Chromatin dynamics in DNA double-strand break repair

INAUGURALDISSERTATION

zur

Erlangung der Würde eines Doktors der Philosophie

vorgelegt der

Philosophisch-Naturwissenschaftlichen Fakultät

der Universität Basel

von

Andrew Ciaran Seeber

aus Irland

Basel, 2017

Genehmigt von der Philosophisch-Naturwissenschaftlichen Fakultät

auf Antrag von

Prof. Dr. Susan M. Gasser

Prof. Dr. Noel F. Lowndes

Basel, den 13 Dezember 2016

Prof. Dr. Jörg Schibler

Dekan

Table of Contents

Thesis Overview

This thesis consists of 7 chapters and the appendices. Each chapter starts with a summary sheet consisting of a title, author list, and summary; if parts or the whole of the chapter has been published, the summary sheet details where and when, and my contribution where other authors were involved.

Chapter 1 is an overview of chromatin organization and dynamics in the context of double-strand break (DSB) repair, and largely stems from a published review. It also contains additional sections discussing the role of modeling chromatin using polymer models, and repair choice in heterochromatin.

Chapter 2 is a more specific published review of the roles of nucleosome remodeling enzymes in DSB repair. It also contains two important tables. One lists the composition and classifications of Swr1-like, Snf2-like and Rad54-like chromatin remodelers in *S. cerevisiae* and humans. The other contains information about the specific subunits of these remodeling complexes and their roles in DSB repair. The second part of Chapter 2, a published editorial, covers my 2013 Genes and Development manuscript where I not only discuss the potential roles of increased DSB and genome-wide chromatin mobility, but also speculate on the possible mechanisms that drive this increased motion.

Chapters 3, 4, 5 and 6 are experimental chapters:

- Chapter 3 is a study on the dynamics of spontaneous repair foci. Importantly, this work also shows that cohesin and the nucleolus constrain chromatin motion.

- Chapter 4 describes a set of experiments where the phenomenon of genome-wide increased chromatin movement in response to DNA damage checkpoint activation is investigated. This study shows that checkpoint activation is both necessary and sufficient for increased chromatin movement in response to DNA damage. It also implicates INO80 as being the key regulator of chromatin movement downstream of the checkpoint.

- Chapter 5 contains a set of follow-up experiments that continues the research done in Chapters 3 and 4, building on previous work of Vincent Dion, Frank Neumann and Patrick Heun. This follow-up research combines an updated imaging regime with a collaboration between the group of Susan Gasser and that of French theoretical physicist David Holcman. This fruitful collaboration allowed us to develop a workflow based on polymer models that can predict local changes in chromatin structure using single particle analysis of chromatin loci.

- Chapter 6 is a large body of experiments that elucidate how the Mre11-Rad50-Xrs2 (MRX) and Replication Protein A (RPA) complexes can interact both at DSBs and at replication forks. In addition, we show for the first time that the MRX complex can physically link two sister chromatids together at a DSB, and that failure to do so reduces repair efficiency.

Chapter 7 summarizes the main conclusions of this thesis and discusses the future directions subsequent research stemming from this work may follow.

Finally, the appendices contain a list of abbreviations, my non-thesis related contributions, my curriculum vitae, and acknowledgments.

This thesis includes the following publications:

Peer-reviewed publications

Dion, V., Kalck, V., **Seeber, A.**, Schleker, T., and Gasser, S.M. (2013). Cohesin and the nucleolus constrain the mobility of spontaneous repair foci. EMBO Reports 14, 984-991.

Seeber, A., Dion, V., and Gasser, S.M. (2013). Checkpoint kinases and the INO80 nucleosome remodeling complex enhance global chromatin mobility in response to DNA damage. Genes & Development 27, 1999-2008.

Seeber, A., Hegnauer, A.M., Hustedt, N., Deshpande, I., Poli, J., Eglinger, J., Pasero, P., Gut, H., Shinohara, M., Hopfner, K.P., Shimada, K., Gasser, S.M. (2016). RPA Mediates Recruitment of MRX to Forks and Double-Strand Breaks to Hold Sister Chromatids Together. Molecular Cell, 64, 951-966.

Amitai, A.*, **Seeber, A.***, Gasser, S.M., Holcman, D. (2017). Visualization of Chromatin Decompaction and Break Site Extrusion as Predicted by Statistical Polymer Modeling of Single-Locus Trajectories. Cell Reports, 18, 1200-1214.

*equal contribution

Review articles and editorials

Seeber, A.*, Hauer, M.*, and Gasser, S.M. (2013). Nucleosome remodelers in double-strand break repair. Current Opinion in Genetics & Development 23, 174-184.

Seeber, A., Dion, V., and Gasser, S.M. (2014). Remodelers move chromatin in response to DNA damage. Cell Cycle 13, 877-878.

Seeber, A., and Gasser, S.M. (2016). Chromatin organization and dynamics in double-strand break repair. Current Opinion in Genetics & Development 43, 9-16.

*equal contribution

CHAPTER 1: AN INTRODUCTION TO CHROMATIN ORGANIZATION AND DYNAMICS IN DOUBLE-STRAND BREAK REPAIR

Based on:

Andrew Seeber and Susan M. Gasser

Friedrich Miescher Institute for Biomedical Research, Maulbeerstrasse 66, 4058 Basel, Switzerland

Current Opinion in Genetics and Development 2016, Volume 43, pp 9-16

Summary

Chromatin is organized and segmented into a landscape of domains that serve multiple purposes. In contrast to transcription, which is controlled by defined sequences and initiates at distinct sites, DNA damage can occur anywhere in the genome. Repair accordingly must occur everywhere, yet it is inevitably affected by its chromatin environment. In this introduction, an expanded version of a published review, we summarize recent work investigating how changes in chromatin organization facilitate and/or guide DNA double-strand break repair. I specifically assess how breaks are repaired, and by which repair pathways, in heterochromatin or euchromatin. I examine recent live-cell studies on the dynamics of chromatin and the mechanisms that regulate its movement, and discuss the role of polymer models in our quest to understand DNA damage repair and repair pathway choice.

Author contributions: A.S. and S.M.G. wrote the manuscript. A.S. designed the figures.

Chromatin on the move

It has been almost 20 years since John Sedat's laboratory showed that chromatin in the interphase nucleus is mobile using live-cell imaging of GFP-tagged loci (Marshall et al., 1997). At the time this stood in contradiction to datasets from fluorescence recovery after photobleaching (FRAP) (Abney et al., 1997), and from imaging UV-induced damage in interphase chromosomes (Cremer et al., 1982), which both argued that chromatin position is static. On the other hand, it was obvious that chromatin must be able to move to enable biological events like meiotic homolog pairing, homologous recombination (HR), chromatin condensation and gene activation through long-range enhancer–promoter interactions. The Sedat laboratory resolved this issue by showing that chromatin does indeed move randomly in both *S. cerevisiae* and *D. melanogaster* within constrained volumes, which are on a scale below the resolution of FRAP. This seminal work additionally showed that size does not matter (i.e. a yeast CEN-containing plasmid, which clusters with other centromeres, was no more mobile than a whole chromosome), although excised chromatin rings without a centromere move more than whole chromosomes (Gartenberg et al., 2004; Neumann et al., 2012). This underscores the fact that centromeres connect to interphase microtubules and constrain chromatin movement, at least in yeast (Marshall et al., 1997). Recent articles have now addressed many of the questions raised by these early studies, the foremost being, 'Does chromatin movement have a biological function and how is it regulated?'

DNA damage induces chromatin mobility

Double-strand break (DSB) repair by homologous recombination (summarized in Figure 1) with an ectopic or non-sister donor sequence requires a physical search for the homologous template. This has long been considered one of the central mechanisms that would require chromatin movement. Investigations into this hypothesis have led to the discovery that endonuclease-induced DSBs in budding yeast move more than uncleaved loci (Dion et al., 2012; Mine-Hattab and Rothstein, 2012). This is regulated by the DNA damage checkpoint kinase Mec1-Ddc2 (or ATR-ATRIP in mammals). Intriguingly, an induced DSB affects more than just the surrounding chromatin: the Rothstein group was the first to report an apparent increase in chromatin mobility for genomic loci far from the break site (Miné-Hattab and Rothstein, 2012). Later work confirmed this generalized increase in chromatin mobility (Seeber et al., 2013a) which, although less pronounced than DSB movement, was ATP-dependent, sensitive to the number of DSBs induced, and dependent on checkpoint kinase activation, including the downstream kinase Rad53 (Seeber et al., 2013a). This link was recently shown to be relevant for mammalian cells, as ionizing radiation (IR) -induced damage triggers increased locus movement, in a manner dependent on the repair factor 53BP1 and the ATM kinase (Lottersberger et al., 2015).

A recent study by the Durocher group proposed that an essential budding yeast kinetochore protein, Cep3, as the relevant target of the checkpoint kinase that controls chromatin movement, both locally and globally (Strecker et al., 2016). The authors suggested that a point mutation, *cep3-S575A*, which compromises a Rad53 phosphoacceptor site in Cep3, completely abrogated the enhanced movement that accompanies a targeted DSB, as well as the global chromatin movement response (Dion et al., 2012). The authors hypothesized that damage-induced phosphorylation of Cep3 triggers a release of centromeres from the interphase spindle that links them to a membrane-spanning spindle pole body (SPB). This release is proposed to generally enhance chromatin movement. They did not detect any change in distance between the SPB and yeast centromeres following cut induction, but they did score, using a relative mean square displacement assay, an enhanced relative mobility between the SPB and a centromere, which was dependent on the phosphoacceptor site in Cep3. Linking this to damage,

they showed that cells treated with Zeocin, a radiomimetic drug previously used to induce global chromatin mobility (Seeber et al., 2013a), led to the declustering of kinetochores near the SPB. However, the *cep3-S575A* mutation had no effect on repair by homologous recombination. Unfortunately, the study failed to monitor the efficiency of DSB induction in the *cep3-S575A* mutant, leaving open alternative interpretations for the lack of increased mobility (e.g. less efficient cleavage or impaired checkpoint activation would similarly fail to increase mobility). Nor did they separate the cells they analyzed by their phase of the cell cycle. Given that there are significant differences in basal level mobility between G1- and S-phase chromatin (Dion et al., 2013; Heun et al., 2001), cell cycle effects must also be carefully controlled for. Nonetheless, this study raises the question of whether enhanced movement is really necessary for homology search

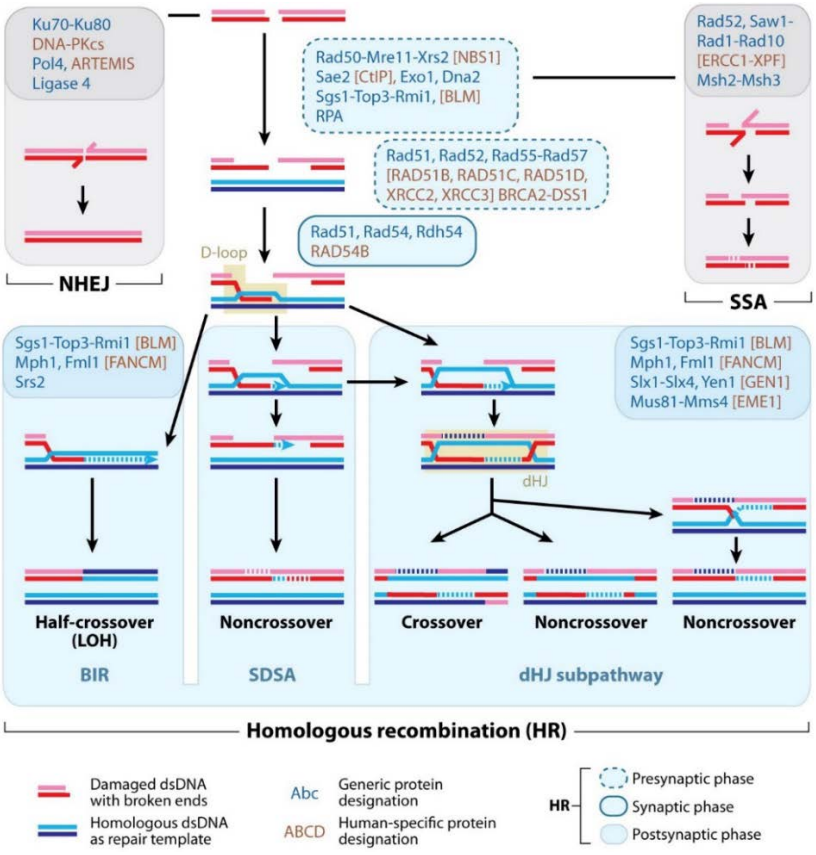

Figure 1: Double-strand break repair pathways. Blue protein names refer to *S. cerevisiae* proteins. If different, the corresponding human name is in brackets and brown. Proteins without a yeast homologue are brown with no bracket. Dashed lines indicate DNA synthesis. DSBs can be repaired by at least three pathways: non-homologous end joining (NHEJ) where the ends of a break are religated together; single-strand annealing (SSA), a template-independent (but homology-dependent) repair mechanism in which the copy number of tandem repeats can be reduced after DSB resection. Alternatively, a variety of homologous recombination mechanisms can be used to repair the break including break induced replication (BIR) when homology is restricted to one end, for example at a collapsed replication fork or uncapped telomeres. This can result in loss of heterozygosity. On the other hand, synthesis dependent strand annealing (SDSA), a template-dependent repair mechanism that proceeds without Holliday junction intermediates leads to non-crossover products. Finally, resolution of double Holiday junctions by resolvases lead to either crossover or non-crossover products. Adapted from (Heyer et al., 2010).

It is certainly possible that increased chromatin mobility does not necessarily facilitate homologous recombination. However, due to a lack of consensus in the field, this hypothesis is neither proven nor rejected. In opposition to the hypothesis that chromatin movement is sufficient to increase homology search efficiency, it has been shown that deletion of the Swr1 chromatin remodeler prevents increased DSB movement, yet it almost doubles the rate of HR with an ectopic repair template (Horigome et al., 2014). In addition, as stated above, *cep3-S575A* does not have increased DSB movement but appears to be as proficient as wildtype for HR using a number of strains carrying breaks and repair templates on different chromosomes (Strecker et al., 2016). In support of the link, a deletion of the *S. cerevisiae* gene *RAD9*, which is required for increased DSB movement, has been shown to increase the time it takes for a DSB to invade its template (Dion et al., 2013). However, Rad9 affects many aspects of DNA repair, including checkpoint activation (Sun et al., 1998) and long-range resection (Chen et al., 2012). Also in support of the homology search hypothesis is the finding that artificial targeting of INO80 to an inducible DSB increases the rate of recombination with an ectopic donor (Neumann et al., 2012). Moreover, cells treated with Latrunculin A, an actin depolymerizing drug which strongly decreases chromatin movement (Spichal et al., 2016), also exhibit a strong decrease in HR. Use of drugs such as Latrunculin A will, of course, affect more than just chromatin movement, and none of the above assays directly measures search time. A live-cell, quantitative experiment that measures homology search still needs to be done, and only that will prove the hypothesis right or finally lay it to rest.

The 2016 Strecker et al., paper has raised a number of other confounding issues.

1) Strecker et al. show that both telomere and centromere detachment are necessary to give rise to the same amount of mobility as that of a DSB. However, they later show that *cep3-S575A* is sufficient to ablate increased movement of a DSB. Since it is unlikely that *cep3-S575A* will lead to detachment of telomeres, is the release of telomeres necessary of damage induced movement? In fact, there is no evidence that telomeres detach from the nuclear periphery after DSB induction. In the case of global chromatin mobility, it has been shown for at least a single telomere that Zeocin did not change its nuclear position (Seeber et al., 2013b).

2) Strecker et al. show that DSB mobility relies partially on the checkpoint kinase Mec1 (ATR), but deletion of *TEL1 (ATM)* seemingly has no effect. However, the double knockout of both proteins completely abrogates increased DSB movement. Furthermore, they show that Rad53, a downstream kinase and target of Mec1, is required for increased DSB movement. This result directly contradicts an earlier report that showed Rad53 is not required for DSB movement although it does stimulate non-break site or general chromatin movement (Dion et al., 2012; Seeber et al., 2013a). Thus, while genome-wide increased chromatin movement in response to DNA damage clearly requires a full blown checkpoint, including Mec1 and Rad53, it is unclear whether the same degree of checkpoint activation is required to increase the movement of DSBs.

3) Strecker et al. confirm the necessity of the chromatin remodeler, INO80, in DSB mobility. However, the link between INO80 and *cep3-S575A* is unclear. The authors show that mutants of INO80 that cannot remodel nucleosomes also have less damage-induced phosphorylation of Cep3; however, there is still sufficient phosphorylation of Cep3 that some increase in mobility of a DSB should be observable. Therefore, the role of INO80 in DSB mobility cannot simply be through Cep3. In addition, it is troubling that the authors have an inconsistent set of results: on the one hand, INO80 is resistant to Zeocin by drop assay, but on the other hand has reduced rates of recombination. It is difficult to imagine a scenario in which this result makes sense, but it may be due to the proclivity of INO80 mutants to become polyploid (Chambers et al., 2012). INO80 mutants have been shown to be sensitive to Zeocin, γIR or induced DSBs by a number of groups (Papamichos-Chronakis et al.,

2006; Papamichos-Chronakis et al., 2011; Seeber et al., 2013b; Shen et al., 2000; van Attikum et al., 2007). This raises questions about the INO80 deficient strain used. Lastly, the shorter DSB-induced cell cycle arrest lengths of INO80 mutants found by Strecker et al. directly contradict earlier reports that show INO80 mutants fail to escape DSB-induced checkpoint arrest (Papamichos-Chronakis et al., 2006) and cannot efficiently resume replication after checkpoint activation following treatment with HU (Shimada et al., 2008) or MMS (Falbo et al., 2009). Lastly, Strecker et al., failed to measure the cut efficiencies of the HO endonuclease for any of their strains, nor did they track Rad52 foci that colocalised with their locus of interest. Therefore, if one of their mutants had less HO induction, or if day-to-day variation resulted in some experiments having poor cut efficiency, they would never know. This caveat combined with the fact that Strecker et al., merged the trajectories of G1 and S phase cells, means that the core conclusions of this paper are not supported by the evidence presented and need to be repeated in a correct and controlled manner.

Clearly, not all damage in yeast triggers enhanced movement (Dion et al., 2013), nor does all damage activate the Mec1-Ddc2/Rad53 checkpoint. Spontaneous damage or DNA-protein adducts that are repaired by exchange with a sister chromatid, or by precise non-homologous end-joining, appear not to trigger changes in chromatin mobility (Dion et al., 2013), nor do they shift to the nuclear periphery for repair (Nagai et al., 2008). Too much movement at a DSB is, moreover, deleterious, particularly in repetitive regions in mammalian cells where extensive movement correlates with translocations and deletion events (Roukos et al., 2013). Intriguingly, the rate of misrepair is strongly affected by the position of the observed locus on a chromosome arm in both yeast and mammals (Hakim et al., 2012; Lee et al., 2016; Rocha et al., 2012; Zhang et al., 2012). This initiated an examination of how nuclear compartments, which often stem from local chromatin structure (Burman et al., 2015), influence pathways of repair. It has been observed that breaks in heterochromatin behaved differently from breaks in euchromatic zones, particularly in mammals and flies (Chiolo et al., 2011; Lemaitre et al., 2014; Ryu et al., 2015; Tsouroula et al., 2016). Thus, chromatin movement can provide a means to escape an unfavorable chromatin compartment or access a set of factors that were unavailable in the lesion's original context.

Telomeres are an excellent case in point: they are highly repetitive yet, when unprotected, they act like a single-ended DSB (Marcomini and Gasser, 2015). Budding yeast telomeres are clustered at the nuclear periphery and form heterochromatic regions (Taddei and Gasser, 2012). The clustering of telomeric ends has raised the question of whether the mobility of telomeres is controlled in response to damage or uncapping.

A study by the Greenberg laboratory investigated what happens to telomere movement during repair or maintenance by the recombination-dependent pathway called alternative lengthening of telomeres, or ALT. They found that DSB signaling at an ALT telomere causes long-range movement and clustering of chromosome ends, which is thought to favor homology-driven maintenance of telomere repeats (Cho et al., 2014). The alternative, i.e. activating end-joining at a telomere, can be dangerous. Previous work from the de Lange laboratory had shown that uncapped telomeres (which lack the protective telomere binding protein TRF2) show increased movement, which correlated with enhanced rates of telomere end-to-end fusion. Both movement and end-to-end fusion depended on 53BP1 (Dimitrova et al., 2008). Recent work from this group has further investigated telomere damage. They find that SUN-domain-containing proteins, which are a component of LINC complex (see below) and bridge the nucleoskeleton to the cytoskeleton, promote increased dynamics of dysfunctional uncapped telomeres, enhancing the rate of untimely end-to-end fusions by NHEJ (Lottersberger et al., 2015). The authors also showed a role for cytoskeleton-bound kinesins in telomere fusions and the repair of internal breaks, suggesting that an active, kinesin-driven movement

of the nucleus or elements in the nuclear envelope affect DSB repair. This is reminiscent of a study in yeast which showed that kinesins can promote movement of subtelomeric DSBs (Chung et al., 2015). In summary, increased movement of a telomere can be useful for ALT-like telomere recombination, yet is deleterious in conditions that generate uncapped or dysfunctional ends, for it leads to telomere-telomere fusions. The difference between the two may be related to the degree of resection at the telomere. The next section will discuss new articles that look at the effect of chromatin structure, actin, and microtubules on chromatin motion.

Chromatin structure, actin, and microtubules affect chromatin mobility

The budding yeast genome is organized in a Rabl configuration where the centromeres are attached to the SPB and the telomeres are attached to the periphery (Bystricky et al., 2005; Duan et al., 2010). Forced detachment of the centromere from the SPB increases chromatin movement (Strecker et al., 2016; Verdaasdonk et al., 2013a), as does telomere release from the periphery (Hediger et al., 2002) or the loss of anchorage by ablation of SIR-mediated silencing (Hediger et al., 2002; Taddei et al., 2004). However, a chromosome that is detached from its perinuclear anchor is still more confined than a free-floating plasmid ring (Neumann et al., 2012; Strecker et al., 2016), suggesting that there are additional constraints on chromosomes. One constraint stems from the inherent structure of the chromatin fiber, while the second is the tethering of sister chromatids through cohesin (Dion et al., 2013). Consistently, there is accumulating evidence that supports the notion that altered chromatin fiber organization, i.e. nucleosome eviction or remodeling, increases movement. Notably, the targeting of a functional nucleosome remodeler, INO80, to a chromosomal locus (Neumann et al., 2012; Spichal et al., 2016) or the INO80-dependent eviction of nucleosomes at the *PHO5* locus in the absence of phosphate both increase the movement of an appropriately tagged locus.

Interestingly, DNA damage also changes chromatin structure. A new study in yeast shows that Zeocin-induced damage leads to the degradation of 30% of the four core histones within 30-60 mins (Hauer et al., 2017). This induces chromatin decompaction, and increases both the flexibility of the chromatin fiber and its mobility, in a manner dependent on the DNA damage checkpoint and INO80. Furthermore, either the artificial reduction of histone proteins H3/H4, or the use of a mutant that naturally has lower levels of histones (*nhp6Δ*), triggers decompaction and increased chromatin movement (Hauer et al., 2017). This result contradicts an earlier report where the shutdown of histone H3 production was thought to decrease locus mobility (Verdaasdonk et al., 2013a). The difference may reflect the fact that nucleosome depletion and enhanced chromatin flexibility requires the loss of both H3 and H4. Furthermore, it was shown that H4 (but not H3) shutdown leads to a declustering of kinetochores (Bouck and Bloom, 2007), an event that may also contribute to the increased chromatin movement observed by Hauer et al. The influence of inherent chromatin structure on mobility is consistent with the finding that histone modifications correlate with the propensity for translocations in mammalian cells (Burman et al., 2015). A very recent paper (Adam et al., 2016) also documents a similar unfolding and expansion of chromatin in response to UV-induced damage in mammalian cells, although in this case the effect stemmed largely from histone mobilization and replacement, rather than degradation (Adam et al., 2016).

Besides inherent changes in chromatin structure, accumulating evidence also implicates microtubules and the actin cytoskeleton as drivers of nuclear and/or chromatin movement. In Sedat's study, the depolymerization of microtubules by Nocodazole was shown to increase chromatin movement in budding yeast (Marshall et al., 1997). This suggested that microtubules mediated constraint, although it was not clear whether this effect arose from direct interactions between chromatin and microtubules or indirect contact through the nuclear envelope. The LINC complex can connect cytoskeletal

filaments (Chang et al., 2015) through Klarsicht, ANC-1, and Syne homology proteins (KASH, also known as Nesprin) on the outer nuclear membrane, to their ligands, the SUN-domain proteins, which span the perinuclear space and protrude into the nucleoplasm. Some SUN-domain proteins interact with chromatin, specifically telomeres (Chang et al., 2015), and resected DSBs in budding yeast (Horigome et al., 2014; Kalocsay et al., 2009; Oza et al., 2009; Swartz et al., 2014).

Work from the de Lange laboratory showed for the first time that, in contrast to yeast, the treatment of mammalian cells with dysfunctional telomeres with the microtubule poisons Taxol or Nocodazole actually decreased their movement in a reversible manner (Lottersberger et al., 2015). Importantly, the authors showed that removal of SUN1/2, an essential bridge from the cytoskeleton to the inner nuclear membrane, decreased movement, similar to the microtubule poisons. The reduced movement, due either to depolymerization of the cytoskeleton or loss of this cytoskeleton-to-nucleus link, also reduced the rate of telomere-telomere fusions. Importantly, Taxol treatment also seemed to decrease the movement of IR-induced foci, and not only dysfunctional telomeres. This implies that the forces applied to the chromosomes through the microtubules can be transduced to internal chromatin. Although a mechanism through which cytoskeleton-associated kinesins drive SUN-domain-bound telomeres into a clustered, bouquet arrangement is well-characterized in meiotic prophase (Scherthan et al., 2001), this checkpoint kinase-induced event in mitosis does not entail bouquet formation and is most likely differently regulated.

In budding yeast, as mentioned above, the depolymerization of microtubules had the opposite effect on chromatin movement: mobility increased after Nocodazole treatment, consistent with data showing that the deletion of *CSM4*, a putative LINC protein, similarly led to increased subtelomere movement (Spichal et al., 2016). Nocodazole has also been shown to increase distance of a centromere to the nuclear periphery (Bystricky et al., 2004; Heun et al., 2001) This may be due to the loss of microtubules that tether interphase centromeres to the SPB (Jin et al., 2000), or the disruption of a network of intranuclear microtubules (Laporte et al., 2013), something unique to budding yeast. It is noteworthy that, in meiosis, bouquet formation is also driven by cytoplasmic actin filaments in budding yeast, rather than microtubules, suggesting that in this species actin filaments replace microtubules in some aspects of nuclear movement.

Nonetheless, in all eukaryotes, actin forms a cytoplasmic network of filaments and it is found, at least in its monomeric 'G' form, inside the nucleus in a range of protein complexes, the most prominent of which are chromatin remodelers (Kapoor et al., 2013). Work from the Fabre laboratory has recently shown that both cytoplasmic and nuclear actin contribute to chromatin motion, through a mechanism that appears to be independent of the putative budding yeast LINC (Spichal et al., 2016). Treatment of yeast cells with the actin filament poison Latrunculin A (LatA) was sufficient to decrease the movement of a locus. While this suggests that cytoplasmic actin filaments might move the yeast nucleus, much like microtubules do in *S. pombe* and mice, it is also possible that LatA affects movement indirectly by altering nuclear G-actin. Intriguingly, the targeting of the actin-containing remodeler INO80, which increases the movement of a locus under normal conditions (Neumann et al., 2012), fails to do so when cells are treated with LatA. This result suggests that LatA may bind nuclear actin and disrupt the function of the INO80 complex (Kapoor et al., 2013). This mechanism might affect other actin-containing chromatin modulating complexes as well, such as NuA4 (TIP60), Swi/Snf, or SWR1 (SRCAP). Since INO80 is necessary for the eviction and degradation of histones in response to DNA damage (Hauer et al., 2017), LatA could interfere with INO80-mediated changes in the nucleosome packing, thereby abrogating the damage-associated increase in chromatin mobility.

A summary of chromatin movement studies unrelated to DNA repair and in other organisms

This introduction has so far focused on studies of chromatin movement that are either linked to DNA damage in some way, most of which were performed in yeast. In this section I will list and briefly summarize some studies on chromatin movement that are unrelated to DNA repair or are performed in organisms other than yeast. Early work on chromatin motion in living human cells relied on the incorporation of fluorescently labeled deoxy- or ribo-NTP analogs (Manders et al., 1999; Zink et al., 1998) or by the addition of peptide nucleic acid (PNA) probes (Molenaar et al., 2003). Other studies have used histones tagged with photoactivatable or photoconvertible fluorophores to study motion in living cells (Kruhlak et al., 2006; Liu et al., 2015; Wiesmeijer et al., 2008). More recent studies on chromatin motion have started to employ advanced techniques such as displacement correlation spectroscopy (DCS) (Zidovska et al., 2013), which allowed the authors to detect coherent movement of chromatin across micron-scale ranges (Bruinsma et al., 2014). Other laboratories have developed new microscopes such as the Double-Helix Point Spread Function (DH-PSF) microscope (Backlund et al., 2014) and the aberration-corrected Multifocus Microscope (MFM)(Abrahamsson et al., 2013), to study chromatin motion in 3D without needing to acquire z-stacks. This enables fast 3D image acquisition without a moving piezo stage.

In addition to the development of new microscopes, researchers are developing new methods of visualizing chromatin in living cells. The ParB-*parS* system works in a similar way to the traditional GFP-LacI/*laco* method but differs substantially in one respect. The ParB protein, which may be tagged with a fluorophore, can oligomerize at *parS* (also called INT) sites, recruiting 100-200 molecules (Saad et al., 2014). The *parS* DNA is ~1kb in length, considerably shorter than the ~10kb of a *lacO* array. The current state-of-the-art for live imaging of chromatin in mammalian cells is the use of fluorescently tagged Cas9 enzymes with guide RNAs specific for a genomic locus of interest (Chen et al., 2013; Chen et al., 2016; Ma et al., 2015). These systems are flexible, since only the guide sgRNA needs to be changed to target a different genomic locus. It is now possible to do two-color CRISPR imaging by using fluorescently tagged Cas9 proteins from either *Staphylococcus aureus* or *Streptococcus pyogenes* (Chen et al., 2016).

Chromatin movement appears to be conserved across species with the diffusion coefficient ranging from 10^{-4} to 10^{-3} $\mu m^2/s$, such as in mammalian cells, bacteria, yeast, and *Drosophila* (Bornfleth et al., 1999; Bronstein et al., 2009; Chubb et al., 2002; Dion et al., 2012; Heun et al., 2001; Levi et al., 2005; Marshall et al., 1997; Pliss et al., 2013; Seeber et al., 2013a; Vazquez et al., 2001; Weber et al., 2012). However, chromatin movement can change during cell differentiation. Dynamic imaging of *Drosophila* imaging discs has shown that in cells that are differentiated, chromatin is more constrained (Thakar and Csink, 2005). This result is consistent with the observation that mature *Drosophila* spermatocytes show more constrained chromatin motion than spermatocytes not yet fully differentiated (Vazquez et al., 2001). Currently, chromatin motion has not been studied in a quantitative manner in embryonic stem cells or in induced pluripotent cells.

In budding yeast, less movement is observed in S phase than in G1 (Dion et al., 2013; Heun et al., 2001). This correlates inversely with the number of active replications forks (Heun et al., 2001), which could constrain movement through replication origin clustering which itself may require cohesin. Importantly the cleavage of cohesin in S phase is sufficient to reduce constraint in S phase cells to G1 levels (Dion et al., 2013). Early work in mammalian cells showed that there did not appear to be much change between chromatin motion in mid to late G1, and early S through G2 phase (Walter et al., 2003; Wiesmeijer et al., 2008). However, chromatin motion in early G1 was significantly higher,

suggesting that there are physical parameters that control the motion of a locus. Other researchers have refined this by tracking large ~1 Mbp chromatin domains in mammalian cells. They have found that chromosome domains that replicate early are less constrained than those that replicate late (Pliss et al., 2013). Importantly it reduces movement (Horigome et al., 2014).

The effects of subnuclear chromatin organization on DNA repair

There is no doubt that chromatin movement exists, and is enhanced by some types of DNA damage; but the question persists, why? It has been proposed that chromatin compartments affect the efficiency of certain repair pathways or, at the very least, favor/disfavor certain damage processing steps. This last section will examine how subnuclear compartments, like the nuclear envelope and the nucleolus, affect DSB repair.

The nuclear pore complex (NPC) contains >30 different nuclear pore proteins (nucleoporins), creating a complex with eight-fold symmetry that spans the nuclear envelope and gates traffic between the cytoplasm and the nucleus (Bukata et al., 2013). In budding yeast, the NPC is a binding site for persistent DSBs (Kalocsay et al., 2009; Nagai et al., 2008; Oza et al., 2009) including breaks that occur at collapsed forks (Nagai et al., 2008; Su et al., 2015) or in subtelomeric regions (Therizols et al., 2006). In addition, the Sad1-Unc-84-related (SUN) domain protein Mps3, which acts as an alternative binding site for resected DSBs in S phase, is embedded in the inner nuclear membrane (Oza et al., 2009). This same phenomenon occurs in fission yeast (Swartz et al., 2014). DSB-break recruitment to either the NPC or to Mps3/Sad1 has different requirements to recruitment to pores (Horigome et al., 2014; Oza et al., 2009), and appears to favor distinct features of repair (summarized in Figure 2).

DSB recruitment to the NPC is independent of cell-cycle stage, does not require the recombinase Rad51 nor the INO80 chromatin remodeling (Horigome et al., 2014) complex, and is independent of extensive resection (at least in G1 phase cells (Neumann et al., 2012; Strecker et al., 2016)). In contrast, Mps3-DSB interaction occurs in S/G2 phase, and requires resection, the ssDNA binding factor Rad51, and INO80. Importantly, the SWR1 chromatin remodeler and its deposition of Htz1 (H2A.Z) at breaks contribute to the peripheral relocation for either site of anchorage. The outcomes of relocation are deduced from the phenotypes that arise from ablation of one anchor. Based on such an analysis, it would seem that Mps3 helps suppress illegitimate recombination, perhaps by anchoring or protecting the resected ends until an appropriate template appears (Swartz et al., 2014). The NPC complex, on the other hand, appears to promote alternative repair pathways, such as template switching at a broken replication fork, or BIR at single-ended breaks (Horigome et al., 2016). The Mekhail group found that Cohibin (a complex consisting of Lsr4-Csm1 and kinesin-14) is necessary for a subtelomeric DSB and the NPC to interact (Chung et al., 2015). Lsr4-Csm1 is involved in rDNA stabilization through perinuclear anchoring (Chan et al., 2011), but it has not been implicated in the recovery from persistent DSBs or collapsed replication forks.

Earlier work had shown that the Slx5/Slx8 SUMO-targeted ubiquitin ligase (STUbL) not only interacts with nuclear pores, but is also recruited to persistent DSBs, both in yeast (Horigome et al., 2016; Nagai et al., 2008) and in *Drosophila* (Ryu et al., 2015). It was therefore examined whether Slx5/Slx8 (degringolade or Dgrn in flies; RNF4 in mammals) was required for the relocation of DSBs to the periphery or if it acts only after recruitment. Considering that STUbLs contain small ubiquitin-like modifier (SUMO) interacting motifs (SIMs) (Mullen and Brill, 2008), and that many repair proteins are SUMOylated (Sarangi and Zhao, 2015), this role of Slx5/Slx8 immediately raised the question whether or not SUMO ligases are involved in DSB relocation. Four recent papers (Churikov et al., 2016; Horigome et al., 2016; Ryu et al., 2015; Su et al., 2015) have examined the roles of Slx5/Slx8 and SUMO ligases at DSBs, eroded telomeres, and collapsed replication forks in budding yeast and

Drosophila, producing a coherent picture of the role of SUMO and its ligands in break relocation (Figure 3).

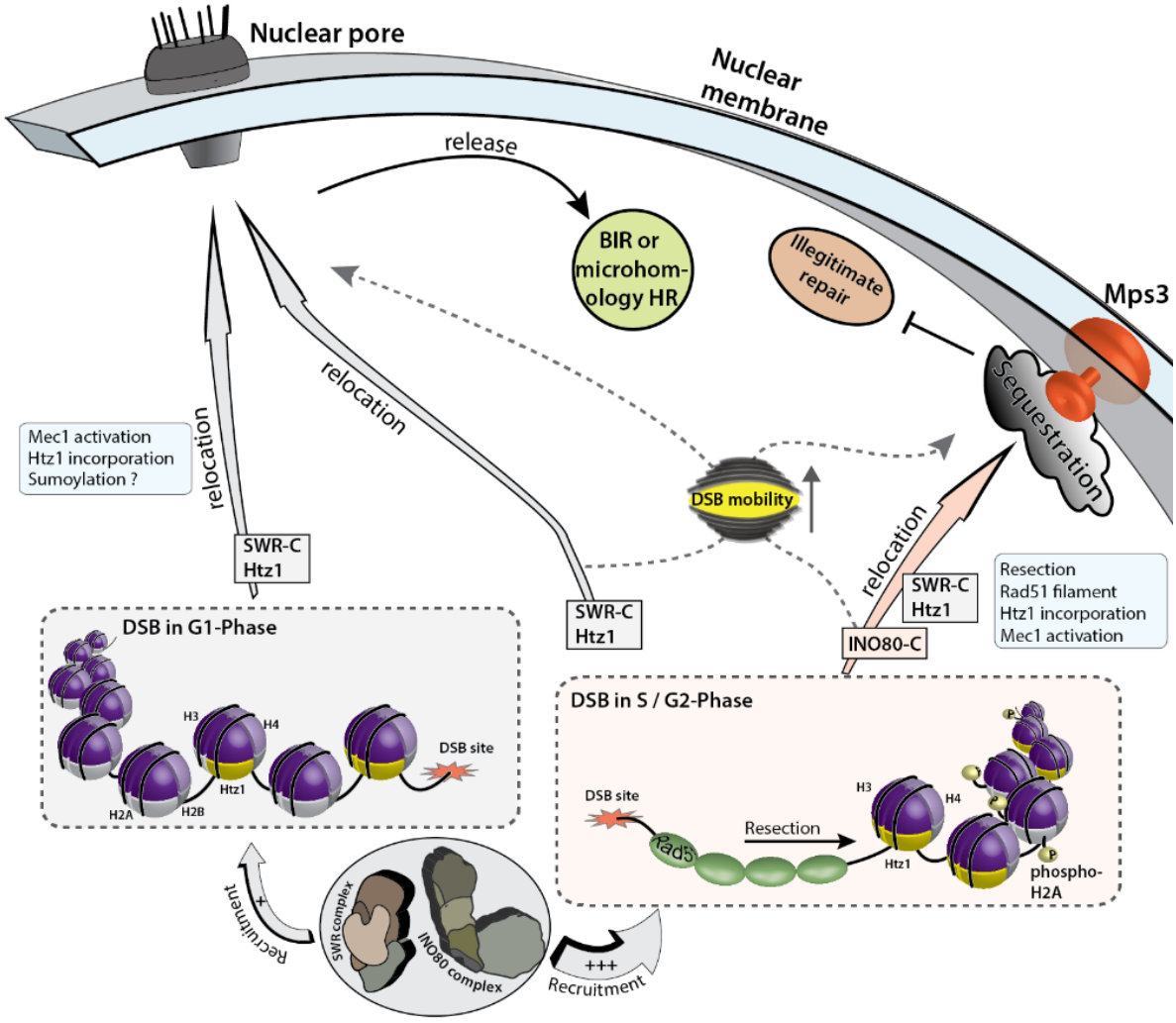

Figure 2: The roles of SWR-C and INO80-C in DSB relocation during G1 and S/G2 phase. DSBs signal the recruitment of a multitude of repair factors including the Swr1 complex (SWR-C) and the INO80 complex (INO80-C). SWR-C and INO80-C are preferentially recruited to DSBs in S/G2 phase. A DSB has different protein requirements for relocation to the periphery during the cell cycle. In S/G2 phase, INO80 promotes the relocation of the DSB to Mps3 and requires resection and Rad51 binding. SWR-C and the deposition of Htz1 (H2A.Z) are required for relocation to either the nuclear pores or Mps3. Mps3 may suppress illegitimate recombination, possibly by anchoring or protecting the resected ends until an appropriate template appears. The nuclear pore complex promotes alternative repair pathways such as BIR. Adapted from Gerhold et al., 2015.

In *S. cerevisiae*, there are four SUMO E3 ligases, Siz1, Siz2 (mammalian PIAS homologs), Mms21 (which binds the Smc5/6 complex), and the meiosis-specific Cst9. SUMOylation events mediated by both Siz2 and Mms21 are implicated in DSB relocation to the nuclear periphery (Horigome et al., 2016). Interestingly, the relocation has different requirements at different points during the cell cycle. PolySUMOylation by Siz2 or Mms21 in G1 phase recruits Slx5/Slx8 to the break, which then allows relocation to pores. An artificial poly-SUMO construct was sufficient to shift an undamaged site to NPCs, in a Slx5-dependent manner, while a similarly targeted mono-SUMO construct was not able to (Horigome et al., 2016). In S phase, on the other hand, monoSUMOylation was sufficient to shift resected damage to the SUN-domain protein, Mps3, in a manner independent of Slx5/Slx8 (Horigome et al., 2016). This is reminiscent of an earlier report that a targeted yKu80-SUMO fusion shifts internal loci and/or telomeres to Mps3 (Ferreira et al., 2011). Thus, there are cell cycle-, and SUMO chain-dependent pathways that direct damage to one or another perinuclear processing sites, obviously with different repair outcomes.

At pores, both imprecise non-homologous end joining (NHEJ) and break-induced replication (BIR) are compromised by mutations in Nup84 (the binding site for Slx5) and by loss of the STUbL itself (Horigome et al., 2016). This observation is bolstered by the fact that the tethering of a subtelomeric DSB to the NPC results in hyperactive BIR, as well as moderately increasing imprecise NHEJ (Chung et al., 2015). In an analogous study using *Drosophila* cells, Chiolo and colleagues first showed that DSB relocate away from heterochromatin to enable recombination to occur (Chiolo et al., 2011). This required both SUMOylation by SUMO E3 ligases, and the *Drosophila* Slx5/Slx8 equivalent Dgrn (Ryu et al., 2015). However, in flies not only the NPC, but also the Mps3 homologues, Koi and Spag4, appear to recruit the STUbL (Dgrn) and its RENi cofactor (Rad60) to the periphery. These work together with the Smc5/6-SUMO ligase complex (Mms21), triggering the recruitment of hetero-chromatic DSBs to pores (Ryu et al., 2015) (Figure 3). In yeast, the proximity of the proteasome to the NPC may justifies relocation of the break, while in flies it is unclear whether further processing of the break or protein degradation of a STUbL target is necessary for repair.

Importantly, it is not only artificially induced breaks that find their way to the nuclear periphery: two important recent studies have shown that both eroded telomeres and replication damage associated with expanded triplet repeats shift transiently in S phase to pores for processing and release (Churikov et al., 2016; Su et al., 2015). The Lisby and Geli laboratories looked at telomeres in a telomerase-deficient yeast strain, and found that shortened telomeres are relocated to the NPC in a very similar SUMO-dependent pathway. The shift, and Slx5/Slx8 itself, were both required to enable recombination-mediated elongation of the short terminal TG-tract, generating type II survivors in which TG repeats are maintained by recombination (ALT in mammals) (Churikov et al., 2016; Figure 4). Finally, an analysis of expanded CAG triplet repeats (Figure 4), which serve as hotspots for replication fork collapse in S phase, showed that these also relocate transiently in late S phase to the NPC, again in a Slx5/Slx8-dependent manner (Su et al., 2015). Unlike flies, the Mps3 protein was not involved although Mps3 does interfere with the relocation of DSBs to pores in S phase in yeast (Horigome et al., 2014). This may argue for S-phase modification or possibly the interaction of a subpopulation of Mps3 with nuclear pores. Failure to recruit the CAG repeat to the periphery led to both expansions and deletions of the CAG tract (Su et al., 2015). Taken together, these studies collectively define a conserved pathway through which damage is shifted from its normal subnuclear context to the nuclear pore, in a manner dependent on SUMOylation. Failure to move appears to be detrimental to recovery (Figures 3 and 4), and the shift of damage to a favored site of repair in all cases depends on SUMOylation.

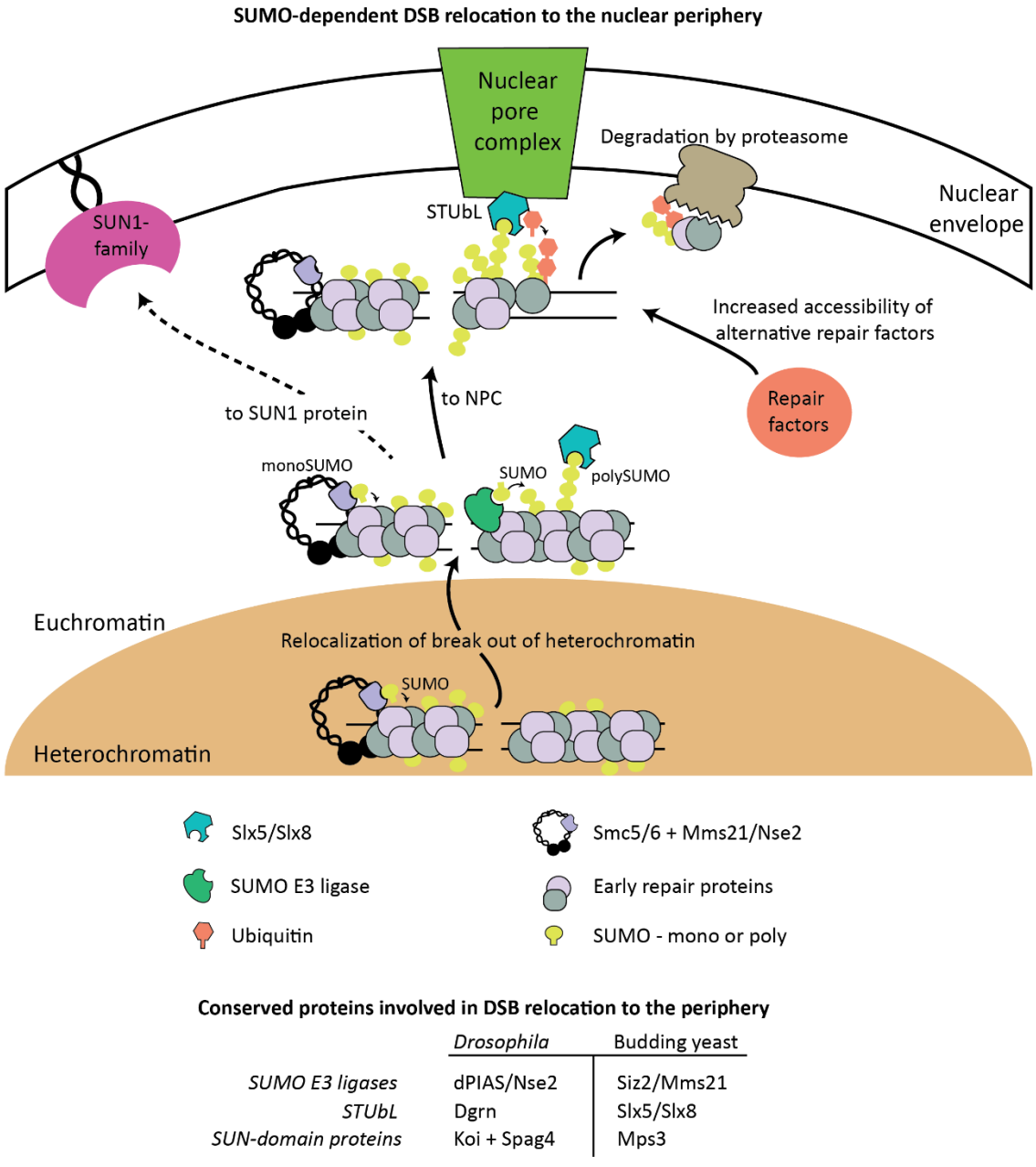

Conserved proteins involved in DSB relocation to the periphery

	Drosophila	Budding yeast
SUMO E3 ligases	dPIAS/Nse2	Siz2/Mms21
STUbL	Dgrn	Slx5/Slx8
SUN-domain proteins	Koi + Spag4	Mps3

Figure 3: Relocation of a DSB to the nuclear periphery in yeast and *Drosophila*. DSBs can occur in heterochromatin or euchromatin. SMC5/SMC6 and its associated E3 ligase, Mms21, mediate monoSUMOylation which allows DSBs to shift out of heterochromatin and enables repair. Recruitment of additional SUMO E3 ligases (e.g. Siz2/PIAS homologues) to the DSBs promotes polySUMOylation, which facilitates STUbL-dependent relocalization of the lesion to the NPC, where proteins are ubiquitylated and degraded by the proteasome. This is thought to allow alternative repair factors to bind the DSB, mediating BIR or imprecise NHEJ. MonoSUMOylated DSBs can also shift to SUN-domain proteins embedded in the nuclear envelope independent of STUbL interactions. This occurs particularly in S-phase cells, where breaks are readily resected and bound by Rad51.

Nonetheless, many open questions remain. It is unclear whether one or many proteins are SUMOylated, and which are degraded following STUbL-mediated ubiquitination. Interestingly, recent work shows that nuclear pore proteins are targets of Slx5/Slx8 (Nino et al., 2016). Epistasis mapping studies place the proteasome in the same pathway as Nup84 and Slx5/Slx8 for the recovery from difficult-to-repair breaks (Nagai et al., 2008), yet why must targeted protein degradation occur near the pore? What is gained by clustering or targeting damage through SUMOylation and SIM-containing proteins? An alternative hypothesis proposes that the nuclear periphery serves a structural role, that allows it to bring free ends or common sequences together, so that the homology search for difficult-to-repair breaks becomes a 2-, rather than 3-dimensional search.

Besides the nuclear envelope, the nucleolus (which harbors the rDNA repeats) is a major organizing element of the nucleus. Previous studies in *S. cerevisiae* found that DSBs induced in the rDNA context also shift away from the nucleolus to allow break processing and Rad51 loading, and repair by homologous recombination (Torres-Rosell et al., 2007) (Figure 4). The shift out of the nucleolus depended on the SMC5/6- Mms21 SUMO ligase, and in this case it appeared that Rad52 was the essential target of SUMOylation. Failure to modify Rad52 and shift away from the nucleolus resulted in aberrant recombination events (Torres-Rosell et al., 2007). Two new studies have addressed this issue in mammalian cells (Harding et al., 2015; van Sluis and McStay, 2015) with results remarkably similar to those from budding yeast. Persistent nucleolar DSBs were observed to shift from the core of the nucleolus to its periphery (Harding et al., 2015; van Sluis and McStay, 2015). While Harding et al. found that most DSBs in the rDNA were efficiently repaired by NHEJ, both studies showed that persistent DSBs led to an ATM-dependent inhibition of Pol1 transcription and nucleolar rearrangements. The relocation of the rDNA break from the interior of the nucleolus to its periphery allowed HR factors to be recruited (van Sluis and McStay, 2015). This supports the notion that certain chromatin compartments are refractory to repair, apparently in all eukaryotic organisms. Domains that are rich in repeats appear to require special measures and tailor-made pathways for DSB repair. The parallels in the roles of chromatin movement, SUMOylation, and nuclear pores in DSB repair from yeast to humans, as highlighted above and in many other recent studies (Goodarzi et al., 2008; Janssen et al., 2016; Lomax et al., 2013; Noon et al., 2010), secures this as a highly promising field of research.

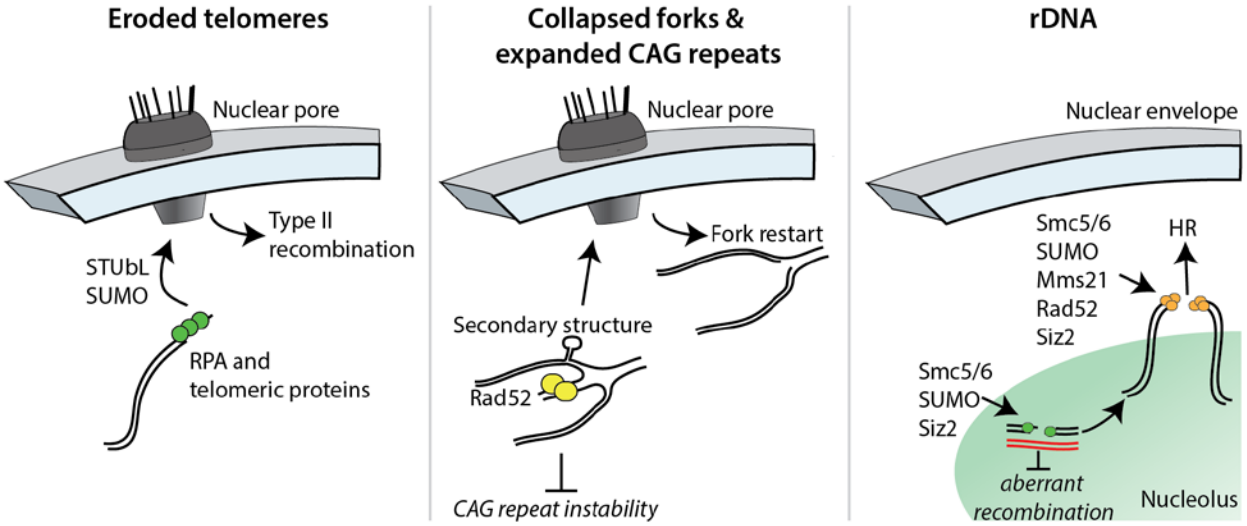

Figure 4: Relocation of eroded telomeres, collapsed forks/expanded CAG repeats and the rDNA. For explanation see above paragraphs. Figure adapted from Gerhold et al., 2015.

Repair pathway choice in Heterochromatin vs Euchromatin

When a break occurs, the repair choice can be affected by the surrounding chromatin. A comprehensive study by Janssen et al. measured the relative contributions of different repair mechanisms at controlled endonuclease DSBs in both euchromatin and heterochromatin in *Drosophila melanogaster* larval imaginal discs. Using a variety of tests, including live-cell imaging and repair product sequencing, the authors showed that both HR and NHEJ are used to repair DSBs in both euchromatin and heterochromatin. Interestingly, the authors conclude that the majority (~80%) of DSBs in heterochromatin are repaired by NHEJ and that 70% of all breaks move to the nuclear periphery independent of Rad51, Ku70, or CtIP (Sae2 in *S. cerevisiae*). This implies that DSB relocalization occurs independently of the repair pathway used (Janssen et al., 2016). Importantly, the authors provide strong evidence that there is no difference in repair kinetics between euchromatic and heterochromatic lesions for a single endonuclease-induced DSB. This contrasts what has been observed for irradiation-(IR) induced damage where is has been observed that heterochromatic breaks are repaired more slowly (Chiolo et al., 2011; Goodarzi et al., 2008; Noon et al., 2010). This difference may be due to the fact that DSBs represent only a small fraction (1%) of the lesions induced by IR: the predominant type of damage is single-strand breaks or purine/pyrimidine lesions (Lomax et al., 2013; Povirk et al., 1996). In addition, it remains possible that the position of the break is indeed important, and that using a single-break induced site does not represent an average view for all positions. In line with this, another study using mammalian cells looked at the repair of CRISPR/Cas9-induced DSBs in a variety of heterochromatic regions (Tsouroula et al., 2016). The authors found that there is a striking difference between pericentric and centromeric heterochromatin with repair choices being affected, in addition, by cell cycle stage. Specifically, centromeric DSBs recruit RPA and Rad51 throughout the cell cycle, independent of DNA replication. Pericentric heterochromatic DSBs appear to only recruit Rad51 in post-replicative chromatin at the periphery of the heterochromatic domain (Tsouroula et al., 2016). While contradictions persist, the tools developed in these studies are powerful systems in which to study DSBs within the context of chromatin in living animal tissue and eukaryotic cells.

The role of polymer models in understanding chromatin dynamics

Mean square displacement (MSD) analysis is the most common way to examine the properties of a trajectory obtained from single-particle tracking of chromosomal loci. An important parameter that can be obtained is the radius of confinement (Rc) which is proportional to the MSD plateau (Dion and Gasser, 2013). Other than the Rc, there are a number of parameters that can be determined, the two most prominent being the diffusion coefficient, and the scaling factor or anomalous exponent (α), which describes the character of the movement, i.e. sub-diffusive, Brownian, super-diffusive (Dion and Gasser, 2013; Wang et al., 2015). While other reviews cover this topic more comprehensively (Wang et al., 2015), it should be noted that there is considerable effort being put into getting more out of chromatin motion studies than just the degree of confinement. Methods to integrate biological data and polymer models are still under development but appear promising. Three recent papers have used Rouse polymer models (for discussion on whether Rouse models are correct for modeling yeast chromatin motion see (Wang et al., 2015)) to either extract forces acting on chromatin (Amitai et al., 2015; Verdaasdonk et al., 2013b) or to try to assess chromatin flexibility (Hajjoul et al., 2013). While such studies are still in their infancy, we are close to a point where modeling of chromatin structure with polymers will enable novel biological predictions. This will require refinement and development of local interaction models, coupled with large, whole genome models such as those generated by chromosome conformation capture techniques. The outcome should eventually be a multi-scale model of the nucleus with which to study chromatin organization under changing conditions, i.e. DSB repair.

References

Abney, J.R., Cutler, B., Fillbach, M.L., Axelrod, D., and Scalettar, B.A. (1997). Chromatin Dynamics in Interphase Nuclei and Its Implications for Nuclear Structure. The Journal of cell biology *137*, 1459-1468.

Abrahamsson, S., Chen, J., Hajj, B., Stallinga, S., Katsov, A.Y., Wisniewski, J., Mizuguchi, G., Soule, P., Mueller, F., and Darzacq, C.D. (2013). Fast multicolor 3D imaging using aberration-corrected multifocus microscopy. Nature methods *10*, 60-63.

Adam, S., Dabin, J., Chevallier, O., Leroy, O., Baldeyron, C., Corpet, A., Lomonte, P., Renaud, O., Almouzni, G., and Polo, S.E. (2016). Real-Time Tracking of Parental Histones Reveals Their Contribution to Chromatin Integrity Following DNA Damage. Molecular Cell *64*, 65-78.

Amitai, A., Toulouze, M., Dubrana, K., and Holcman, D. (2015). Analysis of single locus trajectories for extracting in vivo chromatin tethering interactions. PLoS Comput Biol *11*, e1004433.

Backlund, M.P., Joyner, R., Weis, K., and Moerner, W. (2014). Correlations of three-dimensional motion of chromosomal loci in yeast revealed by the double-helix point spread function microscope. Molecular biology of the cell *25*, 3619-3629.

Bornfleth, H., Edelmann, P., Zink, D., Cremer, T., and Cremer, C. (1999). Quantitative motion analysis of subchromosomal foci in living cells using four-dimensional microscopy. Biophysical journal *77*, 2871-2886.

Bouck, D.C., and Bloom, K. (2007). Pericentric chromatin is an elastic component of the mitotic spindle. Current biology *17*, 741-748.

Bronstein, I., Israel, Y., Kepten, E., Mai, S., Shav-Tal, Y., Barkai, E., and Garini, Y. (2009). Transient anomalous diffusion of telomeres in the nucleus of mammalian cells. Physical review letters *103*, 018102.

Bruinsma, R., Grosberg, A.Y., Rabin, Y., and Zidovska, A. (2014). Chromatin hydrodynamics. Biophys J *106*, 1871-1881.

Bukata, L., Parker, S.L., and D'Angelo, M.A. (2013). Nuclear pore complexes in the maintenance of genome integrity. Curr Opin Cell Biol *25*, 378-386.

Burman, B., Zhang, Z.Z., Pegoraro, G., Lieb, J.D., and Misteli, T. (2015). Histone modifications predispose genome regions to breakage and translocation. Genes & development *29*, 1393-1402.

Bystricky, K., Heun, P., Gehlen, L., Langowski, J., Gasser, S.M. (2004). Long-range compaction and flexibility of interphase chromatin in budding yeast analyzed by high-resolution imaging techniques. Proc Natl Acad Sci U S A, *101,* 16495-16500.

Bystricky, K., Laroche, T., van Houwe, G., Blaszczyk, M., and Gasser, S.M. (2005). Chromosome looping in yeast telomere pairing and coordinated movement reflect anchoring efficiency and territorial organization. The Journal of cell biology, *168*, 375-387.

Chambers, A.L., Ormerod, G., Durley, S.C., Sing, T.L., Brown, G.W., Kent, N.A., and Downs, J.A. (2012). The INO80 chromatin remodeling complex prevents polyploidy and maintains normal chromatin structure at centromeres. Genes & development *26*, 2590-2603.

Chan, J.N., Poon, B.P., Salvi, J., Olsen, J.B., Emili, A., and Mekhail, K. (2011). Perinuclear cohibin complexes maintain replicative life span via roles at distinct silent chromatin domains. Developmental cell *20*, 867-879.

Chang, W., Worman, H.J., and Gundersen, G.G. (2015). Accessorizing and anchoring the LINC complex for multifunctionality. The Journal of cell biology *208*, 11-22.

Chen, B., Gilbert, L.A., Cimini, B.A., Schnitzbauer, J., Zhang, W., Li, G.-W., Park, J., Blackburn, E.H., Weissman, J.S., and Qi, L.S. (2013). Dynamic imaging of genomic loci in living human cells by an optimized CRISPR/Cas system. Cell *155*, 1479-1491.

Chen, B., Hu, J., Almeida, R., Liu, H., Balakrishnan, S., Covill-Cooke, C., Lim, W.A., and Huang, B. (2016). Expanding the CRISPR imaging toolset with Staphylococcus aureus Cas9 for simultaneous imaging of multiple genomic loci. Nucleic acids research, gkv1533.

Chen, X., Cui, D., Papusha, A., Zhang, X., Chu, C.D., Tang, J., Chen, K., Pan, X., and Ira, G. (2012). The Fun30 nucleosome remodeller promotes resection of DNA double-strand break ends. Nature *489*, 576-580.

Chiolo, I., Minoda, A., Colmenares, S.U., Polyzos, A., Costes, S.V., and Karpen, G.H. (2011). Double-strand breaks in heterochromatin move outside of a dynamic HP1a domain to complete recombinational repair. Cell *144*, 732-744.

Cho, N.W., Dilley, R.L., Lampson, M.A., and Greenberg, R.A. (2014). Interchromosomal Homology Searches Drive Directional ALT Telomere Movement and Synapsis. Cell *159*, 108-121.

Chubb, J.R., Boyle, S., Perry, P., and Bickmore, W.A. (2002). Chromatin motion is constrained by association with nuclear compartments in human cells. Current Biology *12*, 439-445.

Chung, D.K., Chan, J.N., Strecker, J., Zhang, W., Ebrahimi-Ardebili, S., Lu, T., Abraham, K.J., Durocher, D., and Mekhail, K. (2015). Perinuclear tethers license telomeric DSBs for a broad kinesin-and NPC-dependent DNA repair process. Nature communications *6*.

Churikov, D., Charifi, F., Eckert-Boulet, N., Silva, S., Simon, M.-N., Lisby, M., and Géli, V. (2016). SUMO-Dependent Relocalization of Eroded Telomeres to Nuclear Pore Complexes Controls Telomere Recombination. Cell reports *15*, 1242-1253.

Cremer, T., Cremer, C., Baumann, H., Luedtke, E., Sperling, K., Teuber, V., and Zorn, C. (1982). Rabl's model of the interphase chromosome arrangement tested in Chinise hamster cells by premature chromosome condensation and laser-UV-microbeam experiments. Human genetics *60*, 46-56.

Dimitrova, N., Chen, Y.C.M., Spector, D.L., and de Lange, T. (2008). 53BP1 promotes non-homologous end joining of telomeres by increasing chromatin mobility. Nature *456*, 524-U551.

Dion, V., and Gasser, S.M. (2013). Chromatin movement in the maintenance of genome stability. Cell *152*, 1355-1364.

Dion, V., Kalck, V., Horigome, C., Towbin, B.D., and Gasser, S.M. (2012). Increased mobility of double-strand breaks requires Mec1, Rad9 and the homologous recombination machinery. Nat Cell Biol *14*, 502-509.

Dion, V., Kalck, V., Seeber, A., Schleker, T., and Gasser, S.M. (2013). Cohesin and the nucleolus constrain the mobility of spontaneous repair foci. EMBO reports *14*, 984-991.

Duan, Z., Andronescu, M., Schutz, K., McIlwain, S., Kim, Y.J., Lee, C., Shendure, J., Fields, S., Blau, C.A., and Noble, W.S. (2010). A three-dimensional model of the yeast genome. Nature *465*, 363-367.

Falbo, K.B., Alabert, C., Katou, Y., Wu, S., Han, J., Wehr, T., Xiao, J., He, X., Zhang, Z., and Shi, Y. (2009). Involvement of a chromatin remodeling complex in damage tolerance during DNA replication. Nature structural & molecular biology *16*, 1167-1172.

Ferreira, H.C., Luke, B., Schober, H., Kalck, V., Lingner, J., and Gasser, S.M. (2011). The PIAS homologue Siz2 regulates perinuclear telomere position and telomerase activity in budding yeast. Nat Cell Biol *13*, 867-874.

Gartenberg, M.R., Neumann, F.R., Laroche, T., Blaszczyk, M., and Gasser, S.M. (2004). Sir-mediated repression can occur independently of chromosomal and subnuclear contexts. Cell *119*, 955-967.

Gerhold, C.B., Hauer, M.H., and Gasser, S.M. (2015). INO80-C and SWR-C: guardians of the genome. J Mol Biol *427*, 637-651.

Goodarzi, A.A., Noon, A.T., Deckbar, D., Ziv, Y., Shiloh, Y., Lobrich, M., and Jeggo, P.A. (2008). ATM signaling facilitates repair of DNA double-strand breaks associated with heterochromatin. Mol Cell *31*, 167-177.

Hajjoul, H., Mathon, J., Ranchon, H., Goiffon, I., Mozziconacci, J., Albert, B., Carrivain, P., Victor, J.-M., Gadal, O., and Bystricky, K. (2013). High-throughput chromatin motion tracking in living yeast reveals the flexibility of the fiber throughout the genome. Genome research *23*, 1829-1838.

Hakim, O., Resch, W., Yamane, A., Klein, I., Kieffer-Kwon, K.R., Jankovic, M., Oliveira, T., Bothmer, A., Voss, T.C., Ansarah-Sobrinho, C.*, et al.* (2012). DNA damage defines sites of recurrent chromosomal translocations in B lymphocytes. Nature *484*, 69-74.

Harding, S.M., Boiarsky, J.A., and Greenberg, R.A. (2015). ATM Dependent Silencing Links Nucleolar Chromatin Reorganization to DNA Damage Recognition. Cell reports *13*, 251-259.

Hauer, M., Seeber, A., Singh, V., Thierry, R., Ragna, S., Amitai, A., Kryzhanovska, M., Eglinger, J., Holcman, D., Owen-Hughes, T., and Gasser, S.M. (2017). Histone Degradation in Response to DNA Damage Enhances Chromatin Dynamics and Recombination Rates. NSMB *24,* 99-107.

Hediger, F., Neumann, F.R., Van Houwe, G., Dubrana, K., and Gasser, S.M. (2002). Live imaging of telomeres: yKu and Sir proteins define redundant telomere-anchoring pathways in yeast. Current biology *12*, 2076-2089.

Heun, P., Laroche, T., Shimada, K., Furrer, P., and Gasser, S.M. (2001). Chromosome dynamics in the yeast interphase nucleus. Science *294*, 2181-2186.

Heyer, W.D., Ehmsen, K.T., and Liu, J. (2010). Regulation of homologous recombination in eukaryotes. Annu Rev Genet *44*, 113-139.

Horigome, C., Bustard, D.E., Marcomini, I., Delgoshaie, N., Tsai-Pflugfelder, M., Cobb, J.A., and Gasser, S.M. (2016). PolySUMOylation by Siz2 and Mms21 triggers relocation of DNA breaks to nuclear pores through the Slx5/Slx8 STUbL. Genes Dev *30*, 931-945.

Horigome, C., Oma, Y., Konishi, T., Schmid, R., Marcomini, I., Hauer, M.H., Dion, V., Harata, M., and Gasser, S.M. (2014). SWR1 and INO80 chromatin remodelers contribute to DNA double-strand break perinuclear anchorage site choice. Mol Cell *55*, 626-639.

Janssen, A., Breuer, G.A., Brinkman, E.K., van der Meulen, A.I., Borden, S.V., van Steensel, B., Bindra, R.S., LaRocque, J.R., and Karpen, G.H. (2016). A single double-strand break system reveals repair dynamics and mechanisms in heterochromatin and euchromatin. Genes & Development *30*, 1645-1657.

Jin, Q.W., Fuchs, J., and Loidl, J. (2000). Centromere clustering is a major determinant of yeast interphase nuclear organization. Journal of cell science *113*, 1903-1912.

Kalocsay, M., Hiller, N.J., and Jentsch, S. (2009). Chromosome-wide Rad51 spreading and SUMO-H2A. Z-dependent chromosome fixation in response to a persistent DNA double-strand break. Molecular cell *33*, 335-343.

Kapoor, P., Chen, M., Winkler, D.D., Luger, K., and Shen, X. (2013). Evidence for monomeric actin function in INO80 chromatin remodeling. Nat Struct Mol Biol *20*, 426-432.

Kruhlak, M.J., Celeste, A., Dellaire, G., Fernandez-Capetillo, O., Müller, W.G., McNally, J.G., Bazett-Jones, D.P., and Nussenzweig, A. (2006). Changes in chromatin structure and mobility in living cells at sites of DNA double-strand breaks. The Journal of cell biology *172*, 823-834.

Laporte, D., Courtout, F., Salin, B., Ceschin, J., and Sagot, I. (2013). An array of nuclear microtubules reorganizes the budding yeast nucleus during quiescence. J Cell Biol *203*, 585-594.

Lee, C.-S., Wang, R.W., Chang, H.-H., Capurso, D., Segal, M.R., and Haber, J.E. (2016). Chromosome position determines the success of double-strand break repair. Proceedings of the National Academy of Sciences *113*, E146-E154.

Lemaitre, C., Grabarz, A., Tsouroula, K., Andronov, L., Furst, A., Pankotai, T., Heyer, V., Rogier, M., Attwood, K.M., Kessler, P*., et al.* (2014). Nuclear position dictates DNA repair pathway choice. Genes Dev *28*, 2450-2463.

Levi, V., Ruan, Q., Plutz, M., Belmont, A.S., and Gratton, E. (2005). Chromatin dynamics in interphase cells revealed by tracking in a two-photon excitation microscope. Biophysical journal *89*, 4275-4285.

Liu, J., Vidi, P.-A., Lelièvre, S.A., and Irudayaraj, J.M. (2015). Nanoscale histone localization in live cells reveals reduced chromatin mobility in response to DNA damage. J Cell Sci *128*, 599-604.

Lomax, M., Folkes, L., and O'Neill, P. (2013). Biological consequences of radiation-induced DNA damage: relevance to radiotherapy. Clinical oncology *25*, 578-585.

Lottersberger, F., Karssemeijer, R.A., Dimitrova, N., and de Lange, T. (2015). 53BP1 and the LINC Complex Promote Microtubule-Dependent DSB Mobility and DNA Repair. Cell *163*, 880-893.

Ma, H., Naseri, A., Reyes-Gutierrez, P., Wolfe, S.A., Zhang, S., and Pederson, T. (2015). Multicolor CRISPR labeling of chromosomal loci in human cells. Proceedings of the National Academy of Sciences *112*, 3002-3007.

Manders, E.M., Kimura, H., and Cook, P.R. (1999). Direct imaging of DNA in living cells reveals the dynamics of chromosome formation. The Journal of cell biology *144*, 813-822.

Marcomini, I., and Gasser, S.M. (2015). Nuclear organization in DNA end processing: Telomeres vs double-strand breaks. DNA repair *32*, 134-140.

Marshall, W.F., Straight, A., Marko, J.F., Swedlow, J., Dernburg, A., Belmont, A., Murray, A.W., Agard, D.A., and Sedat, J.W. (1997). Interphase chromosomes undergo constrained diffusional motion in living cells. Curr Biol *7*, 930-939.

Mine-Hattab, J., and Rothstein, R. (2012). Increased chromosome mobility facilitates homology search during recombination. Nat Cell Biol *14*, 510-517.

Miné-Hattab, J., and Rothstein, R. (2012). Increased chromosome mobility facilitates homology search during recombination. Nature cell biology *14*, 510-517.

Molenaar, C., Wiesmeijer, K., Verwoerd, N.P., Khazen, S., Eils, R., Tanke, H.J., and Dirks, R.W. (2003). Visualizing telomere dynamics in living mammalian cells using PNA probes. The EMBO journal *22*, 6631-6641.

Mullen, J.R., and Brill, S.J. (2008). Activation of the Slx5-Slx8 ubiquitin ligase by poly-small ubiquitin-like modifier conjugates. J Biol Chem *283*, 19912-19921.

Nagai, S., Dubrana, K., Tsai-Pflugfelder, M., Davidson, M.B., Roberts, T.M., Brown, G.W., Varela, E., Hediger, F., Gasser, S.M., and Krogan, N.J. (2008). Functional targeting of DNA damage to a nuclear pore-associated SUMO-dependent ubiquitin ligase. Science *322*, 597-602.

Neumann, F.R., Dion, V., Gehlen, L.R., Tsai-Pflugfelder, M., Schmid, R., Taddei, A., and Gasser, S.M. (2012). Targeted INO80 enhances subnuclear chromatin movement and ectopic homologous recombination. Genes Dev *26*, 369-383.

Nino, C., Guet, D., Gay, A., Brutus, S., Jourquin, F., Mendiratta, S., Salamero, J., Geli, V., Dargemont, C. (2016). Posttranslational marks control architectural and functional plasticity of the nuclear pore complex basket. J Cell Biol *212,* 167-180.

Noon, A.T., Shibata, A., Rief, N., Lobrich, M., Stewart, G.S., Jeggo, P.A., and Goodarzi, A.A. (2010). 53BP1-dependent robust localized KAP-1 phosphorylation is essential for heterochromatic DNA double-strand break repair. Nat Cell Biol *12*, 177-184.

Oza, P., Jaspersen, S.L., Miele, A., Dekker, J., and Peterson, C.L. (2009). Mechanisms that regulate localization of a DNA double-strand break to the nuclear periphery. Genes Dev *23*, 912-927.

Papamichos-Chronakis, M., Krebs, J.E., and Peterson, C.L. (2006). Interplay between Ino80 and Swr1 chromatin remodeling enzymes regulates cell cycle checkpoint adaptationin response to DNA damage. Genes & Development *20*, 2437-2449.

Papamichos-Chronakis, M., Watanabe, S., Rando, O.J., and Peterson, C.L. (2011). Global regulation of H2A. Z localization by the INO80 chromatin-remodeling enzyme is essential for genome integrity. Cell *144*, 200-213.

Pliss, A., Malyavantham, K.S., Bhattacharya, S., and Berezney, R. (2013). Chromatin dynamics in living cells: identification of oscillatory motion. Journal of cellular physiology *228*, 609-616.

Povirk, L.F. (1996). DNA damage and mutagenesis by radiomimetic DNA-cleaving agents: bleomycin, neocarzinostatin and other enediynes. Mutation research. *355*, 71–89.

Rocha, P.P., Micsinai, M., Kim, J.R., Hewitt, S.L., Souza, P.P., Trimarchi, T., Strino, F., Parisi, F., Kluger, Y., and Skok, J.A. (2012). Close proximity to Igh is a contributing factor to AID-mediated translocations. Mol Cell *47*, 873-885.

Roukos, V., Voss, T.C., Schmidt, C.K., Lee, S., Wangsa, D., and Misteli, T. (2013). Spatial dynamics of chromosome translocations in living cells. Science *341*, 660-664.

Ryu, T., Spatola, B., Delabaere, L., Bowlin, K., Hopp, H., Kunitake, R., Karpen, G.H., and Chiolo, I. (2015). Heterochromatic breaks move to the nuclear periphery to continue recombinational repair. Nat Cell Biol *17*, 1401-1411.

Saad, H., Gallardo, F., Dalvai, M., Tanguy-le-Gac, N., Lane, D., and Bystricky, K. (2014). DNA dynamics during early double-strand break processing revealed by non-intrusive imaging of living cells. PLoS genetics *10*, e1004187.

Sarangi, P., and Zhao, X. (2015). SUMO-mediated regulation of DNA damage repair and responses. Trends Biochem Sci *40*, 233-242.

Scherthan, H. (2001). A bouquet makes ends meet. Nature reviews Molecular cell biology *2*, 621-627.

Seeber, A., Dion, V., and Gasser, S.M. (2013a). Checkpoint kinases and the INO80 nucleosome remodeling complex enhance global chromatin mobility in response to DNA damage. Genes & development *27*, 1999-2008.

Seeber, A., Dion, V., and Gasser, S.M. (2013b). Checkpoint kinases and the INO80 nucleosome remodeling complex enhance global chromatin mobility in response to DNA damage. Genes & development *27*, 1999-2008.

Shen, X., Mizuguchi, G., Hamiche, A., and Wu, C. (2000). A chromatin remodelling complex involved in transcription and DNA processing. Nature *406*, 541-544.

Shimada, K., Oma, Y., Schleker, T., Kugou, K., Ohta, K., Harata, M., and Gasser, S.M. (2008). Ino80 chromatin remodeling complex promotes recovery of stalled replication forks. Current Biology *18*, 566-575.

Spichal, M., Brion, A., Herbert, S., Cournac, A., Marbouty, M., Zimmer, C., Koszul, R., and Fabre, E. (2016). Evidence for a dual role of actin in regulating chromosome organization and dynamics in yeast. J Cell Sci *129*, 681-692.

Strecker, J., Gupta, G.D., Zhang, W., Bashkurov, M., Landry, M.-C., Pelletier, L., and Durocher, D. (2016). DNA damage signalling targets the kinetochore to promote chromatin mobility. Nature cell biology *18*, 281-290.

Su, X.A., Dion, V., Gasser, S.M., and Freudenreich, C.H. (2015). Regulation of recombination at yeast nuclear pores controls repair and triplet repeat stability. Genes Dev *29*, 1006-1017.

Sun, Z., Hsiao, J., Fay, D.S., and Stern, D.F. (1998). Rad53 FHA domain associated with phosphorylated Rad9 in the DNA damage checkpoint. Science *281*, 272-274.

Swartz, R.K., Rodriguez, E.C., and King, M.C. (2014). A role for nuclear envelope-bridging complexes in homology-directed repair. Mol Biol Cell *25*, 2461-2471.

Taddei, A., Hediger, F., Neumann, F.R., Bauer, C., and Gasser, S.M. (2004). Separation of silencing from perinuclear anchoring functions in yeast Ku80, Sir4 and Esc1 proteins. The EMBO Journal *23*, 1301-1312.

Taddei, A., and Gasser, S.M. (2012). Structure and function in the budding yeast nucleus. Genetics **192**, 107-129.

Thakar, R., and Csink, A.K. (2005). Changing chromatin dynamics and nuclear organization during differentiation in Drosophila larval tissue. J Cell Sci *118*, 951-960.

Therizols, P., Fairhead, C., Cabal, G.G., Genovesio, A., Olivo-Marin, J.C., Dujon, B., and Fabre, E. (2006). Telomere tethering at the nuclear periphery is essential for efficient DNA double strand break repair in subtelomeric region. J Cell Biol *172*, 189-199.

Torres-Rosell, J., Sunjevaric, I., De Piccoli, G., Sacher, M., Eckert-Boulet, N., Reid, R., Jentsch, S., Rothstein, R., Aragon, L., and Lisby, M. (2007). The Smc5-Smc6 complex and SUMO modification of Rad52 regulates recombinational repair at the ribosomal gene locus. Nat Cell Biol *9*, 923-931.

Tsouroula, K., Furst, A., Rogier, M., Heyer, V., Maglott-Roth, A., Ferrand, A., Reina-San-Martin, B., and Soutoglou, E. (2016). Temporal and Spatial Uncoupling of DNA Double Strand Break Repair Pathways within Mammalian Heterochromatin. Mol Cell *63*, 293-305.

van Attikum, H., Fritsch, O., and Gasser, S.M. (2007). Distinct roles for SWR1 and INO80 chromatin remodeling complexes at chromosomal double-strand breaks. Embo J *26*, 4113-4125.

van Sluis, M., and McStay, B. (2015). A localized nucleolar DNA damage response facilitates recruitment of the homology-directed repair machinery independent of cell cycle stage. Genes Dev *29*, 1151-1163.

Vazquez, J., Belmont, A.S., and Sedat, J.W. (2001). Multiple regimes of constrained chromosome motion are regulated in the interphase Drosophila nucleus. Current Biology *11*, 1227-1239.

Verdaasdonk, J.S., Vasquez, P.A., Barry, R.M., Barry, T., Goodwin, S., Forest, M.G., and Bloom, K. (2013a). Centromere tethering confines chromosome domains. Mol Cell *52*, 819-831.

Verdaasdonk, J.S., Vasquez, P.A., Barry, R.M., Barry, T., Goodwin, S., Forest, M.G., and Bloom, K. (2013b). Centromere tethering confines chromosome domains. Molecular cell *52*, 819-831.

Walter, J., Schermelleh, L., Cremer, M., Tashiro, S., and Cremer, T. (2003). Chromosome order in HeLa cells changes during mitosis and early G1, but is stably maintained during subsequent interphase stages. The Journal of cell biology *160*, 685-697.

Wang, R., Mozziconacci, J., Bancaud, A., and Gadal, O. (2015). Principles of chromatin organization in yeast: relevance of polymer models to describe nuclear organization and dynamics. Current opinion in cell biology *34*, 54-60.

Weber, S.C., Spakowitz, A.J., and Theriot, J.A. (2012). Nonthermal ATP-dependent fluctuations contribute to the in vivo motion of chromosomal loci. Proceedings of the National Academy of Sciences *109*, 7338-7343.

Wiesmeijer, K., Krouwels, I.M., Tanke, H.J., and Dirks, R.W. (2008). Chromatin movement visualized with photoactivable GFP-labeled histone H4. Differentiation *76*, 83-90.
Zhang, Y., McCord, R.P., Ho, Y.-J., Lajoie, B.R., Hildebrand, D.G., Simon, A.C., Becker, M.S., Alt, F.W., and Dekker, J. (2012). Spatial organization of the mouse genome and its role in recurrent chromosomal translocations. Cell *148*, 908-921.
Zidovska, A., Weitz, D.A., and Mitchison, T.J. (2013). Micron-scale coherence in interphase chromatin dynamics. Proceedings of the National Academy of Sciences *110*, 15555-15560.
Zink, D., Cremer, T., Saffrich, R., Fischer, R., Trendelenburg, M.F., Ansorge, W., and Stelzer, E.H. (1998). Structure and dynamics of human interphase chromosome territories in vivo. Human genetics *102*, 241-251.

Available online at www.sciencedirect.com

ScienceDirect

Current Opinion in Genetics & Development

Chromatin organization and dynamics in double-strand break repair

Andrew Seeber[1,2] and Susan M Gasser[1,2]

Chromatin is organized and segmented into a landscape of domains that serve multiple purposes. In contrast to transcription, which is controlled by defined sequences at distinct sites, DNA damage can occur anywhere. Repair accordingly must occur everywhere, yet it is inevitably affected by its chromatin environment. In this review, we summarize recent work investigating how changes in chromatin organization facilitate and/or guide DNA double-strand break repair. In addition, we examine new live cell studies on the dynamics of chromatin and the mechanisms that regulate its movement.

Addresses
[1] Friedrich Miescher Institute for Biomedical Research, Maulbeerstrasse 66, CH-4058 Basel, Switzerland
[2] University of Basel, Faculty of Natural Sciences, Klingelbergstrasse 50, CH-4056 Basel, Switzerland

Corresponding author: Gasser, Susan M (susan.gasser@fmi.ch)

Current Opinion in Genetics & Development 2017, **43**:9–16

This review comes from a themed issue on **Genome architecture and expression**

Edited by **Bart Deplancke** and **Charles Sagerstrom**

http://dx.doi.org/10.1016/j.gde.2016.10.005

Chromatin on the move

It has been almost 20 years since John Sedat's laboratory showed that chromatin is mobile using live cell imaging of GFP-tagged loci [1]. At the time this stood in contradiction to datasets from fluorescence recovery after photobleaching (FRAP) [2], and from imaging UV-induced damage within interphase chromosomes [3], which both argued that chromatin position is static. On the other hand, it was obvious that chromatin must be able to move to enable biological events like meiotic homolog pairing, homologous recombination (HR), chromatin condensation and gene activation through long-range enhancer–promoter interactions. The Sedat laboratory resolved this issue by showing that chromatin does indeed move randomly in both *S. cerevisiae* and *D. melanogaster* within constrained volumes, which are on a scale below the resolution of FRAP. This seminal work additionally showed that size does not matter (i.e. a yeast CEN-containing plasmid, which clusters with other centromeres, was no more mobile than a whole chromosome), and that microtubules constrain chromatin movement, at least in yeast [1]. Recent articles now address many of the questions raised by these early studies, the foremost being, 'Does chromatin movement have a biological function and how is it regulated?'

DNA damage induces chromatin mobility

Double-strand break (DSB) repair by homologous recombination with an ectopic or non-sister donor sequence requires a physical search for the homologous template. This has long been considered one of the central mechanisms that would require chromatin movement. Investigations into this hypothesis led to the discovery that endonuclease-induced DSBs in budding yeast move more than uncleaved loci [4,5]. This is regulated by the DNA damage checkpoint kinase, Mec1-Ddc2 (or ATR-ATRIP in mammals). Intriguingly, an induced DSB affects more than just the surrounding chromatin: the Rothstein group was first to report an apparent increase in chromatin mobility for genomic loci far from the break site [5]. Later work confirmed this generalized increase in chromatin mobility [6], which, although less pronounced than DSB movement, was ATP-dependent, sensitive to the number of DSBs induced, and dependent on checkpoint kinase activation, including the downstream kinase, Rad53 [6]. This link was recently shown relevant for mammalian cells, as ionizing radiation (IR)-induced damage triggers increased locus movement, in a manner dependent on the repair factor 53BP1 and the ATM kinase, 53BP1 [7••].

A recent study by the Durocher group proposed an essential budding yeast kinetochore protein, Cep3, as the relevant target of the checkpoint kinase that controls chromatin movement, both locally and globally [8••]. The authors suggested that a point mutation, *cep3-S575A*, which compromises a Rad53 phosphoacceptor site in Cep3, completely abrogated the enhanced movement that accompanies a targeted DSB, as well as the global chromatin movement response [4]. The authors hypothesized that damage-induced phosphorylation of Cep3 triggers a release of centromeres from the interphase spindle that links them to a membrane spanning spindle pole body (SPB). This release is proposed to generally enhance chromatin movement. They did not detect any change in distance between the SPB and yeast centromeres

following cut induction, but they did score, using a relative mean square displacement assay, an enhanced relative mobility between the SPB and a centromere, which was dependent on the phosphoacceptor site in Cep3. Linking this to damage, they showed that cells treated with Zeocin, a radiomimetic drug previously used to induce global chromatin mobility [6], led to the declustering of kinetochores near the SPB. However, the *cep3-S575A* mutation had no effect on repair by homologous recombination. Unfortunately, the study failed to monitor the efficiency of DSB induction in the *cep3-S575A* mutant, leaving alternative interpretations possible for the lack of increased mobility (i.e. less efficient cleavage or impaired checkpoint activation, would similarly fail to increase mobility). Given that there are significant differences in basal level mobility between G1- and S-phase chromatin [9], cell cycle effects must also be carefully controlled for. Nonetheless, this study raises the question whether enhanced movement is really necessary for homology search.

Clearly, not all damage in yeast triggers enhanced movement [9], nor does all damage activate the Mec1-Ddc2/Rad53 checkpoint. Spontaneous damage or DNA-protein adducts that are repaired by exchange with a sister chromatid, or by precise non-homologous end-joining, appear not to trigger changes in chromatin mobility [9], nor do they shift to the nuclear periphery for repair [10]. Too much movement at a DSB was, moreover, deleterious, particularly in repetitive regions in mammalian cells where extensive movement correlated with translocations and deletion events [11]. Intriguingly, the rate of misrepair was strongly affected by the position of the observed locus in the nucleus in both yeast and mammals [12,13,14,15]. This initiated an examination of how nuclear compartments, which often stem from local chromatin structure [16], influence pathways of repair. It was observed that breaks in heterochromatin behaved differently from breaks in euchromatic zones particularly in mammals and flies [17,18,19,20••]. Thus, chromatin movement can provide a means to escape an unfavorable chromatin compartment or access a set of factors that were unavailable in the lesion's original context. Telomeres are an excellent case in point: they are highly repetitive, yet when unprotected, they act like a single-ended DSB [21]. This raised the question whether the mobility of telomeres is controlled and whether their movement affects telomere maintenance during end uncapping.

A study by the Greenberg laboratory investigated what happens to telomere movement during repair or maintenance by recombination-dependent pathway called alternative lengthening of telomeres, or ALT. They found that DSB signaling at an ALT telomere causes long range movement and clustering of chromosome ends, which is thought to favor homology-driven maintenance of telomere repeats [22••]. The alternative, i.e. activating a DSB response at a telomere, can be dangerous. Previous work from the de Lange laboratory had shown that uncapped telomeres (which lack the protective telomere binding protein TRF2) show increased movement, which correlated with enhanced rates of telomere end-to-end fusion. Both movement and end-to-end fusion depended on 53BP1 [23]. Recent work from this group investigated telomere damage further and showed that SUN-domain-containing proteins, which bridge from the nucleoskeleton to the cytoskeleton in the LINC complex (see below), promote increased dynamics of dysfunctional uncapped telomeres, enhancing the rate of untimely end-to-end fusions by NHEJ [7••]. The authors also showed a role for cytoskeleton-bound kinesins in telomere fusions and the repair of internal breaks, suggesting that an active, kinesin-driven movement of the nucleus or elements in the nuclear envelope affect DSB repair. This is reminiscent of a study in yeast which showed that kinesins can promote movement of subtelomeric DSBs [24•]. In summary, increased movement of a telomere can be useful for ALT-like telomere recombination, yet is deleterious in conditions that generate uncapped or dysfunctional ends, for it leads to telomere-telomere fusions. The next section will discuss new articles that look at the effect of chromatin structure, actin and microtubules on chromatin motion.

Chromatin structure, actin and microtubules affect chromatin mobility

The budding yeast genome is organized in a Rabl configuration where the centromeres are attached to the SPB and the telomeres are attached to the periphery [25,26]. Forced detachment of the centromere from the SPB increases chromatin movement [8••,27], as does telomere release from the periphery [28] or the loss of anchorage by ablation of SIR-mediated silencing [8••,29]. However, a chromosome that is detached from its perinuclear anchor is still more confined than a free-floating plasmid ring [8••,30], suggesting that there are additional constraints on chromosomes. One constraint stems from the inherent structure of the chromatin fiber, while the second is the tethering of sister chromatids through cohesin [9]. Consistently, there is accumulating evidence that supports the notion that altered chromatin fiber organization, that is, nucleosome eviction or remodeling, increases movement. Notably, the targeting of a functional nucleosome remodeler, INO80, to a chromosomal locus [30,31••] or the INO80-dependent eviction of nucleosomes at the *PHO5* locus in the absence of phosphate, both increase the movement of an appropriately tagged locus.

Interestingly, DNA damage also changes chromatin structure. A new study in yeast shows that Zeocin-induced damage leads to the degradation of ~30% of the four core histones within a short time [32]. This induces chromatin decompaction, and increases both the flexibility of the chromatin fiber and its mobility, in manner dependent on the DNA damage checkpoint and INO80. Furthermore,

either the artificial reduction of histone proteins H3/H4, or the use of a mutant that naturally has lower levels of histones (*nhp6Δ*), triggers decompaction and increased chromatin movement [32]. This result contradicts an earlier report where the shutdown of histone H3 production was proposed to decrease locus mobility [27]. The difference may reflect that fact nucleosome depletion and enhanced chromatin flexibility requires the loss of both H3 and H4. Furthermore, it was shown that H4 (but not H3) shutdown leads to a declustering of kinetochores [33], an event that may also contribute to the increased chromatin movement observed by Hauer *et al*. The influence of inherent chromatin structure on mobility is consistent with the finding that histone modifications correlate with the propensity for translocations in mammalian cells [16]. A very recent paper [34••] also documents a similar unfolding and expansion of chromatin in response to UV-induced damage in mammalian cells, although in this case the effect stem largely from histone mobilization and replacement, rather than degradation [34••].

Besides inherent changes in chromatin structure, accumulating evidence also implicates microtubules and the actin cytoskeleton as drivers of nuclear and/or chromatin movement. In Sedat's study, the depolymerisation of microtubules by Nocodazole was shown to increase chromatin movement in budding yeast [1]. This suggested that microtubules mediated constraint, although it was not clear whether this effect arose from direct interactions between chromatin and microtubules or indirect contact through the nuclear envelope. The LINC complex can connect cytoskeletal filaments [35] through Klarsicht, ANC-1, and Syne homology proteins (KASH also known as Nesprin) on the outer nuclear membrane, to their ligands, the SUN-domain proteins, which span the perinuclear space and protrude into the nucleoplasm. Some SUN-domain proteins interact with chromatin, specifically telomeres [35], and resected DSBs in budding yeast [36,37,38••,39•].

Work from the de Lange laboratory showed for the first time that, in contrast to yeast, the treatment of mammalian cells with dysfunctional telomeres with the microtubule poisons Taxol or Nocodazole actually decreased their movement in a reversible manner [7••]. Importantly, the authors showed that removal of SUN1/2, an essential bridge from the cytoskeleton to the inner nuclear membrane, decreased movement, similar to the microtubule poisons. The reduced movement, due either to depolymerization of the cytoskeleton or loss of this cytoskeleton-to-nucleus link, also reduced the rate of telomere-telomere fusions. Importantly, Taxol treatment also seemed to decrease the movement of IR-induced foci, and not only dysfunctional telomeres. This implies that the forces applied to the chromosomes through the microtubules can be transduced to internal chromatin. Whereas a mechanism through which cytoskeleton-associated kinesins drive SUN-domain-bound telomeres into a clustered, bouquet arrangement is well-characterised in meiotic prophase, this checkpoint kinase-induced event in mitosis does not entail bouquet formation and is most likely differently regulated.

In budding yeast, as mentioned above, the depolymerization of microtubules had the opposite effect on chromatin movement: mobility increased after Nocodazole treatment, consistent with data showing that the deletion of *CSM4*, a putative LINC protein, similarly led to increased subtelomere movement [31••]. This may be due to the loss of microtubules that tether interphase centromeres to the SPB [40], or the disruption of a network of intranuclear microtubules [41], something quite unique to budding yeast. It is noteworthy that in meiosis, bouquet formation is also driven by cytoplasmic actin filaments in budding yeast, rather than microtubules, suggesting that in this species actin filaments replace microtubules for some aspects of nuclear movement.

Nonetheless, in all eukaryotes, actin forms a cytoplasmic network of filaments and it is found, at least in its monomeric 'G' form, inside the nucleus in a range of protein complexes, the most prominent of which are chromatin remodelers [42]. Work from the Fabre laboratory has recently shown that both cytoplasmic and nuclear actin contribute to chromatin motion, through a mechanism that appears to be independent of the putative budding yeast LINC [31••]. Treatment of yeast cells with the actin filament poison Latrunculin A (LatA) was sufficient to decrease the movement of a locus. While this suggests that cytoplasmic actin filaments might move the yeast nucleus, much like microtubules do in *S. pombe* and mice, it is also possible that LatA affects movement indirectly by altering nuclear G-actin. Intriguingly, the targeting of the actin-containing remodeler INO80, which increases the movement of a locus under normal conditions [30], fails to do so when cells are treated with LatA. This result suggests that LatA may bind nuclear actin and disrupt the function of the INO80 complex [42]. This mechanism might affect other actin-containing chromatin modulating complexes, as well, such as NuA4 (TIP60), Swi/Snf, or SWR1 (SRCAP). Since INO80 is necessary for the eviction and degradation of histones in response to DNA damage [32], LatA could interfere with INO80-mediated changes in the nucleosome packing, thereby abrogating the damage-associated increase in chromatin mobility.

The effects of subnuclear chromatin organization on DNA repair

There is no doubt that chromatin movement exists, and is enhanced by some types of DNA damage; but the question persists, why? It has been proposed that chromatin compartments affect the efficiency of certain repair pathways,

or, at the very least, favor/disfavor certain damage processing steps. This last section will examine how subnuclear compartments, like the nuclear envelope and the nucleolus, affect DSB repair.

The nuclear pore complex (NPC) contains > 30 different nuclear pore proteins (nucleoporins), creating a complex with eight-fold symmetry that spans the nuclear envelope and gates traffic between the cytoplasm and the nucleus [43]. In budding yeast, the NPC is a binding site for persistent DSBs [10,36,37] including breaks that occur at collapsed forks [10,44•] or in subtelomeric regions [45]. In addition, embedded in the inner nuclear membrane is the Sad1-Unc-84-related (SUN) domain protein Mps3, which acts as an alternative binding site for resected DSBs in S phase [37]. This same phenomenon occurs in fission yeast [39•]. DSB break recruitment to either the NPC or to Mps3/Sad1 has different requirements than recruitment to pores [37,38••], and appears to favor distinct features of repair.

DSB recruitment to the NPC is independent of cell-cycle stage, does not require the recombinase Rad51 nor the INO80 chromatin remodeling complex, and is independent of extensive resection (at least in G1 phase cells; [8••,30,38••]). In contrast, Mps3-DSB interaction occurs in S/G2 phase, requires resection, the ssDNA binding factor, Rad51, and INO80. Importantly, the SWR1 chromatin remodeler and its deposition of Htz1 (H2A.Z) at breaks, contributes to the peripheral relocation to either site of anchorage. The outcomes of relocation are deduced from the phenotypes that arise from ablation of one or the other anchors. Based on such an analysis, it would seem that that Mps3 helps suppress illegitimate recombination, perhaps by anchoring or protecting the resected ends until an appropriate template appears [39•]. The NPC complex, on the other hand, appears to promote alternative repair pathways, such as template switching at a broken replication fork, or BIR at single-ended breaks [46••]. The Durocher group finds that Cohibin (a complex consisting of Lsr4-Csm1 and kinesin-14) is necessary for a subtelomeric DSB and the NPC to interact [24•]. Lsr4-Csm1 is involved in rDNA stabilization through perinuclear anchoring [47], but it has not been implicated the recovery from persistent DSBs or collapsed replication forks.

Earlier work had shown that the Slx5/Slx8 SUMO-targeted ubiquitin ligase (STUbL) not only interacts with nuclear pores, but is also recruited to persistent DSBs, both in yeast [10,46••] and in *Drosophila* [20••]. It was therefore examined whether Slx5/Slx8 (Degringolade or Dgrn in flies; RNF4 in mammals) was required for the relocation of DSBs to the periphery or if it acts only after recruitment. Considering that STUbLs contain small ubiquitin-like modifier (SUMO) interacting motifs (SIMs) [48], and that many repair proteins are SUMOylated [49], this role of Slx5/Slx8 immediately raised the question whether or not SUMO ligases were involved in DSB relocation. Four new papers [20••,44•,46••,50•] have examined the roles of Slx5/8 and SUMO ligases at DSBs, eroded telomeres and collapsed replication forks in budding yeast and *Drosophila*, producing a coherent picture of the role of SUMO and its ligands in break relocation (Figure 1).

In *S. cerevisiae*, there are four SUMO E3 ligases, Siz1, Siz2 (mammalian PIAS homologs), Mms21 (which binds the Smc5/6 complex), and the meiosis specific Cst9. SUMOylation events mediated by both Siz2 and Mms21 are implicated in DSB relocation to the nuclear periphery [46••]. Interestingly, the relocation has different requirements during the cell cycle. PolySUMOylation by Siz2 or Mms21 in G1 phase recruits Slx5/Slx8 to the break which then allows relocation. An artificial poly-SUMO construct was sufficient to shift an undamaged site to NPCs, in a Slx5-dependent manner, while a similarly targeted mono-SUMO construct was not able to [46••]. In S phase, on the other hand, monoSUMOylation was sufficient to shift resected damage to the SUN-domain protein, Mps3, in a manner independent of Slx5/Slx8 [46••]. This is reminiscent of an earlier report that a targeted yKu80-SUMO fusion shifts internal loci and/or telomeres to Mps3 [51]. Thus, there are cell cycle-, and SUMO chain-dependent pathways that direct damage to one or another perinuclear processing sites, obviously with different repair outcomes.

At pores both imprecise non-homologous end joining (NHEJ) and break-induced replication (BIR) are compromised by mutations in Nup84 (the binding site for Slx5) and by loss of the STUbL itself [46••]. This observation is bolstered by the fact that the tethering of a subtelomeric DSB to the NPC resulted in hyperactive BIR, as well as moderately increasing imprecise NHEJ [24•]. In an analogous study using *Drosophila* cells, Chiolo and colleagues first showed that DSB relocate away from heterochromatin to enable recombination to occur [19]. This required both SUMOylation by SUMO E3 ligases, and the *Drosophila* Slx5/Slx8 equivalent Dgrn [20••]. However, in flies not only the NPC, but also the Mps3 homologues, Koi and Spag4, appear to recruit the STUbL (Dgrn) and its RENi cofactor (Rad60) to the periphery. These work in concert with the Smc5/6-SUMO ligase complex (Mms21), triggering the recruitment of heterochromatic DSBs to pores [20••]. It is proposed that in yeast, the proximity of the proteasome to the NPC justifies relocation, while in flies it is unclear whether further processing of the break or protein degradation of a STUbL target, is necessary for repair.

Importantly, it is not only artificially induced breaks that find their way to the nuclear periphery: two important recent studies show that both eroded telomeres and replication damage associated with expanded triplet

Figure 1

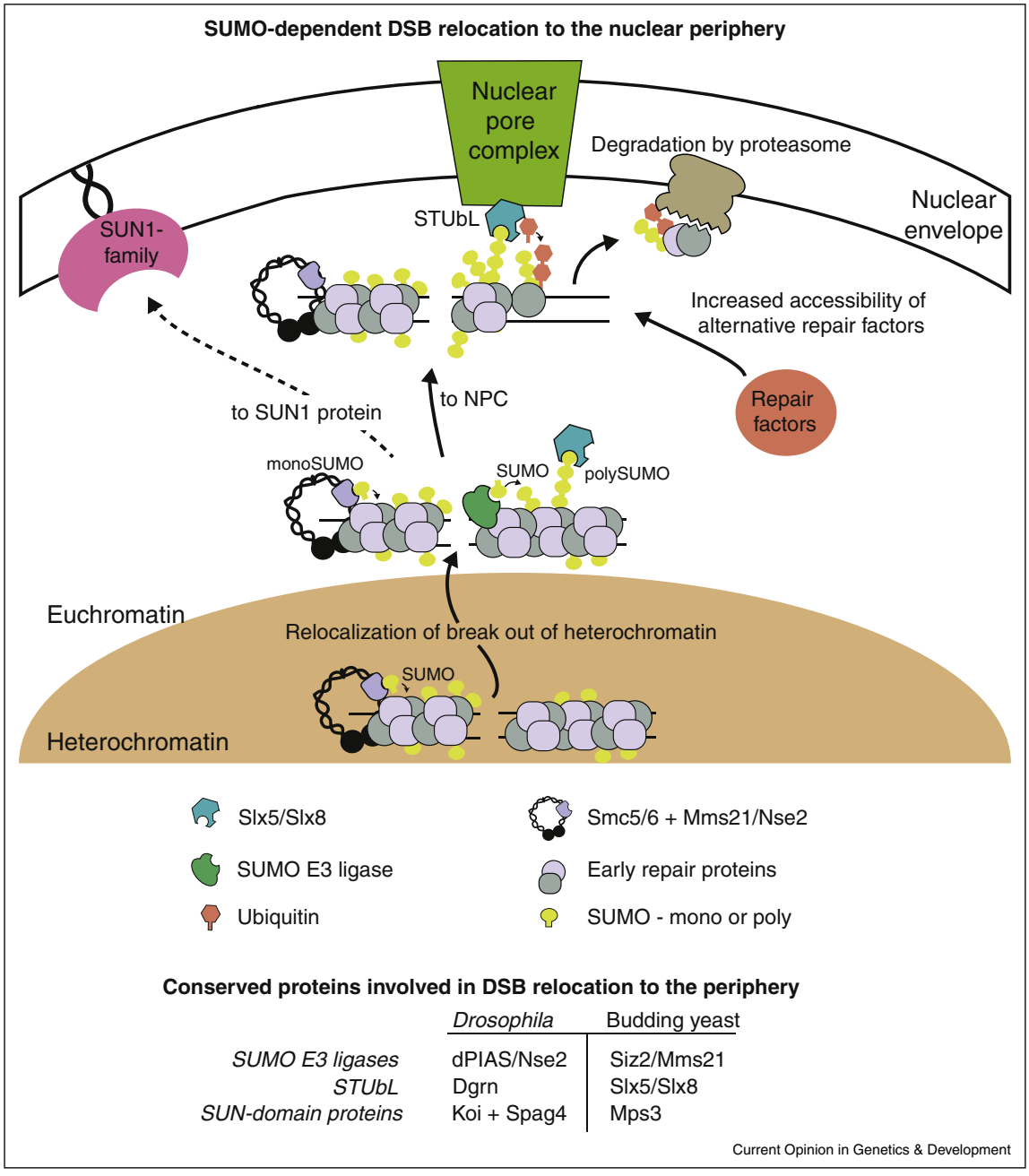

Relocation of a DSB to the nuclear periphery in yeast and Drosophila.
DSBs can occur in heterochromatin or euchromatin. SMC5/SMC6 and its associated E3 ligase Mms21, mediate monoSUMOylation which allows DSBs to shift out of heterochromatin and enable repair. Recruitment of additional SUMO E3 ligases (e.g. Siz2/PIAS homologues) to the DSBs promotes polySUMOylation which facilitates STUbL dependent relocalization of the lesion to the NPC, where proteins are ubiquitylated and degraded by the proteasome. This is thought to allow alternative repair factors to bind the DSB, mediating BIR or imprecise NHEJ. MonoSUMOylated DSBs can also shift to SUN-domain proteins embedded in the nuclear envelope independent of STUbL interactions. This occurs particularly in S-phase cells where breaks are readily resected and bound by Rad51.

repeats, shift transiently to pores for processing and release [44•,50•]. The Lisby and Geli laboratories looked at telomeres in a telomerase-deficient yeast strain, and found that shortened telomeres are relocated to the NPC in a very similar SUMO-dependent pathway. The shift, and Slx5/Slx8 itself were both required to enable recombination-mediated elongation of the short terminal TG-tract, generating type II survivors in which TG

repeats are maintained by recombination (ALT in mammals) [50•]. Finally, an analysis of expanded CAG triplet repeats, which serve as hot spots for replication fork collapse in S phase, showed that these also relocate transiently in late S phase to the NPC, again in a Slx5/8-dependent manner [44•]. Unlike flies, the Mps3 protein was not involved. Failure to recruit the CAG repeat to the periphery led to both expansions and deletions of the CAG tract [44•]. Taken together, these studies collectively define a conserved pathway through which damage is shifted from its normal subnuclear context to the nuclear pore, in a manner dependent on SUMOylation. Failure to move appears to be detrimental to recovery (Figure 1), and the shift of damage to a favored site of repair in all cases depends on SUMOylation.

Nonetheless, many open questions remain. It remains unclear whether one or many proteins are SUMOylated, and which are degraded following STUbL-mediated ubiquitination. Epistasis mapping studies place the proteasome in the same pathway as Nup84 and Slx5/Slx8 for the recovery from difficult-to-repair breaks [10], yet it is unclear why targeted protein degradation must occur near the pore. What is gained by clustering or targeting damage through SUMOylation and SIM-containing proteins? An alternative hypothesis proposes that the nuclear periphery serves to bring free ends or common sequences together, so that the homology search for difficult-to-repair breaks becomes a 2-, rather than 3-dimensional search.

Besides the nuclear envelope, the nucleolus which harbors the rDNA repeats, is a major organizing element of the nucleus. Previous studies in *S. cerevisiae* found that DSBs induced in the rDNA context, also shift away from the nucleolus to allow break processing and Rad51 loading, and repair by homologous recombination [52]. The shift out of the nucleolus depended on the SMC5/6-Mms21 SUMO ligase, and in this case it appeared that Rad52 was the essential target of SUMOylation. Failure to modify Rad52 and shift away from the nucleolus, resulted in aberrant recombination events [52]. Two new studies have addressed this issue in mammalian cells [53•,54] with results remarkably similar to those from budding yeast. Persistent nucleolar DSBs were observed to shift from the core of the nucleolus to its periphery [53•,54]. While Haring *et al.*, found that most DSBs in the rDNA were efficiently repaired by NHEJ, both studies showed that persistent DSBs led to an ATM-dependent inhibition of Pol1 transcription, and nucleolar rearrangements. The relocation of the rDNA break from the interior of the nucleolus to its periphery allowed HR factors to be recruited [53•]. This supports the notion that certain chromatin compartments are refractory to repair, apparently in all eukaryotic organisms. Domains that are rich in repeats appear to require special measures and tailor-made pathways for DSB repair. The parallels in the roles of chromatin movement, SUMOylation, and nuclear pores in DSB repair from yeast to humans, as highlighted above and in many other recent studies [55,56,57,58], secures this as a highly promising field of research.

Acknowledgments

The Gasser laboratory is supported by the Novartis Research Foundation, the Swiss National Science Foundation, and the Human Frontiers Science Program.

References and recommended reading

Papers of particular interest, published within the period of review, have been highlighted as:

- • of special interest
- •• of outstanding interest

1. Marshall W, Straight A, Marko J, Swedlow J, Dernburg A, Belmont A, Murray A, Agard D, Sedat J: **Interphase chromosomes undergo constrained diffusional motion in living cells**. *Curr Biol* 1997, **7**:930-939.

2. Abney JR, Cutler B, Fillbach ML, Axelrod D, Scalettar BA: **Chromatin dynamics in interphase nuclei and its implications for nuclear structure**. *J Cell Biol* 1997, **137**:1459-1468.

3. Cremer T, Cremer C, Baumann H, Luedtke E, Sperling K, Teuber V, Zorn C: **Rabl's model of the interphase chromosome arrangement tested in chinise hamster cells by premature chromosome condensation and laser-uv-microbeam experiments**. *Hum Genet* 1982, **60**:46-56.

4. Dion V, Kalck V, Horigome C, Towbin BD, Gasser SM: **Increased mobility of double-strand breaks requires mec1, rad9 and the homologous recombination machinery**. *Nat Cell Biol* 2012, **14**:502-509.

5. Miné-Hattab J, Rothstein R: **Increased chromosome mobility facilitates homology search during recombination**. *Nat Cell Biol* 2012, **14**:510-517.

6. Seeber A, Dion V, Gasser SM: **Checkpoint kinases and the ino80 nucleosome remodeling complex enhance global chromatin mobility in response to DNA damage**. *Genes Develop* 2013, **27**:1999-2008.

7. •• Lottersberger F, Karssemeijer RA, Dimitrova N, de Lange T: **53bp1 and the linc complex promote microtubule-dependent dsb mobility and DNA repair**. *Cell* 2015, **163**:880-893.
This study shows that in mammalian cells distribution of microtubules or severing the link between the nucleus and the cytoplasm decreases movement of uncapped telomeres, which in turn decreases the rate of telomere fusions.

8. •• Strecker J, Gupta GD, Zhang W, Bashkurov M, Landry M-C, Pelletier L, Durocher D: **DNA damage signalling targets the kinetochore to promote chromatin mobility**. *Nat Cell Biol* 2016, **18**:281-290.
This study identifies a phosphorylation mutant of the essential kinetochore protein Cep3 that is a target of the DNA damage response checkpoint. This mutant fails to increase movement at the site of DSBs but yet has no recombination defects.

9. Dion V, Kalck V, Seeber A, Schleker T, Gasser SM: **Cohesin and the nucleolus constrain the mobility of spontaneous repair foci**. *EMBO Reports* 2013, **14**:984-991.

10. Nagai S, Dubrana K, Tsai-Pflugfelder M, Davidson MB, Roberts TM, Brown GW, Varela E, Hediger F, Gasser SM, Krogan NJ: **Functional targeting of DNA damage to a nuclear pore-associated sumo-dependent ubiquitin ligase**. *Science* 2008, **322**:597-602.

11. Roukos V, Voss TC, Schmidt CK, Lee S, Wangsa D, Misteli T: **Spatial dynamics of chromosome translocations in living cells**. *Science* 2013, **341**:660-664.

12. Lee C-S, Wang RW, Chang H-H, Capurso D, Segal MR, Haber JE: **Chromosome position determines the success of double-strand break repair**. *Proc Natl Acad Sci* 2016, **113**:E146-E154.

13. Hakim O, Resch W, Yamane A, Klein I, Kieffer-Kwon KR, Jankovic M, Oliveira T, Bothmer A, Voss TC, Ansarah-Sobrinho C, Mathe E *et al.*: **DNA damage defines sites of recurrent chromosomal translocations in b lymphocytes**. *Nature* 2012, **484**:69-74.

14. Rocha PP, Micsinai M, Kim JR, Hewitt SL, Souza PP, Trimarchi T, Strino F, Parisi F, Kluger Y, Skok JA: **Close proximity to igh is a contributing factor to aid-mediated translocations**. *Mol Cell* 2012, **47**:873-885.

15. Zhang Y, McCord RP, Ho Y-J, Lajoie BR, Hildebrand DG, Simon AC, Becker MS, Alt FW, Dekker J: **Spatial organization of the mouse genome and its role in recurrent chromosomal translocations**. *Cell* 2012, **148**:908-921.

16. Burman B, Zhang ZZ, Pegoraro G, Lieb JD, Misteli T: **Histone modifications predispose genome regions to breakage and translocation**. *Genes Develop* 2015, **29**:1393-1402.

17. Tsouroula K, Furst A, Rogier M, Heyer V, Maglott-Roth A, Ferrand A, Reina-San-Martin B, Soutoglou E: **Temporal and spatial uncoupling of DNA double strand break repair pathways within mammalian heterochromatin**. *Mol Cell* 2016, **63**:293-305.

18. Lemaitre C, Grabarz A, Tsouroula K, Andronov L, Furst A, Pankotai T, Heyer V, Rogier M, Attwood KM, Kessler P, Dellaire G *et al.*: **Nuclear position dictates DNA repair pathway choice**. *Genes Develop* 2014, **28**:2450-2463.

19. Chiolo I, Minoda A, Colmenares SU, Polyzos A, Costes SV, Karpen GH: **Double-strand breaks in heterochromatin move outside of a dynamic hp1a domain to complete recombinational repair**. *Cell* 2011, **144**:732-744.

20. •• Ryu T, Spatola B, Delabaere L, Bowlin K, Hopp H, Kunitake R, Karpen GH, Chiolo I: **Heterochromatic breaks move to the nuclear periphery to continue recombinational repair**. *Nat Cell Biol* 2015, **17**:1401-1411.

This study shows that in *Drosophila* cells DSBs in heterochromatin move to the nuclear periphery in a manner dependent on SUMO E3 ligases and STUbL/RENi.

21. Marcomini I, Gasser SM: **Nuclear organization in DNA end processing: Telomeres vs double-strand breaks**. *DNA Rep* 2015, **32**:134-140.

22. •• Cho NW, Dilley RL, Lampson MA, Greenberg RA: **Interchromosomal homology searches drive directional alt telomere movement and synapsis**. *Cell* 2014, **159**:108-121.

This study shows that ALT telomeres show directed motion. This facilitates the search for other telomeres enable repair. This requires Rad51 and Hop2-Mnd1.

23. Dimitrova N, Chen Y-CM, Spector DL, de Lange T: **53bp1 promotes non-homologous end joining of telomeres by increasing chromatin mobility**. *Nature* 2008, **456**:524-528.

24. • Chung DK, Chan JN, Strecker J, Zhang W, Ebrahimi-Ardebili S, Lu T, Abraham KJ, Durocher D, Mekhail K: **Perinuclear tethers license telomeric dsbs for a broad kinesin-and npc-dependent DNA repair process**. *Nat Commun* 2015:6.

Here the authors provide evidence that kinesins and the NPC are important to repair DSBs by BIR.

25. Bystricky K, Laroche T, van Houwe G, Blaszczyk M, Gasser SM: **Chromosome looping in yeast: telomere pairing and coordinated movement reflect anchoring efficiency and territorial organization**. *J Cell Biol* 2005, **168**:375-387.

26. Duan Z, Andronescu M, Schutz K, McIlwain S, Kim YJ, Lee C, Shendure J, Fields S, Blau CA, Noble WS: **A three-dimensional model of the yeast genome**. *Nature* 2010, **465**:363-367.

27. Verdaasdonk JS, Vasquez PA, Barry RM, Barry T, Goodwin S, Forest MG, Bloom K: **Centromere tethering confines chromosome domains**. *Mol Cell* 2013, **52**:819-831.

28. Hediger F, Neumann FR, Van Houwe G, Dubrana K, Gasser SM: **Live imaging of telomeres: Yku and sir proteins define redundant telomere-anchoring pathways in yeast**. *Curr Biol* 2002, **12**:2076-2089.

29. Gartenberg MR, Neumann FR, Laroche T, Blaszczyk M, Gasser SM: **Sir-mediated repression can occur independently of chromosomal and subnuclear contexts**. *Cell* 2004, **119**:955-967.

30. Neumann FR, Dion V, Gehlen LR, Tsai-Pflugfelder M, Schmid R, Taddei A, Gasser SM: **Targeted ino80 enhances subnuclear chromatin movement and ectopic homologous recombination**. *Genes Develop* 2012, **26**:369-383.

31. •• Spichal M, Brion A, Herbert S, Cournac A, Marbouty M, Zimmer C, Koszul R, Fabre E: **Evidence for a dual role of actin in regulating chromosome organization and dynamics in yeast**. *J Cell Sci* 2016, **129**:681-692.

Here the authors show that depolymerization of actin filaments reduces chromatin movement. They also show provide some evidence to support a role for not only cytoplasmic actin but also nuclear actin in chromatin movement that likely works through the INO80 complex.

32. Hauer M, Seeber A, Singh V, Thierry R, Amitai A, Eglinger J, Holcman D, Owen-Hughes T, Gasser S: **Histone degradation in response to DNA damage triggers general chromatin decompaction**. *NSMB* in press.

33. Bouck DC, Bloom K: **Pericentric chromatin is an elastic component of the mitotic spindle**. *Curr Biol* 2007, **17**:741-748.

34. •• Adam S, Dabin J, Chevallier O, Leroy O, Baldeyron C, Corpet A, Lomonte P, Renaud O, Almouzni G, Polo SE: **Real-time tracking of parental histones reveals their contribution to chromatin integrity following DNA damage**. *Mol Cell* 2016.

This study shows that following UV irradiation in mammalian cells, chromatin expands due to a mobilization of histones, as tracked by following histone H3. They show that parental histones rapidly redistribute leading to both chromatin opening and histone mobilization.

35. Chang W, Worman HJ, Gundersen GG: **Accessorizing and anchoring the linc complex for multifunctionality**. *J Cell Biol* 2015, **208**:11-22.

36. Kalocsay M, Hiller NJ, Jentsch S: **Chromosome-wide rad51 spreading and sumo-h2a. Z-dependent chromosome fixation in response to a persistent DNA double-strand break**. *Mol Cell* 2009, **33**:335-343.

37. Oza P, Jaspersen SL, Miele A, Dekker J, Peterson CL: **Mechanisms that regulate localization of a DNA double-strand break to the nuclear periphery**. *Genes Develop* 2009, **23**:912-927.

38. •• Horigome C, Oma Y, Konishi T, Schmid R, Marcomini I, Hauer MH, Dion V, Harata M, Gasser SM: **Swr1 and ino80 chromatin remodelers contribute to DNA double-strand break perinuclear anchorage site choice**. *Mol Cell* 2014, **55**:626-639.

This study shows the importance of Htz1 (H2A.Z) and the Swr1 chromatin remodeling complex in relocation of DSBs to the nuclear periphery. Differential binding sites at the nuclear periphery and their respective requirements are identified here.

39. • Swartz RK, Rodriguez EC, King MC: **A role for nuclear envelope-bridging complexes in homology-directed repair**. *Mol Biol Cell* 2014, **25**:2461-2471.

Here the authors use *S. pombe* as a model for studying the position and movement of DSBs. They prove an involvement of SUN domain proteins and their bridge to the cytoskeleton in tethering DSBs to the nuclear envelope.

40. Jin QW, Fuchs J, Loidl J: **Centromere clustering is a major determinant of yeast interphase nuclear organization**. *J Cell Sci* 2000, **113**:1903-1912.

41. Laporte D, Courtout F, Salin B, Ceschin J, Sagot I: **An array of nuclear microtubules reorganizes the budding yeast nucleus during quiescence**. *J Cell Biol* 2013, **203**:585-594.

42. Kapoor P, Chen M, Winkler DD, Luger K, Shen X: **Evidence for monomeric actin function in ino80 chromatin remodeling**. *Nat Struct Mol Biol* 2013, **20**:426-432.

43. Bukata L, Parker SL, D'Angelo MA: **Nuclear pore complexes in the maintenance of genome integrity**. *Curr Opin Cell Biol* 2013, **25**:378-386.

44. • Su XA, Dion V, Gasser SM, Freudenreich CH: **Regulation of recombination at yeast nuclear pores controls repair and triplet repeat stability**. *Genes Develop* 2015, **29**:1006-1017.

This study uses triplet repeat sequences as a form of replication induced damage. The authors show that repeat instability is enhanced if relocation to the NPC cannot occur for instance in a Slx5/Slx8 mutant.

45. Therizols P, Fairhead C, Cabal GG, Genovesio A, Olivo-Marin JC, Dujon B, Fabre E: **Telomere tethering at the nuclear periphery is essential for efficient DNA double strand break repair in subtelomeric region**. *J Cell Biol* 2006, **172**:189-199.

46. •• Horigome C, Bustard DE, Marcomini I, Delgoshaie N, Tsai-Pflugfelder M, Cobb JA, Gasser SM: **Polysumoylation by siz2 and mms21 triggers relocation of DNA breaks to nuclear pores through the slx5/slx8 stubl**. *Genes Develop* 2016, **30**:931-945.

This study details how PolySUMOylation along with its ligand STUbL Slx5/8 controls relocation of DSBs to the NPC and shows that it increases BIR and imprecise NHEJ. Additionally, the authors show the relative contributions of mono- versus poly-SUMOylation in DSB relocation to the periphery.

47. Chan JN, Poon BP, Salvi J, Olsen JB, Emili A, Mekhail K: **Perinuclear cohibin complexes maintain replicative life span via roles at distinct silent chromatin domains**. *Develop Cell* 2011, **20**:867-879.

48. Mullen JR, Brill SJ: **Activation of the slx5-slx8 ubiquitin ligase by poly-small ubiquitin-like modifier conjugates**. *J Biol Chem* 2008, **283**:19912-19921.

49. Sarangi P, Zhao X: **Sumo-mediated regulation of DNA damage repair and responses**. *Trends Biochem Sci* 2015, **40**:233-242.

50. • Churikov D, Charifi F, Eckert-Boulet N, Silva S, Simon M-N, Lisby M, Géli V: **Sumo-dependent relocalization of eroded telomeres to nuclear pore complexes controls telomere recombination**. *Cell Reports* 2016, **15**:1242-1253.

This study shows that eroded telomeres are recruited to the NPC in a SUMO and Slx5/Slx8 dependent manner. This favors type II recombination of telomeres which is analogous to ALT in mammals.

51. Ferreira HC, Luke B, Schober H, Kalck V, Lingner J, Gasser SM: **The pias homologue siz2 regulates perinuclear telomere position and telomerase activity in budding yeast**. *Nat Cell Biol* 2011, **13**:867-874.

52. Torres-Rosell J, Sunjevaric I, De Piccoli G, Sacher M, Eckert-Boulet N, Reid R, Jentsch S, Rothstein R, Aragon L, Lisby M: **The smc5-smc6 complex and sumo modification of rad52 regulates recombinational repair at the ribosomal gene locus**. *Nat Cell Biol* 2007, **9**:923-931.

53. • van Sluis M, McStay B: **A localized nucleolar DNA damage response facilitates recruitment of the homology-directed repair machinery independent of cell cycle stage**. *Genes Develop* 2015, **29**:1151-1163.

This study shows that DSBs that are induced in the rDNA move from the nucleolar interior to the periphery. This allows repair factors that would otherwise be excluded from the nucleoli to access the DSB. Interestingly, the authors show that rDNA DSBs are repaired by HR even in G1.

54. Harding SM, Boiarsky JA, Greenberg RA: **Atm dependent silencing links nucleolar chromatin reorganization to DNA damage recognition**. *Cell Rep* 2015, **13**:251-259.

55. Janssen A, Breuer GA, Brinkman EK, van der Meulen AI, Borden SV, van Steensel B, Bindra RS, LaRocque JR, Karpen GH: **A single double-strand break system reveals repair dynamics and mechanisms in heterochromatin and euchromatin**. *Genes Develop* 2016, **30**:1645-1657.

56. Noon AT, Shibata A, Rief N, Lobrich M, Stewart GS, Jeggo PA, Goodarzi AA: **53bp1-dependent robust localized kap-1 phosphorylation is essential for heterochromatic DNA double-strand break repair**. *Nat Cell Biol* 2010, **12**:177-184.

57. Goodarzi AA, Noon AT, Deckbar D, Ziv Y, Shiloh Y, Lobrich M, Jeggo PA: **Atm signaling facilitates repair of DNA double-strand breaks associated with heterochromatin**. *Mol cell* 2008, **31**:167-177.

58. Lomax M, Folkes L, O'Neill P: **Biological consequences of radiation-induced DNA damage: relevance to radiotherapy**. *Clin Oncol* 2013, **25**:578-585.

CHAPTER 2: NUCLEOSOME REMODELERS IN DOUBLE-STRAND BREAK REPAIR

This chapter consists of two parts based on the following publications:

Seeber, A., Hauer, M., and Gasser, S.M. (2013). Nucleosome remodelers in double-strand break repair. Current Opinion in Genetics & Development 23, 174-184.

Author contributions: A.S., M.H. and S.M.G. wrote the manuscript. A.S. and M.H. designed the figures.

Seeber, A., Dion, V., and Gasser, S.M. (2014). Remodelers move chromatin in response to DNA damage. Cell Cycle 13, 877-878.

Author contributions: A.S. and S.M.G. wrote the manuscript. A.S. designed the figure.

Summary

ATP-dependent nucleosome remodelers use ATP hydrolysis to shift, evict, and exchange histone dimers or octamers and have well-established roles in transcription. Earlier work has suggested a role for nucleosome remodelers such as INO80 in double-strand break (DSB) repair. The first publication within this chapter is a review that begins with an update on recent studies that explore how remodelers are recruited to DSBs. We examine their impact on various steps of repair, focusing on resection and the formation of the Rad51-ssDNA nucleofilament. Finally, we will explore new studies that implicate remodelers in the physical movement of chromatin in response to damage. The second part of this chapter is an editorial covering the publication in Chapter 4 and discusses the role of chromatin mobility in DSB repair. Specifically, repair of DSBs occurs either by homologous recombination (HR) or non-homologous end-joining (NHEJ). A fundamental distinction between the two pathways lies in the requirement for a homologous sequence that templates the repair: this is needed for HR but not for NHEJ. In S-phase cells, the template most often used is the sister chromatid. If the break occurs in G1 phase (particularly in haploid cells, like yeast), or if both sisters are damaged, the homologue or an ectopic sequence with appropriate homology must be used as a template. For that to occur, the damage and the intact homologous sequence must first physically meet, through a process called homology search. This occurs after resection and binding of Rad51, Rad52 and requires Rad51. Various nucleosome remodelers are implicated in each step including RSC, INO80 (resection) and Fun3 (long range resection). In mammalian nuclei homology search involves the scanning of thousands of millions of base pairs for an exact copy of the damaged site. Not surprisingly, ectopic recombination (i.e. recombination with a homologue or a non-sister chromosome) is relatively rare in complex genomes, while it occurs quite efficiently in yeast.

Available online at www.sciencedirect.com

SciVerse ScienceDirect

Current Opinion in Genetics & Development

Nucleosome remodelers in double-strand break repair

Andrew Seeber[1,2,4], Michael Hauer[1,3,4] and Susan M Gasser[1,2]

ATP-dependent nucleosome remodelers use ATP hydrolysis to shift, evict and exchange histone dimers or octamers and have well-established roles in transcription. Earlier work has suggested a role for nucleosome remodelers such as INO80 in double-strand break (DSB) repair. This review will begin with an update on recent studies that explore how remodelers are recruited to DSBs. We then examine their impact on various steps of repair, focusing on resection and the formation of the Rad51-ssDNA nucleofilament. Finally, we will explore new studies that implicate remodelers in the physical movement of chromatin in response to damage.

Addresses
[1] Friedrich Miescher Institute for Biomedical Research, Maulbeerstrasse 66, CH-4058 Basel, Switzerland
[2] University of Basel, Faculty of Natural Sciences, Klingelbergstrasse 50, CH-4056 Basel, Switzerland
[3] University of Tuebingen, Interfaculty Institute for Cell Biology, Department of Molecular Biology, Auf der Morgenstelle 15, D-72076 Tuebingen, Germany

Corresponding author: Gasser, Susan M (susan.gasser@fmi.ch)
[4] These authors contributed equally to this work.

Current Opinion in Genetics & Development 2013, **23**:174–184

This review comes from a themed issue on **Genome architecture and expression**

Edited by **Genevieve Almouzni** and **Frederick Alt**

For a complete overview see the Issue and the Editorial

Available online 23rd January 2013

0959-437X/$ – see front matter,

http://dx.doi.org/10.1016/j.gde.2012.12.008

Introduction

In eukaryotic cells, the genomic DNA is wrapped around histone proteins to form a compact nucleosomal fiber. This form of chromatin is bound and protected by a variety of factors, yet is nonetheless susceptible to environmentally induced damage. Once damaged, repair and checkpoint signaling machineries recruit chromatin modifying enzymes to render damaged DNA accessible to repair. This is mediated both by enzymes that modify histones and by ATP-dependent nucleosome remodelers that can shift, evict and exchange histone dimers or octamers, facilitating the different steps of the repair process. Histone modifications coordinate repair with other DNA-based functions, such as transcription and replication. Recent work also suggests that nucleosome remodelers enhance micromovement [1•] and possibly evict proteins that inhibit the repair process [2••]. Finally, the re-establishment of the initial chromatin structure requires histone chaperones and various modifying enzymes that deposit or remove acetyl-groups, methyl-groups and ubiquitin from histone tails [3]. It is likely that active nucleosome remodeling is required as well for proper recovery after repair.

All remodelers of the SWI2/SNF2 family contain related, large catalytic ATPase subunits. A new phylogenetic analysis has replaced the classical grouping (SWI/SNF, ISWI, CHD and INO80) of the various remodelers, splitting them into six major families, namely the Snf2-like, Swr1-like, SMARCAL1, Rad54-like, Rad5/16-like and ERCC6/SSO1653-like [4] (Table 1). SWI/SNF members of the Snf2-like family contain a bromodomain which binds acetylated histone tails. ISWI remodelers have HAND, SANT and SLIDE domains involved in DNA binding in the context of nucleosomes. The Snf2-like family also includes CHD remodelers, which contain a tandem chromodomain that mediates binding to methylated histones. INO80 complexes fall into the Swr1-like class, which has a characteristic insert in the middle of the ATPase domain, and contain a RuvB-like DNA helicase, Rvb1/2 in yeast or TIP49a,b in mammals. Most remodeling complexes harbor a number of additional subunits, among them actin and actin related proteins (Arps), some of which are shared, others unique to specific remodelers (Table 1) [5].

Previous work had shown that mutation or down-regulation of some remodeler subunits renders cells hypersensitive to DNA damage [6]. This phenotype, however, can stem from effects either on transcription, replication, or the repair pathway itself. To study the direct involvement of chromatin remodelers in double strand break (DSB) repair, chromatin immunoprecipitation (ChIP) and fluorescent imaging studies have monitored whether or not a given ATP-dependent nucleosome remodeler was recruited to a unique DSB or to a zone of laser-induced damage. These approaches have implicated many remodelers directly in steps of repair, and most frequently in repair by homologous recombination (HR), but more recently, also by non-homologous end joining (Table 2). Given the broader effect of remodelers on chromatin composition, we will hereafter refer to them as chromatin remodelers, rather than nucleosome remodelers. In this review, we provide an overview about the various roles that remodeling complexes play during DSB repair. Crucial to understand is how remodelers are initially recruited to DSBs, how they impact the various steps of repair and how they affect the formation of the Rad51-ssDNA nucleofilament. Recent studies also implicate chromatin remodelers in changing the physical movement of DNA in response to damage.

Table 1

Composition and classification of nucleosome remodelers in *S. cerevisiae* and Human.

Grouping			Organism					
Family	Subfamily & Composition		*S. cerevisiae*			Human		
Swr1 like	Ino80	Complex	**INO80**			**INO80**		
		ATPase	Ino80			hINO80		
		Orthologous subunits	Rvb1*, Rvb2*			TIP49A*, TIP49B*		
			Arp4*, Arp5*, Arp8, Act1			BAF53a*, ARP5, ARP8		
			Taf14					
			Ies2			hIES2		
			Ies6			hIES6		
		Unique	Ies1, Ies3-5, Nhp10			Amida, NFRKB, MCRS1, FLJ90652, FLJ20309		
	Swr1	Complex	**SWR1**			**SRCAP**	**TRRAP/Tip60**	
		ATPase	Swr1			SRCAP	p400	
		Orthologous subunits	Rvb1*, Rvb2*			Tip49a*, Tip49b*	Tip49a*, Tip49b*	
			Arp4*, Arp6, Act1			BAF53a*, Arp6	BAF53a*, Actin	
			Yaf9			GAS41*	GAS41*	
			Swc4/Eaf2			DMAP1*	DMAP1*	
			Swc2/Vps72			YL-1*	YL-1*	
			Bdf1				BRD8/TRCp120	
			H2AZ, H2B			H2AZ, H2B		
			Swc6/Vps71			Znf-HIT1		
		Unique	Swc3,5,7				Tip60, MRG15, MRGX, FLJ11730, MRGBP, EPC1,EPC-like, ING3	
	Etl1	Complex	**FUN30**			**SMARCAD1**		
		ATPase	Fun30			SMARCAD1		
		Subunits	Not identified			Not identified		
Snf2 like	Mi-2	Complex	**No homolog**			**NuRD**		
		ATPase				CHD3/Mi-2α CHD4/Mi-2β		
		Subunits				MBD2,MBD3, MTA1-3, HDAC1-2, RbAp46 or 48, p66α, p66β		
	Chd1	Complex	**CHD1**			**CHD1**		
		ATPase	Chd1			CHD1		
		Subunits	monomeric			monomermic		
	Alc1	**Complex**	**No homolog**			**ALC1**		
		ATPase				ALC1		
		Subunits				Not identified		
	Snf2	Complex	**SWI/SNF**	**RSC**		**BAF**	**PBAF**	
		ATPase	Swi2/Snf2	Sth1		BRG1/SMARCA4 or hBRM/SMARCA2	BRG1	
		Orthologous subunits				BAF250a/ARID1A or BAF250b/ARID1B or		
				Rsc1, Rsc2, Rsc4		BAF180*, BAF200/ARID2*	BAF180*, BAF200/ARID2*	
			Swi3	Rsc8		BAF155/SMARCC1* and/or BAF170/SMARCC2*	BAF155/SMARCC1* and/or BAF170/SMARCC2*	
			Swp73	Rsc6		BAF60a/SMARCD1*	BAF60a/SMARCD1*	
			Arp7*, Arp9*	Arp7*, Arp9*		BAF53a*	BAF53a*	
			Snf5	Sfh1		BAF47/hSNF5/SMARCB1*	BAF47/hSNF5/SMARCB1*	
						BAF57/SMARCE1*	BAF57/SMARCE1*	
						β-actin*	β-actin*	
		Unique	Swi1/Adr6, Swp82, Taf14, Snf6, Snf11	Rsc3, Rsc5, Rsc7, Rsc9, Rsc10, Rsc30, Htl1, Lbd7, Rtt102		BAF45a or BAF45d		
	Iswi	Complex	**ISW1a**	**ISW1b**	**ISW2**	**ACF**	**CHRAC**	**NURF**
		ATPase	Isw1*	Isw1*	Isw2	hSNF2H		hSNF2L
		Orthologous subunits			Itc1	WCRF180/ hACF1*	WCRF180/ hACF1*	BPTF
					Dpb4		hCHRAC17	RbAp46
					Dls1		hCHRAC15	RbAp48
		Unique	Ioc3	Ioc2, Ioc4				
Rad54 like	Rad54	Complex	**Rad54**			**Rad54**		
		ATPase	Rad54			Rad54		

*Subunits shared within different remodeling complexes of the same organism.

Recruitment of chromatin remodelers to a DSB

The INO80 nucleosome remodeler is recruited to DSBs in both yeast and man. In yeast, the INO80 complex is made up of 15 subunits including Ino80, Rvb1/2, Arp5/8, Arp4, Act1, Nhp10 and Ies3. Its recruitment to DSBs in yeast requires an interaction with phosphorylated H2A (γH2A); mutation of the phosphoacceptor site on yeast H2A reduced INO80 binding at an induced DSB [7]. The subunits implicated in this interaction are Nhp10 and Ies3

Table 2

A summary of [chromatin remodelers], the relevant subunit and key findings reported in this review

Family & Subunits					Remodeler subunit functions addressed in this review		
Grouping[4]		Name of Remodeling complex	Core Subunits [4,5]	Remodeler complex function/Remarks	Subunit (organism)	(Proposed) function of subunit during DNA damage repair	Ref.
Family	Sub family						
Swr1 like	Etl1	Fun30	non identified	In budding yeast, Fun30 promotes long range DNA end resection & regulates centromere function. In fission yeast, Fft3 acts as a protector of heterochromatic regions.	Fun30(*Sce*)	A novel remodeling enzyme with higher activity in histone dimer exchange than nucleosome repositioning. Promotes long range DNA end resection and checkpoint adaptation through removal of Rad9. Regulates the function and architecture of centromeric chromatin via nucleosome remodeling and blocking of transcription over centromeres.	[38] [2,42] [40]
		Fft3/Fun30	non identified		Fft3 (*Spo*)	Localizes at known insulator elements, protecting centromeres and subtelomeres from euchromatin spreading. Fft3 controls the identity of heterochromatic regions.	[41]
		SMARCAD1	non identified	Closest homolog to yeast Fun30 with roles in the maintenance of silent chromatin and novel functions in DNA end resection and repair	SMARCAD1(*Hsa*)	Role in DNA end resection, knockdowns result in homologous recombination and RPA foci formation defects.	[42]
	Ino80	INO80	15	INO80 has been studied for many years in yeast, plants and humans. It plays a role in many steps of DSB repair via homologous recombination: implications have been made in resection, nucleofilament formation and the dynamics of a DSB fiber.	Arp4 (*Sce*)	Arp4 is lost upon Arp8 deletion and it physically associates with γH2A, promoting INO80 recruitment to the site of a DSB.	[7,63]
					ARP5 (*Hsa*)	Mammalian ARP5 shuffles between the cytoplasm and the nucleus, promoting initial H2A.X phosphorylation and INO80 binding to γ H2A.X upon damage.	[11]
					Arp5 (*Ath*)	Arp5 is essential in plants to promote resistance to DNA damaging agents.	[12]
					ARP8 (*Hsa*)	Major role in recruiting INO80 to sites of damage, independent of H2A.X phosphorylation. Novel findings link ARP8 to RPA foci formation and ssDNA accumulation, implying a role in resection.	[10,35]
					Arp8 (*Sce*)	Stabilizes Arp4 and Actin in INO80. Increases the movement and the recombination rate of a locus when targeted onto chromatin. Promotes Rad51 recruitment to sites of damage in haploid cells.	[1,7,8,47,63]
					Nhp10 (*Sce*)	Required for Arp4 dependent interaction of INO80 with γH2A.	[7]
					Ies3 (*Sce*)	Promotes γH2A dependent recruitment of INO80 to DSBs (lost from the complex in *nhp10Δ*).	[7]
					Act1 (*Sce*)	Like Arp4, is lost upon deletion of Arp8.	[7,63]
	Swr1	Swr1	19	Among other roles, the yeast SWR1 remodeling complex deposits H2A.Z (Htz1 in yeast) at DSBs by catalyzing the replacement of H2A–H2B dimers with H2A.Z–H2B dimmers. This reaction occurs stepwise and in an unidirectional manner.			[13]
		TTRAP/Tip60	22		P400(*Hsa*)	The catalytic subunit P400 can exchange H2A.Z onto nucleosomes at DSBs. Incorporation of H2A.Z along with other modifications subsequently facilitates loading of brca1 complexes.	[17]
	Ino80, Swr1	INO80, SRCAP TTRAP/Tip60	15,13,22	TIP49a/b acts as a part of many human remodeling complexes with potential roles in DNA repair	TIP49a; TIP49b (*Hsa*)	The yeast homolog Rvb1/Rvb2 unwinds DNA at 3' ssDNA overhangs, implying a role in processing resected ends. Promotes RAD51 foci accumulation at DSBs by relaxing chromatin and making it accessible for the repair machinery.	[37,45,46]
Snf2 like	Mi-2	NuRD	12	The NuRD complex has a well established role in deacetylating chromatin, repressing transcription and regulating development *in vitro* as well as remodeling nucleosomes *in vitro*. Its function during DNA damage repair can vary with the composition of the complex (CHD3 or CHD4 containing).	CHD3(*Hsa*)	Acts as a heterochromatin factor and is released via ATM dependent KAP1 phosphorylation upon damage. Loss of CHD3 leads to chromatin relaxation and priming breaks for repair.	[31]
					CHD4(*Hsa*)	Is recruited to sites of DNA damage (PARylation dependent) where it promotes Ubiquitination of histones and thereby the recruitment of BRCA1 and RNF168. CHD4 has a function in G2/M checkpoint maintenance.	[26,64] [26]
	Alc1	ALC1/CHD1L	1	ALC1 was identified as a novel, CHD1-like (CHD1L) remodeler. Its recruitment to breaks is adenosine 5'-diphosphate (ADP)-ribose (PAR) dependent.	ALC1(*Hsa*)	ALC1 re-positions nucleosomes in-vitro. Interacts with NHEJ proteins, probably priming breaks for repair by NHEJ.	[28-30]
	Snf2	RSC	18	The yeast RSC complex is known to prime the DSB site for repair by mobilizing nucleosomes and loading Mre11. Novel results implicate RSC in DNA end resection, even though cells depleted for RSC are still proficient in SSA.			[2,34,65]
		SWI/SNF	11	Yeast SWI/SNF has broad roles in regulating transcription, mitotic exit and activation of weak replication origins. In yeast and humans, SWI/SNF remodeling complexes localize to DSBs and play distinct roles in repair events as well as regulating the damage response checkpoint.	BAF170(*Hsa*)	Mediates SWI/SNF recruitment to DSB sites after damage in an ATM/ATR phosphorylation dependent manner (enhanced by BRIT1/MCPH1).	[23]
					BRG1(*Hsa*)	Impacts the DNA damage checkpoint through interaction with p53 and the acetyl transferase CBP. Binds and propagates γH2A.X via its interaction with H3K14–Indication of a novel, cooperative activation loop with H3 HAT Gcn5 upon DNA damage.	[21,66,67]
					hBRM(*Hsa*)	In contrast to BAF170, this alternative SWI/SNF catalytic subunit plays no role in regulating the DNA damage response.	[66]
Rad54 like	Rad54	Rad54	1	Rad54 is not a classic SNF2 remodeling enzyme but able to slide and remodel nucleosomes *in vitro*. Rad54 plays a major role in middle to late steps during homologous recombination and was recently implicated in regulating the dynamics of a DNA DSB fiber.	Rad54 yeast & human	Facilitates strand invasion and slides nucleosomes *in vitro*. Stabilizes the Rad51 ssDNA nucleofilament. Promotes homologous recombination.	[50,51,59]
					Rad54(*Sce*)	Essential for the increased movement and nuclear search volume of an Isce1 induced DSB.	[50]
					Rad54(*Hsa*)	Recruitment to DSBs is independent of ATP usage but dissociation from chromatin and the relocalization of damage foci to the nuclear periphery requires ATP hydrolysis.	[47]

(a subunit which is lost upon deletion of *NHP10*) [8], and Arp4, with Arp4 having been shown to physically associate with γH2A [9]. The story appears to be different in mammals, where INO80 is recruited to laser-induced sites of damage independently of γH2A.X, but in a manner sensitive to loss of Arp8 [10]. shRNA against other INO80 subunits did not have an effect on recruitment, but it should be noted that the INO80 subunits studied were only reduced to levels ranging from 20% to 40% of wild-type levels. It remains possible that other INO80 subunits play a role in the recruitment to DSBs, but that the shRNA knock-down was not sufficient to impair binding at the break. Another mammalian study shows that Arp5 interacts with γH2A.X and promotes its initial phosphorylation [11]. In the same vein, a new report using *Arabidopsis* shows that Arp5 is required to prevent sensitivity to DNA damaging agents, highlighting the importance of this subunit [12]. Collectively these findings argue that in higher eukaryotes the initial recruitment of INO80 is mediated by Arp8, while Arp5 subsequently interacts with and facilitates the spread of γH2AX.

Also recruited by interaction with γH2A.X is the INO80-related yeast remodeler SWR1 (p400 or SRCAP in man). The SWR1 remodeler has been shown to deposit H2A.Z (Htz1 in yeast), a conserved variant of H2A, by catalyzing the replacement of H2A–H2B dimers with H2A.Z–H2B dimers in a stepwise and unidirectional manner [13]. H2A.Z is found enriched near the TSS of genes, as well as in some heterochromatic regions. A number of papers implicate H2A.Z or Htz1 in repair pathways [14] and, not surprisingly, mutants in Swr1 or Swr1 complex components are sensitive to DNA damaging agents [15,16]. In mammalian cells, H2A.Z can be exchanged onto nucleosomes at DSBs by TRRAP/TIP60's p400 ATPase domain, the recruitment of which depends on γH2A.X, as in yeast [36]. At the DSB, H2A.Z exchange is required for the acetylation of histone H4 by TIP60, and for histone ubiquitination by RNF8. H2A.Z then ultimately leads to enhanced Ku recruitment, favoring repair by NHEJ, whereas its absence, leads to extensive resection and inaccurate repair [17•].

The SWI/SNF remodeling complex has also been shown to be recruited to DSBs [18], although the mechanism of recruitment is unknown, particularly in yeast. In one report, a null mutant of the yeast SWI/SNF subunit Snf2 did not result in enhanced sensitivity to UV or ionizing radiation (IR) [19], while in other yeast backgrounds *SNF2* or *SNF5* deletions rendered cells susceptible to either HU or bleomycin treatment [18]. Indeed, in this paper, SWI/SNF2 subunits could be detected at DSBs by ChIP one hour after damage induction [18]. What SWI/SNF achieves at DSBs in yeast is unclear, as it appears to be dispensable for HR if the donor sequence is euchromatic. On the other hand, SWI/SNF was shown to be necessary for the eviction of heterochromatin factors (Sir3) from donor sequences *in vitro* [20]. This occurs during mating type switching, which requires invasion of the resected DNA strands from *MAT* into silent chromatin at *HM* loci.

In humans, the SWI/SNF complex contains one of two catalytic subunits, BRG1 or BRM, along with many BRG1/BRM associated factors (BAFs) [5]. A recent study proposed a positive feedback loop, in which the histone acetyl transferase (HAT) GCN5 binds to γH2A.X upon damage, acetylating adjacent H3 molecules, which would be recognized by the bromodomain of BRG1. SWI/SNF is then thought to facilitate access to the damage extending phosphorylation of H2A.X and thus more acetylation [21•]. However, other HATs, such as Tip60, p300 and CBP have been shown to work with SWI/SNF at DSBs in NHEJ [22].

In a more general way, DSBs undergo a series of dependent events which involve ubiquitination, acetylation of H3K14 and finally the acetylation-dependent recruitment and active remodeling by the SWI/SNF subunit BRG1.

In one study, SWI/SNF was shown to be recruited to neocarzinostatin induced DSBs in a manner promoted by BRIT1/MCPH1, an early DNA damage response protein. This entailed the ATR/ATM dependent phosphorylation of the SWI/SNF subunit, BAF170. Chromatin cannot relax as monitored by MNase sensitivity assays upon BRIT/MCPH1 depletion, which coincides with defects in both HR and NHEJ in mammalian cells [23].

In conclusion, human SWI/SNF has previously unappreciated roles in promoting the early spread of γH2A.X and histone acetylation at DSBs. Whether NHEJ and HR pathways have a differential dependence on SWI/SNF is not yet clear.

Repressive Snf2-like remodeling complexes of the Mi-2 and CHD class (such as CHD1 and NuRD complexes) are unique in the sense that their catalytic subunits contain a characteristic N-terminal tandem chromodomain, which directs them to methylated histones. This domain, at least for Chd1, regulates its ATPase motor dynamics [24•]. CHD1 and NuRD have clear roles in transcriptional regulation, histone dynamics and gene silencing [5], whereas their impact on DSB repair is only starting to be revealed.

In mammalian cells, shRNA knockdowns of NuRD subunits, CHD4 or MTA2, resulted in increased levels of spontaneous damage and persistent p53 activation [25•]. CHD4 also promotes ubiquitination of histones, which correlates with recruitment of BRCA1 and RNF168 and maintenance of the G2/M checkpoint. Further studies

showed that the NuRD components CHD4 and MTA1 are recruited to sites of IR-induced DNA damage. This recruitment takes place in a previously unappreciated, polyadenosine 5′-diphosphate (ADP)-ribose (PARylation)-dependent manner, but is independent of H2A.X phosphorylation [26•,27••]. It was also shown that components of the Polycomb Repressive Complex 1 (PRC1), such as MEL-18, are recruited to DSBs in a PARylation-dependent manner, and that PARylation is required to exclude nascent RNA as well as RNA polymerase II from regions of laser induced damage [27••]. Thus PARylation and NuRD recruitment appear to repress transcription at breaks. Speculation on the role of heterochromatin proteins in DSB repair is discussed elsewhere [3]. PARylation is also crucial for the recruitment of another human Snf2-like chromatin remodeler, ALC1, also known as CHD1L. ALC1 is targeted to sites of phleomycin-induced damage through its interaction with poly-ADP ribose. ALC1 overexpression delays or impedes repair, based on the comet assay. It is thought that ALC1 may promote NHEJ through its physical interactions with Ku70, XRCC1, DNA-PKcs and the histone chaperone APLF. Its interaction with subunits of the RPA complex may also suggest a role in HR, or another pathway of repair requiring DNA resection [28–30].

Finally, the related NuRD complex ATPase, CHD3, was shown to be lost from lesions induced in KAP-1-enriched heterochromatic domains [26•]. This effect is regulated by ATM dependent phosphorylation of KAP-1 at Ser824. Once KAP-1 is phosphorylated (pKAP-1), its direct interaction with CHD3 is disrupted, resulting in CHD3 loss from the domain. The ensuing chromatin relaxation is thought to promote DNA accessibility of heterochromatic regions, thereby facilitating repair [31••,32]. This is consistent with the role proposed for CHD3 and MI-2 in promoting chromatin compaction and gene repression [33].

The closest yeast equivalent to mammalian CHD3, CHD4 and ALC1 ATPases is the monomeric Chd1 remodeler (Table 1). Computational studies showed that yeast and other lower eukaryotes lack KAP-1-like proteins and PAR, and so far there have been no recent studies that link yeast Chd1 to DSB repair. In summary, these results identify ALC1 and CHD4 as active factors in genome maintenance that recruit DNA damage response factors, possibly favoring repair, while the related CHD3-containing NuRD remodeler complex needs to be lost from heterochromatic sites in order to aid repair. This suggests that the chromatin context of the DNA damage strongly influences which remodeler is important for subsequent repair events. Furthermore, depending on whether the situation calls for NHEJ-mediated or HR-mediated repair, resection may either need to be attenuated or promoted by remodeling complexes.

Role of chromatin remodelers in resection

The Swr1-like remodeler INO80 [7] and the Snf2-like remodeler RSC [34] were the first chromatin remodeling complexes to be associated with resection (for an in depth analysis see [6]). A recent study on mammalian INO80 and one of its subunits, Arp8, shows the importance of INO80 in RPA filament formation after damage [35•]. This is consistent with its previously demonstrated role in resection in yeast [36]. We note that, TIP49a,b which is part of the human INO80, SCRAP and TTRAP/Tip60 complexes [5] and yeast Rvb1/Rvb2 of INO80 and SWR1, have been shown to be ATP-dependent helicases that unwind DNA at 3′ ssDNA overhangs of at least 30 nucleotides in length, in a 3′ to 5′ direction [37]. These *in vitro* findings suggest that complexes containing TIP49a,b (or Rvb1/Rvb2) may be generally involved in processing resected DNA ends.

Fun30 is a poorly characterized chromatin remodeler of the Etl1 Snf2-like nucleosome remodeler family [4,38,39••]. The previous best described role of Fun30 was the protection of centromeres by maintaining the integrity of centromeric chromatin [40,41]. Three new studies highlight the role of Fun30 in Sgs1 and Exo1 dependent long-range resection at a DSB [2,40,42••]. Fun30 appears to be the most important chromatin remodeler for long-range resection in yeast, although this role is partially redundant with that of INO80 and RSC near the DSB [2]. This also appears to hold true in mammals for SMARCAD1, the closest human homologue of Fun30 [42••]. Intriguingly, Fun30 becomes partly dispensable when recruitment of the checkpoint mediator Rad9 is ablated. Rad9 inhibits resection at DSBs [43,44] thus favoring NHEJ over HR. Fun30 is proposed to remove Rad9 (Figure 1) and thus promote resection and HR [2,39••]. Consistently, when Fun30 is deleted, Rad9 spreads outwards from the DSB, presumably antagonizing resection [2]. This paper also offers evidence indicating that CHD1, SWR1, Rad54 and ISW1 remodeling factors do not play any significant role in resection, though Rad54 is epistatic with Fun30 with respect to its damage sensitivity [2].

Cells without intact INO80, SWR1 and RSC are still proficient in single-strand annealing (SSA), a repair mechanism that requires extensive resection to repair a DSB. However, *fun30Δ* strains are defective in repair by SSA, highlighting the importance of this protein's involvement in long range resection [2,39••]. Importantly, Fun30 does not seem to be involved in strand invasion or in later steps of HR. However, like *rdh54Δ* strains, *fun30Δ* strains are defective in adaptation to a single DSB, due to the hyperactivation of Mec1 (ATR kinase) through Mre11 [39••]. These papers have now added Fun30 to the list of DNA damage response factors, although little is known about the complex(es) it forms.

Figure 1

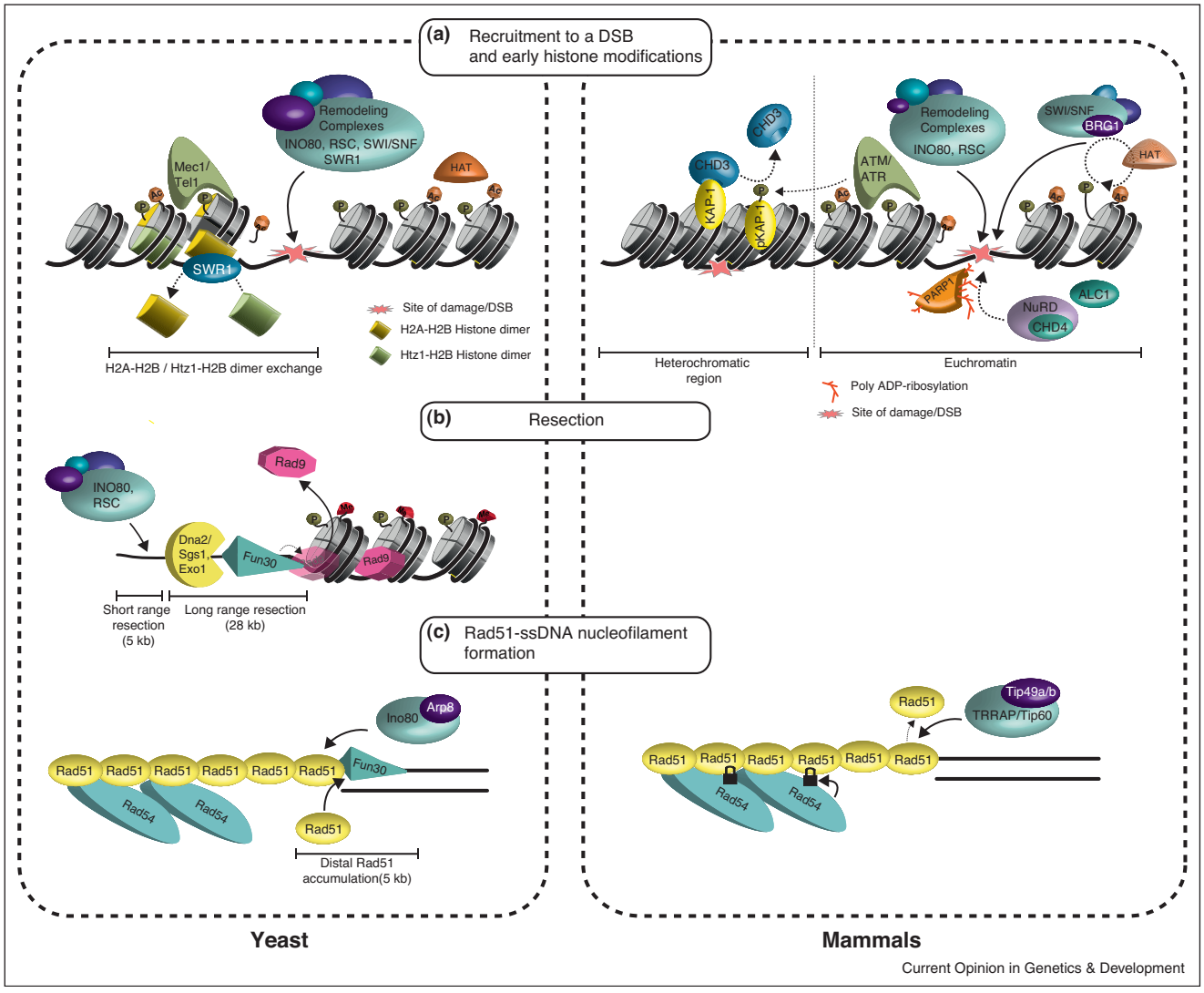

Chromatin remodeling at different steps during HR. **(a)** Formation of a DSB activates the DNA damage response followed by an orchestrated localization of repair factors to the site of damage, priming it for repair. The events occurring in budding yeast are on the left and those in mammals on the right. One of the first steps during DSB repair is the acetylation of histones, combined with phosphorylation by checkpoint kinases. The combination recruits chromatin remodeling complexes to the site of damage. Upon binding, remodelers change the local occupancy and histone composition of nucleosomes around the DSB, facilitating the accessibility for subsequent repair factors. In mammals both acetylation and the recruitment of remodelers associated with transcriptional repression is documented. In heterochromatic regions the CHD3-containing NuRD complex is evicted from heterochromatin. This may facilitate the opening of these compacted chromatin regions. PARylation is also important in recruiting NuRD complex components such as CHD4 and ALC1 (CHD1L) near the lesion. **(b)** The next step in HR requires resection of the dsDNA at the break site, generating a 3′ overhang. RSC and INO80 have a role in short range resection while Fun30 is essential for long range resection. Following DSB formation, Fun30 accumulates at distal sites from the break, removing the resection barrier imposed by Rad9 binding. Once Rad9 is removed, the exonucleases Dna2/Sgs1 and Exo1 can produce long ssDNA overhangs. **(c)** Following resection, the ssDNA binding protein Rad51 is loaded onto DNA and forms the ssDNA nucleofilament. Rad54 stabilizes the Rad51 filament. In haploid yeast cells, Arp8 within the INO80 complex is required for efficient accumulation of Rad51 at DSBs. In mammals Tip49a,b in the human TRRAP/Tip60 promotes Rad51 focus formation at DSBs.

Rad51-ssDNA filament formation

After resection, one of the next steps in HR is the formation of a Rad51 filament along the ssDNA strand. This is facilitated by a number of remodelers. For example when Fun30 is deleted, Rad51 levels at distal sites from a DSB (5 kb) are greatly reduced and accumulate slowly over time. Even though basal protein levels are reduced, this defect in recruitment and accumulation is not seen within proximal sites to the DSB (1 kb) [2].

The same holds true for Tip49a-depleted or Tip49b-depleted human cells where Rad51 focus accumulation

is strongly reduced in response to IR, rendering cells sensitive to damaging agents. Indeed, the amount of soluble Rad51 accumulates, and the level of chromatin-bound Rad51 decreases, upon Tip49a/b depletion. The authors also show that relaxing chromatin before DSB induction, using sodium butyrate to provoke hyperacetylation, restores the number of Rad51 foci to wild-type levels, possibly achieving the same opening of chromatin as that effected by the Tip49/TRRAP/Tip60 complex [45,46]. Alternatively, SRCAP may be involved. One model proposes that the role of Tip49 within the TTRAP–Tip60 complex is to relax chromatin by acetylation, enabling the access of the repair machinery at the break site. Mammalian INO80 does not seem to be important for the recruitment of Rad51, but rather affects the recruitment of early repair proteins such as 53BP1, which may antagonize HR [35•]. In contrast, in haploid yeast Rad51 recruitment to an irreparable DSB is diminished in *arp8*Δ cells [47]. We note that when a donor is present and the DSB was repairable by HR in yeast, as in the mammalian study, INO80 mutants did not show a defect in Rad51 recruitment [48]. Given that yeast Rad51 activity is enhanced in diploids, it may be that Arp8 becomes dispensable in diploid cells for Rad51-filament formation [49].

Rad54 also plays a role in stabilizing Rad51 ssDNA filaments [50,51]. Evidence from a new mammalian study indicates that Rad54 dependent accumulation of Rad51 does not require the ATPase domain of Rad54, although ATP hydrolysis is required for the dissociation of Rad54 from the filament. Following IR induced damage over five hours, the authors observed an increase in the number of Rad54-GFP foci at the nuclear periphery. After another five hours the number of foci at the periphery dropped to the same levels as at the beginning of the experiment. In a Rad54-GFP ATPase mutant, the number of foci at the periphery continued to accumulate over the course of the experiment. The authors interpret this effect as relocation of a DSB to the nuclear periphery. However, this result could also indicate that DSBs are repaired faster in internal regions (euchromatin) than at the periphery (heterochromatin), or that foci persist longer in less accessible peripheral heterochromatin [52••]. Finally, displacement of yeast heterochromatin factors by the SWI/SNF remodeler complex was shown to promote Rad51 mediated joint-molecule formation and Rad54 dependent strand invasion, priming the DSB for repair by HR *in vitro* [20]. Taken together, these observations support the model that SWI/SNF ATPases facilitate Rad51 focus formation while Rad54 promotes filament assembly.

Dynamics of the DSB fiber

The least understood step in HR is homology search [53] (Figure 2). This process implies that a DSB scans the nucleus for its homologous template, in order to anneal and finally carry out repair by recombination. Undamaged chromatin moves within the nucleus, but it is constrained by the continuity of the chromatin fiber [54]. Both sides of a break remain linked by the MRN/MRX complex, yet changes in chromatin structure could change the persistence length of the chromatin fiber [1]. Recently it was tested whether the mobility of a DNA locus changes upon DSB induction and the impact of such movement on HR-mediated repair. Two studies in budding yeast have shown that DNA bearing a DSB in S-phase cells moves through a nuclear volume approximately 4-times larger than that of undamaged DNA [55••,56••]. Similarly, in mammalian cells the mobility of IR induced foci was found to increase over that of undamaged chromatin [57•]. While yeast and man share this phenomenon, a small increase in radius of constraint in yeast can enhance access to more than 60% of the genome, while in mammalian cells the same radius of movement might only mean that damage shifts from a compacted domain of chromatin to an open space nearby, without accessing a large part of the genome.

In support of the idea that chromatin mobility enhances HR, it was shown that the decreased chromatin mobility scored in a *rad9*Δ strains, correlated with lower rates of heteroduplex formation, when the donor sequence sits on a nonhomologous chromosome [55••]. The ATR homologue Mec1 was also implicated in the increased mobility of the DSB [55••].

One way in which random chromatin movement can be increased is through the removal of nucleosomes, which might increase the flexibility of a compacted chromatin fiber. In support of this model, work from the Gasser laboratory showed that the targeting of INO80 increased chromatin mobility in a manner dependent on its ATPase activity. At the *PHO5* promoter the increased movement could be correlated with nucleosome displacement by INO80 [1]. Consistently, the enhanced movement scored at an induced DSB was partially reduced in an *arp8*Δ strain [1], while the loss of Rad51 or of Rad54's ATPase activity completely eliminated damage-induced chromatin mobility [55••]. Since Rad51 helps recruit Rad54, and Rad54 in turn stabilizes the Rad51-ssDNA fiber, it is unclear whether the Rad54 ATPase action or the creation of the Rad51-ssDNA filament, or both enhance movement [55••].

Rad54 remodels chromatin [58] in a manner that correlates both with its dsDNA translocation activity, and its ATPase activity [50,51]. Thus, Rad54 may actively slide nucleosomes away from the resected DSB [59], which could, based on the action of other chromatin remodelers, increase the radius of the random walk movement of the DSB, due to reduced constraint on the damaged chromatin fiber. Interestingly, Rad54 molecules in human do not need their ATPase domains to associate

Figure 2

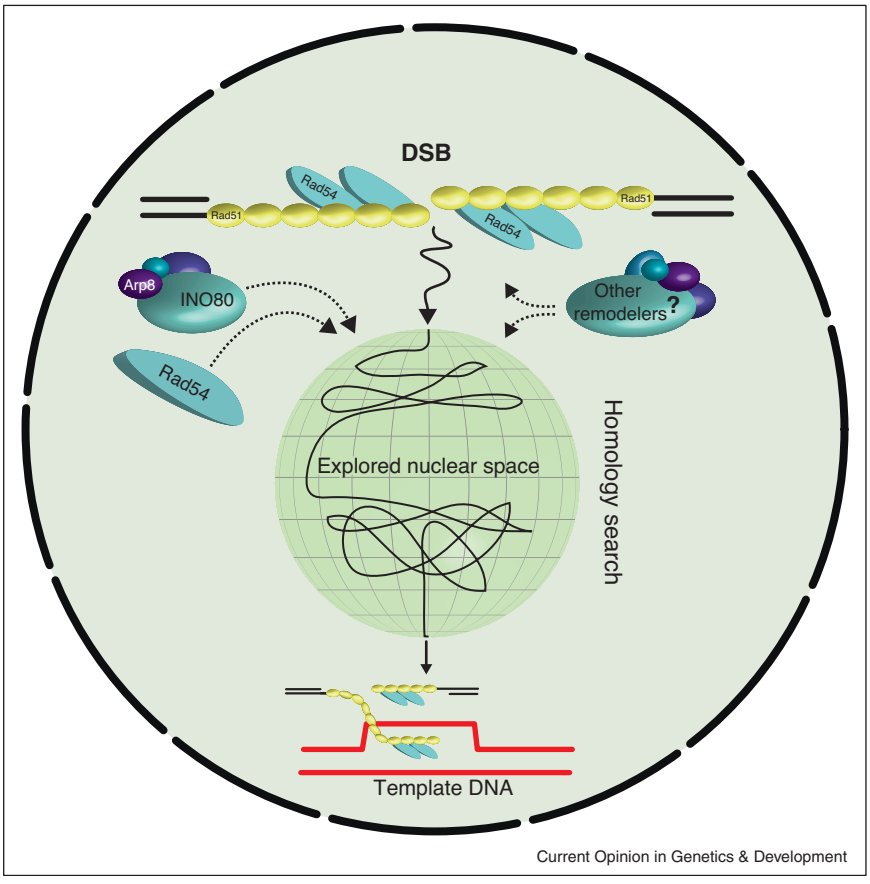

A speculative role of chromatin remodelers in homology search. In order to repair a lesion by HR, the homologous template needs to be identified and bound. The homologous template can be the sister chromatid after replication, although in special cases, repair occurs with ectopic homologous sequences. Several studies suggest that the efficiency of homology search is rate-limiting for DSB repair by HR with ectopic donors [53,62]. Upon damage, DSBs become more mobile, which may facilitate the homology search through nuclear space. This increase in mobility is dependent on the ATPase activities of INO80 and Rad54, both of which can remodel nucleosomes. Other chromatin remodeling complexes may also be involved in homology search dynamics.

with DSBs, and lack of ATPase activity inhibits its turnover at sites of damage, as shown by FRAP [52••]. Thus, it could also be the release of Rad54 that enhances movement of the resected break. In mammalian cells, but not in yeast, hINO80 binds to and promotes the expression of the *RAD54* gene, which suggests that INO80 may also have indirect effects in DSB repair. Indeed, enhanced expression of Rad54 can complement the DNA repair defect of human Ino80-deficient cells [60].

The specific mechanism of how remodelers increase chromatin mobility is still an open question. Multiple effects, including release from anchoring molecules, reduced persistence length, or the effect of the ATPase itself, are all possibilities. Some insight may be gained by identifying and comparing the effects of different remodeler subtypes in regard to chromatin mobility.

Conclusions

Up to this point only a few studies of chromatin remodelers in damage have scored defects in repair that could be traced unambiguously to the remodeler's activity at the site of damage. This may in part reflect redundancy in the function of chromatin remodelers, but may also simply arise from the fact that the appropriate read-outs were not yet monitored. Many unanswered questions remain. It is still unclear why so many chromatin remodeling factors are recruited to double-strand breaks. It is unclear how chromatin remodelers increase mobility of chromatin, why some damage shows movement while other do not, and what the impact of chromatin mobility is on repair. What role do remodelers play in the late stages of HR or in the restoration of chromatin after repair? The literature currently implicates histone chaperones in this step leaving the role for remodelers largely open [3]. The fate of nucleosomes during the DNA damage response is

an open question. Certainly, there has to be nucleosome eviction during resection to form an overhang for HR. The possibility remains that half nucleosomes remain bound, although it is unlikely that the Rad51 fiber contains nucleosomes. Improved methods for quantifying histone abundance at sites of damage would help to resolve this question. The fact that many cancers have mutations in subunits of chromatin remodeling complexes [61] indicates that these enzymes remain an unexplored source of diagnostic targets to help screen for diseases that stem from genomic instability.

Acknowledgments

The Gasser laboratory is supported by the Novartis Research Foundation, the Marie Curie networks Image-DDR and Nucleosome 4D, and the Swiss National Science Foundation. We thank H. Ferreira, V. Dion and F. Clarke for constructive advice on the writing.

References and recommended reading

Papers of particular interest, published within the period of review, have been highlighted as:

- • of special interest
- •• of outstanding interest

1. • Neumann FR, Dion V, Gehlen LR, Tsai-Pflugfelder M, Schmid R, Taddei A, Gasser SM: **Targeted INO80 enhances subnuclear chromatin movement and ectopic homologous recombination**. *Genes Dev* 2012, **26**:369-383.
The authors show that targeting the INO80 complex to a locus increases its mobility within the yeast nucleus. This was correlated with higher rates of spontaneous gene conversion, and with nucleosome eviction at the *PHO5* promoter. The increase in mobility at a DSB is Arp8-dependent. The authors propose a model where by nucleosome eviction increases chromatin mobility by enhancing the flexibility of the chromatin fiber.

2. •• Chen X, Cui D, Papusha A, Zhang X, Chu CD, Tang J, Chen K, Pan X, Ira G: **The Fun30 nucleosome remodeller promotes resection of DNA double-strand break ends**. *Nature* 2012, **489**:576-580.
One of three important studies on the role of Fun30 in double-strand break repair. Here the authors highlight Fun30 as nucleosome remodeler that promotes resection of DSBs through a mechanism that seems to promote the removal of Rad9. They also show the relative roles of the RSC and INO80 remodeling complexes in resection.

3. Soria G, Polo Sophie E, Almouzni G: **Prime, repair, restore: the active role of chromatin in the DNA damage response**. *Mol Cell* 2012, **46**:722-734.

4. Flaus A, Martin DM, Barton GJ, Owen-Hughes T: **Identification of multiple distinct Snf2 subfamilies with conserved structural motifs**. *Nucleic Acids Res* 2006, **34**:2887-2905.

5. Clapier CR, Cairns BR: **The biology of chromatin remodeling complexes**. *Annu Rev Biochem* 2009, **78**:273-304.

6. Chambers AL, Downs JA: **The RSC and INO80 chromatin-remodeling complexes in DNA double-strand break repair**. *Prog Mol Biol Transl Sci* 2012, **110**:229-261.

7. van Attikum H, Fritsch O, Hohn B, Gasser SM: **Recruitment of the INO80 complex by H2A phosphorylation links ATP-dependent chromatin remodeling with DNA double-strand break repair**. *Cell* 2004, **119**:777-788.

8. Morrison AJ, Highland J, Krogan NJ, Arbel-Eden A, Greenblatt JF, Haber JE, Shen X: **INO80 and γ-H2AX interaction links ATP-dependent chromatin remodeling to DNA damage repair**. *Cell* 2004, **119**:767-775.

9. Downs JA, Allard S, Jobin-Robitaille O, Javaheri A, Auger A, Bouchard N, Kron SJ, Jackson SP, Cote J: **Binding of chromatin-modifying activities to phosphorylated histone H2A at DNA damage sites**. *Mol Cell* 2004, **16**:979-990.

10. Kashiwaba S, Kitahashi K, Watanabe T, Onoda F, Ohtsu M, Murakami Y: **The mammalian INO80 complex is recruited to DNA damage sites in an ARP8 dependent manner**. *Biochem Biophys Res Commun* 2010, **402**:619-625.

11. Kitayama K, Kamo M, Oma Y, Matsuda R, Uchida T, Ikura T, Tashiro S, Ohyama T, Winsor B, Harata M: **The human actin-related protein hArp5: nucleo-cytoplasmic shuttling and involvement in DNA repair**. *Exp Cell Res* 2009, **315**:206-217.

12. Kandasamy MK, McKinney EC, Deal RB, Smith AP, Meagher RB: **Arabidopsis actin-related protein ARP5 in multicellular development and DNA repair**. *Dev Biol* 2009, **335**:22-32.

13. Luk E, Ranjan A, Fitzgerald PC, Mizuguchi G, Huang Y, Wei D, Wu C: **Stepwise histone replacement by SWR1 requires dual activation with histone H2A.Z and canonical nucleosome**. *Cell* 2010, **143**:725-736.

14. Bao YH: **Chromatin response to DNA double-strand break damage**. *Epigenomics* 2011, **3**:307-321.

15. Kalocsay M, Hiller NJ, Jentsch S: **Chromosome-wide Rad51 spreading and SUMO-H2A.Z-dependent chromosome fixation in response to a persistent DNA double-strand break**. *Mol Cell* 2009, **33**:335-343.

16. Morillo-Huesca M, Clemente-Ruiz M, Andujar E, Prado F: **The SWR1 histone replacement complex causes genetic instability and genome-wide transcription misregulation in the absence of H2A.Z**. *PLoS ONE* 2010, **5**:e12143.

17. • Xu Y, Ayrapetov MK, Xu C, Gursoy-Yuzugullu O, Hu Y, Price BD: **Histone H2A.Z controls a critical chromatin remodeling step required for DNA double-strand break repair**. *Mol Cell* 2012, **48**:723-733.
Convincing evidence is put forth for a functional role of H2A.Z deposition by p400 and subsequent acetylation by Tip60 in mammals at dSBs in mammalian cells, Incorporation of H2A.Z along with acetylation of H4 facilitates relaxation of chromatin and allows for subsequent modifications such as ubiquitination and loading of KU to mediate repair by NHEJ.

18. Chai B, Huang J, Cairns BR, Laurent BC: **Distinct roles for the RSC and Swi/Snf ATP-dependent chromatin remodelers in DNA double-strand break repair**. *Genes Dev* 2005, **19**:1656-1661.

19. Shen X, Mizuguchi G, Hamiche A, Wu C: **A chromatin remodelling complex involved in transcription and DNA processing**. *Nature* 2000, **406**:541-544.

20. Sinha M, Watanabe S, Johnson A, Moazed D, Peterson CL: **Recombinational repair within heterochromatin requires ATP-dependent chromatin remodeling**. *Cell* 2009, **138**:1109-1121.

21. • Lee HS, Park JH, Kim SJ, Kwon SJ, Kwon J: **A cooperative activation loop among SWI/SNF, gamma-H2AX and H3 acetylation for DNA double-strand break repair**. *EMBO J* 2010, **29**:1434-1445.
The authors provide evidence of a positive feedback loop between SWI/SNF, H3 acetylation and phosphorylation of H2A.X, facilitating DSB repair.

22. Ogiwara H, Ui A, Otsuka A, Satoh H, Yokomi I, Nakajima S, Yasui A, Yokota J, Kohno T: **Histone acetylation by CBP and p300 at double-strand break sites facilitates SWI/SNF chromatin remodeling and the recruitment of non-homologous end joining factors**. *Oncogene* 2011, **30**:2135-2146.

23. Peng G, Yim EK, Dai H, Jackson AP, Burgt I, Pan MR, Hu R, Li K, Lin SY: **BRIT1/MCPH1 links chromatin remodelling to DNA damage response**. *Nat Cell Biol* 2009, **11**:865-872.

24. • Hauk G, McKnight JN, Nodelman IM, Bowman GD: **The chromodomains of the Chd1 chromatin remodeler regulate DNA access to the ATPase motor**. *Mol Cell* 2010, **39**:711-723.
This study solved the crystal structure of yeast Chd1 and proposes a model where the chromodomains of Chd1 allow it to distinguish between nucleosomes and naked DNA by controlling access to its ATPase motor.

25. • Smeenk G, Wiegant WW, Vrolijk H, Solari AP, Pastink A, van Attikum H: **The NuRD chromatin-remodeling complex regulates signaling and repair of DNA damage**. *J Cell Biol* 2010, **190**:741-749.
Knockdown of *MTA2* or *CHD4*, which encode components of the NuRD complex, leads to accumulation of DNA damage as well as sensitivity to IR. CHD4 stimulates RNF8/RNF168 dependent ubiquitin conjugates, and promotes DSB repair and checkpoint activation in response to IR.

26. • Polo SE, Kaidi A, Baskcomb L, Galanty Y, Jackson SP: **Regulation of DNA-damage responses and cell-cycle progression by the chromatin remodelling factor CHD4**. *EMBO J* 2010, **29**:3130-3139.
CHD4 promotes DSB repair and cell survival after damage as well as acting as a regulator of G1/S cell cycle progression by controlling p53 deacetylation.

27. •• Chou DM, Adamson B, Dephoure NE, Tan X, Nottke AC, Hurov KE, Gygi SP, Colaiacovo MP, Elledge SJ: **A chromatin localization screen reveals poly (ADP ribose)-regulated recruitment of the repressive polycomb and NuRD complexes to sites of DNA damage**. *Proc Natl Acad Sci U S A* 2010, **107**:18475-18480.
The authors find that components of mammalian Polycomb Repressive Complex 1 (PRC1), such as MEL-18, like MTA1 and CHD4 of the NuRD complex, are recruited to sites of laser induced damage in a PARP dependent manner. They show that exclusion of nascent transcripts as well as RNA polymerase II from sites of laser induced damage was dependent on PARP. They propose a model whereby PARP promotes transcriptional repression at sites of DNA damage.

28. Ahel D, Horejsi Z, Wiechens N, Polo SE, Garcia-Wilson E, Ahel I, Flynn H, Skehel M, West SC, Jackson SP *et al.*: **Poly(ADP-ribose)-dependent regulation of DNA repair by the chromatin remodeling enzyme ALC1**. *Science* 2009, **325**:1240-1243.

29. Ahel I, Ahel D, Matsusaka T, Clark AJ, Pines J, Boulton SJ, West SC: **Poly(ADP-ribose)-binding zinc finger motifs in DNA repair/checkpoint proteins**. *Nature* 2008, **451**:81-85.

30. Gottschalk AJ, Timinszky G, Kong SE, Jin J, Cai Y, Swanson SK, Washburn MP, Florens L, Ladurner AG, Conaway JW *et al.*: **Poly(ADP-ribosyl)ation directs recruitment and activation of an ATP-dependent chromatin remodeler**. *Proc Natl Acad Sci U S A* 2009, **106**:13770-13774.

31. •• Goodarzi AA, Kurka T, Jeggo PA: **KAP-1 phosphorylation regulates CHD3 nucleosome remodeling during the DNA double-strand break response**. *Nat Struct Mol Biol* 2011, **18**:831-839.
The authors show that the mammalian remodeler CHD3 is lost from heterochromatin upon damage following the phosphorylation of KAP-1 by ATM. Loss of CHD3 results in chromatin relaxation which could help facilitate repair in heterochromatic regions, by antagonizing chromatin compaction.

32. Goodarzi AA, Noon AT, Deckbar D, Ziv Y, Shiloh Y, Lobrich M, Jeggo PA: **ATM signaling facilitates repair of DNA double-strand breaks associated with heterochromatin**. *Mol Cell* 2008, **31**:167-177.

33. Denslow SA, Wade PA: **The human Mi-2//NuRD complex and gene regulation**. *Oncogene* 2007, **26**:5433-5438.

34. Shim EY, Hong SJ, Oum JH, Yanez Y, Zhang Y, Lee SE: **RSC mobilizes nucleosomes to improve accessibility of repair machinery to the damaged chromatin**. *Mol Cell Biol* 2007, **27**:1602-1613.

35. • Gospodinov A, Vaissiere T, Krastev DB, Legube G, Anachkova B, Herceg Z: **Mammalian Ino80 mediates double-strand break repair through its role in DNA end strand resection**. *Mol Cell Biol* 2011, **31**:4735-4745.
Here the authors show that mammalian INO80 is required for efficient DSB repair. They show that 53BP1 but not Rad51 focus formation is impaired upon human Ino80 depletion. This led them to investigate the role of INO80 in early steps of repair and they find that the complex mediates 5′–3′ resection of DSB ends.

36. van Attikum H, Fritsch O, Gasser SM: **Distinct roles for SWR1 and INO80 chromatin remodeling complexes at chromosomal double-strand breaks**. *EMBO J* 2007, **26**:4113-4125.

37. Papin C, Humbert O, Kalashnikova A, Eckert K, Morera S, Kas E, Grigoriev M: **3′- to 5′ DNA unwinding by TIP49b proteins**. *FEBS J* 2010, **277**:2705-2714.

38. Awad S, Ryan D, Prochasson P, Owen-Hughes T, Hassan AH: **The Snf2 homolog Fun30 acts as a homodimeric ATP-dependent chromatin-remodeling enzyme**. *J Biol Chem* 2010, **285**:9477-9484.

39. •• Eapen VV, Sugawara N, Tsabar M, Wu WH, Haber JE: **The *Saccharomyces cerevisiae* chromatin remodeler Fun30 regulates DNA end-resection and checkpoint deactivation**. *Mol Cell Biol* 2012, **32**:4727-4740.
One of three important studies on the role of Fun30 in double strand break repair. The authors show that Fun30 promotes 5′ to 3′ resection of DSBs. Deletion of *FUN30* results in a ~3.3 fold reduction in the speed of resection. They also show that Fun30 is important for the adaptation of DNA damage checkpoint arrested cells with an unrepaired DSB to resume cell cycle progression.

40. Durand-Dubief M, Will WR, Petrini E, Theodorou D, Harris RR, Crawford MR, Paszkiewicz K, Krueger F, Correra RM, Vetter AT *et al.*: **SWI/SNF-like chromatin remodeling factor Fun30 supports point centromere function in *S. cerevisiae***. *PLoS Genet* 2012, **8**:e1002974.

41. Stralfors A, Walfridsson J, Bhuiyan H, Ekwall K: **The FUN30 chromatin remodeler, Fft3, protects centromeric and subtelomeric domains from euchromatin formation**. *PLoS Genet* 2011, **7**:e1001334.

42. •• Costelloe T, Louge R, Tomimatsu N, Mukherjee B, Martini E, Khadaroo B, Dubois K, Wiegant WW, Thierry A, Burma S *et al.*: **The yeast Fun30 and human SMARCAD1 chromatin remodellers promote DNA end resection**. *Nature* 2012, **489**:581-584.
One of three important studies on the role of Fun30 in double strand break repair. In addition to showing that yeast Fun30 plays a role in resection these authors show that the closest human homologue, SMARCAD1 also is recruited to and plays a role in repair of DSBs.

43. Lazzaro F, Sapountzi V, Granata M, Pellicioli A, Vaze M, Haber JE, Plevani P, Lydall D, Muzi-Falconi M: **Histone methyltransferase Dot1 and Rad9 inhibit single-stranded DNA accumulation at DSBs and uncapped telomeres**. *EMBO J* 2008, **27**:1502-1512.

44. Lydall D, Weinert T: **Yeast checkpoint genes in DNA damage processing: implications for repair and arrest**. *Science* 1995, **270**:1488-1491.

45. Gospodinov A, Tsaneva I, Anachkova B: **RAD51 foci formation in response to DNA damage is modulated by TIP49**. *Int J Biochem Cell Biol* 2009, **41**:925-933.

46. Murr R, Loizou JI, Yang YG, Cuenin C, Li H, Wang ZQ, Herceg Z: **Histone acetylation by Trrap–Tip60 modulates loading of repair proteins and repair of DNA double-strand breaks**. *Nat Cell Biol* 2006, **8**:91-99.

47. Tsukuda T, Fleming AB, Nickoloff JA, Osley MA: **Chromatin remodelling at a DNA double-strand break site in *Saccharomyces cerevisiae***. *Nature* 2005, **438**:379-383.

48. Tsukuda T, Lo YC, Krishna S, Sterk R, Osley MA, Nickoloff JA: **INO80-dependent chromatin remodeling regulates early and late stages of mitotic homologous recombination**. *DNA Repair (Amst)* 2009, **8**:360-369.

49. Morgan EA, Shah N, Symington LS: **The requirement for ATP hydrolysis by *Saccharomyces cerevisiae* Rad51 is bypassed by mating-type heterozygosity or RAD54 in high copy**. *Mol Cell Biol* 2002, **22**:6336-6343.

50. Mazin AV, Mazina OM, Bugreev DV, Rossi MJ: **Rad54, the motor of homologous recombination**. *DNA Repair (Amst)* 2010, **9**:286-302.

51. Ceballos SJ, Heyer WD: **Functions of the Snf2/Swi2 family Rad54 motor protein in homologous recombination**. *Biochim Biophys Acta* 2011, **1809**:509-523.

52. •• Agarwal S, van Cappellen Wa, Guénolé A, Eppink B, Linsen SEV, Meijering E, Houtsmuller A, Kanaar R, Essers J: **ATP-dependent and independent functions of Rad54 in genome maintenance**. *J Cell Biol* 2011, **192**:735-750.
The authors show that human Rad54 is required for the timely accumulation of Rad51 at DSBs that is independent of Rad54's ATPase activity. They also show that Rad54's ATPase activity is required for the redistribution of DSB repair sites within the nucleus.

53. Gehlen LR, Gasser SM, Dion V: **How broken DNA finds its template for repair: a computational approach**. *Prog Theor Phys Suppl* 2011, **191**:20.

54. Gartenberg MR, Neumann FR, Laroche T, Blaszczyk M, Gasser SM: **Sir-mediated repression can occur independently of chromosomal and subnuclear contexts**. *Cell* 2004, **119**:955-967.

55. Dion V, Kalck V, Horigome C, Towbin BD, Gasser SM: **Increased
•• mobility of double-strand breaks requires Mec1, Rad9 and the homologous recombination machinery**. *Nat Cell Biol* 2012, **14**:502-509.
This study along with that of Mine-Hattab and Rothstein shows that a DSB is more mobile than its undamaged counterpart. A nick induced by collision of the replication fork with protein adduct does not increase in mobility. Dion *et al.* show that the chromatin remodeler Rad54, and specifically its ATPase activity, are required for increased chromatin mobility upon damage, as is Rad9 and Mec1. The rate of heteroduplex formation with an ectopic donor is reduced in a *rad9* mutant.

56. Mine-Hattab J, Rothstein R: **Increased chromosome mobility
•• facilitates homology search during recombination**. *Nat Cell Biol* 2012, **14**:510-517.
This study shared many of the same findings as Dion *et al.*, but performed the study in diploid yeast cells. Increased mobility depends in part on Sae2. Importantly, Mine-Hattab and Rothstein show that not only a DSB but also a non-homologous, undamaged chromosomal locus increases in mobility when cells incur damage.

57. Krawczyk PM, Borovski T, Stap J, Cijsouw T, ten Cate R,
• Medema JP, Kanaar R, Franken NA, Aten JA: **Chromatin mobility is increased at sites of DNA double-strand breaks**. *J Cell Sci* 2012, **125**:2127-2133.
Here the authors show that DSB foci are more mobile than undamaged chromatin. They also show that drugs such as Curcumin or azacitidine, which affect chromatin structure, can reduce mobility.

58. Zhang Z, Fan HY, Goldman JA, Kingston RE: **Homology-driven chromatin remodeling by human RAD54**. *Nat Struct Mol Biol* 2007, **14**:397-405.

59. Alexeev A, Mazin A, Kowalczykowski SC: **Rad54 protein possesses chromatin-remodeling activity stimulated by the Rad51-ssDNA nucleoprotein filament**. *Nat Struct Biol* 2003, **10**:182-186.

60. Park EJ, Hur SK, Kwon J: **Human INO80 chromatin-remodelling complex contributes to DNA double-strand break repair via the expression of Rad54B and XRCC3 genes**. *Biochem J* 2010, **431**:179-187.

61. Luijsterburg MS, van Attikum H: **Chromatin and the DNA damage response: the cancer connection**. *Mol Oncol* 2011, **5**:349-367.

62. Wilson JH, Leung WY, Bosco G, Dieu D, Haber JE: **The frequency of gene targeting in yeast depends on the number of target copies**. *Proc Natl Acad Sci U S A* 1994, **91**:177-181.

63. Shen X, Ranallo R, Choi E, Wu C: **Involvement of actin-related proteins in ATP-dependent chromatin remodeling**. *Mol Cell* 2003, **12**:147-155.

64. Larsen DH, Poinsignon C, Gudjonsson T, Dinant C, Payne MR, Hari FJ, Rendtlew Danielsen JM, Menard P, Sand JC, Stucki M *et al.*: **The chromatin-remodeling factor CHD4 coordinates signaling and repair after DNA damage**. *J Cell Biol* 2010, **190**:731-740.

65. Oum JH, Seong C, Kwon Y, Ji JH, Sid A, Ramakrishnan S, Ira G, Malkova A, Sung P, Lee SE *et al.*: **RSC facilitates Rad59-dependent homologous recombination between sister chromatids by promoting cohesin loading at DNA double-strand breaks**. *Mol Cell Biol* 2011, **31**:3924-3937.

66. Naidu SR, Love IM, Imbalzano AN, Grossman SR, Androphy EJ: **The SWI/SNF chromatin remodeling subunit BRG1 is a critical regulator of p53 necessary for proliferation of malignant cells**. *Oncogene* 2009, **28**:2492-2501.

67. Park JH, Park EJ, Hur SK, Kim S, Kwon J: **Mammalian SWI/SNF chromatin remodeling complexes are required to prevent apoptosis after DNA damage**. *DNA Repair (Amst)* 2009, **8**:29-39.

Cell Cycle 13:6, 877–878; March 15, 2014; © 2014 Landes Bioscience

Remodelers move chromatin in response to DNA damage

Andrew Seeber[1,2], Vincent Dion[3], and Susan M Gasser[1,2,*]

[1]Friedrich Miescher Institute for Biomedical Research; Basel, Switzerland; [2]University of Basel; Faculty of Natural Sciences; Basel, Switzerland; [3]University of Lausanne; Center for Integrative Genomics; Lausanne, Switzerland

DNA double-strand breaks (DSBs) are dangerous lesions that occur when both strands of the DNA double helix are broken. Repair of DSBs occurs either by homologous recombination (HR) or non-homologous end-joining (NHEJ). A fundamental distinction between the 2 pathways lies in the requirement for a homologous sequence that templates the repair: this is needed for HR but not for NHEJ. In S-phase cells, the template most often used is the sister chromatid. If the break occurs in G_1 phase (particularly in haploid cells, like yeast) or if both sisters are damaged, the homolog or an ectopic sequence with appropriate homology must be used as a template. For that to occur, the damage and the intact homologous sequence must first physically meet, through a process called homology search. In mammalian nuclei this would involve the scanning of thousands of millions of base pairs for an exact copy of the damaged site. Not surprisingly, ectopic recombination (i.e., recombination with a homolog or a non-sister chromosome) is relatively rare in complex genomes, while it occurs quite efficiently in yeast.

Given the spatial constraint that restricts the mobility of chromosomal loci,[1] it is not surprising that the time it takes for 2 specific sites to collide is rate limiting for HR. Both computer simulations and experiments that monitored recombination rates in yeast support this notion.[2,3]

Intriguingly, last year it was shown, through single-particle tracking with high-resolution time-lapse microscopy in yeast, that fluorescently tagged sites of DSBs move within a larger radius than the same tagged site when it is undamaged.[4,5] Notably, the volume explored increased by ~4-fold. Mutations in repair proteins such as Rad51 and Rad54 or in the DNA damage checkpoint kinase Mec1 (ATR) were shown to be important for the increased mobility. Two studies reported similar phenomena, yet they differed in one aspect: one suggested that loci unlinked to the damage might also increase in mobility after exposure to ionizing irradiation, while the other did not observe this after induction of a single DSB or on low level Zeocin. The discrepancy was recently resolved by showing that the genome-wide response to damage that leads to increased chromatin mobility depends on the activation of the DNA damage checkpoint response (DDR).[6] The DDR is not immediately induced in the presence of a single DSB, nor in the presence of low levels of Zeocin, while higher levels of Zeocin activate the DDR rapidly and, indeed, induce the general chromatin response.[6]

Genetic dependence on DNA damage checkpoint kinases was shown by mutating either Mec1 and/or its downstream target kinase Rad53. In both mutants, the ectopic or general increase in mobility was impaired. Remarkably, an artificial activation of Mec1 kinase by juxtaposition of its binding partner Ddc2 and the kinase co-activator Ddc1 led to a similar increase in chromatin mobility in the absence of DNA damage, ruling out potential indirect effects of Zeocin and/or DNA damage.

In contrast to the increased movement scored for the DSB site itself, this general increase in mobility was not dependent on Rad51. Thus the mechanism that acts at the site of damage (in cis) differs at least in part from that which increases chromatin mobility in trans.[6]

Increases in chromatin mobility could be a direct consequence of nucleosome remodeling that would change the flexibility of a chromatin fiber. Previous work has shown that the targeting of the INO80 nucleosome remodeling complex leads to an increase in the mobility of an intact locus. Studies of the yeast *PHO5* promoter showed that the INO80-dependent increase in mobility correlated with the removal of nucleosomes. Since the INO80 complex is a known target of the DDR, the INO80 complex was tested for contributions to the DDR-induced increase in chromatin mobility. Indeed, deletion of INO80 subunits that compromise its ATP-dependent nucleosome remodeling activity reduced the DDR-induced increase in chromatin mobility at ectopic sites. Ablation of other remodelers, such as Chd1 and Swr1, did not.[6]

A number of open questions remain (**Fig. 1**). First and foremost, what is the structural change in chromatin that leads to increased mobility of a given tagged locus? Does the increased mobility correlate with nucleosome displacement, loss of other factors, or disruption of an anchor? Finally, how do checkpoint kinases regulate INO80?

Whereas both homology search and the flexibility of the chromatin fiber may be different in mammalian cells, it is nonetheless plausible that the effects observed are relevant beyond yeast. For instance, a DSB array that leads to a translocation in mouse fibroblasts has a higher mobility than that of a non-translocating array.[7]

*Correspondence to: Susan M Gasser; Email: susan.gasser@fmi.ch
Submitted: 10/25/2013; Accepted: 11/05/2013; Published Online: 02/14/2014
http://dx.doi.org/10.4161/cc.28200
Correspondence to: Seeber A, et al. Genes Dev 2013; 27:1999-2008; PMID:24029917; http://dx.doi.org/10.1101/gad.222992.113

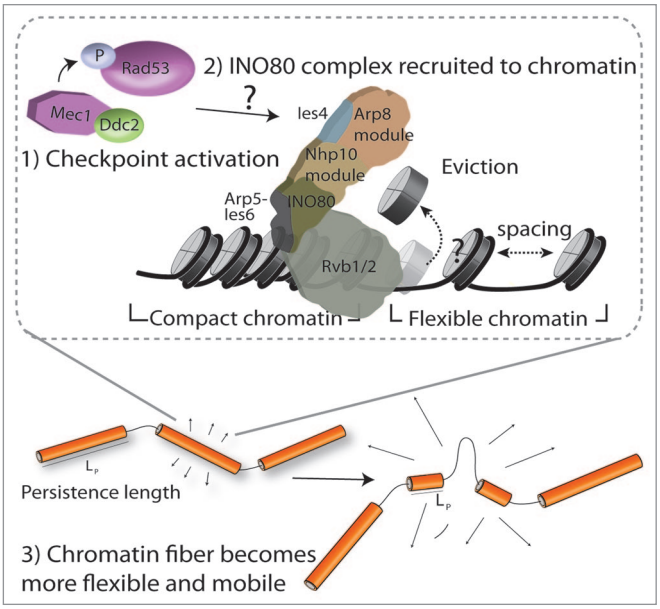

Figure 1. Hypothetical model of INO80 mediated enhanced chromatin mobility. Checkpoint activation due to DNA damage targets the INO80 nucleosome remodelling complex to chromatin. INO80 evicts nucleosomes and makes chromatin more flexible. Due to the actions of INO80 the persistence length of the chromatin fiber is reduced allowing for chromatin to move more freely.

Since NHEJ is the preferred mode of repair in mammalian cells, and not HR, it may only be an exceptional type of break that requires a homology search, and therefore enhanced movement. Indeed, homology search in mammals may normally be actively suppressed to prevent unwanted translocations or deletions. It will be intriguing to see if remodelers that favor NHEJ, such as the SWI/SNF remodeler BRM,[8] antagonize movement in mammalian cells, by perhaps counteracting the activity of INO80. Fortunately the tools are in hand to test such hypotheses, both in mammalian and yeast cells.

References

1. Dion V and Gasser SM. Cell 2013; 152:1355-64; PMID:23498942; http://dx.doi.org/10.1016/j.cell.2013.02.010
2. Agmon N, et al. Nat Cell Biol 2013; 15:694-9; PMID:23644470; http://dx.doi.org/10.1038/ncb2745
3. Gehlen L, et al. Progress of Theoretical Physics Supplement 2011; 191:20-9; http://dx.doi.org/10.1143/PTPS.191.20
4. Dion V, et al. Nat Cell Biol 2012; 14:502-9; PMID:22484486; http://dx.doi.org/10.1038/ncb2465
5. Miné-Hattab J, et al. Nat Cell Biol 2012; 14:510-7; PMID:22484485; http://dx.doi.org/10.1038/ncb2472
6. Seeber A, et al. Genes Dev 2013; 27:1999-2008; PMID:24029917; http://dx.doi.org/10.1101/gad.222992.113
7. Roukos V, et al. Science 2013; 341:660-4; PMID:23929981; http://dx.doi.org/10.1126/science.1237150
8. Ui A, et al. Oncogene 2013; PMID:23584481; http://dx.doi.org/10.1038/onc.2013.125

CHAPTER 3: COHESIN AND THE NUCLEOLUS CONSTRAIN THE MOBILITY OF SPONTANEOUS REPAIR FOCI

Vincent Dion, Veronique Kalck, Andrew Seeber, Thomas Schleker, and Susan M. Gasser

Friedrich Miescher Institute for Biomedical Research, Maulbeerstrasse 66, 4058 Basel, Switzerland

EMBO reports, Volume 14, pp 984-991

Summary

The regulation of chromatin mobility in response to DNA damage is important for homologous recombination in yeast. Anchorage reduces rates of recombination, whereas increased chromatin mobility correlates with more efficient homology search. Here we tracked the mobility and localization of spontaneous S-phase lesions bound by Rad52, and found that these foci have reduced movement, unlike enzymatically induced double-strand breaks. Moreover, spontaneous repair foci were positioned in the nuclear core, abutting the nucleolus. We show that cohesin and nucleolar integrity constrain the mobility of these foci, consistent with the notion that spontaneous, S-phase damage is preferentially repaired from the sister chromatid.

This article was of particular significance since it showed that not all types of damage show increased chromatin movement and that foci of different tagged repair enzymes including Rad51, Rad52, and Rad54 are enriched in the nuclear core. In addition, we show the nucleolus constrains movement of spontaneous Rad52-YFP foci. Importantly, this work confirms that chromatin movement is greater in G1 than in S phase as proposed by Heun et al., 2001. Here it is shown that the decreased S phase movement is due to cohesin loading.

Author contributions: V.D. and S.M.G planned experiments and wrote the manuscript. V.D. and V.K. performed most of the experiments. A.S. performed experiments in Figure 5G. T.S. performed experiment in Figure S3.

EMBO reports

TRANSPARENT PROCESS

scientific report

Cohesin and the nucleolus constrain the mobility of spontaneous repair foci

Vincent Dion[1], *Véronique Kalck*[1], *Andrew Seeber*[1,2], *Thomas Schleker*[1†] & *Susan M. Gasser*[1,2+]

[1]Friedrich Miescher Institute for Biomedical Research, and [2]Faculty of Natural Sciences, University of Basel, Basel, Switzerland

The regulation of chromatin mobility in response to DNA damage is important for homologous recombination in yeast. Anchorage reduces rates of recombination, whereas increased chromatin mobility correlates with more efficient homology search. Here we tracked the mobility and localization of spontaneous S-phase lesions bound by Rad52, and find that these foci have reduced movement, unlike enzymatically induced double-strand breaks. Moreover, spontaneous repair foci are positioned in the nuclear core, abutting the nucleolus. We show that cohesin and nucleolar integrity constrain the mobility of these foci, consistent with the notion that spontaneous, S-phase damage is preferentially repaired from the sister chromatid.

Keywords: DNA damage; Rad52 foci; chromatin dynamics; cohesin; nucleolus

EMBO *reports* (2013) **14,** 984–991. doi:10.1038/embor.2013.142

INTRODUCTION

Double-strand breaks (DSB) are particularly deleterious DNA lesions, as inappropriate repair can lead to translocations and genome instability [1]. Budding yeast efficiently repairs DSBs by homologous recombination (HR), which requires physical contact with a homologous template. Sister chromatids are the favoured template in S- and G2-phase cells, as they are exact copies of the damaged site, and are held together by cohesin. If a sister chromatid is unavailable or is similarly damaged, then a genome-wide search for a homologous template might take place [2].

In budding yeast, the Rad52 epistasis group composed of Mre11, Rad50, Xrs2, Rad52, Rad51 and Rad54, is responsible for catalyzing HR [3]. Each member is sequentially recruited to the DSB along with mediators of the DNA damage response, including the checkpoint kinase adaptor Rad9 (53BP1/BRCA1 in humans) [4]. These factors, when fused to a fluorescent protein, form microscopically discernible repair centres at the sites of damage [5], and are therefore convenient tools to study repair dynamics in living cells.

[1]Friedrich Miescher Institute for Biomedical Research, Maulbeerstrasse 66, [2]Faculty of Natural Sciences, University of Basel, CH-4056 Basel, Switzerland
[†]Present address: BioCampus Straubing GmbH, Europaring 4, 94315 Straubing, Germany
[+]Corresponding author. Tel: +41 61 697 5025; Fax: +41 61 697 3976; E-mail: susan.gasser@fmi.ch

Received 17 May 2013; revised 13 August 2013; accepted 13 August 2013; published online 10 September 2013

Most studies on mobility of repair foci have focused on Rad52, which accumulates at DSBs after resection [5] and disappears once pairing with the homologous template has occurred [6]. Rad52 foci form only in S-phase cells [7]. Quantitation of Rad52 focus mobility showed that enzymatically induced site-specific DSBs move within a larger volume than the same locus undamaged [6,8]. The enhanced mobility of Rad52 foci requires Rad51 and Rad54, as well as the checkpoint kinase, Mec1 and the checkpoint adaptor protein Rad9 [6,8]. Consistent with the notion that movement facilitates the homology search, increased mobility at DSBs correlates with faster production of repair intermediates and higher rates of recombination [8,9]. Moreover, artificially tethered domains recombine less frequently [10].

Locus mobility might also be harnessed to relocate a DSB away from domains that are repressive for HR, such as heterochromatin or the nucleolus [11–13], and can shift DSBs that lack a homologous donor for HR towards nuclear pores [14]. The proposal that chromatin mobility promotes the efficiency of DSB repair, particularly when a homology search beyond the sister chromatid is required [15], is consistent with a recent study that examined the effect of nuclear architecture on ectopic recombination in yeast [10].

Importantly, DSBs are not the only lesions that generate Rad52 foci. For example, the repair of replication fork collision with a covalent DNA-protein adduct similarly recruits Rad52 [16], as do other spontaneous lesions in S-phase cells [7]. These spontaneous lesions generally do not activate the DNA damage checkpoint or arrest the cell cycle. Unlike enzymatically induced DSBs, they appear to reflect damage on one of the two sister chromatids, which are held together by cohesin following replication. Indeed, spontaneous Rad52 foci appear to stem largely from gaps behind the replication fork [17], making them structurally distinct from the breaks induced by enzymes that repeatedly cleave both sister chromatids. Intriguingly, these two types of lesions segregate spatially within the yeast nucleus: irreparable DSBs were shown to shift to the nuclear envelope [14,18], whereas spontaneous Rad52 foci are predominantly found in the nuclear core [19].

Here we have explored the constraints that influence repair centre movement and position. Our results implicate cohesin and the nucleolus in constraining damage mobility, and support the hypothesis that reduced movement reflects the repair of spontaneous lesions by exchange with the sister chromatid.

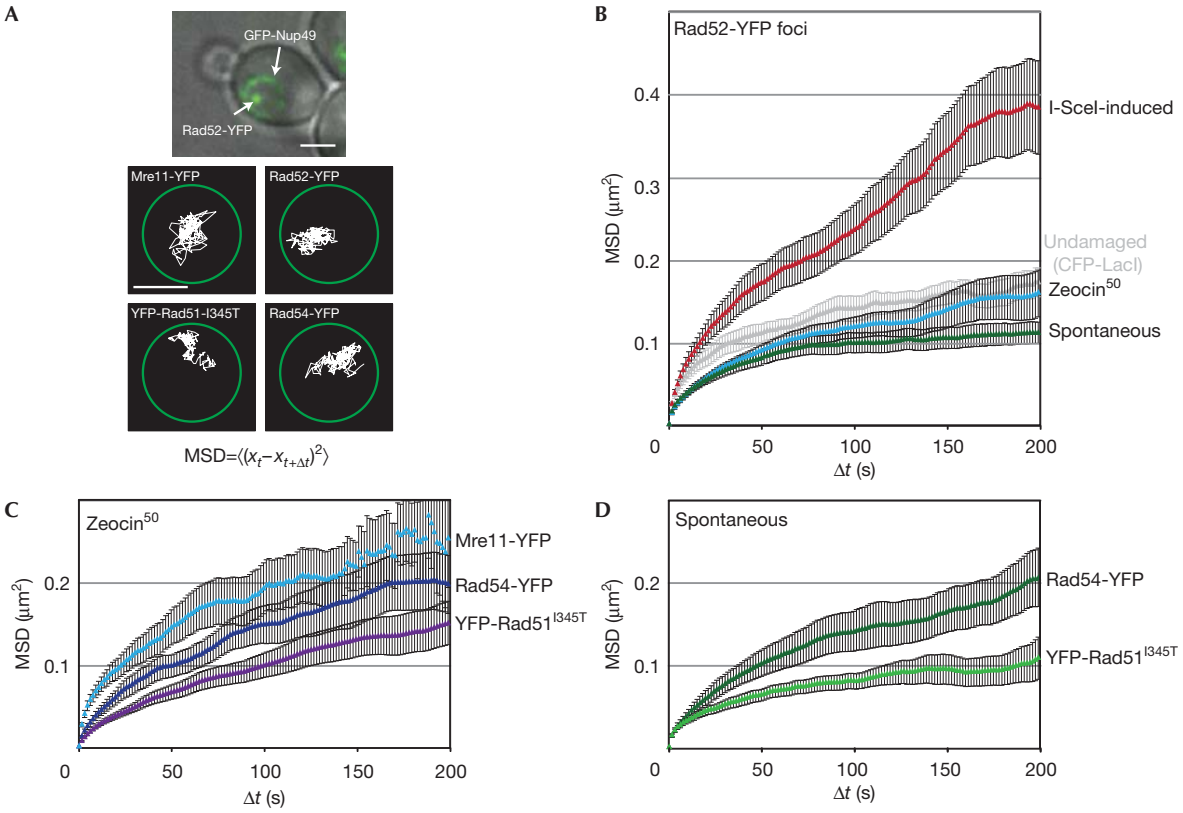

Fig 1 | The mobility of damaged DNA at various stages of repair. (**A**) Example of a Rad52-YFP focus in an S-phase cell (contrast-adjusted) in GA7997 (top). Scale bar, 2 μm. Bottom: Traces of Mre11-YFP (GA5832), Rad52-YFP (GA5820), YFP-Rad51^{I345T} (GA6057) and Rad54-YFP (GA5833) on Zeocin addition. Scale bar, 1 μm. (**B**) MSD analysis of I-SceI-induced Rad52-YFP foci and the same undamaged locus (*ZWF1*; in grey; 17 movies) in GA6208, Zeocin-induced (50 μg/ml for 1 h; 28 movies) and spontaneous (21 movies) Rad52-YFP foci in GA5820. The data in this panel are from [8]. (**C,D**) MSD analysis of Mre11-YFP (12 movies), YFP-Rad51^{I345T} (21 movies) and Rad54-YFP (10 movies) foci induced with 50 μg/ml Zeocin for 1 h (**C**) and for those that arose spontaneously (**D**; YFP-Rad51^{I345T}: 16 movies; YFP-Rad54: 13 movies). All movies were taken in S-phase, except for Mre11-YFP, which is six from each S and G1 phases. Error bars represent the standard error. GFP, green fluorescent protein; MSD, mean square displacement; YFP, yellow fluorescent protein.

RESULTS AND DISCUSSION

Mean square displacement (MSD) analysis robustly quantifies the mobility of diffusing, fluorescently tagged chromosomal loci and repair foci [6,8,9,15]. In such analyses, the position of a moving spot is monitored from frame to frame, and the square of the distance travelled by the locus is plotted against increasing time intervals (Fig 1A). The resulting MSD curve, averaged over several independent time-lapse series, generally reaches a plateau proportional to the square of the radius of constraint (Rc). This is a useful measure that indicates the nuclear volume (nvol) within which a fluorescent spot can move. All movement parameters relevant for this study are compiled in supplementary Table S1 online.

We have previously shown that the undamaged *ZWF1* locus on chromosome 14, has an Rc of about 0.51 μm in S-phase cells, which is equivalent to ~18% of the nvol (Fig 1B) [8]. Once an I-SceI-induced DSB is generated at this locus, the Rc value of the resulting Rad52-YFP focus increases to 0.7 μm (47% of nvol; Fig 1B) [8]. Not every Rad52 focus showed a similar mobility, however. For example, Rad52 foci induced by a limited dose of Zeocin (50 μg/ml for 1 h) have a mobility identical to that of an undamaged locus (Fig 1B). Similarly slow movement was detected for damage induced by the covalent binding of a mutated Flpase to DNA [8]. Surprisingly, spontaneous S-phase Rad52-YFP foci had an even lower Rc value (0.37 μm or 7% nvol; Fig 1B). We asked if spontaneous lesions were enriched in the ribosomal DNA (rDNA), but lesion localization by anti-Rad52 chromatin immunoprecipitation and deep sequencing failed to show significant enrichment for rDNA sequences (data not shown). Thus, we conclude that the type of DNA lesion determines the mobility of Rad52 foci.

In order to characterize the molecular constraints on spontaneously occurring S-phase damage, we asked whether the mobility of damaged DNA varies with different steps of the repair process. To this end, we fluorescently tagged several repair proteins besides Rad52, namely Mre11 (which binds transiently to the initial lesion in both S and G1 phases) and Rad51 and Rad54 (which both bind after 5′ end-resection). We determined the mobility of repair foci arising either spontaneously in S phase, or as a result of exposure to low-dose treatment with Zeocin, which induces single-strand nicks nine times more frequently than DSBs [20] (Fig 1C,D). As Rad51 is not functional when fused to YFP [5], we tracked both

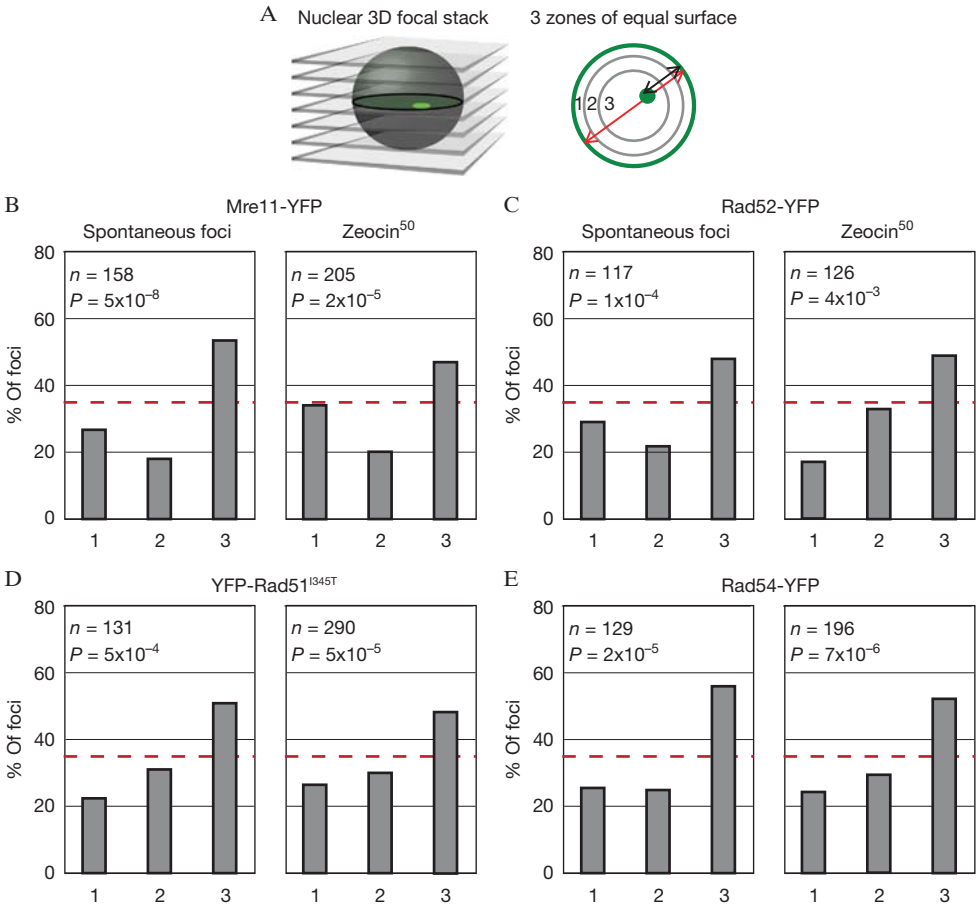

Fig 2 | Repair foci of tagged HR repair factors are enriched in the nuclear core. (**A**) Radial positions of repair foci were obtained by taking three-dimensional focal stacks of yeast nuclei and dividing the slice in which the spot is in focus into three zones of equal surface, with zone 1 being peripheral. (**B–E**) Zoning analysis of spontaneous and Zeocin-induced (50 μg/ml Zeocin for 1 h) Mre11-YFP foci (B; GA5832), Rad52-YFP (**C**; GA5820), YFP-Rad51^{I345T} (**D**; GA6057), and Rad54-YFP (**E**; GA5833). Number of nuclei analysed (*n*) and the *P*-value for a χ^2 test versus an expected random distribution are given. HR, homologous recombination; YFP, yellow fluorescent protein.

YFP-rad51 and a mutant of Rad51 that restores its activity in context of the YFP fusion, YFP-Rad51^{I345T} [21].

Mre11 is part of the early-binding MRN complex that holds the two free ends of a DSB together, and has a role in end-resection [3,22,23]. Whereas spontaneous Mre11 foci were too short-lived to be imaged reliably, both Zeocin-induced and I-SceI-induced foci of Mre11 could be tracked in both G1- and S-phase cells. I-SceI-induced Mre11 foci showed a high degree of mobility in both stages of the cell cycle (Rc = 0.81–0.82 μm; supplementary Fig S1A online), even though resection occurs only in S phase. Zeocin-induced Mre11-YFP foci had a lower Rc than I-SceI-induced foci (0.59 μm compared with 0.84 μm), yet was also unchanged between G1- and S-phase cells (supplementary Fig S1B online). Intriguingly, Zeocin-induced foci had a slightly higher mobility than undamaged loci in S phase, suggesting that the first response to damage is enhanced movement, which, for a short time, overrides the differences in constraint on chromatin mobility that correlate with stages of the cell cycle [24].

The tracking of spontaneous foci formed by a functional Rad51 fusion (YFP-Rad51^{I345T}) showed behaviour similar to Rad52-YFP foci: spontaneous damage was more constrained than Zeocin-induced foci (7% versus ~18% of nvol, respectively, Fig 1C,D). This was not the case for Rad54-YFP foci, which in both cases showed movement similar to that of an undamaged locus (~18% of nvol). Given that Rad54 acts after Rad51 and Rad52, it might be that at late steps in the repair process, damage-induced changes in mobility are exhausted. Importantly, there was no instance in which either spontaneous or low-level Zeocin-induced foci showed the high level of mobility that is typical of an I-SceI-induced, irreparable DSB. Indeed, one major difference between I-SceI-induced damage and spontaneous Rad52 foci is that the latter do not activate the checkpoint kinase Mec1, which is required for enhanced DSB movement [8].

To test whether perinuclear anchoring accounts for the reduced mobility of spontaneous or low-level Zeocin-induced damage, we determined the radial position of the resulting repair foci using a well-characterized 3-zone assay [25,26] (Fig 2A). We find that all types of spontaneous foci (that is, those scored in the mobility assays above) are enriched in the nuclear interior (Fig 2B–E). This resembles the distribution of Rad52 foci that arise from cleavage at the *MAT* locus, which is rapidly repaired by recombination with sequences at *HMR* or *HML* [19]. This result argues that the low

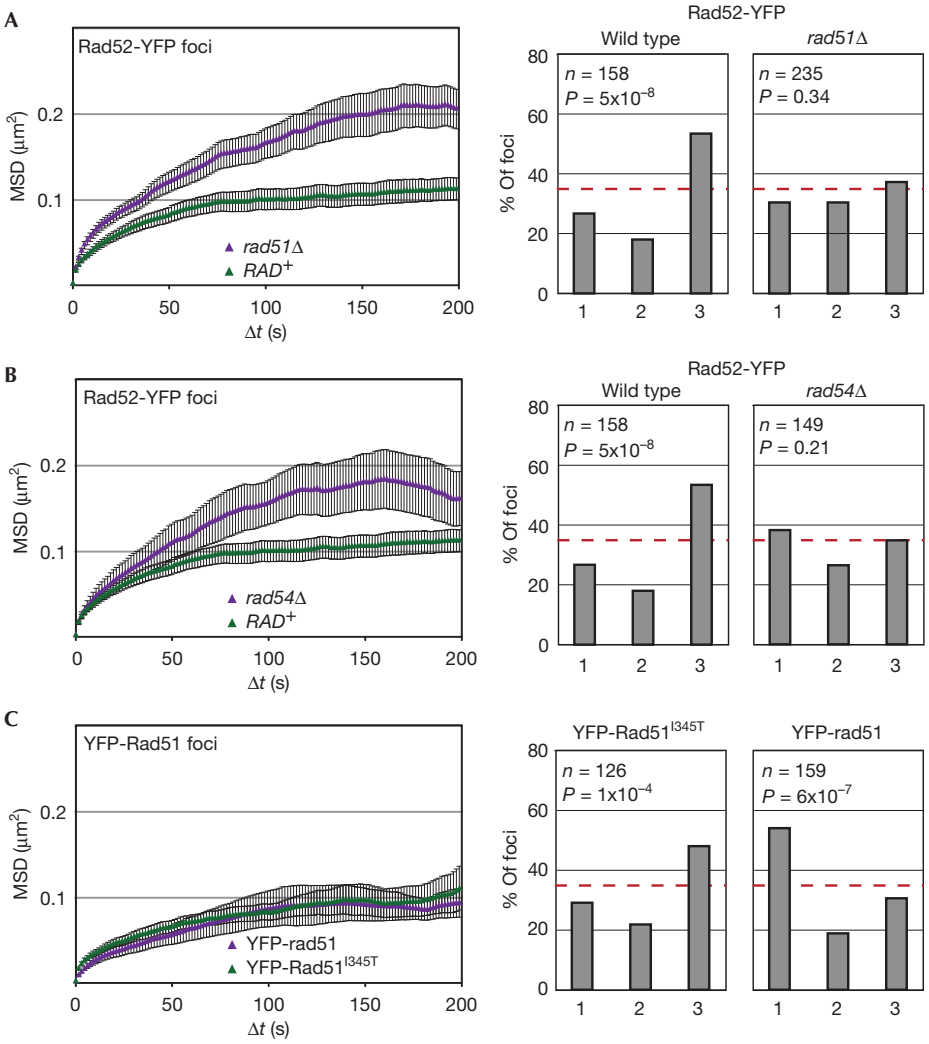

Fig 3 | HR factors help constrain the mobility and non-peripheral enrichment of repair foci. (**A–C**) MSD analyses of spontaneous Rad52-YFP foci in *rad51Δ* (GA5836; 28 movies) and *rad54*Δ (GA6110; 13 movies) strains. MSD was also performed on foci of YFP-rad51 (GA6106; 9 movies) and YFP-Rad51^{I345T} (GA6057; 16 movies). Spontaneous Rad52-YFP foci in wild type (GA5820) and YFP-Rad51^{I345T} (GA6057) cells as in Fig 1. To the right are zoning assays of spontaneous Rad52 foci in wild type, *rad51*Δ *or rad54*Δ strains, or for YFP-rad51 (GA6106) and YFP-Rad51^{I345T} (GA6057) in a wild-type background Number of nuclei analysed (*n*) and the *P*-value for a χ^2 test versus an expected random distribution are given. The error bars on the MSD curves represent the s.e. HR, homologous recombination; MSD, mean square displacement; YFP, yellow fluorescent protein.

mobility of spontaneous foci does not reflect their association with nuclear pores or other peripheral anchorage sites.

We next examined whether the increased mobility of Zeocin-induced damage over spontaneous foci reflects differential activation of the DNA damage checkpoint response, as appears to be the case for I-SceI-induced DSBs [8]. To this end, we monitored the mobility of spontaneous and Zeocin-induced Rad52-YFP foci, as well as that of an undamaged locus, in a *rad9* mutant, which impairs checkpoint activation. While we found a slight increase in the mobility of undamaged DNA in *rad9*Δ cells, there was no longer a difference in the mobility of spontaneous and Zeocin-induced Rad52 foci (supplementary Fig S2 online). Thus, the slight increase in mobility of a Zeocin-induced focus over a spontaneous focus might indeed reflect activation of the DNA damage response.

It remained to determine what elements restrict the mobility of spontaneous Rad52 foci. Given that Rad51 and Rad54 actively contribute to the enhanced movement of an I-SceI-induced DSB [8], we targeted these ATPases for deletion. Intriguingly, we found that loss of Rad51 or Rad54 partially relaxed the constraint on spontaneous Rad52-YFP foci (Fig 3A,B), which is the opposite of their effect on an induced DSB [8]. Nonetheless, in neither mutant did the Rad52 focus reach the mobility observed for an induced DSB.

The subnuclear distribution of spontaneous Rad52-YFP foci was also altered in cells lacking Rad51 or Rad54, as spontaneous foci were now randomly distributed, rather than being internally enriched (Fig. 3A,B). This suggests that spontaneous damage becomes irreparable in these mutants, and moves, like an irreparable DSB, to the nuclear periphery. Consistent with this interpretation, we found that foci containing the non-functional

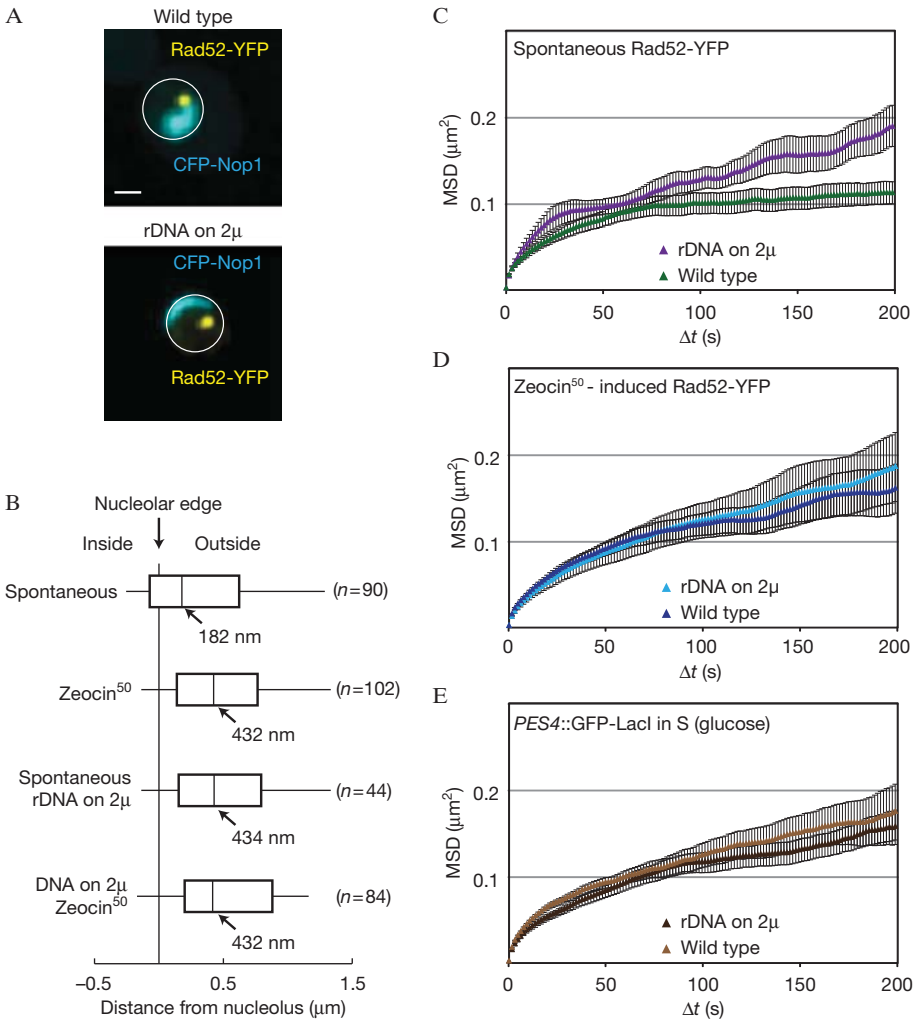

Fig 4 | Spontaneous Rad52-YFP foci are constrained by the nucleolus. (**A**) Representative images of wild-type cells (GA5820) and those harbouring the rDNA on a multicopy plasmid (GA7997), both expressing CFP-Nop1. The CFP-Nop1 signal in the strain carrying the rDNA on a plasmid was ~10-fold lower than in wild type, and thus brightness is adjusted. Scale bar, 1 μm. (**B**) Distances between Rad52-YFP foci and the nucleolus marked by CFP-Nop1 in GA5820 and GA7997. The number of nuclei analysed (*n*) is given for each condition. (**C,D**) MSD analyses of spontaneous (**C**) and Zeocin-induced (**D**) Rad52-YFP foci in both wild-type cells with (GA5820; 21 and 28 movies, respectively) or without the rDNA on a 2 μ plasmid (GA7997; 16 and 26 movies, respectively). 50 μg/ml Zeocin treatment was for 1 h. (**E**) MSD analysis of the LacO-tagged *PES4* locus in wild type (GA1461; 20 movies) and in cells with the 5S and 35S on a 2 μ plasmid (GA8147; 22 movies). Analyses were done on S-phase cells. The error bars on the MSD curves represent the s.e. CFP, cyan fluorescent protein; MSD, mean square displacement; rDNA, ribosomal DNA; YFP, yellow fluorescent protein.

YFP-rad51 fusion were enriched at the nuclear periphery, whereas functional YFP-Rad51^{I345T} foci stayed internal (Fig 3C). In both strains, however, the foci showed constrained mobility (Fig 3C). Thus, the presence of Rad51 at spontaneous lesions seems to constrain mobility, and its ability to support HR determines whether the resulting repair focus will be internal (that is, HR positive) or peripheral (HR negative). In conclusion, both the mobility and localization of repair foci are influenced by HR proteins. In their absence, a default state might prevail, which confers mobility equivalent to the undamaged site with no preferential position within the nucleus. Alternatively, the nature of the underlying lesion might change fundamentally in *rad51*Δ or *rad54*Δ cells, which might also alter mobility or position of the repair foci.

We next looked for structures that might constrain repair foci in the nuclear interior. One of the few identified substructures in the yeast nuclear core that could anchor foci is the nucleolus, which occupies about a third of the nvol. Indeed, mammalian chromosomal loci associated with the nucleolus are slow moving [27]. We scored the position of spontaneous and Zeocin-induced Rad52-YFP foci relative to the periphery of the nucleolus, which we tagged with a fluorescent marker (Fig 4A). The distances measured between the centre of each spontaneous Rad52-YFP focus and the nucleolar periphery yielded a median of 182 nm, whereas the more mobile Zeocin-induced foci were further away (median = 432 nm; $P = 0.003$; Fig 4B). These results indicate that the spontaneous repair foci are adjacent to the nucleolar surface,

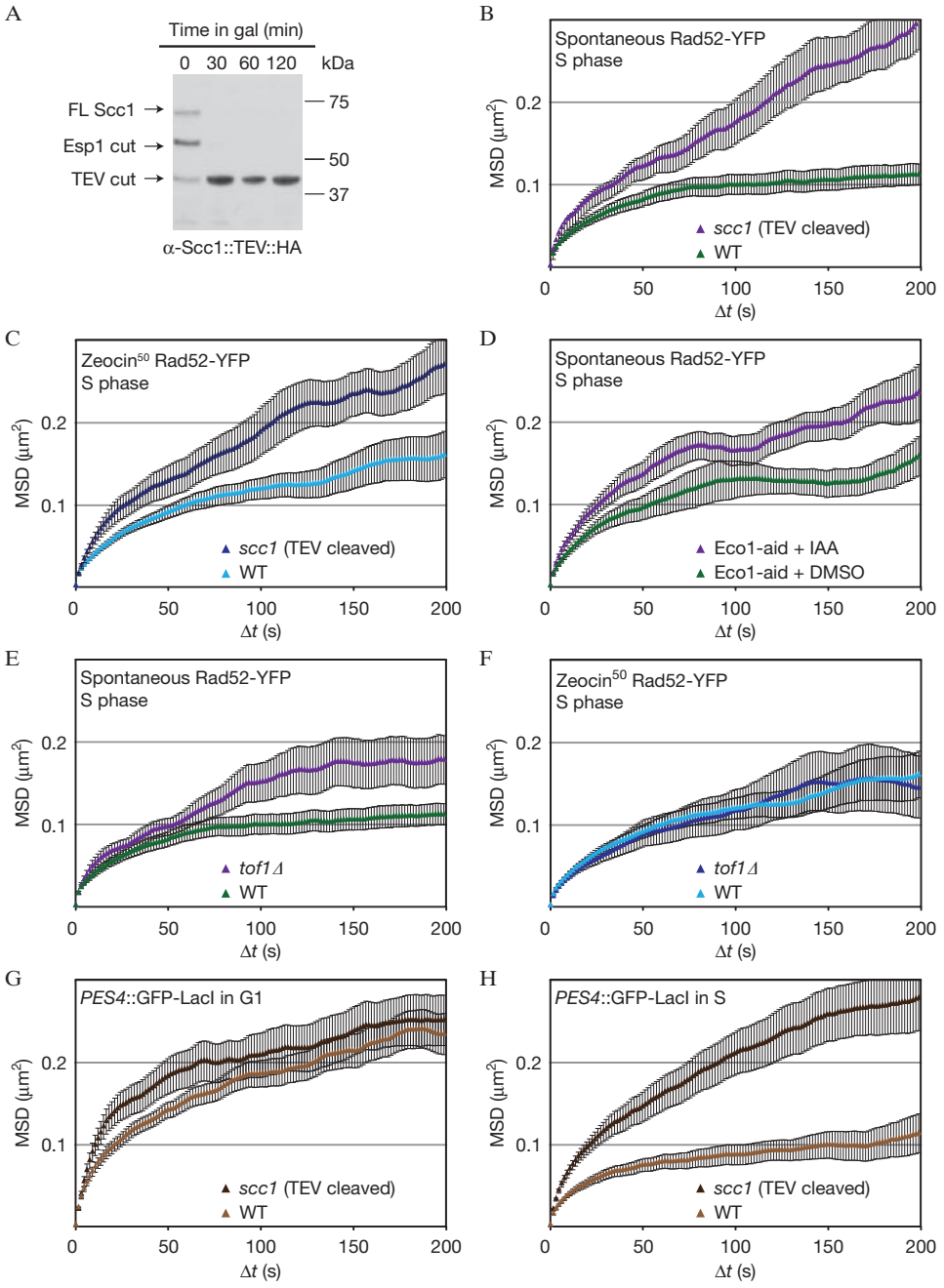

Fig 5 | Sister chromatid cohesion constrains Rad52-YFP foci and undamaged chromatin. (**A**) Western blot showing efficient cleavage of Scc1::TEV on TEV induction in GA7757. (**B,C**) MSD analyses of spontaneous (**B**) and Zeocin-induced (C; 50 μg/ml for 1 h) Rad52-YFP foci after cleavage of cohesin (GA7757; 11 and 12 movies, respectively) compared with wild type (GA5820; 21 and 28 movies as in Fig 1). (**D**) MSD analysis of spontaneous Rad52-YFP foci in cells containing the Eco1-aid allele (GA8193) treated with DMSO (12 movies) or auxin (IAA; 14 movies). Only S-phase cells were analyzed. (**E,F**) MSD analysis of spontaneous and Zeocin-induced Rad52-YFP foci in *tof1*Δ cells (GA8160; 11 and 12 movies, respectively) compared with wild-type cells (GA5820; 21 and 28 movies, respectively). (**G,H**) MSD curves of LacO-tagged *PES4* in GA1461 (wild type) and after cleavage of Scc1 (GA8112) in G1 (**D**; 26 and 22 movies, respectively) and S phase (**E**; 14 and 19 movies, respectively). The error bars on the MSD curves represent the s.e. MSD, mean square displacement; YFP, yellow fluorescent protein.

even though they are not enriched for rDNA lesions. Consistently, immunostaining of spontaneously occurring γH2A foci in S-phase cells also revealed strong enrichment at the nucleolar periphery (supplementary Fig S3 online).

If spontaneous, slow-moving Rad52-YFP foci are juxtaposed to the nucleolus, then, we reasoned that changing the shape and size of the nucleolus should alter the organization and mobility of these repair foci. To test this, we obtained a strain that carries its only

copies of the 5S and 35S rDNA genes on a multicopy plasmid [28]. In this strain, the nucleolus, detected by CFP-Nop1 fluorescence, is reduced by ~10-fold (Fig 4A). In this strain, spontaneous foci no longer associate with the nucleolar periphery (Fig 4B) and their mobility increases slightly, reaching the mobility of Zeocin-induced foci (Fig 4C). In contrast, the mobility of Zeocin-induced Rad52-YFP foci is not different between the wild-type cells and the rDNA-plasmid strain, consistent with the fact that they are not associated with the nucleolar surface (Fig 4D). Similarly, there is no general increase in chromatin mobility: the MSD curve for the undamaged *PES4* locus was unaltered (Fig 4E). We conclude that an intact nucleolar structure helps restrain the mobility of a spontaneous Rad52 focus.

While constraint is reduced in the strain with defective nucleolar structure, the Rad52 foci in these cells do not become as mobile as an I-SceI-induced DSB. This argues that additional forces restrict the movement of spontaneous and Zeocin-induced foci. As these foci arise almost exclusively in S-phase cells [7], when the sister chromatid is synthesized, we surmised that the damaged site and its sister might be linked to each other by a ring-like complex called cohesin [29]. The cohesin ring is closed at one end by a protein called Scc1, whose cleavage releases the sister chromatids from each other in mitosis [30].

To see if the tethering of sister chromatids by cohesion confers constraint on spontaneous sites of damage, we took advantage of a Scc1 construct (Scc1::TEV) that contains a TEV protease cleavage site [30]. In a strain carrying a galactose-inducible TEV construct, the addition of galactose provokes complete cleavage of Scc1 within 30 min (Fig 5A). We found that Scc1::TEV cleavage led to increased Rc values for both spontaneous and Zeocin-induced Rad52-YFP foci (0.59 and 0.56 μm, respectively; Fig 5B,C).

To confirm a role for sister chromatid cohesion (SCC) in constraining locus mobility, we exploited an allele of *ECO1*, which is fused to an auxin-inducible degron (Eco1-aid). Upon addition of auxin, Eco1 is rapidly degraded and sister chromatids separate [31]. Adding DMSO alone increased the mobility of both spontaneous Rad52 foci and undamaged loci slightly (Fig 5D, supplementary Fig S4A online), yet the addition of auxin led to an additional increase in mobility, exclusively in the Eco1-aid containing strain (Fig 5D, supplementary Fig S4A online). We therefore conclude that cohesin-dependent SCC restrains spontaneous Rad52-YFP foci in S-phase cells.

We further confirmed the role of SCC in constraining Rad52-YFP focus mobility by testing a *tof1* mutant, which also compromises the establishment of cohesion at forks and damage [32]. We find that chromatin mobility at an undamaged locus is only slightly affected in this background (supplementary Fig S4B online). On the other hand, *tof1*Δ increased the mobility of spontaneous Rad52-YFP foci (Fig 5E), but not that of Zeocin-induced foci (Fig 5F). We propose that Tof1-established SCC specifically confers constraint at spontaneous Rad52-YFP foci.

Next, we asked whether the increase in mobility due to loss of cohesin was specific to repair foci. We tracked the undamaged LacO-tagged *PES4* locus in G1- and S-phase cells, with and without Scc1 cleavage by TEV, because *PES4,* like most genomic loci, moves less in S-phase than in G1-phase cells [24]. Cleaving Scc1 did not increase chromatin mobility in G1, but led to a substantial increase in Rc in S-phase cells, suggesting that cohesin-mediated SCC is also responsible for cell cycle differences in mobility and not only for damage-specific constraint (Fig 5G,H). This is actually expected, as cohesin is not only loaded at sites of damage.

Finally, we tested whether contact with the nucleolar surface and SCC work together to constrain Rad52-YFP foci. Although Scc1 cleavage led to a dissolution of nucleolar structure (supplementary Fig S4C online), *tof1*Δ cells retain normal nucleolar shape, which we monitor by CFP-Nop1 (supplementary Fig S4C online). In the strain with plasmid-borne rDNA loci and reduced nucleolar structure (Fig 4A), we additionally deleted *TOF1,* yet this did not further increase in the mobility of either spontaneous or Zeocin-induced Rad52-YFP foci (supplementary Fig S4DE online). This argues that the effects of SCC and of nucleolar structure are epistatic with respect to their impact on the mobility of Rad52 foci.

Our work suggests that both cohesin-mediated SCC and some aspects of nucleolar structure constrain the movement of spontaneous Rad52-YFP foci. What could the biological implications of confining spontaneous repair centres be? We propose a model whereby the slow mobility of repair centres favours repair with the tethered sister chromatid, while reducing the likelihood of deleterious ectopic recombination. In support of this hypothesis, the *scc1-73* mutant is defective in sister chromatid exchange, but has increased rates of ectopic recombination [33]. Moreover, several mutants defective in sister chromatid recombination, including those of H3K56 acetyltransferase Rtt109 and the repair factor Smc5/6, are defective in maintaining Rad52 foci outside of the nucleolus and have been associated with specific defects in sister chromatid recombination, while remaining competent for HR with ectopic donors [10,11,34–37]. Together with these results, our study supports a model whereby both chromatin mobility and the molecules that constrain it contribute to genome stability in face of a diverse range of genetic insults.

METHODS

Yeast strains and plasmids. The supplementary material online contains details about the strains and plasmids (supplementary Tables S2 and S3).

Microscopy. MSD and zoning analyses were done as described [8,9,19]. Time-lapse data for a given strain are based on several independent cultures or colonies of a given strain, filmed at different times. Details of the Zeocin treatment as well as the degradation of Scc1::TEV and Eco1-aid can be found in the supplementary information online.

Statistics. The *P*-values reported for the zoning assays represent a χ^2 test with d.f. = 2 comparing the experimental results to an expected random distribution. For the difference in the distance of the Rad52-YFP focus to the nucleolar periphery, we used a two-tailed Student's *t*-test. The error on the Rc was determined as described [8,9].

Supplementary information is available at EMBO *reports* online (http://www.emboreports.org).

ACKNOWLEDGEMENTS

We thank A. Ponti and R. Thierry for the Imaris add-on, R. Rothstein, O. Fritsch, F. Uhlmann, and L. Symington for strains and reagents. We are grateful to the FMI microscopy core for technical help, and F. Hamaratoglu and N. Hustedt for critical reading of the manuscript. This work has been supported by the Friedrich Miescher Institute for Biomedical Research, by a project grant from the Swiss National Foundation to S.M.G., the Swiss National Science Foundation "Frontiers

in Genetics" programme, and a Terri Fox Foundation postdoctoral fellowship to V.D. (#19759).

Author contributions: V.D. and A.S. designed the experiments, carried them out, interpreted results and contributed to the writing; V.K. and T.S. carried out the experiments and interpreted the results, and S.M.G., helped to design the experiments, interpreted the results and contributed to writing.

CONFLICT OF INTEREST

The authors declare that they have no conflict of interest.

REFERENCES

1. Alt FW, Zhang Y, Meng FL, Guo C, Schwer B (2013) Mechanisms of programmed DNA lesions and genomic instability in the immune system. *Cell* **152:** 417–429
2. Gehlen LR, Gasser SM, Dion V (2011) How broken DNA finds its template for repair: a computational approach. *Prog Theoret Physics Suppl* **191:** 20–29
3. Heyer WD, Ehmsen KT, Liu J (2010) Regulation of homologous recombination in eukaryotes. *Annu Rev Genet* **44:** 113–139
4. Finn K, Lowndes NF, Grenon M (2012) Eukaryotic DNA damage checkpoint activation in response to double-strand breaks. *Cell Mol Life Sci* **69:** 1447–1473
5. Lisby M, Barlow JH, Burgess RC, Rothstein R (2004) Choreography of the DNA damage response: spatiotemporal relationships among checkpoint and repair proteins. *Cell* **118:** 699–713
6. Mine-Hattab J, Rothstein R (2012) Increased chromosome mobility facilitates homology search during recombination. *Nat Cell Biol* **14:** 510–517
7. Lisby M, Rothstein R, Mortensen UH (2001) Rad52 forms DNA repair and recombination centers during S phase. *Proc Natl Acad Sci USA* **98:** 8276–8282
8. Dion V, Kalck V, Horigome C, Towbin BD, Gasser SM (2012) Increased mobility of double-strand breaks requires Mec1, Rad9 and the homologous recombination machinery. *Nat Cell Biol* **14:** 502–509
9. Neumann FR, Dion V, Gehlen LR, Tsai-Pflugfelder M, Schmid R, Taddei A, Gasser SM (2012) Targeted INO80 enhances subnuclear chromatin movement and ectopic homologous recombination. *Genes Dev* **26:** 369–383
10. Agmon N, Liefshitz B, Zimmer C, Fabre E, Kupiec M (2013) Effect of nuclear architecture on the efficiency of double-strand break repair. *Nat Cell Biol* **15:** 694–699
11. Torres-Rosell J *et al* (2007) The Smc5-Smc6 complex and SUMO modification of Rad52 regulates recombinational repair at the ribosomal gene locus. *Nat Cell Biol* **9:** 923–931
12. Chiolo I, Minoda A, Colmenares SU, Polyzos A, Costes SV, Karpen GH (2011) Double-strand breaks in heterochromatin move outside of a dynamic HP1a domain to complete recombinational repair. *Cell* **144:** 732–744
13. Jakob B, Splinter J, Conrad S, Voss KO, Zink D, Durante M, Lobrich M, Taucher-Scholz G (2011) DNA double-strand breaks in heterochromatin elicit fast repair protein recruitment, histone H2AX phosphorylation and relocation to euchromatin. *Nucleic Acids Res* **39:** 6489–6499
14. Nagai S *et al* (2008) Functional targeting of DNA damage to a nuclear pore-associated SUMO-dependent ubiquitin ligase. *Science* **322:** 597–602
15. Dion V, Gasser SM (2013) Chromatin movement in the maintenance of genome stability. *Cell* **152:** 1355–1364
16. Nielsen I, Bentsen IB, Lisby M, Hansen S, Mundbjerg K, Andersen AH, Bjergbaek L (2009) A Flp-nick system to study repair of a single protein-bound nick *in vivo*. *Nat Methods* **6:** 753–757
17. Gonzalez-Prieto R, Munoz-Cabello AM, Cabello-Lobato MJ, Prado F (2013) Rad51 replication fork recruitment is required for DNA damage tolerance. *EMBO J* **32:** 1307–1321
18. Oza P, Jaspersen SL, Miele A, Dekker J, Peterson CL (2009) Mechanisms that regulate localization of a DNA double-strand break to the nuclear periphery. *Genes Dev* **23:** 912–927
19. Bystricky K, Van Attikum H, Montiel MD, Dion V, Gehlen L, Gasser SM (2009) Regulation of nuclear positioning and dynamics of the silent mating type loci by the yeast Ku70/Ku80 complex. *Mol Cell Biol* **29:** 835–848
20. Povirk LF (1996) DNA damage and mutagenesis by radiomimetic DNA-cleaving agents: bleomycin, neocarzinostatin and other enediynes. *Mutat Res* **355:** 71–89
21. Fung CW, Mozlin AM, Symington LS (2009) Suppression of the double-strand-break-repair defect of the *Saccharomyces cerevisiae* rad57 mutant. *Genetics* **181:** 1195–1206
22. Lobachev K, Vitriol E, Stemple J, Resnick MA, Bloom K (2004) Chromosome fragmentation after induction of a double-strand break is an active process prevented by the RMX repair complex. *Curr Biol* **14:** 2107–2112
23. Kaye JA, Melo JA, Cheung SK, Vaze MB, Haber JE, Toczyski DP (2004) DNA breaks promote genomic instability by impeding proper chromosome segregation. *Curr Biol* **14:** 2096–2106
24. Heun P, Laroche T, Shimada K, Furrer P, Gasser SM (2001) Chromosome dynamics in the yeast interphase nucleus. *Science* **294:** 2181–2186
25. Heun P, Laroche T, Raghuraman MK, Gasser SM (2001) The positioning and dynamics of origins of replication in the budding yeast nucleus. *J Cell Biol* **152:** 385–400
26. Meister P, Gehlen LR, Varela E, Kalck V, Gasser SM (2010) Visualizing yeast chromosomes and nuclear architecture. *Methods Enzymol* **470:** 535–567
27. Chubb JR, Boyle S, Perry P, Bickmore WA (2002) Chromatin motion is constrained by association with nuclear compartments in human cells. *Curr Biol* **12:** 439–445
28. Johzuka K, Horiuchi T (2009) The cis element and factors required for condensin recruitment to chromosomes. *Mol Cell* **34:** 26–35
29. Nasmyth K, Haering CH (2009) Cohesin: its roles and mechanisms. *Annu Rev Genet* **43:** 525–558
30. Uhlmann F, Wernic D, Poupart MA, Koonin EV, Nasmyth K (2000) Cleavage of cohesin by the CD clan protease separin triggers anaphase in yeast. *Cell* **103:** 375–386
31. Lopez-Serra L, Lengronne A, Borges V, Kelly G, Uhlmann F (2013) Budding yeast Wapl controls sister chromatid cohesion maintenance and chromosome condensation. *Curr Biol* **23:** 64–69
32. Mayer ML *et al* (2004) Identification of protein complexes required for efficient sister chromatid cohesion. *Mol Biol Cell* **15:** 1736–1745
33. Tittel-Elmer M, Lengronne A, Davidson MB, Bacal J, Francois P, Hohl M, Petrini JH, Pasero P, Cobb JA (2012) Cohesin association to replication sites depends on rad50 and promotes fork restart. *Mol Cell* **48:** 98–108
34. De Piccoli G *et al* (2006) Smc5-Smc6 mediate DNA double-strand-break repair by promoting sister-chromatid recombination. *Nat Cell Biol* **8:** 1032–1034
35. Cortes-Ledesma F, Aguilera A (2006) Double-strand breaks arising by replication through a nick are repaired by cohesin-dependent sister-chromatid exchange. *EMBO Rep* **7:** 919–926
36. Wurtele H *et al* (2012) Histone H3 lysine 56 acetylation and the response to DNA replication fork damage. *Mol Cell Biol* **32:** 154–172
37. Munoz-Galvan S, Jimeno S, Rothstein R, Aguilera A (2013) Histone H3K56 acetylation, Rad52, and non-DNA repair factors control double-strand break repair choice with the sister chromatid. *PLoS Genet* **9:** e1003237

Supplementary methods:

Drug treatments and growth conditions: Zeocin treatments were done at a concentration of 50μg/ml for 1 hour. We then imaged the cells for 5 min/movie within the following hour. The distances between the nucleolus and the Rad52-YFP foci were determined using a custom made add-on to Imaris, which is available upon request. The add-on uses Imaris' spot finder and surface tool functions and determines the shortest distance between the spot and the surface. Scc1::TEV cleavage was done as described for I-SceI-induced DSBs [8]. We imaged the cells 30 min after galactose addition, which induces the expression of TEV, and no longer than 1.5 hour afterwards. During this time, samples are collected for Western blotting against HA-tagged Scc1::TEV, which was detected using the 12CA5 antibody. The auxin (1mM) and DMSO treatments in Fig. 5D were done for 1hr in G1-arrested cells. Cells were then released into S in the presence of auxin or DMSO and spontaneous Rad52-YFP foci arising during that first S-phase were tracked. Data presented for spontaneous, I-SceI-induced and Zeocin-induced Rad52-YFP foci are from [8]. Movies for spontaneous Rad52-YFP foci were obtained from cells growing in glucose or in galactose. Unlike what we observed for some tagged chromosomal loci, there was no difference between the two carbon sources for these foci.

Immunofluorescence: All immunostaining was done as described [36] using, as primary antibodies, a rabbit polyclonal against γH2A (SG-2397) described earlier (T. Schleker, unpublished), a mouse monoclonal antibody against Nop1 (A66; [37]) and counterstaining with DAPI.

Table S1: Summary of movement parameters

Focus tracked	Locus	Genotype	Treatment	Carbon source	Cell cycle	D (x10^{-3} μm^2/s)	Rc (μm)	No. of cells
CFP-LacI	*ZWF1*	WT	None	Gal	G1	2.2 ± 0.3	0.64 ± 0.07	9
	*ZWF1**	WT	None	Gal	S	1.3 ± 0.2	0.54 ± 0.05	12
GFP-LacI	*PES4*	WT	None	Gal	G1	1.6 ± 0.2	0.54 ± 0.03	26
	PES4	WT	None	Glu	S	0.93 ± 0.05	0.47 ± 0.04	20
	PES4	WT	DMSO	Glu	S	1.2 ± 0.1	0.48 ± 0.05	13
	PES4	WT	Auxin	Glu	S	0.94 ±0.1	0.49 ± 0.05	16
	PES4	*scc1*(TEV-cleaved)	None	Gal	G1	2.4 ± 0.3	0.56 ± 0.03	22
	*PES4***	WT	None	Gal	S	0.77 ± 0.1	0.38 ± 0.04	14
	PES4	*scc1*(TEV-cleaved)	None	Gal	S	1.6 ± 0.2	0.59 ± 0.04	19
	PES4	*tof1*Δ	None	Glu	S	1.0 ± 0.1	0.48 ± 0.03	18
	PES4	rDNA on 2μ	None	Glu	S	0.80 ± 0.06	0.44 ± 0.03	22
mCherry-tetR	*met10***	WT	None	Glu	S	0.8 ± 0.07	0.41 ± 0.03	20
	*met10***	*rad9*⊿	None	Glu	S	0.91 ± 0.07	0.49 ± 0.03	26

Mre11-YFP	-	WT	50µg/ml Zeocin	Glu	G1+S	1.4 ± 0.2	0.59 ± 0.08	12
	-	WT	50µg/ml Zeocin	Glu	G1	1.2 ± 0.9	0.52 ± 0.04	6
	-	WT	50µg/ml Zeocin	Glu	S	1.7 ± 0.3	0.65 ± 0.06	6
	ZWF1	WT	I-SceI	Gal	G1	2.2 ± 0.6	0.82 ± 0.07	11
	ZWF1	WT	I-SceI	Gal	S	2.1 ± 0.8	0.81 ± 0.08	9
Rad52-YFP	*ZWF1**	WT	I-SceI	Gal	S	1.7 ± 0.1	0.70 ± 0.05	17
	-*	WT	None	Glu+Gal	S	0.74 ± 0.1	0.37 ± 0.02	21
	-	*rad51⊿*	None	Glu	S	1.3 ± 0.1	0.51 ± 0.02	28
	-	*rad54⊿*	None	Glu	S	0.95 ± 0.2	0.48 ± 0.04	13
	-	*rad9⊿*	None	Glu	S	0.85 ± 0.01	0.47 ± 0.04	12
	-*	WT	50µg/ml Zeocin	Glu	S	0.77 ± 0.1	0.45 ± 0.04	28
	-	*rad9⊿*	50µg/ml Zeocin	Glu	S	0.93 ± 0.1	0.47 ± 0.03	13
	-	rDNA on 2µ	None	Glu	S	1.1 ± 0.2	0.49 ± 0.03	16
	-	rDNA on 2µ	50µg/ml Zeocin	Glu	S	0.74 ± 0.1	0.48 ± 0.05	26
	-	*scc1*(TEV-cleaved)	None	Gal	S	1.3 ± 0.2	0.61 ± 0.04	11
	-	*scc1*(TEV-cleaved)	50µg/ml Zeocin	Gal	S	1.3 ± 0.2	0.58 ± 0.04	13
	-	*ECO1-aid*	DMSO	Glu	S	0.9 ± 0.1	0.45 ± 0.03	12
	-	*ECO1-aid*	Auxin	Glu	S	1.4 ± 0.2	0.55 ± 0.04	14
	-	*tof1⊿*	None	Glu	S	1.1 ± 0.2	0.47 ± 0.04	11
	-	*tof1⊿*	50µg/ml Zeocin	Glu	S	0.78 ± 0.1	0.44 ± 0.05	12
	-	*tof1⊿* rDNA on 2µ	None	Glu	S	0.75 ± 0.1	0.44 ± 0.04	14
	-	*tof1⊿* rDNA on 2µ	50µg/ml Zeocin	Glu	S	0.74 ±0.1	0.43 ± 0.05	17
YFP-Rad51^{I345T}	-	WT	None	Glu	S	0.60 ± 0.1	0.37 ± 0.04	16
	-	WT	50µg/ml Zeocin	Glu	S	0.59 ± 0.1	0.44 ± 0.04	21
YFP-rad51	-	WT	None	Glu	S	0.56 ± 0.1	0.38 ± 0.03	9
Rad54-YFP	-	WT	None	Glu	S	0.78 ± 0.1	0.51 ± 0.04	13
	-	WT	50µg/ml Zeocin	Glu	S	0.86 ± 0.1	0.50 ± 0.04	10

*: data taken from [8].

**: data taken from A. Seeber, V. Dion, S.M. Gasser, submitted.

Table S2: Strain used in this study*

Strain name	Genotype	Reference
GA1461	*his3*::GFP-LacI::*HIS3* GFP-Nup49 *PES4*::LacO array::*TRP1*	[38]
GA5820	RAD52-YFP GFP-Nup49 *RAD5 ADE2*	[8]
GA5832	Mre11-YFP GFP-Nup49 *RAD5 ADE2*	This study
GA5833	Rad54-YFP GFP-Nup49 *RAD5 ADE2*	This study
GA5836	RAD52-YFP GFP-Nup49 *rad51 RAD5 ADE2*	This study
GA6057	YFP-Rad51-I345T::*URA3*::*rad51* GFP-Nup49 *RAD5 ADE2*	This study
GA6106	YFP-rad51 GFP-Nup49 *RAD5 ADE2*	This study
GA6208	Rad52-YFP GFP-Nup49 *ADE2*::TetR-mCherry::*ade2 lys5*::LacI-CFP-*TRP1*, *leu2*::LoxP, *ZWF1*:cutsite (lmn::lys5::IsceI$_{cs}$::*LEU2*::LacO array::lmn)** *RAD5*	[8]
GA6879	Rad52-YFP GFP-Nup49 *ADE2*::TetR-mCherry::*ade2 lys5*::LacI-CFP-*TRP1*, *leu2*::LoxP, *ZWF1*:cutsite (lmn::lys5::IsceI$_{cs}$::*LEU2*::LacO array::lmn)** *met10*::HIS3::TetO array::LexA *RAD5*	A. Seeber, V. Dion, S.M. Gasser, submitted
GA7173	Mre11-YFP GFP-Nup49 *ADE2*::TetR-mCherry::*ade2 lys5*::LacI-CFP-*TRP1*, *leu2*::LoxP, *ZWF1*:cutsite (lmn::lys5::IsceI$_{cs}$::*LEU2*::LacO array::lmn)** *RAD5*	This study
GA7512	RAD52-YFP GFP-Nup49 *rad9*::NAT^{R} *RAD5 ADE2*	This study
GA7555	Rad52-YFP GFP-Nup49 *ADE2*::TetR-mCherry::*ade2 lys5*::LacI-CFP-*TRP1*, *leu2*::LoxP, *ZWF1*:cutsite (lmn::lys5::IsceI$_{cs}$::*LEU2*::LacO array::lmn)** *met10*::HIS3::TetO array::LexA *rad9*::NAT^{R} *RAD5*	A. Seeber, V. Dion, S.M. Gasser, submitted
GA7757	*scc1*::*HIS3*, Scc1-TEV268-3xHA::*LEU2*, Gal1-10p::NLS-myc9-TEV-NLS2::*TRP1* (10-fold integrants by Southern) RAD52-YFP GFP-Nup49 *ADE2*	This study
GA7869	RAD52-YFP GFP-Nup49 *rad51*::NAT^{R} *RAD5 ADE2*	This study
GA7997	RAD52-YFP GFP-Nup49 rDNA::*HIS3*::hisG 5S and 35S with endogenous promoter on 2μ plasmid (pKJ299-*TRP1*)	This study

GA8112	*scc1*::*HIS3*, Scc1-TEV268-3xHA::*LEU2*, Gal1-10p::NLS-myc9-TEV-NLS2::*TRP1* (10-fold integrants by Southern) RAD52-YFP *his3*::GFP-LacI::*HIS3* GFP-Nup49 *PES4*::LacO array::*TRP1 ADE2*	This study
GA8147	RAD52-YFP GFP-Nup49 rDNA::*HIS3*::hisG *his3*::GFP-LacI::*HIS3 PES4*::LacO array::*TRP1* 5S and 35S with endogenous promoter on 2μ plasmid (pKJ299-*TRP1*)	This study
GA8160	RAD52-YFP GFP-Nup49 *tof1*::*caURA3 RAD5 ADE2*	This study
GA8168	*his3*::GFP-LacI::*HIS3* GFP-Nup49 *PES4*::LacO array::*TRP1 tof1*::*caURA3*	This study
GA8170	RAD52-YFP GFP-Nup49 rDNA::*HIS3*::*hisG tof1*::*caURA3* 5S and 35S with endogenous promoter on 2μ plasmid (pKJ299-*TRP1*)	This study
GA8193	ADH1-OsTir1-9myc::URA3 Eco1-AID::KanMX6 RAD52-YFP GFP-Nup49 *RAD5 ADE2*	This study

*: All strains in this study are *MAT*<u>*a*</u> and isogenic to W303, except for GA1275, which a *MATa* strain isogenic to S288C.

**: lmn are unique sequences from the *lmn*-1 gene from *C. elegans*. Also note that the CFP-LacI is very faint in this strain.

Table S3: Plasmids used in this study

Plasmid name	SG number	Content	Reference
pFN4	1742	CFP-Nop1 CEN/ARS *URA3*	[39]
pVIN-65	2405	I-SceI on Gal1-10 promoter CEN/ARS *URA3*	[8]
pVIN-95	2538	CEN/ARS *URA3*	[8]

<u>Supplementary References:</u>

36. Meister P, Towbin BD, Pike BL, Ponti A, Gasser SM (2010) The spatial dynamics of tissue-specific promoters during C. elegans development. *Genes Dev* **24:** 766-782

37. Teixeira MT, Siniossoglou S, Podtelejnikov S, Benichou JC, Mann M, Dujon B, Hurt E, Fabre E (1997) Two functionally distinct domains generated by in vivo cleavage of Nup145p: a novel biogenesis pathway for nucleoporins. *EMBO J* **16:** 5086-5097

38. Taddei A, Hediger F, Neumann FR, Bauer C, Gasser SM (2004) Separation of silencing from perinuclear anchoring functions in yeast Ku80, Sir4 and Esc1 proteins. *EMBO J* **23:** 1301-1312
39. Bystricky K, Laroche T, van Houwe G, Blaszczyk M, Gasser SM (2005) Chromosome looping in yeast: telomere pairing and coordinated movement reflect anchoring efficiency and territorial organization. *J Cell Biol* **168:** 375-387

Supplementary Figure Legends:

Fig. S1: Mre11-YFP foci move as much in S and G1 phases. A-B) MSD curves for I-SceI-induced Mre11-YFP foci at *ZWF1* in GA7173 and for Zeocin-induced foci (in GA5832) in G1 (Top) and budded S-phase (Bottom) cells. The mobility of I-SceI-induced Rad52-YFP foci and of the undamaged *ZWF1* locus is S-phase cells are from [8].

Fig. S2: The difference in mobility between spontaneous and Zeocin-induced Rad52-YFP foci depends on Rad9. A) MSD analysis of spontaneous and Zeocin-induced (50μg/ml for 1h) Rad52-YFP foci in S-phase *rad9* cells (GA7512). B) MSD analysis of the TetO-tagged *met10* locus in S-phase cells from WT (GA6879) and *rad9⊿* cells (GA7555), see Seeber, Dion, Gasser, submitted.

Fig. S3: Localization of spontaneous γH2A foci near the nucleolus. Nine fluorescently stained S-phase nuclei (GA1275) processed by immunofluorescence for γH2A (red) and the nucleolus (Nop1, green) and DAPI (blue), show that spontaneous γH2A localize near the nucleolar periphery. Scale bar = 1μm.

Fig. S4: Sister chromatid cohesion and Tof1 are required for constrained mobility of spontaneous Rad51-YFP focus mobility. A) MSD analysis of the LacO-tagged *PES4* locus in GA1461 in normally growing S-phase cells (no treatment) or those treated with DMSO or auxin (IAA). B) MSD curve of the LacO-tagged *PES4* locus in WT (GA1461) or *tof1* mutant cells (GA8168). C-D) MSD analysis of spontaneous (C) and Zeocin-induced (D) Rad52-YFP foci in wild-type (GA5820 - data as in Fig. 1), and *tof1* mutant cells (GA8160). E) Nucleolar structure marked by CFP-Nop1 in WT cells (GA5820), in cells where Scc1 is cleaved by induction of TEV in galactose for 1h (GA7757), and in *tof1⊿* cells. F-G) MSD analysis of spontaneous (F) or Zeocin-induced (G) Rad52-YFP foci in *tof1⊿* (GA8170) and in cells that additionally have their rDNA on a 2μ vector.

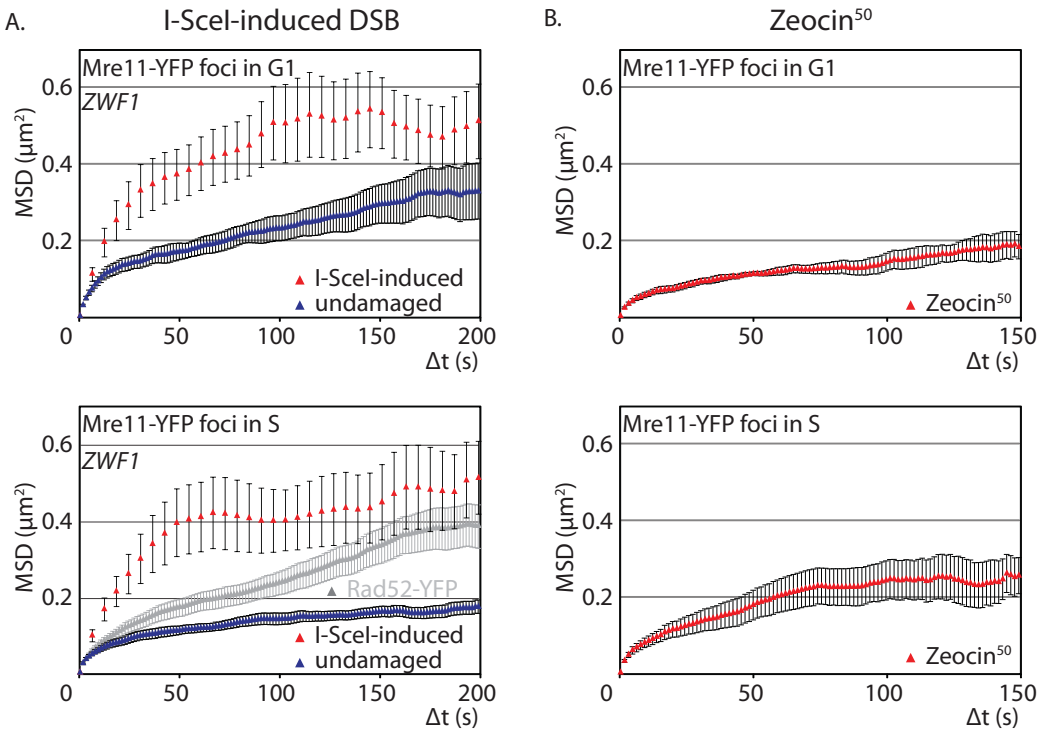
A.
I-SceI-induced DSB
Mre11-YFP foci in G1
ZWF1
MSD (μm²)
0.6
0.4
0.2
0
50
100
150
200
Δt (s)
I-SceI-induced
undamaged
Mre11-YFP foci in S
ZWF1
Rad52-YFP
I-SceI-induced
undamaged
B.
Zeocin50
Mre11-YFP foci in G1
Zeocin50
Mre11-YFP foci in S
Zeocin50

Figure S1

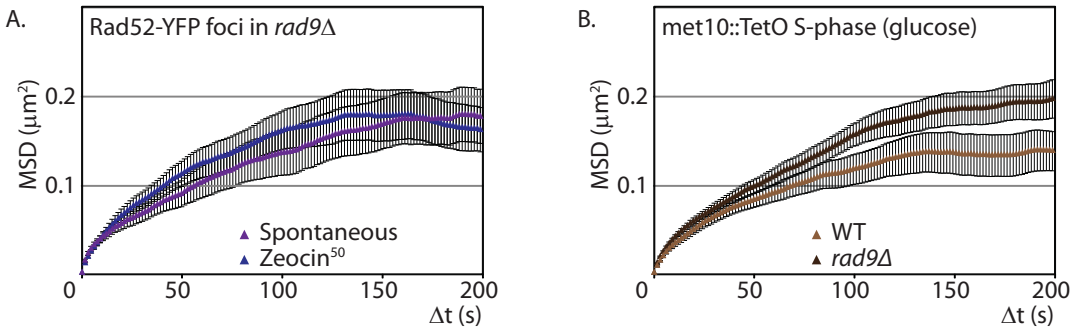
A.
Rad52-YFP foci in rad9Δ
MSD (μm²)
0.2
0.1
0
50
100
150
200
Δt (s)
Spontaneous
Zeocin50
B.
met10::TetO S-phase (glucose)
MSD (μm²)
0.2
0.1
0
50
100
150
200
Δt (s)
WT
rad9Δ

Figure S2

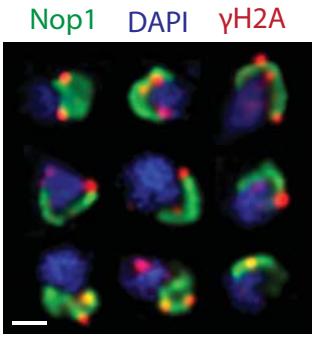

Figure S3

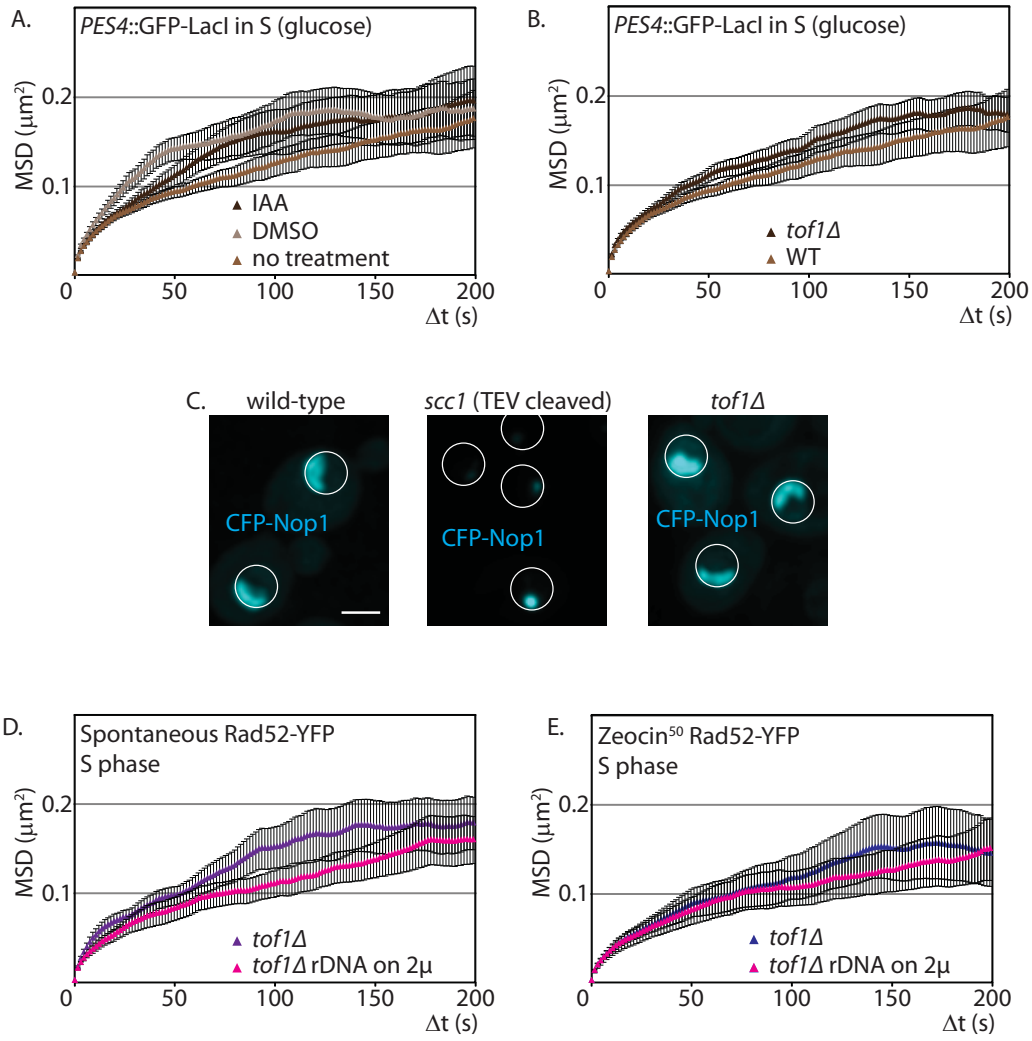
A.
PES4::GFP-LacI in S (glucose)
MSD (μm²)
0.2
0.1
IAA
DMSO
no treatment
0
50
100
150
200
Δt (s)
B.
PES4::GFP-LacI in S (glucose)
MSD (μm²)
0.2
0.1
tof1Δ
WT
0
50
100
150
200
Δt (s)
C.
wild-type
scc1 (TEV cleaved)
tof1Δ
CFP-Nop1
CFP-Nop1
CFP-Nop1
D.
Spontaneous Rad52-YFP
S phase
MSD (μm²)
0.2
0.1
tof1Δ
tof1Δ rDNA on 2μ
0
50
100
150
200
Δt (s)
E.
Zeocin50 Rad52-YFP
S phase
MSD (μm²)
0.2
0.1
tof1Δ
tof1Δ rDNA on 2μ
0
50
100
150
200
Δt (s)

Figure S4

CHAPTER 4: CHECKPOINT KINASES AND THE INO80 NUCLEOSOME REMODELING COMPLEX ENHANCE GLOBAL CHROMATIN MOBILITY IN RESPONSE TO DNA DAMAGE

Andrew Seeber, Vincent Dion, and Susan M. Gasser

Friedrich Miescher Institute for Biomedical Research, Maulbeerstrasse 66, 4058 Basel, Switzerland

Genes and Development 2013, Volume 27, pp 1999-2008

Summary

Double-strand break repair by recombination requires a homology search. In yeast, induced breaks move significantly more than undamaged loci. To examine whether DNA damage provokes an increase in chromatin mobility generally, we tracked undamaged loci under DNA-damaging conditions. We found that the yeast checkpoint factors Mec1, Rad9, and Rad53 are required for genome-wide increases in chromatin mobility, but not the repair protein Rad51. Mec1 activation by targeted Ddc1/Ddc2 enhances chromatin mobility even in the absence of damage. Finally, the INO80 chromatin remodeler is shown to act downstream from Mec1 to increase chromatin mobility, highlighting an additional damage-related role of this nucleosome remodeling complex.

This study was important because it cleared up a controversy at the time of publication, which was whether or not damage-induced global chromatin mobility existed. We showed that damage-induced chromatin mobility did in fact occur and that mobility of undamaged chromosomes increased in a DNA damage-dependent manner. We uncovered the first components of the mechanism of damage-induced mobility, the DNA damage checkpoint and the chromatin remodeling enzyme, INO80. This publication set the stage for determining what drives damage-induced chromatin movement.

Author contributions: A.S., V.D. and S.M.G planned experiments and wrote the manuscript. A.S. performed most of the experiments. V.D. did the Ddc1/2- GFP targeting experiments in Figure 3.

Checkpoint kinases and the INO80 nucleosome remodeling complex enhance global chromatin mobility in response to DNA damage

Andrew Seeber,[1,2] Vincent Dion,[1] and Susan M. Gasser[1,2,3]

[1]Friedrich Miescher Institute for Biomedical Research, CH-4058 Basel, Switzerland; [2]Faculty of Natural Sciences, University of Basel, CH-4056 Basel, Switzerland

Double-strand break repair by recombination requires a homology search. In yeast, induced breaks move significantly more than undamaged loci. To examine whether DNA damage provokes an increase in chromatin mobility generally, we tracked undamaged loci under DNA-damaging conditions. We found that the yeast checkpoint factors Mec1, Rad9, and Rad53 are required for genome-wide increases in chromatin mobility, but not the repair protein Rad51. Mec1 activation by targeted Ddc1/Ddc2 enhances chromatin mobility even in the absence of damage. Finally, the INO80 chromatin remodeler is shown to act downstream from Mec1 to increase chromatin mobility, highlighting an additional damage-related role of this nucleosome remodeling complex.

[*Keywords*: DNA damage response; Mec1; chromatin mobility; double-strand breaks; INO80]

Supplemental material is available for this article.

Received May 29, 2013; revised version accepted August 23, 2013.

DNA double-strand breaks (DSBs) can be repaired by either homologous recombination (HR) or nonhomologous end-joining (NHEJ). Whereas NHEJ is the dominant pathway in G1-phase cells and in mammals, the more efficient and preferred pathway of repair in budding yeast is by HR. In the S and G2 phases of the cell cycle, recombinational repair makes use of the undamaged sister chromatid. However, if a sister chromatid is not present or if both sisters have been damaged, a search for an alternative homologous template ensues. This search appears to be rate-limiting for HR (Wilson et al. 1994; Agmon et al. 2013), and its efficiency was predicted to be affected by the mobility of both the break site and the homologous template (Gehlen et al. 2011). This notion is supported by computer simulations, which show that two randomly moving spots confined within a sphere collide more frequently than they would if one were immobile (Gehlen et al. 2011). New data on recombination rates in yeast support these predictions experimentally (Agmon et al. 2013).

Recent studies have also examined the mechanisms that drive chromatin movement of damaged sites (Dion et al. 2012; Krawczyk et al. 2012; Mine-Hattab and Rothstein 2012; Neumann et al. 2012; for review, see Dion and Gasser 2013). The recruitment of repair proteins, such as the strand exchange protein Rad51, enhances the movement of the broken DNA locus, tagged by Rad52-YFP (Dion et al. 2012). By analogy to the bacterial RecA, which contributes to the sequence search in three-dimensional (3D) space in vitro (Forget and Kowalczykowski 2012), Rad51 has also been suggested to mechanistically drive homology search (Renkawitz et al. 2013). In eukaryotes, Rad51 recruits the Snf2-type ATPase Rad54, which also contributes to the enhanced mobility of a DSB through an unknown mechanism (Dion et al. 2012).

Alongside these repair proteins, the DNA damage response (DDR) pathway appears to regulate the movement of the DSB. The resection of DNA at a cut site leads to activation of the ATR kinase complex Mec1/Ddc2 and, in turn, the downstream checkpoint kinase Rad53. These kinases regulate a number of processes, including cell cycle transitions, transcriptional programs, and DNA repair. Importantly, both Mec1 and its target protein, Rad9, were needed to increase the mobility of a DSB, whereas Rad53 was not (Dion et al. 2012).

It has remained unresolved whether undamaged chromatin also becomes more mobile in a nucleus that contains DNA damage. One report showed that the induction of a DSB at the *MAT* locus on chromosome (Chr) III

[3]**Corresponding author**
E-mail susan.gasser@fmi.ch
Article published online ahead of print. Article and publication date are online at http://www.genesdev.org/cgi/doi/10.1101/gad.222992.113.

in diploid yeast cells led to increased mobility of an undamaged site on the short arm of Chr V (Mine-Hattab and Rothstein 2012). In contrast, Dion et al. (2012) showed that an I-SceI endonuclease-induced DSB in haploid cells did not increase the mobility of an undamaged Chr VI locus, nor did treating cells with the DNA-damaging agent Zeocin at 50 μg/mL. The source of this discrepancy was unclear. Factors likely to influence the outcome include (1) the differential regulation of HR in haploid versus diploid yeast cells, (2) the types and levels of damage induced, or (3) the specific genomic context of the locus monitored; e.g., its proximity to a telomere or centromere. Indeed, the nuclear organization of chromosomes and chromosome territories do seem to affect the efficiency of repair by HR (Agmon et al. 2013). In this study, we set out to resolve this discrepancy. We found that checkpoint kinases in yeast induce a genome-wide alteration in chromatin structure, which is manifested as enhanced locus mobility, even in the absence of DNA damage. This increase in mobility appears to be driven by the INO80 nucleosome remodeling complex.

Results

DNA damage increases global chromatin mobility independently of Rad51

Here we exploited single-particle tracking of fluorescently tagged genomic loci in *Saccharomyces cerevisiae* to quantify the mobility of the chromatin fiber in vivo. To this end, we recorded 3D image stacks on a spinning-disc confocal microscope every 1.5 sec during 5 min. The images were then deconvolved (Ponti et al. 2007) and projected onto a two-dimensional (2D) plane (Fig. 1A). Using the ImageJ plug-in, spots were tracked with respect to the center of the nucleus (SpotTracker) (Sage et al. 2005), and the *X* and *Y* coordinates of the spot as well as the center of the nucleus were determined in each of the 200 images of a typical time-lapse movie. From these values, we calculated the mean-squared displacement (MSD = $\langle X_t - X_{t+\Delta t}\rangle^2$, where *X* is the position of a spot at time *t*). From the MSD plot, we derived the radius of constraint (Rc; the square root of the plateau of the MSD curve multiplied by 5/4) (Meister et al. 2010; Neumann et al. 2012), which is a robust measurement of locus confinement given that thousands of data points were averaged in each graph (Meister et al. 2010).

We tracked genomic loci that were tagged with mCherry-TetR (e.g., the *met10* locus on Chr VI) (Fig. 1A) or GFP-LacI (e.g., *ATG2* on the long arm of Chr XIV or *PES4* and *HXK1*, both on Chr VI). These haploid cells also express yellow fluorescent protein (YFP) fused to Rad52, which is fully functional for HR (Supplemental Table S1; Lisby et al. 2004). To ensure that we tracked an undamaged locus, time-lapse movie data was used only if the genomic tagged locus did not colocalize with Rad52-YFP. Moreover, we confirmed that our imaging regime itself does not induce damage by showing that cells divide with normal kinetics after imaging (Supplemental Fig. S1; Dion et al. 2012).

In line with earlier studies, we measured an Rc of 0.41 μm for the *met10* locus in haploid S-phase cells grown on glucose in the absence of damage (Dion et al. 2012; Mine-Hattab and Rothstein 2012). This value indicates that the locus can sample ~9.5% of the nuclear volume (nvol) (Fig. 1D). We note that movement is higher in G1-phase cells as compared with S-phase cells (Heun et al. 2001) and that the Rc of undamaged loci can range from 0.4 to 0.6 μm, depending on the chromosomal location of the tagged locus (Table 1; Supplemental Fig. S2; Heun et al. 2001; Gartenberg et al. 2004; Bystricky et al. 2009).

To examine the movement of the undamaged locus in a cell responding to DNA damage, we next exposed cells bearing the tagged *met10* locus to increasing doses of Zeocin, a copper-chelated glycopeptide antibiotic that induces both DSBs and single-strand nicks, in the ratio of ~1:9 (Povirk 1996; Burger 1998). After 1 h of treatment with Zeocin, we assessed DDR activation by scoring for phosphorylated forms of H2A and Rad53 (Fig. 1B) and the frequency of Rad52-YFP foci formed (Fig. 1C). Surprisingly, the tagged and undamaged *met10* locus exhibited an increase in mobility after Zeocin treatment, increasing with the concentration of Zeocin used and reaching a maximum of nvol searched of ~34% at 250 μg/mL Zeocin (Fig. 1D). The tracked locus did not colocalize with Rad52-YFP, although each nucleus analyzed had a Rad52-YFP focus elsewhere at both the beginning and end of the movie. In agreement with our previous report, low-level Zeocin (50 μg/mL) did not increase mobility at an undamaged site (Dion et al. 2012), but inducing more damage with higher levels of Zeocin did (Fig. 1C,D).

We then examined whether the increase in chromatin mobility was locus-dependent by scoring the movement of three LacO-tagged loci (*PES4*, *ATG2*, and *HXK1*) on different chromosomes. Each showed an equivalent increase in mobility upon Zeocin treatment, although their chromosomal locations varied significantly, with one being subtelomeric (*HXK1*) (Supplemental Fig. S2A,B). The undamaged loci tested all showed an increase in mobility, albeit slightly less than that scored at the site of damage (Fig. 1E; Table 1).

To rule out that the increase was due to secondary effects unique to Zeocin, we expressed the restriction enzyme EcoRI in yeast cells bearing the tagged *met10* locus. EcoRI induces DSBs that can be monitored through Rad52-YFP foci formation (Fig. 1C). We found that induction of EcoRI also increased the Rc of the undamaged *met10* locus from 0.39 μm to 0.51 μm (from ~9% to ~18% nvol) (Fig. 1F). This increase is more modest than that scored at 250 μg/mL Zeocin and correlates with the reduced number of Rad52 foci formed upon EcoRI induction (Fig. 1C).

Given that specialized chromosomal domains (e.g., telomeres or centromeres) have been implicated in both constraining movement (Heun et al. 2001) and limiting recombination (Agmon et al. 2013), we speculated that the general increase in chromatin movement might arise from the release of perinuclear chromosomal anchorage points. To test this, we scored whether the subtelomeric, LacO-tagged locus *HXK1* loses its anchorage and moves

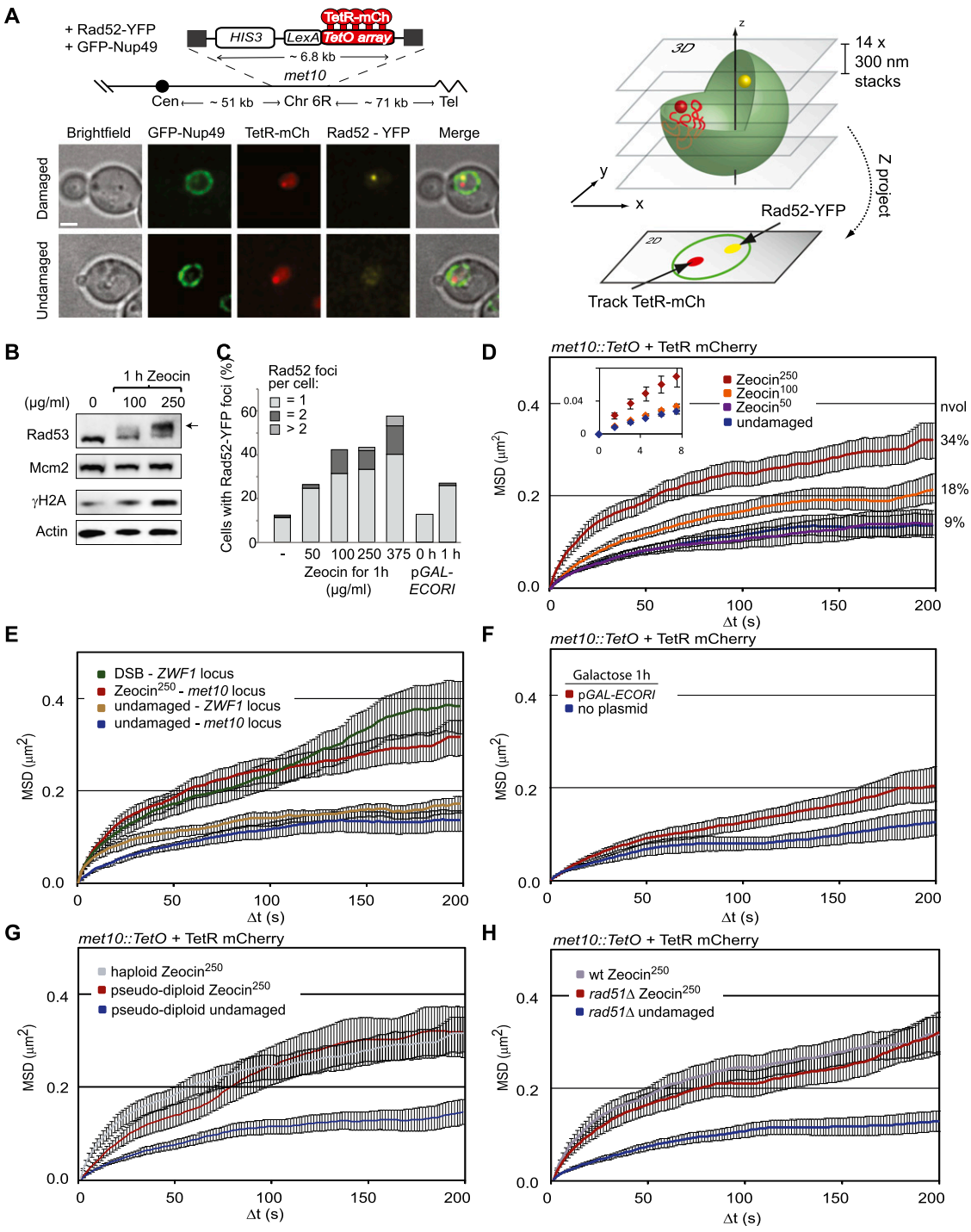

Figure 1. DNA damage causes a global increase in chromatin mobility. (*A*, *top*) Schematic of strain GA-6879 showing the tracked *met10::TetO* Locus. (*Bottom*) S-phase cell (GA-6879) after 1 h of Zeocin or undamaged. Shown is nuclear pore (GFP-Nup49), TetR-mCherry locus, and Rad52-YFP damage focus. Bar, 2 μm. (*Right*) Image stack is projected onto a 2D plane for tracking. (*B*) Western blot of Rad53 and H2A phosphorylation after 1-h Zeocin treatment of GA-6879. Actin and Mcm2 were used as loading controls. (*C*) Rad52-YFP foci accumulation after 1-h treatment with Zeocin or induction of *pGAL-ECORI*. Numbers of nuclei scored: 510 (undamaged), 311 (50 μg/mL Zeocin), 197 (100 μg/mL Zeocin), 395 (250 μg/mL Zeocin), 403 (375 μg/mL Zeocin), 102 (0 h *pGAL-ECORI*), and 124 (1-h *pGAL-ECORI*). (*D–H*) MSD plots of TetO-tagged *met10* in S-phase cells. (*D*) Without damage (blue) or incubated with Zeocin at 50, 100, or 250 μg/mL. The *inset* graph represents the first five time intervals to generate the initial slope. The percentage nuclear volume (nvol) explored is indicated. (*E*) MSD plot of LacO-tagged *ZWF1* (brown) and Rad52-YFP (green) compared with *met10::TetO* either with 1 h of Zeocin (red) or without (blue). *ZWF1* and I-SceI-induced Rad52-YFP from Dion et al. (2012). (*F*) MSD plots of *met10::TetO* after growth in 2% galactose for 1 h either with *pGAL-ECORI* (red) or without (blue). (*G*) MSD plots of *met10::TetO* during S phase in a pseudodiploid strain (GA-7591) with an extra copy of *MAT*α either without damage (blue) or after 1 h of 250 μg/mL Zeocin (red); MSD of *met10::TetO* in haploid GA-6879 (gray). (*H*) MSD of *met10::TetO* in *rad51Δ* cells (GA-7550) without damage (blue) or after 1 h of 250 μg/mL Zeocin (red) or in wild-type cells (GA-6879) in 250 μg/mL Zeocin (light gray). All error bars show the SEM. The numbers of movies tracked and parameters are given in Table 1.

Table 1. *Summary of MSD results presented in this study*

Spot tracked	Locus	Treatment	Features	Rc	Cell number
mCh-TetR	*met10::TetO*	Undamaged		0.41 μm ± 0.03 μm	20
mCh-TetR	*met10::TetO*	Zeocin 50 μg/mL		0.42 μm ± 0.04 μm	17
mCh-TetR	*met10::TetO*	Zeocin 100 μg/mL		0.51 μm ± 0.05 μm	13
mCh-TetR	*met10::TetO*	Zeocin 250 μg/mL		0.63 μm ± 0.04 μm	28
CFP-LacI	*ZWF1*	Undamaged[a]		0.46 μm ± 0.02 μm	20
Rad52-YFP	*ZWF1*	I-Sce1[a]		0.7 μm ± 0.05 μm	17
mCh-TetR	*met10::TetO*	CCCP 40 μM		0.08 μm ± 0.007 μm	10
mCh-TetR	*met10::TetO*	CCCP 40 μM + Zeocin 250 μg/mL		0.2 μm ± 0.06 μm	6
mCh-TetR	*met10::TetO*	Undamaged	Pseudodiploid	0.43 μm ± 0.04 μm	15
mCh-TetR	*met10::TetO*	Zeocin 250 μg/mL	Pseudodiploid	0.64 μm ± 0.05 μm	12
mCh-TetR	*met10::TetO*	Control[a]	No plasmid-gal	0.39 μm ± 0.04 μm	12
mCh-TetR	*met10::TetO*	Induced *ECO-RI*	p*GAL-ECORI*-gal	0.51 μm ± 0.05 μm	15
mCh-TetR	*met10::TetO*	Undamaged	*sml1Δ*	0.35 μm ± 0.02 μm	30
mCh-TetR	*met10::TetO*	Zeocin 250 μg/mL	*sml1Δ*	0.47 μm ± 0.04 μm	26
mCh-TetR	*met10::TetO*	Undamaged	*mec1Δ sml1Δ*	0.32 μm ± 0.03 μm	19
mCh-TetR	*met10::TetO*	Zeocin 250 μg/mL	*mec1Δ sml1Δ*	0.36 μm ± 0.04 μm	16
mCh-TetR	*met10::TetO*	Undamaged	*rad9Δ*	0.49 μm ± 0.03 μm	26
mCh-TetR	*met10::TetO*	Zeocin 250 μg/mL	*rad9Δ*	0.46 μm ± 0.03 μm	21
mCh-TetR	*met10::TetO*	Undamaged	*rad53Δ sml1Δ*	0.39 μm ± 0.02 μm	18
mCh-TetR	*met10::TetO*	Zeocin 250 μg/mL	*rad53Δ sml1Δ*	0.41 μm ± 0.04 μm	24
mCh-TetR	*met10::TetO*	Undamaged	*rad51Δ*	0.40 μm ± 0.04 μm	21
mCh-TetR	*met10::TetO*	Zeocin 250 μg/mL	*rad51Δ*	0.63 μm ± 0.09 μm	13
GFP-LacI	*PES4::LacO*	GFP-LacI	No plasmid-gal	0.38 μm ± 0.04 μm	14
Ddc1/Ddc2-GFP-LacI	*PES4::LacO*	Gal-DDC1/2-FP-LacI	Ddc1/2-GFP-LacI-induced-gal	0.5 μm ± 0.04 μm	16
mCh-TetR	*LEU2::TetO*	GFP-LacI	No Ddc1/2-gal	0.27 μm ± 0.04 μm	11
mCh-TetR	*LEU2::TetO*	Gal-DDC1/2-GFP-LacI	Ddc1/2-GFP-LacI-induced-gal	0.41 μm ± 0.0 μm4	11
mCh-TetR	*LEU2::TetO*	Gal-DDC1/2-LacI (no LacO)	Ddc1/2-GFP-LacI-induced-gal	0.30 μm ± 0.03 μm	9
mCh-TetR	*met10::TetO*	Undamaged	*arp8Δ*	0.42 μm ± 0.02 μm	14
mCh-TetR	*met10::TetO*	Zeocin 250 μg/mL	*arp8Δ*	0.43 μm ± 0.02 μm	13
mCh-TetR	*met10::TetO*	Undamaged	*arp8Δ*$^{+}$*pARP8-URA3*	0.46 μm ± 0.04 μm	16
mCh-TetR	*met10::TetO*	Zeocin 250 μg/mL	*arp8Δ*$^{+}$*pARP8-URA3*	0.63 μm ± 0.05 μm	20
mCh-TetR	*met10::TetO*	Undamaged	*arp5Δ*	0.39 μm ± 0.05 μm	8
mCh-TetR	*met10::TetO*	Zeocin 250 μg/mL	*arp5Δ*	0.44 μm ± 0.04 μm	21
GFP-LacI	*PES4::LacO*	GFP-LacI	*arp8Δ* no Ddc1/2-gal	0.37 μm ± 0.02 μm	15
Ddc1/Ddc2-GFP-LacI	*PES4::LacO*	Gal-DDC1/2-GFP-LacI	*arp8Δ*; Ddc1/2-GFP LacI-induced-gal	0.41 μm ± 0.03 μm	12
mCh-TetR	*LEU2::TetO*	GFP-LacI	*arp8Δ*; Ddc1/2-GFP-LacI-induced-gal	0.30 μm ± 0.02 μm	10
mCh-TetR	*LEU2::TetO*	Gal-DDC1/2-LacI (no LacO)	*arp8Δ*; Ddc1/2-GFP-LacI-induced-gal	0.31 μm ± 0.02 μm	13

Indicated are the exact Rc values calculated from the indicated number of time-lapse series for the indicated loci. The "Features" column lists relevant phenotype/genotype and cell cycle stage and indicates when galactose (gal) replaced glucose.
[a]Data points from Dion et al. (2012).

away from the nuclear envelope after DNA damage. Although *HXK1* shows increased mobility, it does not lose its perinuclear localization upon incubation with Zeocin, suggesting that movement along the nuclear envelope increases (Supplemental Fig. S2D; Supplemental Table S2). This agrees with earlier results showing that yeast telomeres remained associated with the nuclear envelope after single DSB induction (Martin et al. 1999). The observed increase in chromatin mobility in the presence of damage is therefore not a passive event resulting from a loss of telomere anchoring.

Chromatin mobility in general depends on ATP (Heun et al. 2001; Weber et al. 2012), and the ionophore carbonyl cyanide m-chlorophenyl hydrazine (CCCP) was shown to reduce the mobility of chromosomal loci as well as of an excised chromatin ring (Heun et al. 2001; Gartenberg et al. 2004). Consistently, we found that preincubation of cells with 40 μM CCCP suppressed the general chromatin mobility induced by DNA damage (Supplemental Fig. S3A; Supplemental Table S2), suggesting a role for an active mechanism in this process.

The HR repair factors Rad51 and Rad54 are needed to increase mobility at the site of damage itself (Dion et al. 2012; Mine-Hattab and Rothstein 2012). We asked whether repair factors are similarly required for the increased mobility scored at undamaged loci, provoked by DNA lesions elsewhere in the genome. This is not the case; the Rc of the *met10* locus started at the same point in *rad51Δ*

and *RAD51*$^+$ cells and increased after incubation with 250 μg/mL Zeocin to equal degrees, reaching ~34% of nvol in both of these otherwise isogenic haploid strains (Fig. 1H).

In diploid yeast, Rad51 is hyperactive (Morgan et al. 2002), and it was suggested (Ira and Hastings 2012) that this hyperactivity might be responsible for the enhanced mobility observed at unbroken sites in diploid cells. To test this hypothesis, we integrated an extra copy of *MAT* bearing the opposite mating type information (*MAT*$\boldsymbol{\alpha}$) into our wild-type haploid strain (*MAT***a**). Rad51 is hyperactivated in this pseudodiploid strain, as in diploid yeast (Morgan et al. 2002; Haber 2012). Tracking of the *met10* locus yielded an increase in Rc upon treatment with Zeocin (from 0.43 μm to 0.65 μm) in the pseudodiploid that was indistinguishable from that in the haploid strain (Fig. 1G). Thus, the increase in chromatin mobility in response to damage is independent of the Rad51 hyperactivity associated with diploid cells and occurs equally in haploid and diploid strains.

The stage of the cell cycle has a clear effect on chromatin mobility, since in S-phase, movement is much decreased compared with G1 (Heun et al. 2001) due to constraint from sister–sister cohesion (Dion et al. 2013). We were unable to test G1-phase cells, since we used Rad52 focus formation as a marker for damage, and G2-phase nuclei often have distorted nuclear shapes that interfere with accurate tracking. We did score for differences in mobility between early and mid-S phase at *met10* and found a similar increase in response to damage at both stages (Supplemental Fig. S3B,C; Supplemental Table S2). Given that *met10* is early-replicating, it is likely that the tracked loci are replicated and have cohesin loaded (Dion et al. 2013).

The DDR increases global chromatin mobility

An earlier study showed that loss of Mec1, the homolog of human ATR kinase, compromised the increased mobility scored for an induced DSB, while loss of Rad53 (CHK2) did not (Dion et al. 2012). It was therefore of interest to test whether checkpoint kinase activation was necessary for the increase in chromatin mobility genome-wide. This was scored in a *sml1*Δ background because ablation of Sml1 up-regulates dNTP synthesis and suppresses the lethality of *mec1*Δ or *rad53*Δ strains (Zhao et al. 1998). Upon tracking *met10*, we found that the background chromatin mobility (Rc = 0.32 μm) in *mec1*Δ*sml1*Δ cells was nearly unchanged after 1 h of exposure to Zeocin (0.36 μm) (Fig. 2A), and loss of the DDR effector kinase Rad53 completely ablated the damage-induced increase in global chromatin mobility (Fig. 2B). Consistent with earlier observations, *sml1* deletion itself has a partial phenotype: The increase in general chromatin mobility after damage in a *sml1*Δ strain reaches 0.47 μm instead of the 0.65 μm of wild-type cells (Fig. 2C). This lower increase in mobility may reflect the fact that *sml1*Δ strains have altered dNTP levels, although overexpression of the factor Sml1, which down-regulates Rnr1, did not have a similar effect (data not shown). Nonetheless, *mec1*Δ*sml1*Δ or *rad53*Δ*sml1*Δ cells fail to show a damage-induced, global increase in chromatin mobility, while *sml1*Δ cells do.

Next, we tested the role of factors downstream from Mec1. One key target of Mec1 that contributes to both Rad53 activation and the downstream response is the BRCT-containing protein Rad9 (Vialard et al. 1998). Whereas *RAD9* deletion alone increased chromatin mobility in the undamaged state, it completely blocked the general chromatin mobility increase induced by Zeocin (Fig. 2D). By Western blot analysis, we confirmed that checkpoint activation was compromised in all of the DDR mutants tested. Interestingly, although mobility did not increase in the *rad9*Δ mutant, H2A phosphorylation was comparable with that in wild-type cells, indicating that this Mec1 phosphorylation target (γH2AX in mammals) does not induce chromatin movement (Fig. 2E), while the DNA checkpoint signaling cascade, which ends with Rad53 activation, does (Fig. 2F). Interestingly, Rad53, unlike Mec1/Ddc2, has a dispersed nuclear localization, allowing it to propagate changes throughout the nucleoplasm (Melo et al. 2001).

Checkpoint activation without DNA damage increases global chromatin mobility

The question remained whether checkpoint activation is sufficient to enhance chromatin movement in the absence of damage. To examine this, we constructed a strain containing GFP- and LacI-tagged versions of both Ddc1 and Ddc2, whose artificial juxtaposition is sufficient to initiate a damage-independent checkpoint response (Bonilla et al. 2008). Upon expression from a galactose-inducible promoter, these two proteins bound the integrated LacO array at *PES4* near *MET10* and created a GFP focus that could be tracked (Fig. 3A,B). Upon induction of Ddc1/Ddc2-GFP-LacI, the checkpoint was activated as indicated by H2A phosphorylation (Fig. 3C), and the Rc of the tagged *PES4* locus increased from 0.38 μm to 0.5 μm (Fig. 3B,D).

To see whether checkpoint activation in the absence of DNA damage suffices to trigger the general increase in chromatin mobility, we monitored the *LEU2::*TetO locus in these same conditions. Whereas overexpression of Ddc1/2-GFP-LacI without a LacO array at *PES4* did not cause an increase in mobility at *LEU2*, by targeting Ddc1/Ddc2 to *PES4::*LacO, not only did the *PES4* locus increase mobility, but also *LEU2*, albeit to a lower extent (Fig. 3B,E). Given that we saw a dose-dependent increase in mobility with Zeocin, we assume that this more modest increase reflects the efficiency of checkpoint activation. We conclude that DNA damage checkpoint activation is sufficient, even in the absence of DNA damage, to increase both local and global chromatin mobility.

Intact INO80 remodeler complex is required to increase chromatin mobility in trans

Several chromatin remodeling enzymes are targets of Mec1 and the checkpoint response (Morrison et al. 2007; Smolka et al. 2007). Since INO80 is known to increase the mobility of a locus to which it is targeted (Neumann et al.

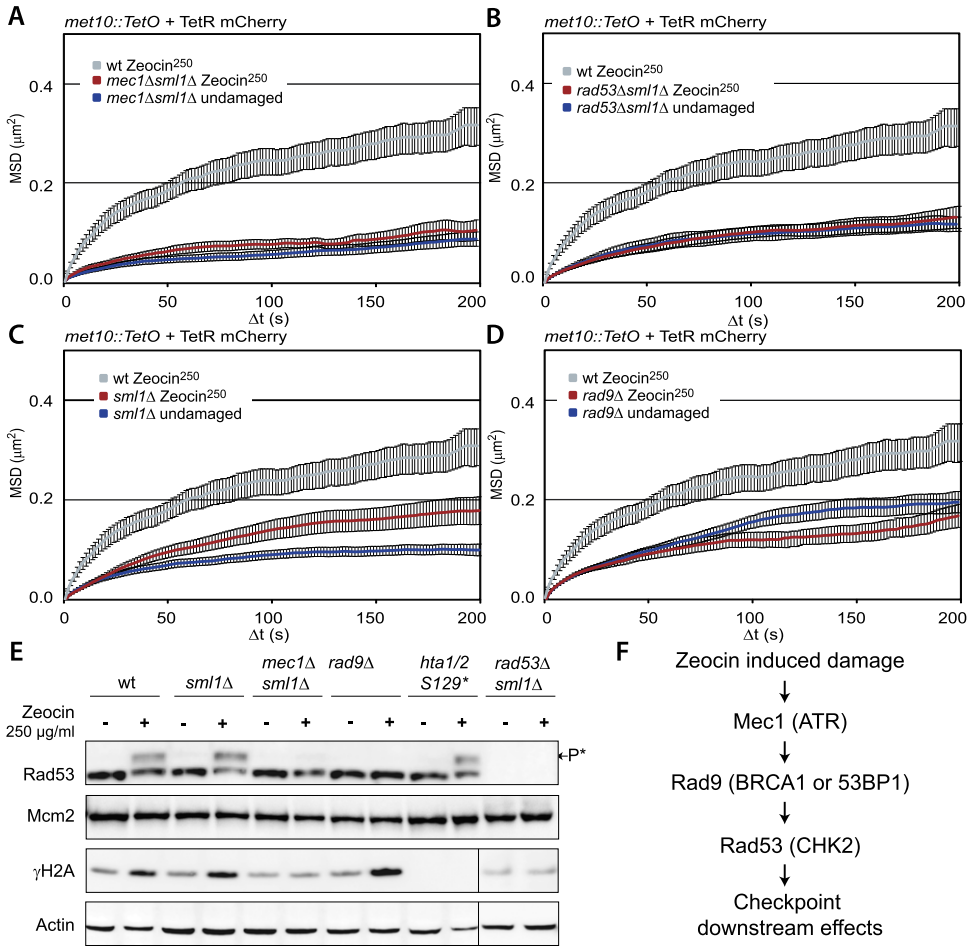

Figure 2. Checkpoint proteins Mec1, Rad9, and Rad53 are essential for damage-induced increases in global chromatin mobility. (*A–D*) MSD of *met10::TetO* in S-phase wild-type GA-6879 after 1 h of 250 μg/mL Zeocin (gray). MSD plots of the same locus without damage (blue) and Zeocin-treated (red) as above in the following backgrounds: *mec1Δsml1Δ* (GA-7556) (*A*), *rad53Δsml1Δ* (GA-7552) (*B*), *sml1Δ* (GA-7553) (*C*), and *rad9Δ* (GA-7555) (*D*). The error bars show the SEM. The numbers of movies tracked and parameters are given in Table 1. (*E*) Western blots showing checkpoint activation after 1 h of Zeocin (250μg/mL) as in Figure 1B, in wild-type (wt) (GA-6879), *sml1Δ* (GA-7553), *mec1Δsml1Δ* (GA-7556), *hta1/2 S129** (GA-4188), *rad9Δ* (GA-7555), and *rad53Δsml1Δ* (GA-7552) cells. (*F*) Scheme of key kinases and regulators in the DNA damage checkpoint.

2012) and has recently been implicated in various DSB repair events (Agmon et al. 2013), we hypothesized that it may have a role in increasing global chromatin mobility. We found that strains lacking either Arp5 or Arp8 abolish increased chromatin mobility after Zeocin treatment (Fig. 4A,B). Complementation of *arp8Δ* with wild-type Arp8 under its endogenous promoter restores chromatin mobility after Zeocin-induced damage just as it restores growth on Zeocin-containing plates (Fig. 4B,C). Importantly, we show that *arp8Δ* does not impair checkpoint activation on Zeocin (Fig. 4D), confirming previously published results on hydroxyurea (van Attikum et al. 2004). In contrast to INO80, we found that the Chd1 and Swr1 chromatin remodelers do not have an effect on global chromatin mobility, nor does the sister chromatid cohesion-promoting factor Tof1 (Supplemental Fig. S4; Supplemental Table S2).

To confirm that the INO80 complex is needed for global chromatin mobility in direct response to Mec1 activation, we targeted Ddc1/Ddc2 to activate movement in the absence of damage. Under these conditions, Arp8 was partially required to increase the mobility of a locus in *cis* (analogous to the partial effect of *arp8Δ* on DSB mobility) (Neumann et al. 2012), and its loss completely compromised the increased mobility of an undamaged locus (*LEU2*) (Fig. 4E,F). We conclude that the INO80 complex acts downstream from checkpoint activation and is needed to increase global chromatin mobility even when the checkpoint is activated artificially, without widespread DNA damage (Bonilla et al. 2008). The model in Figure 5 illustrates the two pathways that lead to enhanced chromatin mobility—one acting locally, and the second affecting chromatin mobility globally—both showing dependence on INO80.

Discussion

This study resolves the discrepancy between previous studies (Dion et al. 2012; Mine-Hattab and Rothstein

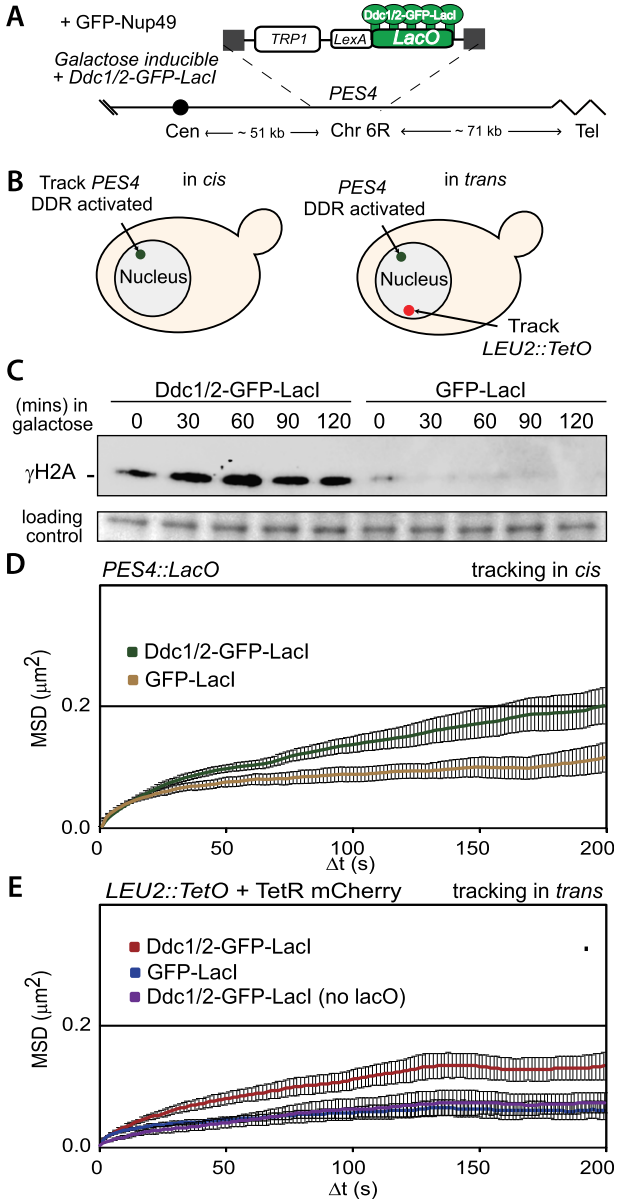

Figure 3. Checkpoint activation is sufficient to enhance both local and global chromatin mobility. (*A*) Schematic of strain GA-7676 showing the tracked locus at *PES4*. (*B*) Cartoon illustrating in *cis* tracking of Ddc1/Ddc2-GFP-LacI foci at *PES4* or in *trans* tracking of mCh-TetO at *LEU2*. (*C*) Western blot for H2A S129 phosphorylation after galactose induction of pGAL-Ddc1/2-GFP-LacI in GA-7676 or a wild-type (wt) strain, GA-1461. (*D*) MSD plots of LacO-tagged *PES4* during S phase after 1 h on galactose in cells expressing Ddc1/Ddc2-GFP-LacI (green; GA-7676) or GFP-LacI (brown; GA-1461). (*E*) TetR-mCherry at *LEU2* in a strain containing GFP-LacI (blue; GA-8088), expressing Ddc1/Ddc2-GFP-LacI in the presence (red; GA-8023) or absence (purple; GA-8158) of *PES4::lacO*. The numbers of movies tracked and parameters are given in Table 1.

2012) with respect to chromatin mobility at undamaged loci in cells exposed to damage. Chromatin mobility does indeed increase globally, yet the increase appears to require a threshold level of damage, which correlates with the induction of the DDR through Mec1 and Rad53 kinases. Low-level damage (e.g., after incubation with 50μg/mL Zeocin) does not provoke a detectable increase in general chromatin movement. We rule out other explanations for the discrepancy, such as cell ploidy or the type of damage induced. Moreover, we can exclude that the global increase in movement arises from chromosome fragmentation given that we scored a checkpoint kinase-dependent increase in mobility in the absence of damage. Finally, by scoring multiple loci, including telomeres, we rule out that the effect depends on the chromosomal context of the locus monitored.

Our studies suggest that changes in chromatin structure that lead to increased mobility in response to DNA damage are different at the site of damage as compared with an undamaged locus. Enhanced mobility in *cis* requires the repair factors Rad51 and Rad54 but is independent of Rad53 kinase activation. Global chromatin mobility increases require the downstream checkpoint kinase Rad53 but not the repair protein Rad51. We note that loss of Arp8 has only a partial effect on the increased mobility of a DSB, while it is essential for the global increase (Fig. 4B,D,F).

We speculate that differential control of chromatin mobility at damaged and undamaged sites may be advantageous to the cell. The enhanced movement of a DSB enhances the probability of harmful translocations or deletions even as it promotes a homology search for HR-mediated repair. The movement, like the checkpoint activation itself, is dependent on the level of damage, consistent with the two being linked. Mec1–Ddc2 activation requires both a threshold and a specific processing event at damage, which may be used to determine in which circumstances global chromatin movement should be enhanced to maximize recombinational repair. The genomic tradeoff for movement is likely to be an elevated risk of deleterious recombination (Dion and Gasser 2013; Seeber et al. 2013).

Several observations suggest that our insights are likely to be relevant to mammalian genomes. For one, recurrent translocations in B lymphocytes occur proportionally to DNA damage (Hakim et al. 2012), and down-regulation of 53BP1 (Rad9) reduces both chromatin mobility and chromosomal end-to-end fusions (Dimitrova et al. 2008). Furthermore, the mobility of arrays that generate translocations in mammalian cells is significantly higher than that of arrays not producing translocations (Roukos et al. 2013). We propose that lesions that do not require a long-range search for a homologous donor and those that do not activate a checkpoint response also fail to trigger a general increase in chromatin mobility.

In summary, we show here that a DNA damage-triggered kinase response controls chromatin organization, with the likely effector being the INO80 complex (Fig. 5). We monitor this as expanded Rc values for undamaged fluorescently tagged chromatin loci. This may reflect local changes in chromatin structure (Neumann et al. 2012) or alterations in the long-range folding of chromatin genome-wide. When S-phase damage is repaired from the sister chromatid, damage movement is

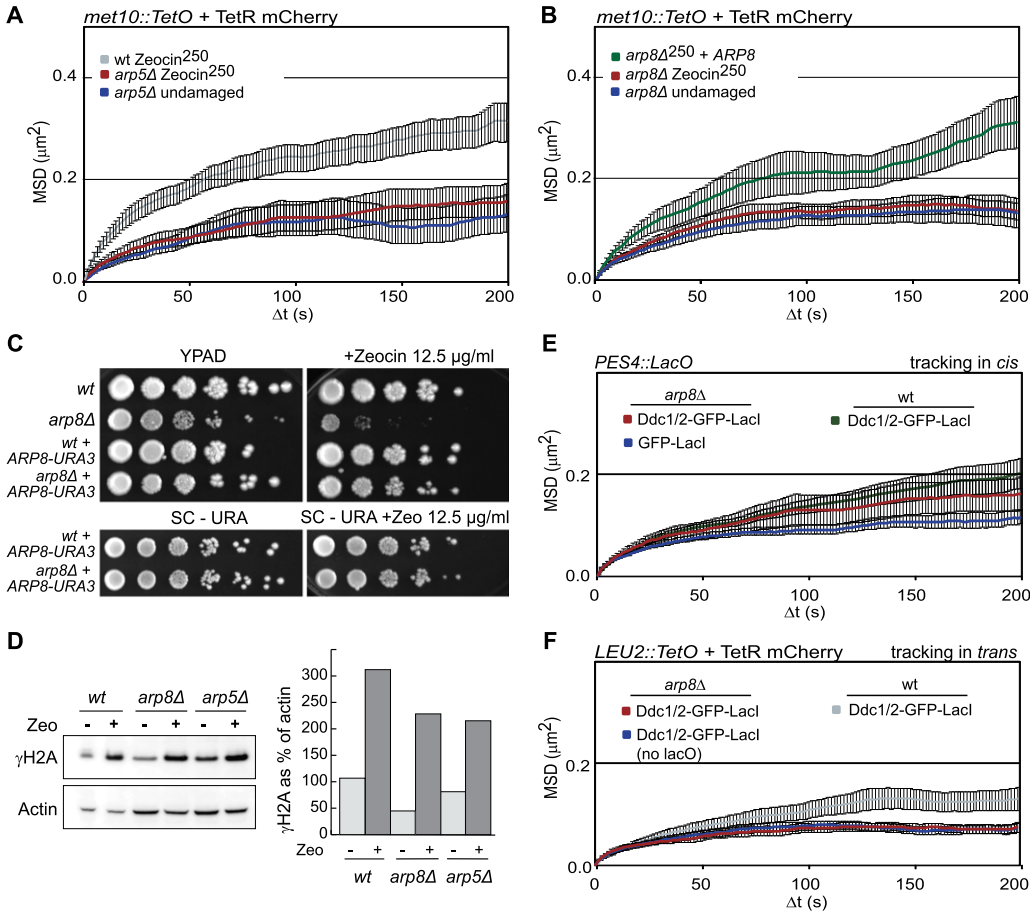

Figure 4. The INO80 complex is required to increase global chromatin mobility. MSD plots of *met10::TetO* during S phase in wild-type cells after 1 h in 250 μg/mL Zeocin (gray) and of the same locus without damage (blue) and treated with Zeocin 250 μg/mL (red) in the following mutant backgrounds: *arp5Δ* (GA-8202) (*A*) and *arp8Δ* (GA-8132) (*B*). (*C*) Serial dilution (10×) showing complementation of *arp8Δ* with p416-*ARP8-URA3* (Shen et al. 2003). (*D*) Western blot of γH2A accumulation after Zeocin treatment. (*E*) MSD plot of LacO-tagged *PES4* during S phase after 1 h on galactose in cells expressing Ddc1/Ddc2-GFP-LacI (red; GA-8203) or GFP-LacI (blue; GA-8204) in *arp8Δ* versus wild-type (green) backgrounds. (*F*) TetR-mCherry at *LEU2* in a strain expressing Ddc1/Ddc2-GFP-LacI (red; GA-8203) or expressing Ddc1/Ddc2-GFP-LacI in the absence of *PES4::lacO* (blue; GA-8204) versus wild-type (gray). The error bars in all panels show the SEM. The numbers of movies tracked and parameters are given in Table 1.

constrained and not enhanced, which can be overcome by destruction of cohesin (Dion et al. 2013). Thus, we speculate that the checkpoint kinases Mec1–Ddc2 and Rad53 modify INO80 and possibly cohesin in response to damage to regulate global chromatin mobility differentially during the DDR.

Materials and methods

Yeast growth conditions and plasmids

Yeast strains used in this study were W303-derived (see Supplemental Table S1). Yeast growth was at 30°C, and imaging was at 25°C. Zeocin exposure experiments were done in synthetic complete (SC) medium with 1-h incubations with drugs prior to microscopy or other assays, which were performed in fresh SC medium. Precise conditions are in the Supplemental Material. *pGAL-ECOR1* plasmid was a gift of Dr. P. Schär, and the pseudodiploid strain was constructed by integrating a *MATα* plasmid at *URA3* (gift of Dr. S. Marcand).

Microscopy, movie analysis, and zoning assay

Live microscopy used an Olympus IX81 microscope equipped with a Yokogawa CSU-X1 scan head, an EM-CCD Cascade II (Photometrics), an ASI MS-2000 Z-piezo stage, and a PlanApo ×100, NA 1.45 total internal reflection fluorescence microscope oil objective. For excitation and exposure times, see the Supplemental Material.

Time-lapse image stacks were analyzed as in Dion et al. (2012) using a custom-made Fiji plug-in (Sage et al. 2005). Analysis of locus position was performed with the zoning assay described in Meister et al. (2010), and phototoxicity was tested by exposing wild-type cells (GA-6879) to standard imaging conditions and then following outgrowth for 5 h by morphological analysis, comparing them with unexposed cells.

Western blotting

DDR activation was scored by Western blotting TCA-precipitated proteins separated on a SDS-PAGE gel (Invitrogen). The antibodies used are noted in the Supplemental Material.

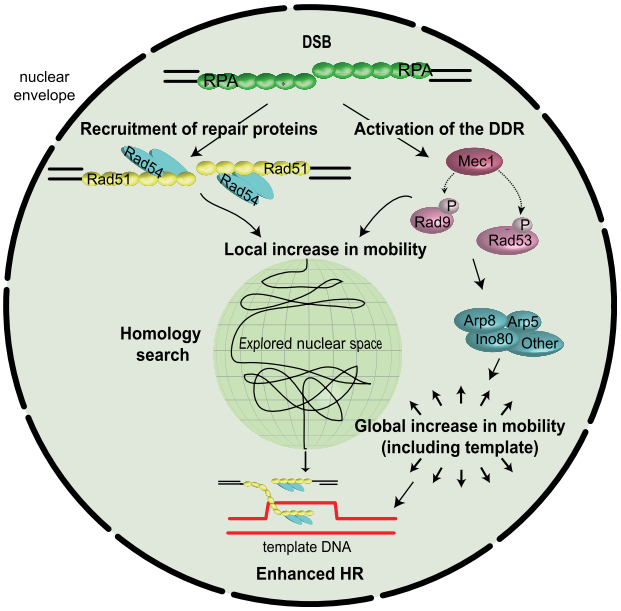

Figure 5. Model of the factors influencing local and global chromatin mobility in response to a DSB. Resection at a DSB leads to accumulation of ssDNA and binding of RPA. This signals the recruitment of repair proteins such as Rad51, Rad52, and finally, Rad54 and activates the DDR. At a DSB, Rad51, Rad54, Rad9, and Mec1 are required to increase DSB mobility (Dion et al. 2012). Global chromatin movement is enhanced by the checkpoint kinase activation and requires Rad53. Downstream from checkpoint activation, the INO80 subunits Arp5 and Arp8 are required to increase mobility globally and have a partial effect on the increase scored at a DSB. Increased mobility of both damaged and undamaged loci would facilitate contact between the DSB and ectopic sites of homology for HR.

Acknowledgments

We thank C. Horigome, U. Rass, I. Marcomini, P. Zeller, M. Hauer, and M. Di Pietro for critical reading and preparation of the manuscript and figures; P. Schär, S. Marcand, and D.P. Toczyski for reagents; and the Friedrich Miescher Institute Facility for Advanced Imaging and Microscopy for technical assistance. The Gasser laboratory is supported by FP7 Marie Curie Network Nucleosome 4D, the Swiss National Science Foundation National Centre for Competence in Research, "Frontiers in Genetics," and the Friedrich Miescher Institute for Biomedical Research. A.S., V.D., and S.M.G. planned experiments and wrote the paper, and A.S. and V.D. performed experiments.

References

Agmon N, Liefshitz B, Zimmer C, Fabre E, Kupiec M. 2013. Effect of nuclear architecture on the efficiency of double-strand break repair. *Nat Cell Biol* **15:** 694–699.

Bonilla CY, Melo JA, Toczyski DP. 2008. Colocalization of sensors is sufficient to activate the DNA damage checkpoint in the absence of damage. *Mol Cell* **30:** 267–276.

Burger RM. 1998. Cleavage of nucleic acids by bleomycin. *Chem Rev* **98:** 1153–1170.

Bystricky K, Van Attikum H, Montiel MD, Dion V, Gehlen L, Gasser SM. 2009. Regulation of nuclear positioning and dynamics of the silent mating type loci by the yeast Ku70/Ku80 complex. *Mol Cell Biol* **29:** 835–848.

Dimitrova N, Chen YC, Spector DL, de Lange T. 2008. 53BP1 promotes non-homologous end joining of telomeres by increasing chromatin mobility. *Nature* **456:** 524–528.

Dion V, Gasser SM. 2013. Chromatin movement in the maintenance of genome stability. *Cell* **152:** 1355–1364.

Dion V, Kalck V, Horigome C, Towbin BD, Gasser SM. 2012. Increased mobility of double-strand breaks requires Mec1, Rad9 and the homologous recombination machinery. *Nat Cell Biol* **14:** 502–509.

Dion V, Seeber A, Gasser SM. 2013. Cohesin and the nucleolus constrain the mobility of spontaneous repair foci. *EMBO Rep* (in press).

Forget AL, Kowalczykowski SC. 2012. Single-molecule imaging of DNA pairing by RecA reveals a three-dimensional homology search. *Nature* **482:** 423–427.

Gartenberg MR, Neumann FR, Laroche T, Blaszczyk M, Gasser SM. 2004. Sir-mediated repression can occur independently of chromosomal and subnuclear contexts. *Cell* **119:** 955–967.

Gehlen L, Gasser SM, Dion V. 2011. How broken DNA finds its template for repair: A computational approach. *Prog Theor Phys* **191:** 20–29.

Haber JE. 2012. Mating-type genes and MAT switching in *Saccharomyces cerevisiae*. *Genetics* **191:** 33–64.

Hakim O, Resch W, Yamane A, Klein I, Kieffer-Kwon KR, Jankovic M, Oliveira T, Bothmer A, Voss TC, Ansarah-Sobrinho C, et al. 2012. DNA damage defines sites of recurrent chromosomal translocations in B lymphocytes. *Nature* **484:** 69–74.

Heun P, Laroche T, Shimada K, Furrer P, Gasser SM. 2001. Chromosome dynamics in the yeast interphase nucleus. *Science* **294:** 2181–2186.

Ira G, Hastings PJ. 2012. DNA breakage drives nuclear search. *Nat Cell Biol* **14:** 448–450.

Krawczyk PM, Borovski T, Stap J, Cijsouw T, Cate RT, Medema JP, Kanaar R, Franken NA, Aten JA. 2012. Chromatin mobility is increased at sites of DNA double-strand breaks. *J Cell Sci* **125:** 2127–2133.

Lisby M, Barlow JH, Burgess RC, Rothstein R. 2004. Choreography of the DNA damage response: Spatiotemporal relationships among checkpoint and repair proteins. *Cell* **118:** 699–713.

Martin SG, Laroche T, Suka N, Grunstein M, Gasser SM. 1999. Relocalization of telomeric Ku and SIR proteins in response to DNA strand breaks in yeast. *Cell* **97:** 621–633.

Meister P, Gehlen LR, Varela E, Kalck V, Gasser SM. 2010. Visualizing yeast chromosomes and nuclear architecture. *Methods Enzymol* **470:** 535–567.

Melo JA, Cohen J, Toczyski DP. 2001. Two checkpoint complexes are independently recruited to sites of DNA damage in vivo. *Genes Dev* **15:** 2809–2821.

Mine-Hattab J, Rothstein R. 2012. Increased chromosome mobility facilitates homology search during recombination. *Nat Cell Biol* **14:** 510–517.

Morgan EA, Shah N, Symington LS. 2002. The requirement for ATP hydrolysis by *S. cerevisiae* Rad51 is bypassed by mating-type heterozygosity or RAD54 in high copy. *Mol Cell Biol* **22:** 6336–6343.

Morrison AJ, Kim JA, Person MD, Highland J, Xiao J, Wehr TS, Hensley S, Bao Y, Shen J, Collins SR, et al. 2007. Mec1/Tel1 phosphorylation of the INO80 chromatin remodeling complex influences DNA damage checkpoint responses. *Cell* **130:** 499–511.

Neumann FR, Dion V, Gehlen LR, Tsai-Pflugfelder M, Schmid R, Taddei A, Gasser SM. 2012. Targeted INO80 enhances subnuclear chromatin movement and ectopic homologous recombination. *Genes Dev* **26:** 369–383.

Ponti A, Schwarb P, Gulati A, Bäcker V. 2007. Huygens remote manager. *Imag Microscopy* **9:** 57–58.

Povirk LF. 1996. DNA damage and mutagenesis by radiomimetic DNA-cleaving agents: Bleomycin, neocarzinostatin and other enediynes. *Mutat Res* **355:** 71–89.

Renkawitz J, Lademann CA, Kalocsay M, Jentsch S. 2013. Monitoring homology search during DNA double-strand break repair in vivo. *Mol Cell.* **50:** 261–272.

Roukos V, Voss TC, Schmidt CK, Lee S, Wangsa D, Misteli T. 2013. Spatial dynamics of chromosome translocations in living cells. *Science* **341:** 660–664.

Sage D, Neumann FR, Hediger F, Gasser SM, Unser M. 2005. Automatic tracking of individual fluorescence particles: Application to the study of chromosome dynamics. *IEEE Trans Image Process* **14:** 1372–1383.

Seeber A, Hauer M, Gasser SM. 2013. Nucleosome remodelers in double-strand break repair. *Curr Opin Genet Dev* **23:** 174–184.

Shen X, Ranallo R, Choi E, Wu C. 2003. Involvement of actin-related proteins in ATP-dependent chromatin remodeling. *Mol Cell* **12:** 147–155.

Smolka MB, Albuquerque CP, Chen SH, Zhou H. 2007. Proteome-wide identification of in vivo targets of DNA damage checkpoint kinases. *Proc Natl Acad Sci* **104:** 10364–10369.

van Attikum H, Fritsch O, Hohn B, Gasser SM. 2004. Recruitment of the INO80 complex by H2A phosphorylation links ATP-dependent chromatin remodeling with DNA double-strand break repair. *Cell* **119:** 777–788.

Vialard JE, Gilbert CS, Green CM, Lowndes NF. 1998. The budding yeast Rad9 checkpoint protein is subjected to Mec1/Tel1-dependent hyperphosphorylation and interacts with Rad53 after DNA damage. *EMBO J* **17:** 5679–5688.

Weber SC, Spakowitz AJ, Theriot JA. 2012. Nonthermal ATP-dependent fluctuations contribute to the in vivo motion of chromosomal loci. *Proc Natl Acad Sci* **109:** 7338–7343.

Wilson JH, Leung WY, Bosco G, Dieu D, Haber JE. 1994. The frequency of gene targeting in yeast depends on the number of target copies. *Proc Natl Acad Sci* **91:** 177–181.

Zhao X, Muller EG, Rothstein R. 1998. A suppressor of two essential checkpoint genes identifies a novel protein that negatively affects dNTP pools. *Mol Cell* **2:** 329–340.

Supplemental Material and Methods

Yeast growth conditions and plasmids

Yeast strains used in this study are in Table S1. Yeast growth was at 30 °C, and imaging at 25 °C. All strains are W303 background (*MAT**a** ade2-1 trp1-1 his3-11 his3-15 ura3-1 leu2-3 leu2-112 RAD5*) and wild-type GA-6879 was previously described (Dion et al. 2012).

Zeocin exposure experiments were done in synthetic complete (SC) media. Cells were incubated with drugs for 1 h prior to microscopy or other assays which were performed in fresh media (SC). For microscopy, cells were grown overnight at 30°C in synthetic complete (SC) media and were diluted in the morning to obtain exponential phase cultures (2 $x10^6$ - 5 x 10^6 cells ml^{-1}). For undamaged conditions, cells were imaged immediately, ensuring that no Rad52-YFP spot was present at the beginning or end of imaging. Zeocin-treated cultures contained drug for 1 h. The Ddc1/Ddc2 targeting was done in synthetic glycerol 3%, lactate 2%, glucose 0.05% (SCGL) media. An overnight pre-culture was diluted and grown 3 hours to ~2.5 x 10^6 cells ml^{-1}. Galactose was added to 2% final volume to induce p*GAL-DDC1-LacI-GFP/DDC2-LacI-GFP* for 30 min, after which the targeted *PES4* locus was tracked in GA-7676 or GA-1461. For an ectopic locus, the TetR-mCherry spot was tracked at *LEU2* in GA-8023 and GA-8088. *pGAL-ECOR1* plasmid was a gift of Dr P. Schär (Schar et al. 2004), and the pseudo-diploid strain was constructed by integrating a *MAT**α*** plasmid at *URA3* (gift of Dr Stephan Marcand; (Frank-Vaillant and Marcand 2002)).

Microscopy

Live microscopy used an Olympus IX81 microscope equipped with a Yokogawa CSU-X1 scan head, an EM-CCD Cascade II (Photometrics), a ASI MS-2000 Z-piezo stage and a PlanApo x100, NA 1.45 total internal reflection fluorescence microscope oil objective. Fluorophores were excited at 567 nm (mCherry, ~30 μW), 515 nm (YFP, ~65 μW) and 491 (GFP, ~75 μW). Time-lapse series (5 min) of 14 optical slices per stack were taken every 1.5 s. Each optical slice required 30 ms exposure, for a total of 420 ms per stack. For zoning assays, 100 nm optical stacks were taken using the 491 nm laser (Meister et al. 2010). Nuclear volumes are based on an average haploid nuclear radius of 0.9 μm.

Movie analysis and Zoning assays

Time-lapse image stacks were analysed as in *(Dion et al. 2012)*, using a custom made Fiji plugin *(Sage et al. 2005)*. Analysis of locus position was performed with the zoning assay described in (Meister et al. 2010).

Phototoxicity

Potential phototoxicity was tested by exposing wild-type cells (GA-6879) to standard imaging conditions, and then following outgrowth for 5 hours by morphological analysis, comparing them to unexposed cells.

Western blotting

DDR activation is scored by Western Blotting of TCA precipitated proteins separated on a SDS-PAGE gel (Invitrogen). Transfer was done using Biorad Turbo blot system onto PVDF membranes. Anti-actin was from Millipore (#MAB1501) and anti-Mcm2 was purchased from Santa Cruz (#6680). Rad53 protein was detected using a custom-made mouse monoclonal antibody (GenScript) against FHA2 domain of Rad53. Anti-γH2A was similarly a custom-made polyclonal antibody that is specific for phospho-S129 in yeast H2A (Schleker 2007)

Supplemental Figure legends and Table S1

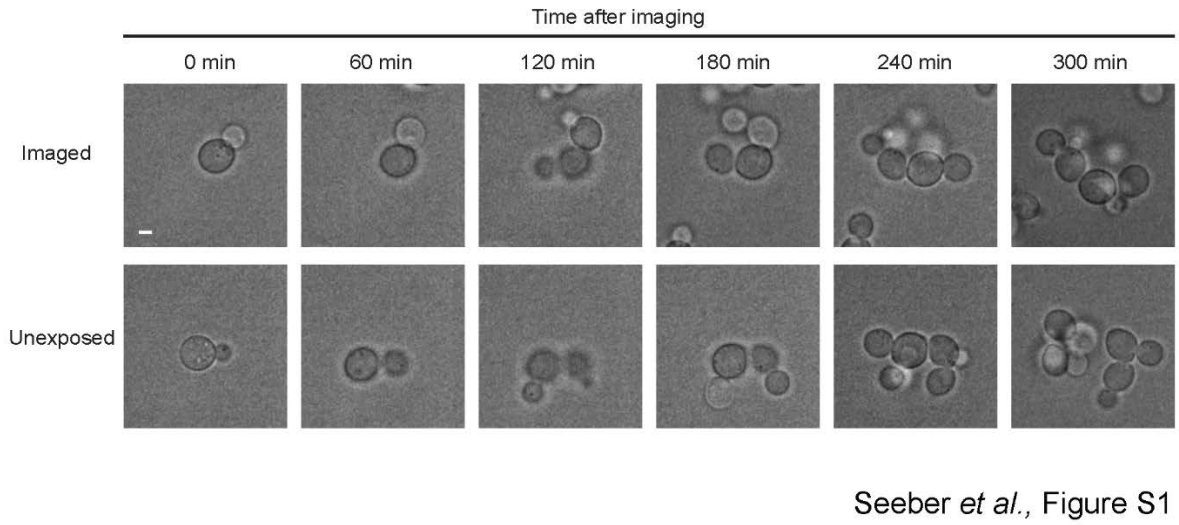

Figure S1: Imaging protocol does not induce cell cycle delays indicative of DDR Wild-type (GA-6879) cells were imaged (top) or (not) with laser line 561 nm taking optical stacks over 4.2 μm with a step size of 300 nm every 1.5s for 5 min. Cells were then monitored for 5 h taking a bright field image every 60 min. Scale bar is 2 μm.

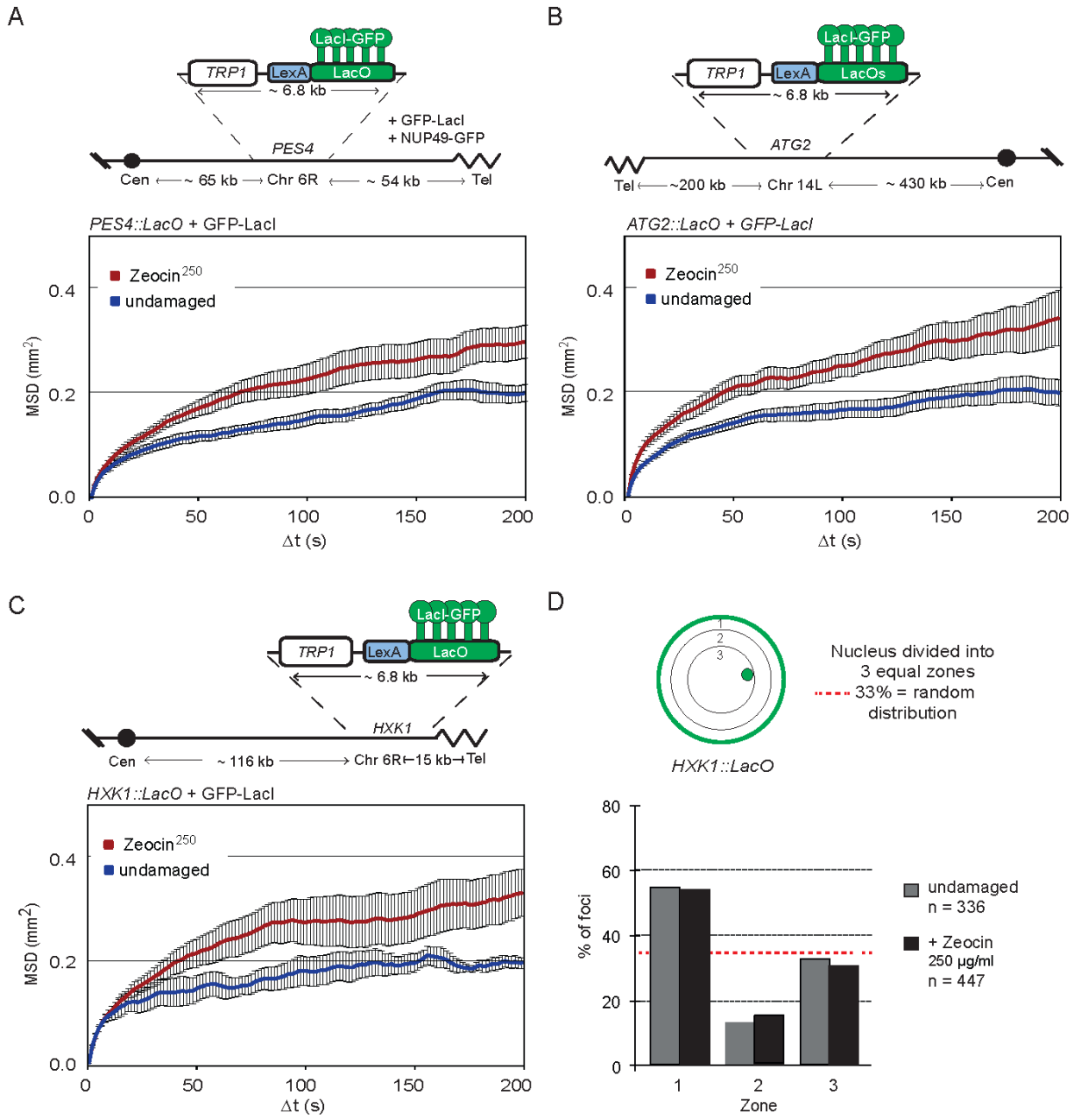

Seeber *et al.*, Figure S2

Figure S2: Zeocin-induced damage increases chromatin mobility at multiple loci including at a telomere. A-C) MSD plots of the indicated *lacO*-tagged locus during S phase in undamaged conditions (blue) and after 1h treatment with 250 µg/ml Zeocin (red). **(A)** Schematic of strain GA-1461 showing the tracked locus at *PES4*. **(B)** Schematic of strain GA-2070 showing the tracked locus at *ATG2 (ARS1412)*. **(C)** Schematic of strain GA-1459 showing the tracked locus at *HXK1 (ARS609)*. **(D)** Zoning assay comparing the location of *HXK1* in strain GA-1459 before and after 1 h treatment with 250 µg/ml Zeocin. Movement parameters are summarized in Table S2.

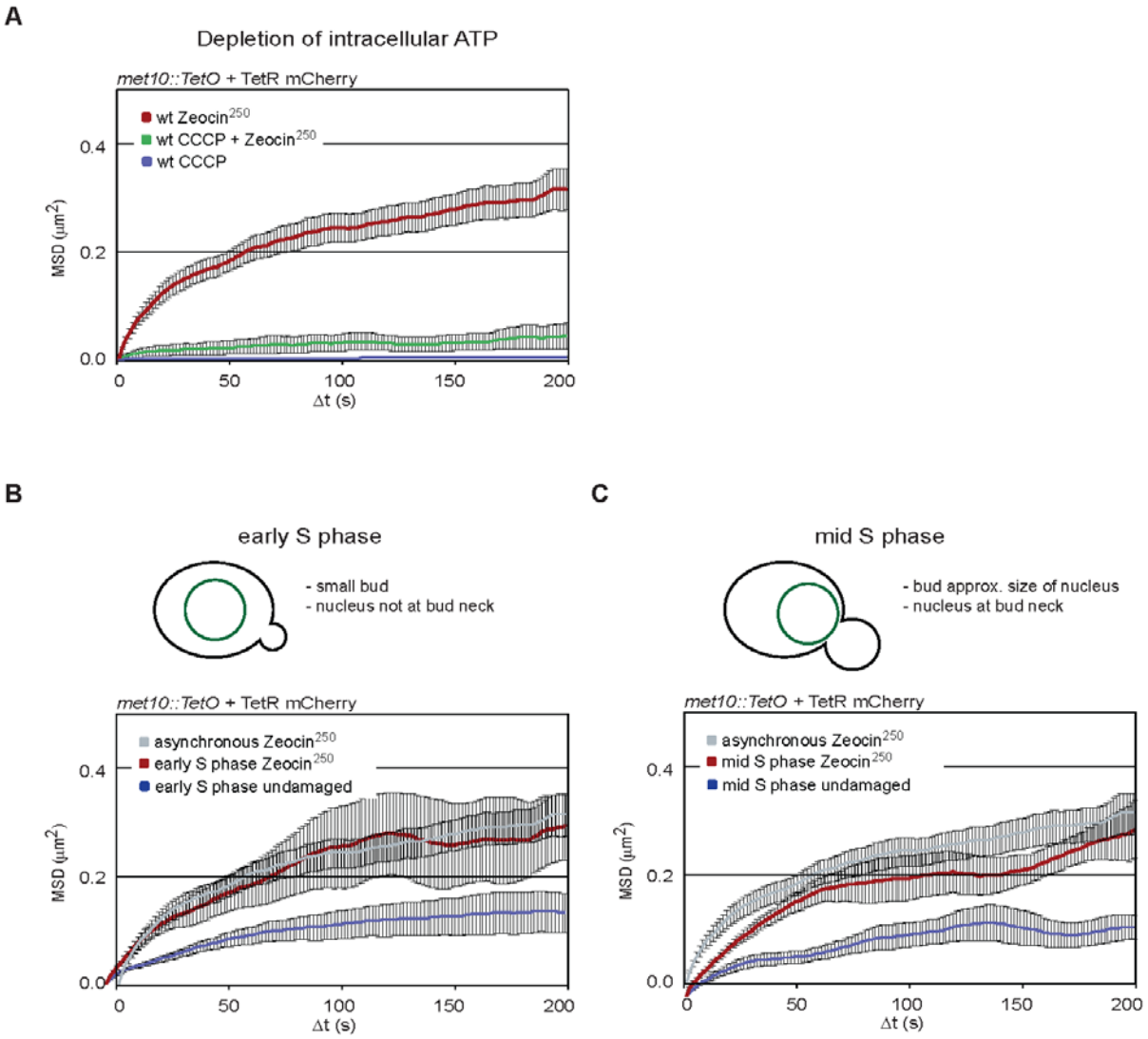

Figure S3: ATP depletion prevents damage dependent increases in chromatin mobility and S-phase stage is not important for chromatin mobility
MSD plots of the indicated *lacO*-tagged locus during S phase **(A)** Effect of 40 µM carbonyl cyanide m-chlorophenyl hydrazine (CCCP) on MSD plots of locus mobility (GA-6879) in the absence (blue), or presence of 250 µg/ml Zeocin (green), or 250 µg/ml Zeocin alone (red).. **B-C** Undamaged conditions (blue) and incubated with Zeocin at 250 µg/ml (red) **(B)** early S-phase cells, **(C)** mid S-phase cells. Asynchronous cells in grey. The error bars show the s.e.m. Movement parameters are summarized in Table S2.

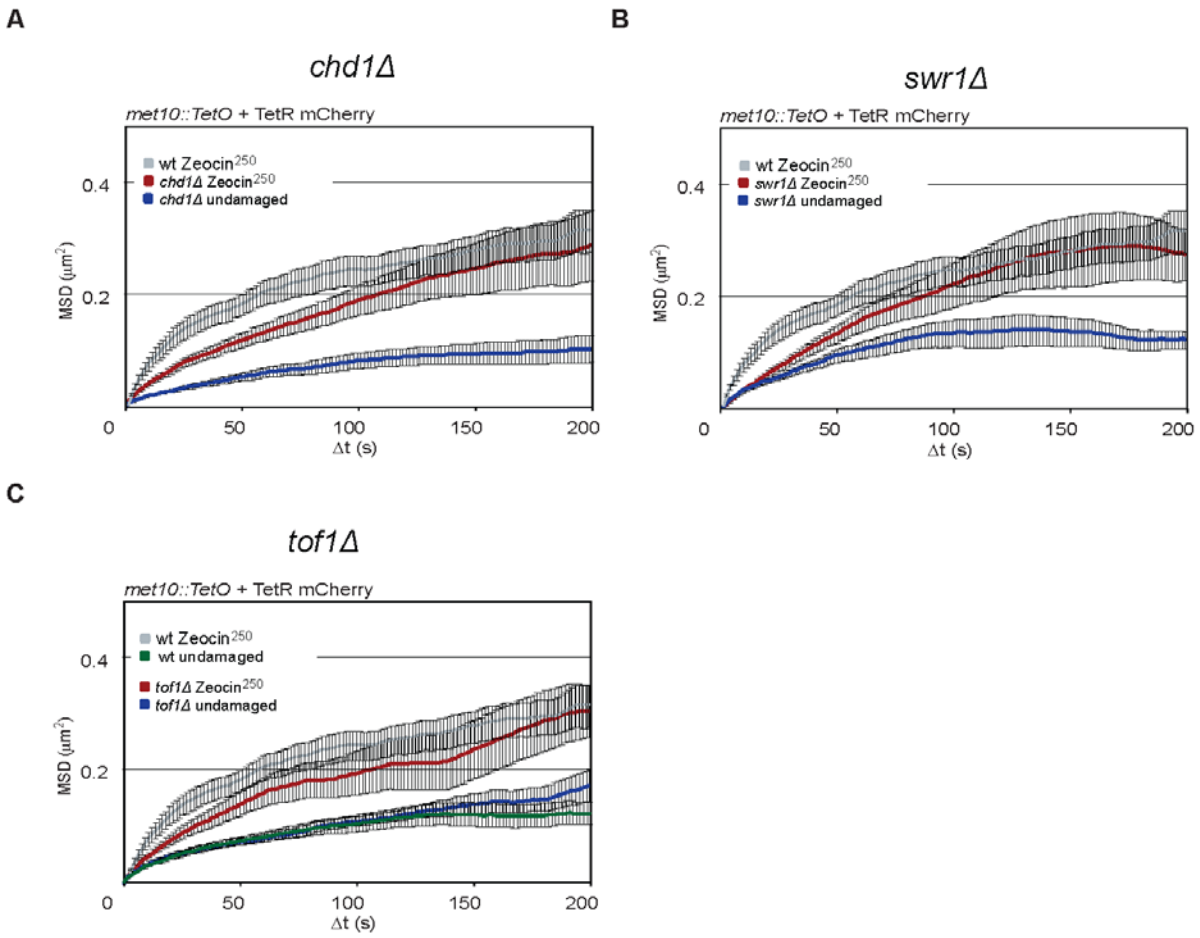

Figure S4: The Chd1 and Swr1 chromatin remodelers and cohesion promoting factor Tof1are dispensable for global chromatin mobility

A-C) MSD plots of *met10::TetO* during S phase in wild-type cells after treatment with 250 μg/ml Zeocin (gray). MSD plots of the same locus in undamaged conditions (blue) and treated with Zeocin 250 μg/ml (red) are shown in the following mutant backgrounds: (A) *chd1⊿* (GA-7723), (B) *swr1⊿* (GA-8185), (C) *tof1⊿* (GA-8186). The error bars show the s.e.m. Movement parameters are summarized in Table S2.

Table S1: Strains used in this study.

All yeast strains are derived from GA-1461 which is in a W303 background.

Strain number	Genotype	Reference
GA-6879	*MAT**a** RAD52-YFP, NUP49-GFP, ADE2::Tet*R-*mCherry, lys5::LacI-CFP-TRP, leu2::LoxP, ZWF1::*cutsite *(Lmn::lys5::IsceIcs::LEU2::lacO* array*::Lmn), met10::lmn* adaptamers*::HIS3::TetOps-Lex* (W303)	(Dion et al. 2012)
GA-7550	*rad51::NAT*, same as GA-6879	This study
GA-1461	*MAT**a**, PES4::4xLexA::lacO array::TRP1, his3-15::GFP-LacI::HIS3, NUP49-GFP* (W303)	(Taddei et al. 2004)
GA-2070	*MAT**a**, ATG2::4xLexA::lacO array, his3-15::GFP-LacI::HIS3, NUP49-GFP* (W303)	(Neumann et al. 2012)
GA-1459	*MAT**a**, Telo 6R::lacO array::TRP1, his3-15::GFP-LacI::HIS3, NUP49-GFP* (W303)	(Heun et al. 2001)
GA-6883	*MAT**a**, RAD52-YFP, NUP49-GFP, ADE2::Tet*R-*mCherry, lys5::LacI-CFP-TRP, leu2::LoxP, ZWF1:cutsite (Lmn::lys5::IsceIcs::LEU2::LacO array::Lmn)*	This study
GA-7591	*MAT**a**, RAD52-YFP, NUP49-GFP, ADE2::Tet*R-*mCherry, lys5::LacI-CFP-TRP, leu2::LoxP, ZWF1:cutsite (Lmn::lys5::IsceIcs::LEU2::LacO array::Lmn), MAT**α**::URA*	This study
GA-7552	*sml1::HIS3, rad53::NAT*, same as GA-6879	This study
GA-7553	*sml1::HIS3*, same as GA-6879	This study
GA-7555	*rad9::NAT*, same as GA-6879	This study
GA-7556	*sml1::HIS3, mec1::NAT*, same as GA-6879	This study
GA-7676	*MAT**a**, GFP-NUP49, Gal-Ddc1-GFP-LacI::URA3, Gal-Ddc2-GFP-LacI::HIS3, PES4::LacO array::LexAx4*	This study
GA-8088	*MAT**a**, GFP-NUP49, PES4::LacO array::LexAx4, LEU2::TetO array*	This study

GA-8023	*MAT**a**, GFP-NUP49, Gal-Ddc1-GFP-LacI::URA3, Gal-Ddc2-GFP-LacI::HIS3, PES4::LacO array::LexAx4, LEU2::TetO array*	This study
GA-8158	*MAT**a**, GFP-NUP49, Gal-Ddc1-GFP-LacI::URA3, Gal-Ddc2-GFP-LacI::HIS3, LEU2::TetO array*	This study
GA-8132	*arp8::NAT*, same as GA-6879	This study
GA-8202	*arp5::NAT*, same as GA-6879	This study
GA-8203	*arp8::NAT*, same as GA-8023	This study
GA-8204	*arp8::NAT*, same as GA-8158	This study
GA-7723	*chd1::NAT*, same as GA-6879	This study
GA-8185	*swr1::NAT*, same as GA-6879	This study
GA-8186	*tof1::NAT*, same as GA-6879	This study

Supplemental Table S2: Summary of MSD results presented in supplemental figures Indicated are the exact Rc and diffusion coefficient values calculated from the indicated number of time-lapse series for the indicated loci. W303 background is considered wild-type. * indicates data points taken from Dion et al., 2012.

Table S2 Summary of MSD results presented in this paper

Spot tracked	Locus	Treatment or damage	Rel. phenotype/ cc stage/sugar	R_c (μm)	Cell No.
mCh - TetR	*met10::TetO*	undamaged	Early S	0.41 ± 0.05	11
mCh - TetR	*met10::TetO*	Zeocin 250	Early S	0.60 ± 0.06	6
mCh - TetR	*met10::TetO*	undamaged	Mid S	0.41 ± 0.03	8
mCh - TetR	*met10::TetO*	Zeocin 250	Mid S	0.62 ± 0.05	9
mCh - TetR	*met10::TetO*	CCCP 40μM		0.08 ± 0.007	10
mCh - TetR	*met10::TetO*	CCCP 40μM +Zeocin 250		0.2 ± 0.06	6
LacI - GFP	*PES4::lacO*	undamaged		0.51 ± 0.02	10
LacI - GFP	*PES4::lacO*	Zeocin 250		0.61 ± 0.03	19
LacI - GFP	*ATG2::lacO*	undamaged		0.51 ± 0.03	19
LacI- GFP	*ATG2::lacO*	Zeocin 250		0.66 ± 0.05	15
LacI -GFP	*HXK1::lacO*	undamaged		0.51 ± 0.1	5
LacI-GFP	*HXK1::lacO*	Zeocin 250		0.64 ± 0.04	12
mCh - TetR	*met10::tetO*	uninduced	p*GAL-ECORI*	0.41 ± 0.03	18
mCh - TetR	*met10::tetO*	undamaged	*chd1⊿*	0.36 ± 0.04	14
mCh - TetR	*met10::tetO*	Zeocin 250	*chd1⊿*	0.61 ± 0.06	17
mCh - TetR	*met10::tetO*	undamaged	*swr1⊿*	0.42 ± 0.02	15
mCh - TetR	*met10::tetO*	Zeocin 250	*swr1⊿*	0.60 ± 0.04	8
mCh - TetR	*met10::tetO*	undamaged	*tof1⊿*	0.47 ± 0.04	13
mCh - TetR	*met10::tetO*	Zeocin 250	*tof1⊿*	0.62 ± 0.05	11

Supplemental References

Dion V, Kalck V, Horigome C, Towbin BD, Gasser SM. 2012. Increased mobility of double-strand breaks requires Mec1, Rad9 and the homologous recombination machinery. *Nature cell biology* **14**: 502-509.

Frank-Vaillant M, Marcand S. 2002. Transient stability of DNA ends allows nonhomologous end joining to precede homologous recombination. *Molecular cell* **10**: 1189-1199.

Heun P, Laroche T, Shimada K, Furrer P, Gasser SM. 2001. Chromosome dynamics in the yeast interphase nucleus. *Science* **294**: 2181-2186.

Meister P, Gehlen LR, Varela E, Kalck V, Gasser SM. 2010. Visualizing yeast chromosomes and nuclear architecture. *Methods in enzymology* **470**: 535-567.

Neumann FR, Dion V, Gehlen LR, Tsai-Pflugfelder M, Schmid R, Taddei A, Gasser SM. 2012. Targeted INO80 enhances subnuclear chromatin movement and ectopic homologous recombination. *Genes Dev* **26**: 369-383.

Sage D, Neumann FR, Hediger F, Gasser SM, Unser M. 2005. Automatic tracking of individual fluorescence particles: application to the study of chromosome dynamics. *IEEE transactions on image processing : a publication of the IEEE Signal Processing Society* **14**: 1372-1383.

Schar P, Fasi M, Jessberger R. 2004. SMC1 coordinates DNA double-strand break repair pathways. *Nucleic acids research* **32**: 3921-3929.

Schleker TA. 2007. Phosphorylation events surrounding the DNA damage response in Saccharomyces cerevisiae in *Philosophisch-Naturwissenschaftlichen Fakultätder*, p. 175. University of Basel, Basel.

Taddei A, Hediger F, Neumann FR, Bauer C, Gasser SM. 2004. Separation of silencing from perinuclear anchoring functions in yeast Ku80, Sir4 and Esc1 proteins. *The EMBO journal* **23**: 1301-1312.

CHAPTER 5: VISUALIZATION OF CHROMATIN DECOMPACTION AND BREAK SITE EXTRUSION AS PREDICTED BY STATISTICAL POLYMER MODELING OF SINGLE-LOCUS TRAJECTORIES

Assaf Amitai*[1], Andrew Seeber*[2], Susan M. Gasser[2], and David Holcman[1]

* equal contribution

1) Institut de Biologie de l'École Normale Supérieure, Ecole Normale Supérieure, 46 rue d'Ulm 75005 Paris, France.
2) Friedrich Miescher Institute for Biomedical Research, Maulbeerstrasse 66, 4058 Basel, Switzerland

Cell Reports 2017, Volume 18, pp 1200-1214

Summary

Chromatin is in constant motion within the nucleus. Changes in DNA dynamics have been extensively studied by fluorescence microscopy and mean squared displacement analysis, leading to diametrically opposed proposals for the forces behind this movement. Here we present an analytical workflow based on an improved imaging regime with higher spatial and temporal resolution, and statistical analyses that extract biophysical parameters from the trajectories. We have applied this to time-lapse imaging of an inducible double-strand break in yeast. Based on the extracted parameters, our modeling predicts chromatin expansion near a break, which we confirm by super-resolution microscopy. We are able to differentiate between extrinsic forces arising from the cytoskeleton and intrinsic forces stemming from changes in local chromatin structure. The actin cytoskeleton contributes to the former, while the INO80 chromatin remodeler is required for local chromatin expansion. Our method can be broadly applied to single-particle trajectories of chromatin polymers.

The importance of this paper is that it describes a polymer model that can faithfully predict chromatin structure at a local level. We show that chromatin movement in *S. cerevisiae* is driven by multiple factors including the actin cytoskeleton as well as changes in chromatin structure. In addition, we make two observations that have broad implications for DSB repair: i) We show that DSBs expand and this depends on the chromatin remodeling enzyme, INO80; ii) We show that for a break to move out of a domain, no active force is needed: one simply needs to modify the surrounding chromatin, and this change in entropy is sufficient to drive it to the surface of the domain.

Author contributions: A.S. and S.M.G planned experiments and analyzed data. A.S. performed most experiments, A.A. and D.H. carried out all polymer modeling and theoretical development of the analysis pipeline and analysis of spot trajectories. All four authors wrote the manuscript. Graphical abstract, and figures were designed by A.S. All data in Figures 1-6 was generated by A.S.

Article

Cell Reports

Visualization of Chromatin Decompaction and Break Site Extrusion as Predicted by Statistical Polymer Modeling of Single-Locus Trajectories

Graphical Abstract

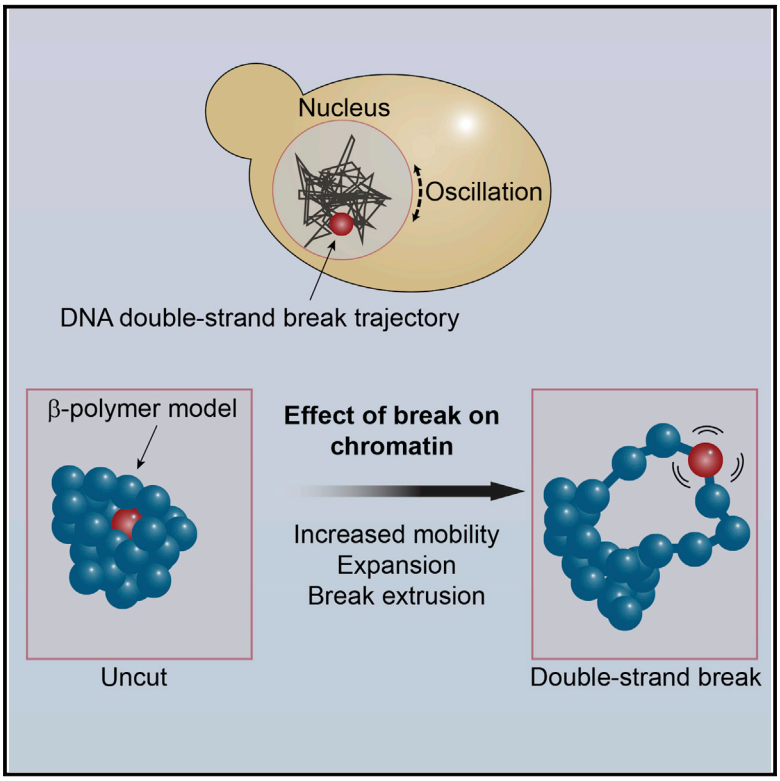

Authors

Assaf Amitai, Andrew Seeber, Susan M. Gasser, David Holcman

Correspondence

susan.gasser@fmi.ch (S.M.G.), david.holcman@ens.fr (D.H.)

In Brief

Amitai et al. present a robust analytical workflow for the analysis of single-particle trajectories. The extracted biophysical parameters allow accurate modeling of chromatin dynamics. The authors predict and show that, at double-strand breaks, chromatin decompacts and induces break relocation, while nuclear oscillation arises from cytoskeleton forces.

Highlights

- A robust analytical workflow for single-particle trajectories is presented
- β-polymer modeling predicts chromatin expansion at double-strand breaks
- Altered nucleosome interaction drives break extrusion from a chromatin domain
- Effects of local chromatin are distinct from actin-driven nuclear oscillation

Amitai et al., 2017, Cell Reports *18*, 1200–1214
January 31, 2017
http://dx.doi.org/10.1016/j.celrep.2017.01.018

CellPress

OPEN ACCESS
CellPress

Cell Reports
Article

Visualization of Chromatin Decompaction and Break Site Extrusion as Predicted by Statistical Polymer Modeling of Single-Locus Trajectories

Assaf Amitai,[1,2,6] Andrew Seeber,[3,4,6] Susan M. Gasser,[3,4,7,*] and David Holcman[1,5,*]
[1]Institut de Biologie de l'École Normale Supérieure, Ecole Normale Supérieure, 46 rue d'Ulm, 75005 Paris, France
[2]Institute for Medical Engineering & Science, Massachusetts Institute of Technology, Cambridge, MA 02139, USA
[3]Friedrich Miescher Institute for Biomedical Research, Maulbeerstrasse 66, 4058 Basel, Switzerland
[4]Faculty of Natural Sciences, University of Basel, 4056 Basel, Switzerland
[5]Department of Applied Mathematics and Theoretical Physics, University of Cambridge and Churchill College, Cambridge CB30DS, UK
[6]Co-first author
[7]Lead Contact
*Correspondence: susan.gasser@fmi.ch (S.M.G.), david.holcman@ens.fr (D.H.)
http://dx.doi.org/10.1016/j.celrep.2017.01.018

SUMMARY

Chromatin moves with subdiffusive and spatially constrained dynamics within the cell nucleus. Here, we use single-locus tracking by time-lapse fluorescence microscopy to uncover information regarding the forces that influence chromatin movement following the induction of a persistent DNA double-strand break (DSB). Using improved time-lapse imaging regimens, we monitor trajectories of tagged DNA loci at a high temporal resolution, which allows us to extract biophysical parameters through robust statistical analysis. Polymer modeling based on these parameters predicts chromatin domain expansion near a DSB and damage extrusion from the domain. Both phenomena are confirmed by live imaging in budding yeast. Calculation of the anomalous exponent of locus movement allows us to differentiate forces imposed on the nucleus through the actin cytoskeleton from those that arise from INO80 remodeler-dependent changes in nucleosome organization. Our analytical approach can be applied to high-density single-locus trajectories obtained in any cell type.

INTRODUCTION

Ever since the first live imaging of chromatin dynamics by single-particle tracking (Marshall et al., 1997), much effort has been invested into understanding the regulation and biological function of DNA movement. Unlike the directional separation of sister chromatids in mitosis, the interphase movement of chromatin is stochastic, yet it is modulated by ATP levels, suggesting that DNA dynamics are influenced by enzymatic events (Heun et al., 2001; Levi et al., 2005; Marshall et al., 1997; Seeber et al., 2013). Indeed, the majority of chromatin movement monitored in eukaryotic nuclei is subdiffusive (Albert et al., 2013; Amitai et al., 2015; Dion and Gasser, 2013; Weber et al., 2012), being restricted to volumes significantly smaller than that of the nucleus, arguing that internal forces constrain chromatin movement (Gartenberg et al., 2004; Bystricky, 2015; Chubb et al., 2002; Marshall, 2002). In budding yeast, such constraint has been altered by either the ablation of sister chromatid cohesion (Dion et al., 2013), the targeting of nucleosome remodelers (Neumann et al., 2012), or the elimination of anchorage sites that tether yeast chromosomes to nuclear substructures, such as the inner nuclear membrane protein Esc1 (Gartenberg et al., 2004), nuclear pores (Horigome et al., 2014), or the spindle pole body (Strecker et al., 2016; Verdaasdonk et al., 2013).

Chromatin movement is thought to facilitate gene induction by allowing distant enhancers and promoters to interact (Amitai and Holcman, 2013a; Bell and Felsenfeld, 1999; Dillon et al., 1997; Ptashne, 1986) or to facilitate the long-range search for sequence homology during DNA double-strand break repair (Agmon et al., 2013; Dion and Gasser, 2013; Miné-Hattab and Rothstein, 2012). More generally, the accessibility of DNA sequence for recognition by either proteins or nucleic acid may benefit from chromatin mobility. As an example, a fluorescently tagged locus with a persistent double-strand break (DSB) in budding yeast, shows greater movement than the same locus undamaged (Dion et al., 2012; Miné-Hattab and Rothstein, 2012). The drivers of this increased mobility and their impact on repair are debated (Dion et al., 2012; Miné-Hattab and Rothstein, 2012; Strecker et al., 2016; Verdaasdonk et al., 2013), yet the fact that increased movement depends on the type of damage incurred (Dion et al., 2012, 2013) and on a kinase-mediated DNA damage checkpoint response (Miné-Hattab and Rothstein, 2012; Seeber et al., 2013; Strecker et al., 2016) argues for physiological relevance.

In mammals as well, the chromatin context of a DSB and the preference of the locus for repair by end joining or ectopic recombination influence whether or not a locus will show enhanced movement following damage induction (Aten et al., 2004; Cho et al., 2014; Jakob et al., 2009; Krawczyk et al., 2012; Kruhlak et al., 2006; Lottersberger et al., 2015; Nelms et al., 1998; Roukos et al., 2013; Soutoglou et al., 2007; Tsouroula et al., 2016).

Radiation-induced foci and uncapped telomeres both show enhanced movement in mammalian cells (Dimitrova et al., 2008; Lottersberger et al., 2015), and in both mammals and flies it was shown that DSBs that occur in heterochromatin must move out of the heterochromatic compartment in order to be repaired by recombination (Chiolo et al., 2011; Jakob et al., 2011; Ryu et al., 2015; Tsouroula et al., 2016). What changes occur on a biophysical level to allow such movements are unclear, but possible triggers could be changes in local chromatin structure, the release of constraints imposed by non-chromatin anchorage sites, or active, motor-driven transport.

To date, the analysis applied to single-particle trajectories (SPTs) of tagged chromatin loci has been inadequate to distinguish between these possibilities. Here, we present a framework for statistical analysis of SPTs over time that allows us to extract a more comprehensive set of biophysical parameters and relate them to polymer models (Amitai and Holcman, 2013b; Amitai et al., 2015). We then use simulations based on the β-polymer model to predict chromatin behavior. Our experimental system is the well-characterized HO endonuclease- induced DSB in budding yeast (Dion et al., 2012; Horigome et al., 2014; Miné-Hattab and Rothstein, 2012; Nagai et al., 2008), which allows us to monitor locus dynamics before and after DSB induction. Polymer modeling predicts that chromatin around a break will expand and that this will drive extrusion of the damage from its local chromatin domain. We confirm chromatin expansion at an induced DSB using quantitative, super-resolution structured illumination microscopy (SIM). Moreover, we demonstrate a significant increase in the anomalous exponent of movement, α, at a DSB in the rDNA, as it shifts from the nucleolus for recombination-mediated repair (Torres-Rosell et al., 2007).

Our approach consists of two parts. First, we extract from single-locus trajectories an ensemble of four statistical parameters derived from polymer model analysis. These parameters provide independent information about the nature of locus movement, allowing us to characterize the origin of the forces acting on chromatin. We then construct a polymer model and simulate chromatin behavior, using empirically extracted biophysical parameters. This analytical approach and predictive modeling enable a biophysical definition of chromatin dynamics and provide a paradigm for the analysis of chromatin movement in other species. In yeast, we show that changes in local chromatin structure at a break can lead to altered dynamics that can affect longer-range aspects of chromatin organization.

RESULTS

We use a well-characterized budding yeast strain carrying a galactose-inducible *HO* gene, which encodes the Homothallic switching endonuclease that, in turn, introduces a double-strand break specifically and uniquely at the *MAT* locus on Chr III (Table S1). Cleavage efficiency is measured for each experiment by qPCR (Table S2). We visualize the locus by tracking a fluorescent LacI-GFP protein bound to an array of *lac* operators (*lacO*) that is inserted near the cut site (Figure 1A). In addition, we have tagged the nuclear pores with a separate red fluorophore (Nup49-Ruby2), which is both brighter than traditional fluorophores and more photostable (Lee et al., 2013). This allows us to use less light to stimulate the fluorochrome, minimizing light-induced damage despite longer acquisition times. Our imaging regimens do not activate the DNA damage response and cells continue to divide after light exposure (Figure S1). The labeling of the nuclear perimeter with Nup49-Ruby2 allows us to align acquired trajectories with respect to the nuclear center, to correct for translational movement.

Previous studies of chromatin dynamics performed SPTs with imaging intervals of 1.5 s for 200 frames (Dion et al., 2012; Neumann et al., 2012; Strecker et al., 2016), 10 s for 80 frames (Miné-Hattab and Rothstein, 2012), 30 s for 20 frames (Verdaasdonk et al., 2013), 100 ms for 300 frames (Spichal et al., 2016), and 15–400 ms for 300 frames (Hajjoul et al., 2013). Without sufficient time points, statistically significant information cannot always be extracted from SPTs. In addition, chromatin motion may show different properties when imaged at different timescales (Amitai et al., 2015; Hajjoul et al., 2013; Levi et al., 2005). We addressed these caveats by acquiring 3D images at two timescales and generating more frames than had previously been published. Namely, 750 or 500 3D stacks of images were obtained for each time-lapse movie at Δt = 80 ms (10 ms per z-slice ×8) or Δt = 300 ms (30 ms per z-slice ×8), respectively (Figure 1A). By selecting a small cropped region on the EM-CCD chip and synchronizing the Piezo z-stage, we could stream acquisitions just above the camera chip readout rate (~9 ms). We simultaneously captured the two fluorophores, i.e., the LacI-GFP at *MAT* and the perinuclear Nup49-Ruby2, and by coupling a EM-CCD camera with 3D deconvolution by Huygens Professional, we could use very-low-light conditions over extended periods of capture. It is important to note that DNA shows significantly less movement in S-phase yeast cells than in G1-phase cells (Dion et al., 2013; Heun et al., 2001); thus, reliable data cannot be extracted from tracking a field of asynchronous yeast cells. Single cells must be selected and the data triaged after determining the cell-cycle stage of each imaged cell. In this study, we selected only small budded S-phase cells for spot tracking.

To extract information from these SPTs we introduce four statistical quantities that can be computed from the data (numerical code to compute the four parameters is accessible at http://bionewmetrics.org/ in the "Nuclear Organization section"). For clarity, and to make this method accessible to a general audience, the majority of the equations defining these parameters are in the Supplemental Information. Their extraction is key to our analysis, because these parameters provide independent, complementary information on first- and second-moment statistics. Each has been studied separately elsewhere and are described below.

1. The length of constraint L_C is defined as the SD of the locus position with respect to its mean averaged over time. This parameter provides estimation for the apparent radius of the volume explored by a finite trajectory. For a trajectory containing N_p points, where $\mathbf{R}_c(k\Delta t)$ is the position of a locus at a time t, L_C is obtained from the empirical estimation:

$$L_C = \sqrt{\mathrm{Var}(\mathbf{R}_c)} \approx \sqrt{\frac{1}{N_p}\sum_{k=1}^{N_p}(\mathbf{R}_c(k\Delta t) - \langle \mathbf{R}_c \rangle)^2}. \quad \text{(Equation 1)}$$

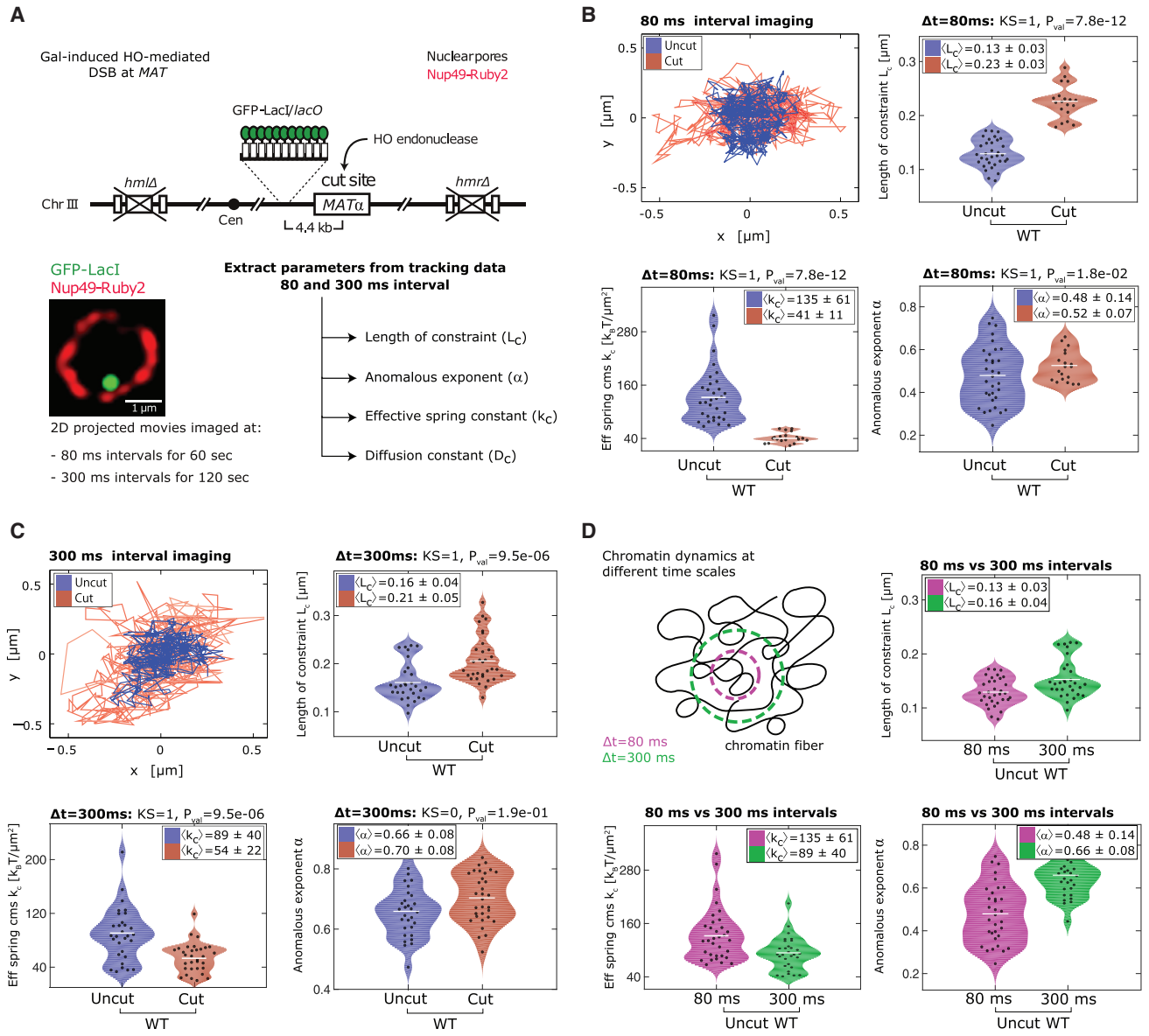

Figure 1. Extraction of Biophysical Parameters of DSB Dynamics Using Two Imaging Regimens

(A) Schematics of the experimental system and description of extracted biophysical parameters. See text and Supplemental Information for definition of length of constraint (Lc), effective spring coefficient (k_c), the anomalous exponent α reflecting an auto-correlation function, and the D_c (diffusion coefficient).

(B) Upper-left quadrant: *MAT* locus trajectories during 60 s (Δt = 80 ms). Other quadrants contain the extracted parameters Lc, kc, and α of cut (red) and uncut (blue) *MAT* loci. Above the panel, the p value of a Kolmogorov-Smirnov (KS) test is indicated. White bar, distribution mean. Strains used are GA-8862/8863 (Table S1).

(C) As in (B) but for Δt = 300 ms during 120 s. For extracted parameters, see Table 1 and Figure S2. Cut efficiencies and nuclei scored are in Table S2.

(D) Monitoring movement at different timescales corresponds to studying the polymer on different scales. The time resolution determines the scale of chromatin dynamics monitored; at a short time resolution (80 ms, pink circle), we observed a smaller element of the chromatin movement than with 300 ms resolution (green circle). Panels present parameters Lc, kc, and α from 80- and 300-ms imaging regimens for an intact locus (see Figures S1 and S2).

It characterizes the confinement of a locus, which in other studies has been reported as the radius of confinement (R_{conf} – not to be confused with R_c). The R_{conf} is computed from the asymptotic plateau of mean square displacement (MSD) curves and is therefore limited to trajectories that plateau. This is strongly influenced by the length of image acquisition. The advantage of computing L_C is that it gives a robust estimate of the volume $V = 4/3\pi L_C^3$ occupied by the trajectory and can be used on any kind of trajectory, as it does not require a plateau (see Supplemental Information).

2. The anomalous exponent α is computed from the auto-correlation (AC, Supplemental Information Equation 11) function for small increments $\boldsymbol{C}(t) = \langle(\mathbf{R_c}(\tau+t) - \mathbf{R_c}(\tau))^2\rangle \approx t^{\alpha}$. It indicates the nature of the locus motion; i.e., α = 1 describes normal diffusion, while

Table 1. Biophysical Parameters Extracted from SPTs before and after DSB Induction

Description	Parameters	Uncut Locus	Cut Locus
Δt = 80 ms			
Length of constraint	L_C	0.13 ± 0.03μm	0.23 ± 0.03μm
Anomalous exponent	α	0.49 ± 0.14	0.52 ± 0.07
Effective spring coefficient	k_c	139 ± 63k_BT/μm^2	41 ± 11k_BT/μm^2
Apparent diffusion constant	D_c	14.3 ± 7.5 × 10^{-3}μm^2/s	27.8 ± 10.8 × 10^{-3}μm^2/s
Δt = 300 ms			
Length of constraint	L_C	0.16 ± 0.04μm	0.21 ± 0.05μm
Anomalous exponent	α	0.66 ± 0.08	0.70 ± 0.08
Effective spring coefficient	k_c	89 ± 40k_BT/μm^2	54 ± 22k_BT/μm^2
Apparent diffusion constant	D_c	3.9 ± 1.1 × 10^{-3}μm^2/s	3.9 ± 1.6 × 10^{-3}μm^2/s

Yeast strains, conditions of imaging, and cut induction are as in Figures 1B and 1C.

$\alpha < 1$ is subdiffusive (constrained) and $\alpha > 1$ is superdiffusive (directed) movement (Kepten et al., 2013; Dion and Gasser, 2013). In practice, we estimated α by fitting the first six points of the AC function of an SPT by a power law t^{α}, as described in the Supplemental Information. Every time point affects the initial slope of the AC function (or the MSD); thus, movies with more time points will ultimately provide the more accurate approximation of α, and a more robust representation of the data.

3. The effective spring coefficient k_c. An external force acting on a chromatin locus can be modeled as a spring force applied on a single monomer belonging to a polymer. This force affects the entire polymer motion and can be recovered from the first-order moment statistics of single-locus trajectories. The spring force acting at position x_a and measured at position x_m is represented by $F = -k_c (x_m - x_a)$, and the spring constant k_c allows us to estimate the effect of local tethering interactions around the locus of interest (Amitai et al., 2015) (see Supplemental Information, Equation 17). This tethering can arise from interactions of the locus with other chromosomes or nuclear substructures, such as the nucleolus or nuclear envelope. While these interactions cannot be measured directly they can be inferred from SPTs.
4. The effective diffusion coefficient D_c reflects the second-order statistical properties of a trajectory. This diffusion coefficient accounts for local crowding that may vary along the trajectory. The estimation procedure is described in the Supplemental Information.

These four parameters are complementary (monitoring first- and second-order moment statistics) and provide an advantage over those extracted previously, which were generally limited to determination of the radius of confinement (R_{conf}) and/or the diffusion coefficient. We use them to characterize the underlying motion of the monitored locus. In summary, the confinement of a locus is measured by L_C, its velocity is D_c, forces acting on a locus is given by k_c, and, importantly, the nature of the motion is described by α.

Induction of a DSB Alters the Biophysical Parameters of a Chromatin Locus

Consistent with previous results that monitored the dynamics of induced DSBs in yeast (Dion et al., 2012; Miné-Hattab and Rothstein, 2012), we find that Lc increases significantly after break induction in both timescales from $L_c^{uncut\ 80ms}$ = 0.13 ± 0.03 μm to $L_c^{cut\ 80ms}$ = 0.23 ± 0.03 μm and $L_c^{uncut\ 300ms}$ = 0.16 ± 0.04 μm to $L_c^{cut\ 300ms}$ = 0.21 ± 0.05 μm (Figures 1B and 1C, summarized in Table 1). Comparing the Lc values for unbroken loci tracked at Δt = 80- versus 300-ms intervals, we find that the 300-ms trajectories have a higher L_C. The 300 ms-interval movies are 120 s long and the 80-ms movies are 60 s long, consistent with the notion that Lc scales with the time during which the locus has explored its surroundings.

The increase in movement upon break induction could reflect the loss of constraint (either from reduced contacts between nucleosomes or reduced interaction with a less mobile nuclear substructure), or stem from an increased external force acting on the nucleus. Yeast chromosomes reversibly interact with nuclear envelope structures (e.g., pores or the spindle pole body [SPB] (Taddei and Gasser, 2012). Such interactions not only constrain movement, but could enhance it, if the nucleus experiences forces leading to rotation or oscillation. To quantify the strength of tethering interactions at the site of a DSB, we approximate the confining tethering force using the classical harmonic potential approximation (Amitai et al., 2015). A binding force is generically parabolic (see Supplemental Information); thus, a tethering force is characterized by a strength k acting on a single monomer R_n: $U = (1/2)k(\mathbf{R}_n - \boldsymbol{\mu})^2$, where μ is the position of the interaction. Reduction of tethering forces should result in increased mobility (Amitai et al., 2015). Based on these modeling predictions, we extracted the effective spring coefficient k_c (Equation 17, Supplemental Information), which measures the averaged external forces affecting the observed locus. We find that k_c decreases significantly for both timescales from $k_c^{uncut\ 80ms}$ = 135 ± 61 k_BT/μm^2 to $k_c^{cut\ 80ms}$ = 41 ± 11 k_BT/μm^2 and $k_c^{uncut\ 300ms}$ = 89 ± 40 k_BT/μm^2 to $k_c^{cut\ 300ms}$ = 54 ± 22 k_BT/μm^2 (Figures 1B and 1C). This decay suggests that there is a local reduction in interactions around the region of the break. This could increase

the territory the spot explores, as reflected in the increase of the length L_C.

Upon cut induction, we also find a small but significant increase in the anomalous exponent α where $\alpha^{uncut\ 80ms} = 0.48 \pm 0.14$ increases to $\alpha^{cut\ 80ms} = 0.52 \pm 0.07$ and $\alpha^{uncut\ 300ms} = 0.66 \pm 0.08$ increases to $\alpha^{cut\ 300ms} = 0.70 \pm 0.08$ (Figures 1B and 1C). Surprisingly, we found that the anomalous exponent α is consistently higher at $\Delta t = 300$ ms ($\alpha^{uncut\ 80ms} = 0.48$ versus $\alpha^{uncut\ 300ms} = 0.66$), even without DSB induction. This difference could arise from the fact that by choosing a time step we implicitly establish a cutoff below which locus dynamics are no longer influenced by the long-range chromatin properties. Vice versa, at larger intervals (e.g., $\Delta t = 300$ ms), the more subtle changes in chromatin dynamics that occur on shorter timescales ($\Delta t = 80$ ms) may be averaged out (see scheme, Figure 1D). Thus, rapid image acquisition allows us to observe fluctuations of polymer structure at the level of short genomic distances, while larger time intervals reveals local fluctuations of chromatin at larger genomic scales. This also provides an explanation of why we observe an increase in the diffusion coefficient after cleavage for the trajectories at $\Delta t = 80$ ms ($D_c^{Uncut\ 80ms} = 15.4 \pm 7.7 \times 10^{-3}\ \mu m^2/s$ to $D_c^{cut\ 80ms} = 27.8 \pm 10.8 \times 10^{-3}\ \mu m^2/s$), but not at $\Delta t = 300$ ms ($D_c^{Uncut\ 300ms} = 3.9 \pm 1.1 \times 10^{-3}\ \mu m^2/s$ versus $D_c^{cut\ 300ms} = 3.9 \pm 1.6 \times 10^{-3}\ \mu m^2/s$; Equation 13, Supplemental Information; Figure S2, Table 1).

Effect of Actin Depolymerization on Chromatin Dynamics

Since the increase in the anomalous exponent α upon DSB induction was small ($\alpha^{uncut\ 80ms} = 0.46$ versus $\alpha^{cut\ 80ms} = 0.52$) and because α increased with longer imaging intervals, we hypothesized that external forces might act on the nucleus that could mask changes in α. While our tracking regimen corrects for translational movement, it cannot account for nuclear rotation or precession. As a simple proof of principle that α increases when an oscillating force is applied to the polymer, we simulated a Rouse polymer ($\alpha = 0.5$) with oscillation period ω (Supplemental Information; Figure S3). We find that when $\omega = 0.04$, α increases from 0.5 to 0.7 (Figure 2A), suggesting that nuclear rotation/precession would increase α and could, therefore, mask changes in this parameter. This simulation was performed for a Rouse polymer, yet simulation of other polymer models would yield the same qualitative behavior.

Next, we tested whether this effect occurs in vivo. Recent work has implicated the cytoskeleton (Lottersberger et al., 2015; Spichal et al., 2016) and KASH proteins, which anchor inner nuclear membrane-spanning SUN domain proteins to the cytoskeleton (Starr and Fridolfsson, 2010) in chromatin movement (Chung et al., 2015; Lottersberger et al., 2015; Spichal et al., 2016). Given that in budding yeast, subcellular organelles are more commonly positioned by actin filaments, rather than by microtubules (MTs), we hypothesized that actin filaments connected to the nuclear envelope could be a source of nuclear rotation, which would, in turn, increase α, as shown by our numerical simulations. To test this hypothesis, we fluorescently labeled the SPB, a structure embedded in the nuclear envelope, by tagging Spc29 with Ruby2. Movement of the SPB reflects that of the entire nucleus (Figure 2B). A 1-hr exposure to 25 μm of the sponge toxin Latrunculin A (LatA) was sufficient to completely depolymerize cytoplasmic actin filaments in yeast (Figure S4). By analyzing SPB trajectories, we found that α decreases significantly upon LatA treatment, from $\alpha^{DMSO} = 0.37 \pm 0.16$ to $\alpha^{LatA} = 0.26 \pm 0.15$ (Figure 2B), suggesting that actin filaments indeed contribute to nuclear rotation/precession. The values for k_c, D_c, and L_c were not significantly reduced after LatA treatment (Figures 2B and S3A). A simple explanation for this phenomenon could be that the nucleus rocks back and forth in the x and y planes, with only the frequency of this motion being reduced by LatA. In this case, the total area scanned by the SPB remains the same, while α, which characterizes its motion, decreases upon actin depolymerization. The fact the second dynamical parameter (D_c) does not change suggests that the frequency of the nuclear precession is large compared to the imaging time step (80 ms). Indeed, given that α is a dynamic parameter computed over the first six time points, it incorporates motion up to 0.48 s. This is illustrated in Figure 2A, where the gap between the curves is larger at longer times.

To see whether nuclear oscillation is necessary for the dynamic changes in chromatin following induction of a DSB, we tracked DSB mobility after treatment with LatA. As observed for the SPB, LatA treatment reduces Lc in the uncut condition ($L_c^{uncut\ No\ drug\ 80ms} = 0.13 \pm 0.03$ μm to $L_c^{uncut\ LatA\ 80ms} = 0.08 \pm 0.03$ μm). Upon cleavage, however, this value increases to $L_c^{cut\ LatA\ 80ms} = 0.15 \pm 0.06$ μm, showing approximately the same fold increase as we observed at a break without LatA (Figure 2C). Thus, the DSB-induced increase in movement is not a result of actin filament-driven dynamics. The spring constant k_c follows the same trend upon LatA exposure (Figure S5B). In other words, tethering forces are released following break induction even in the presence of LatA. Interestingly, the diffusion coefficient of the DSB does not change upon LatA treatment, which we attribute to the timescale of the nuclear oscillations, as explained in the previous paragraph.

We note that the anomalous exponent α decreases strongly upon LatA treatment ($\alpha^{uncut\ No\ drug\ 80ms} = 0.48 \pm 0.14$ to $\alpha^{uncut\ LatA\ 80ms} = 0.30 \pm 0.14$), consistent with the suggestion that actin polymerization indirectly influences the underlying nature of chromatin movement (Spichal et al., 2016). Importantly, however, α again increases strongly from $\alpha^{uncut\ LatA\ 80ms} = 0.30 \pm 0.14$ to $\alpha^{cut\ LatA\ 80ms} = 0.46 \pm 0.14$, upon induction of a DSB, despite the presence of LatA (Figure 2D). The same highly significant change was observed for trajectories taken at $\Delta t = 300$ ms (Figure S5C). Thus, the change in locus dynamics at a DSB is not actin-filament dependent, even though basal chromatin movement is influenced by actin-driven nuclear rotation. Importantly, we show that changes in α can be masked by such oscillations.

Effect of Microtubule Depolymerization on Chromatin Dynamics

Early work had shown that MT depolymerization by Nocodazole in yeast increased chromatin dynamics (Marshall et al., 1997), as it releases centromeres from their attachment to the SPB (Bystricky et al., 2004). In contrast, recent work in a mammalian system showed the opposite effect: MT depolymerization

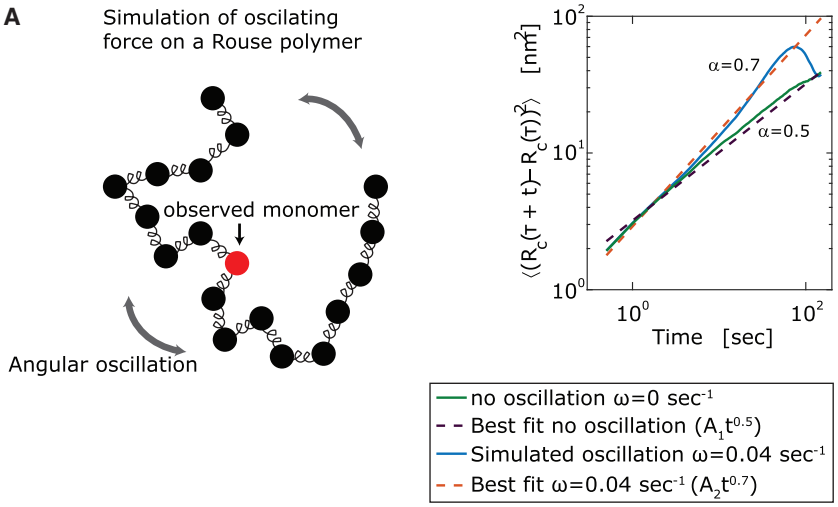

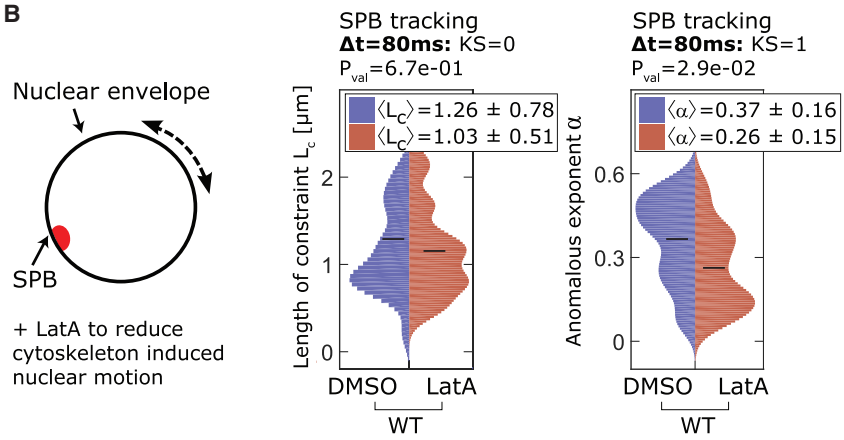

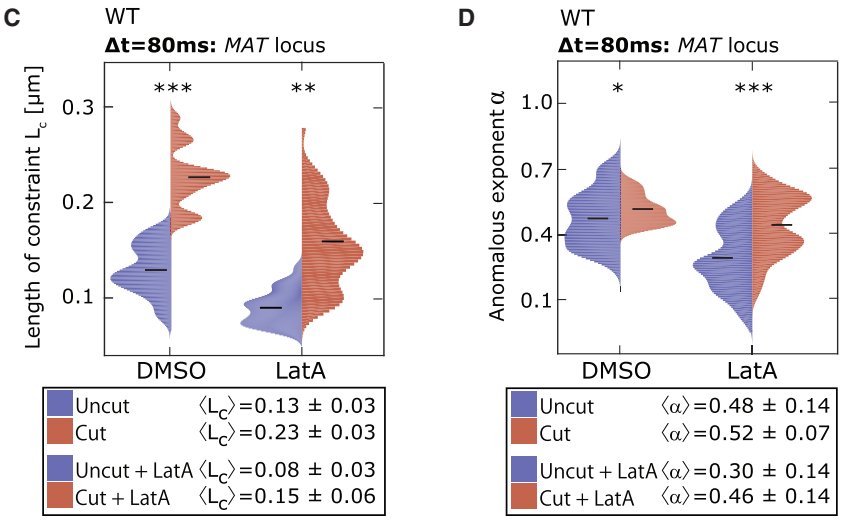

Figure 2. Depolymerization of the Actin Cytoskeleton Reduces Nuclear Rotation but Does Not Prevent DSB-Induced Movement

(A) The effect of rotation on the anomalous exponent α of a monomer within a Rouse polymer. When an angular velocity of ω = 0.04 s^{-1} is applied to the polymer, α increases from 0.5 (Rouse polymer) to 0.7.

(B) The spindle pole body (SPB) is embedded in the nuclear membrane and is visualized by Spc29-Ruby2. Its movement is used to monitor nuclear rotation/precession. Plots show α and Lc of the SPB after 1-hr treatment with the solvent DMSO or 25 μM LatA, which fully depolymerizes actin cables (Figure S4). Strain used is GA-9045.

(C and D) The Lc (C) and α (D) for *MAT*, derived from trajectories taken at Δt = 80 ms ± 25 μM LatA before and after 2 hr DSB induction (for strains, see Figure 1). Corresponding k_c and D_c values, as well as all values for Δt = 300 ms, are in Figure S5. Cut efficiencies are in Table S2.

*p ≤ 0.05, **p ≤ 0.01, ***p ≤ 0.001, respectively. See related Figures S3–S5.

decreased uncapped telomere movement (Lottersberger et al., 2015). Therefore, we revisited this question in yeast to access how MT depolymerization affects chromatin movement. We exposed yeast cells to 50 μM Nocodazole for 1 hr, which is sufficient to arrest cells in G2/M phase due to activation of the spindle assembly checkpoint, and subjected the *lacO*-tagged *MAT* locus to time-lapse imaging, in the presence and absence of a DSB. Interestingly, MT depolymerization (in contrast to actin depolymerization) increased both L_C and α and reduced tethering forces (k_c) at Δt = 80 ms (Figure 3). Following DSB induction, however, there was no further change in movement, with the exception of a marginal decrease in L_C and increase in k_c. Thus, MT depolymerization appears to increase chromatin movement to such an extent that a further increase due to local chromatin changes is not detectable. We attribute the increased chromatin dynamics upon Nocodazole treatment to the depolymerization of the MTs that tether yeast centromeres to the SPB. In mammals, this effect would not be observed since there are no direct MT connections from centrosome to kinetochore in interphase cells. Rather, it was proposed that the effect of Nocodazole in mammalian cells, i.e., the loss of increased chromatin movement after DNA damage (Lottersberger et al., 2015), stems from the loss of the link between cytoplasmic MT and either the nucleoskeleton or chromatin through the LINC complex (Linker of Nucleoskeleton and Cytoskeleton, (Tapley and Starr, 2013)), thus being more similar to the effects of LatA in yeast. Complicating this interpretation is

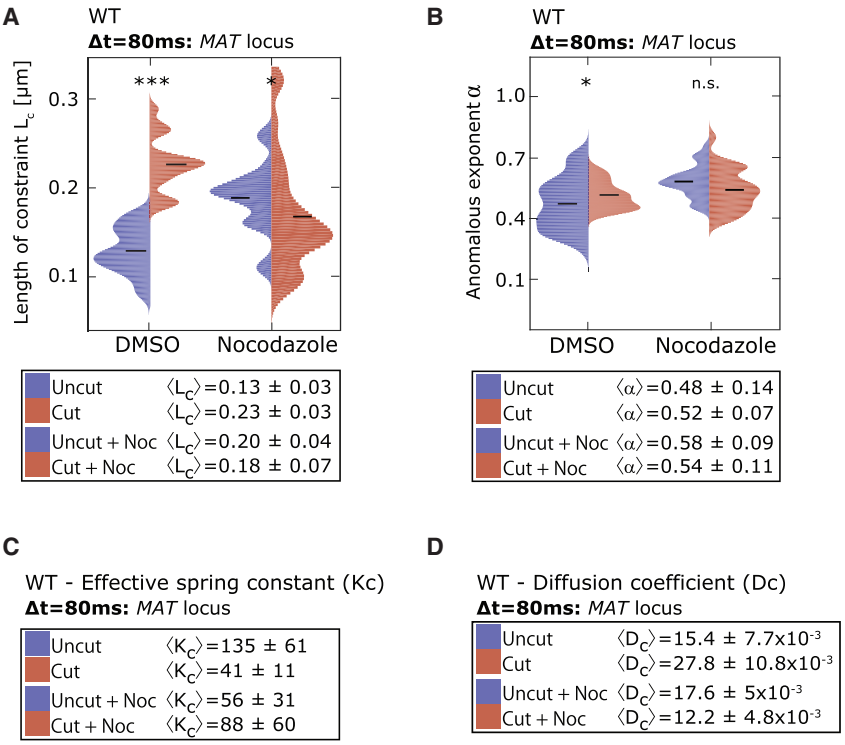

Figure 3. Nocodazole Increases Chromatin Mobility, and There Is No Further Increase after Break Induction

(A–D) The Lc (A) and α (B) values for *MAT*, derived from trajectories taken at $\Delta t = 80$ ms before and after 2 hr DSB induction are given. Strains are as in Figure 1. Where indicated, 50 μM Nocodazole was added for the last hour of HO induction. Corresponding k_c (C) and D_c (D) values are calculated from the same dataset. Cut efficiencies are in Table S2. *$p \leq 0.05$ and ***$p \leq 0.001$.

the fact that Nocodazole may induce cohesin cleavage in HeLa cells (Nakajima et al., 2007), an event that increases chromatin movement in yeast (Dion et al., 2013).

In summary, chromatin dynamics in yeast and mammalian cells showed opposite effects of MT depolymerization: in yeast, MTs can constrain chromatin movement, while actin filaments drive nuclear rotation. Removal of nuclear rotation/precession by LatA created conditions under which changes in SPT parameters were more apparent, while centromere release in yeast seemed to mask enhanced DSB mobility. In contrast, using MSD analysis in mammalian cells cytoplasmic MTs and dynein appeared to drive chromatin movement, an effect that was enhanced during the DNA damage response (Lottersberger et al., 2015). Actin depolymerization had no reported effect.

A Polymer Model Predicts Chromatin Expansion at a DSB

Post-translational modifications on histones and repair/signaling proteins recruited to DSBs are extensive and occur rapidly at DSBs. These include histone acetylation, ubiquitination, and phosphorylation, as well as histone variant exchange and nucleosome eviction by nucleosome remodelers (Smeenk and van Attikum, 2013). Given the large change in α at the site of a DSB once nuclear oscillations were removed ($\alpha^{uncut\ LatA} = 0.30$ to $\alpha^{cut\ LatA} = 0.46$), we next explored the consequence of this change on chromatin structure, using a generalized polymer model called the β-polymer model (Amitai and Holcman, 2013b). This model allows for local interactions between monomers to be calculated from a given anomalous exponent by the relationship $\alpha = 1 - 1/\beta$ (see Supplemental Information). In other words, this polymer model allows us to explore the effects of a changing anomalous exponent on the local organization of the polymer (Figure 4A). This β-polymer model can be used when anomalous exponents are in the range of α = 0–0.5, giving us an advantage over other polymer models, such as the Rouse model in which α must be 0.5. Importantly, while other polymer models can predict anomalous exponents for a chromatin locus with values smaller than 0.5 (Weber et al., 2010), none of them can interpret changes in α of the kind we observe following DNA damage.

To mimic the locus mobility before and after DSB induction, we constructed polymer models with anomalous exponents that were extracted from actual trajectories (Figure 4B). We found that as α increases there is a subsequent decompaction of the polymer (Figure 4B). This is quantified by an increase in the radius of gyration Rg, which is the mean distance of the monomers to the center of mass, from 1.21*b* when α = 0.33, to 2.34*b* when α = 0.5 (here b is distance between two adjacent monomers, for further details see Supplemental Information). Therefore, higher α values are associated with a more open chromatin state. This model thus predicts that chromatin will expand following induction of a DSB (Figure 4B).

To test this prediction, we measured the volumes occupied by the 10 kb of *lacO* array-containing chromatin near the DSB, using 3D super-resolution structured illumination microscopy of GFP-lacI fluorescence (3D-SIM, with an estimated resolution of ~120 nm xy and ~350 nm z; Figure 4C). We quantified the spot volume for hundreds of cells (250–1,030 foci per sample) with and without HO induction. We found that the 3D spot volume increased significantly upon cut induction in S-phase cells, from $V^{uncut} = 0.090 \pm 0.041\ \mu m^3$ to $V^{cut} = 0.109 \pm 0.086\ \mu m^3$ (Figure 4C; Table S4). This striking increase (+20%) confirms the prediction of the β-polymer model and corresponds to an increase in α from 0.33 to 0.45.

Nucleosome Remodeler INO80 Drives Increased α Independent of Actin Dynamics

If decompaction is truly a reflection of altered nucleosome packing, then we should be able to modulate it by eliminating the recruitment of the INO80 remodeler, which is recruited to damage in an Arp8-dependent manner. Loss of INO80 recruitment reduces nucleosome eviction at DSBs and attenuates the

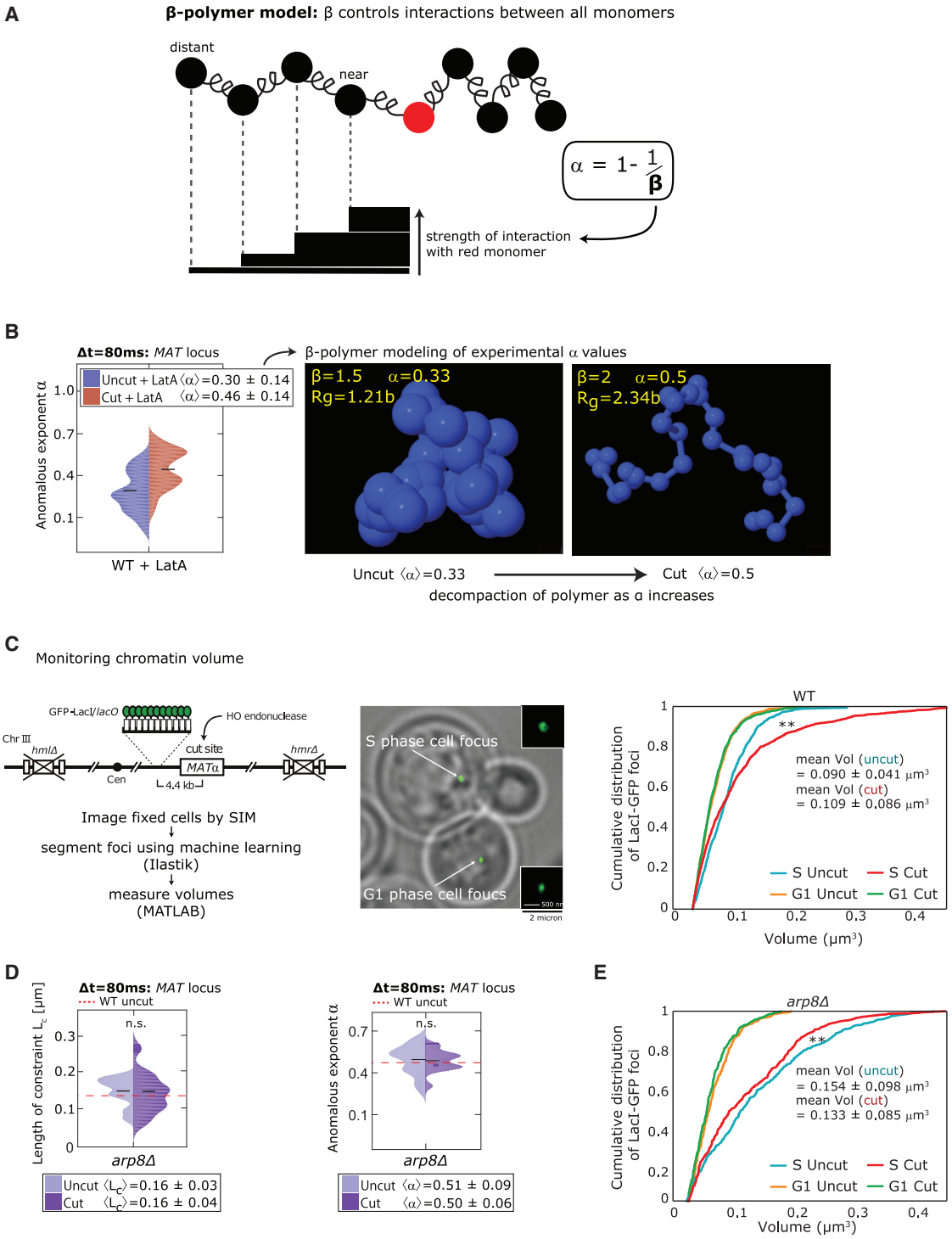

Figure 4. Polymer Simulations Predict Chromatin Expansion at a DSB, which Is Confirmed Experimentally with Structured Illumination Microscopy

(A) The β-polymer model allows for the interactions between all monomers to be controlled and measured in simulations. The strength of interaction of all monomers with any other monomer decays with distance. Anomalous diffusion α is related to β by $\alpha = 1-1/\beta$.

(B) β-polymers where the inter-monomer interactions are modified, with β values corresponding to α values obtained from biological experiments (β = 1.5 gives α = 0.33, and β = 2 gives α = 0.5). The radius of gyration Rg (yellow) measures the degree of compaction. Balls (blue) represent the monomers of radius 0.3*b*.

(C) Experimental system used to acquire and analyze SIM images of the *MAT* locus (left), and an example image showing a G1- and S-phase focus (middle), cumulative distribution function of the 3D volume of spots ± cleavage in wild-type (WT), strain GA-8067 (right). Cells were synchronized with α-factor to obtain G1

(legend continued on next page)

enhanced chromatin dynamics provoked by a DSB (Neumann et al., 2012; Seeber et al., 2013; Strecker et al., 2016). Arp8 is an integral component of the INO80 remodeler that is required for its nucleosome remodeling activity (van Attikum et al., 2007). Interestingly, cells lacking Arp8 have strong recombination defects (Agmon et al., 2013; Strecker et al., 2016) but only mild defects in checkpoint activation or resection (Chen et al., 2012; van Attikum et al., 2007). With this in mind, we tracked locus mobility in an *arp8Δ* strain, before and after DSB induction. Confirming previous reports (Neumann et al., 2012; Strecker et al., 2016), we find that Arp8 is required for increased mobility at the DSB: neither the *Lc*, α, *Dc*, nor k_c changed after cut induction (Figures 4D and S6).

Based on our interpretation of α as an indirect indicator of condensation state (Figure 4A), we monitored locus volume using super-resolution microscopy in the *arp8Δ* strain. The DSB and its surrounding chromatin not only failed to increase spot volume in the absence of Arp8, but volumes were slightly reduced (Figure 4E). This links chromatin expansion at the break to the remodeling activity of INO80 and suggests that INO80 may function at breaks to open chromatin facilitating recruitment of repair proteins (van Attikum et al., 2007).

Increasing α at a DSB Can Provoke Extrusion of Damage from a Chromatin Domain

Our data argue that chromatin expands at a DSB, presumably resulting from a reduction in local forces between monomers (nucleosomes) near the break. Experimentally, we know that DSBs trigger changes in chromatin organization and that they can move from one nuclear sub-compartment to another (Chiolo et al., 2011; Horigome et al., 2014; Jakob et al., 2011; Ryu et al., 2015; Torres-Rosell et al., 2007), yet it is not known how these are related, i.e., whether changes in chromatin at the site of a break affect the long-range architecture of a chromatin domain or a chromosome. Here, we used numerical simulations to ask what happens to the overall structure of a polymer if we reduce the intrinsic interactions of a single monomer, i.e., of a nucleosome near a DSB. The simulations further allow us to modulate the strength of interactions between all monomers, enabling us to test a range of situations that involve changes in specific inter-nucleosomal interactions, mimicking a controlled spread of decondensation from the site of damage.

To account for changes in the chromatin structure and to avoid interpenetration of the chromosome, we added repulsion interactions between each monomer (i.e., Lennard-Jones or LJ interactions) to the β-polymer model (see Figure S7 and Table S3). We considered a polymer of length n = 33, with a coefficient $\beta = 1.5$, where all monomers are highly connected (Figure 5A). We note that with the addition of LJ-interaction forces, the relationship between the exponent of the model and the measured anomalous exponent $\alpha = 1 - 1/\beta$, no longer holds, and the numerically estimated α for a self-avoiding polymer with $\beta = 1.5$ for a given monomer is $\alpha = 0.52$.

We then simulated the effect of a DSB on chromatin organization by reducing interactions of the middle monomer n = *17* (red monomer), such that longer-range connections are lost, and only nearest neighbor contacts remain (green monomers, Figure 5B). Surprisingly, this modification had a dramatic effect on the global structure of the polymer with the middle monomer being extruded to the periphery of the globular chromatin domain (Figure 5B). If we mimic the spreading of decondensation by removal of local forces acting on the two neighbors of the middle monomer (n = 16, 18), the effect is even more pronounced (Figure 5C). In analogy to the documented behavior of a DSB in heterochromatin, we find that the more condensed the polymer is, the more pronounced the extrusion effect will be. Moreover, the extrusion is stable as long as the reduced interactions persist: once shifted, the extruded monomer stays at the periphery of the chromatin domain (Figure S8).

We next simulated the effect of extrusion on movement by following the displacement of either an unmodified monomer (n = 10) or the break-mimicking modified monomer (n = 17) (Figure 5D). While the unmodified monomer does not change its position significantly, the modified monomer is highly mobile. To quantify this effect, we plot the average distance of each monomer from the center of mass (cm) of the polymer (Figure 5E). Before extrusion, the middle monomer was closest to the cm (see Figure 5A), but as forces are reduced on this monomer it moves further away (Figure 5E). Finally, we analyzed α for each monomer during the extrusion process. We find that when the interactions are removed from the middle and two neighbor monomers (Figure 5C), α increases sharply from 0.52 to 0.88 (Figure 5F). This is consistent with our empirical observations of increased α upon DSB induction and local chromatin expansion at the break. This polymer modeling suggests that expansion at the site of the break, reflected as increased α, is sufficient to shift a DSB to the periphery of its local chromatin domain.

Previous work has shown that DSBs that occur in heterochromatin or in the nucleolus must move out of these domains to be repaired by the recombination machinery (Chiolo et al., 2011; Ryu et al., 2015; Torres-Rosell et al., 2007; Tsouroula et al., 2016). To see whether this extrusion correlates with reduced forces at the break (i.e., increased α), we monitored the dynamics of an inducible I-SceI cut site integrated into the yeast rDNA with an adjacent *tetO* array, which is visualized by expressing TetR-mRFP (Torres-Rosell et al., 2007). The yeast strain further expressed a YFP-tagged Rad52, which is largely excluded from the nucleolus, and a plasmid-borne galactose-inducible I-SceI endonuclease, as well as constitutively expressed Nucleolar protein 1 (NOP1)-CFP. Rad52-YFP only co-localizes with the TetR-mRFP array when the locus has been extruded from the nucleolus (Figure 5G). To create the break, we induced I-SceI for 2 hr. To avoid interference by nuclear

cells, and S-phase cells were collected 30 min after release from pheromone. Cut induction was 30 min (see Supplemental Information). **$p \leq 0.01$. For foci counted, cut efficiencies, and statistics, see Tables S2 and S4.

(D) The parameters Lc and α derived from Δt = 80 ms imaging regimen in *arp8Δ* after 2-hr HO induction (strains GA-8921//8922). Cut efficiencies are in Table S2.

(E) Spot volumes as in (C) but for *arp8Δ* (GA-9602). See also Figures S6 and S8.

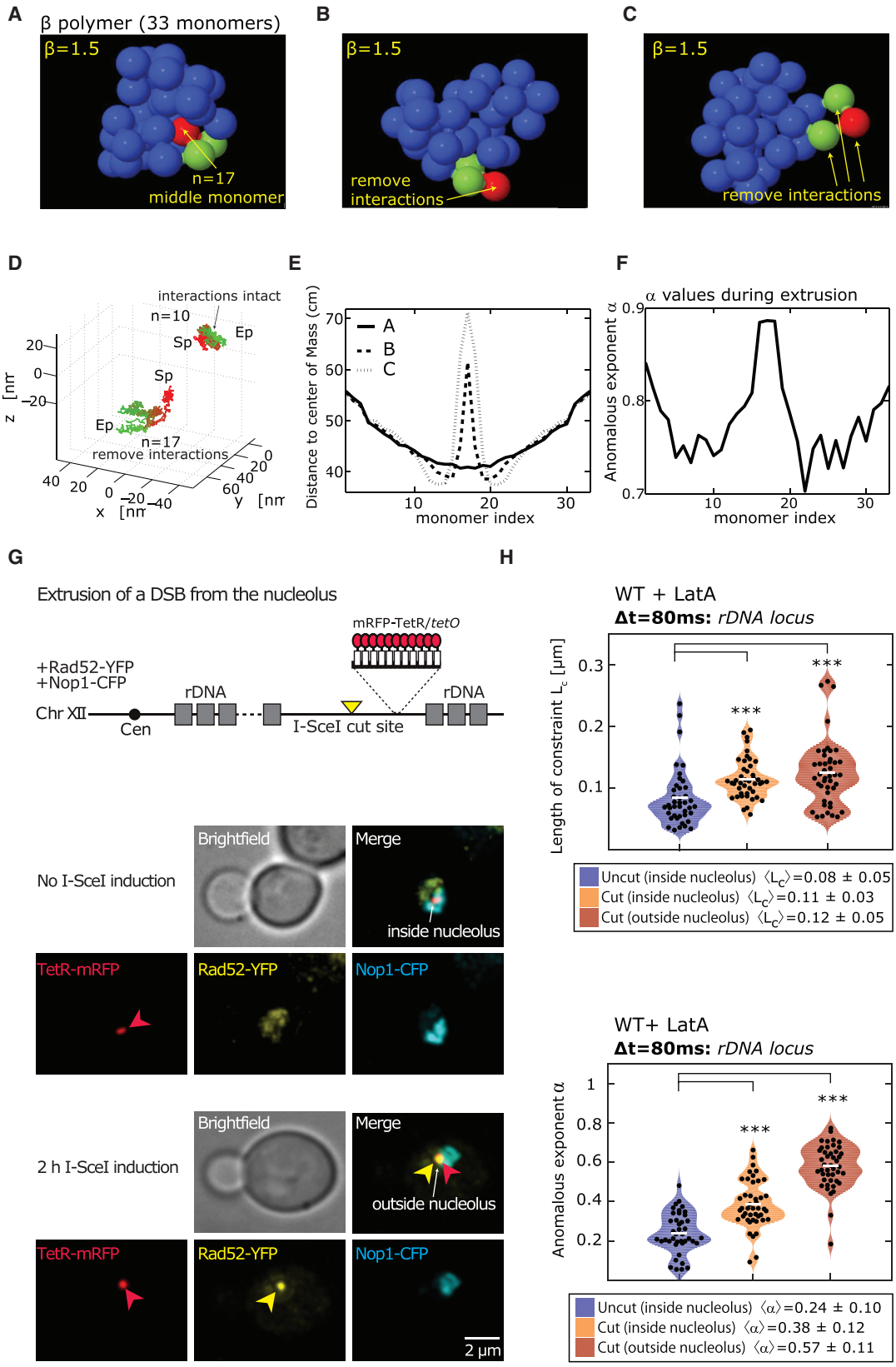

(legend on next page)

oscillation, we included 25 μm LatA during the last hour of cut induction. Dual acquisition (Δt = 80 ms) of TetR-mRFP and Rad52-YFP signals was performed in S-phase cells, where we track three conditions: first, an uncut locus (found within the nucleolus), second, a cut locus (I-SceI is expressed but the array remains within the nucleolus and no Rad52-YFP is bound), and, third, the cut locus that is relocated outside the nucleolus and bound by Rad52-YFP. We find that after break induction *Lc* increases from L_c^{uncut} = 0.08 ± 0.05 μm to $L_c^{cut(inside)}$ = 0.11 ± 0.03 μm and $L_c^{cut(outside)}$ = 0.12 ± 0.05 μm (Figure 5H). Importantly, we find that α increases very strongly both upon cleavage and again upon relocation from the nucleolus (α^{uncut} = 0.24 ± 0.1 μm to $\alpha^{cut(inside)}$ = 0.38 ± 0.12 μm and $\alpha^{cut(outside)}$ = 0.57 ± 0.11 μm). This increase in α likely reflects changes in the contacts at the site of break, further supported by the decrease k_c (Figure S9). It suggests that chromatin surrounding a break, extruded from the nucleolus, is more decondensed than a break within the nucleolus, consistent with a requirement for relocation for Rad52 binding (Torres-Rosell et al., 2007).

Intriguingly, in the absence of LatA the L_C shows the opposite trend: the uncut locus was more dynamic than the cut one (Figure S9). While surprising, we note that the rDNA is segregated from the rest of the nucleus and is attached to the inner nuclear membrane opposite of the SPB by an inner nuclear membrane complex called CLIP (Mekhail and Moazed, 2010) (Figure 6). We hypothesize that the nucleolus is subject to the effects of nuclear precession more than internal loci, and thus an uncut rDNA locus, which is more tightly linked to the nuclear envelope, may be more influenced by cytoskeletal dynamics. After DSB induction, the shift of the locus to the nucleoplasm should reduce nuclear envelope association and Lc or the length of its trajectory within a given time frame may be reduced. Regardless of trajectory length, we found that α increases from α^{uncut} = 0.38 ± 0.06 μm to $\alpha^{cut(outside)}$ = 0.53 ± 0.16 μm, both in the presence and absence of LatA.

Our experimental data thus recapitulate the predicted behavior of the β-polymer model of chromatin surrounding a DSB. The reduction of contacts at the site of a break, observed as domain expansion or an increase in α, reflect a local change in chromatin architecture that allows extrusion to occur. Notably, once chromatin at a DSB has acquired these characteristics, either through the actions of chromatin remodelers such as INO80 (Neumann et al., 2012), or by ubiquitination or SUMOylation of break associated nucleosomes (Horigome et al., 2016; Ryu et al., 2015; Torres-Rosell et al., 2007), break extrusion could occur without a requirement for active translocation. While we do not exclude that directed motion might also occur, the increase in α that leads to extrusion could simply result from reorganization to a minimal energy configuration of the polymer. This biological mechanism may also play a role in other processes that require locus repositioning, for instance, during transcriptional activation.

DISCUSSION

Polymer modeling is a powerful tool to analyze changes in chromatin structure. The choice of polymer model that best recapitulates the behavior of chromatin is open and highly debated. Here, we make the case for a family of polymer models called the β-polymer (Amitai and Holcman, 2013b), as it has the advantage of being able to account for changes in locus dynamics when movement is characterized by variable values for the anomalous exponent α. In addition, we show here that image sampling rate and external forces acting on the nucleus, such as actin filament-driven nuclear oscillation, can strongly affect the results obtained from SPT analysis. These can obscure the underlying properties of chromatin motion and must be taken in to account in live cell chromatin dynamics.

Previous studies of chromatin locus dynamics have relied largely on MSD analysis, which monitors the volume of sampled nuclear space, without shedding light on the nature of the forces acting on the locus in question (reviewed in Dion and Gasser, 2013). In contrast, the analysis workflow presented here dissects the velocity of a locus into external forces acting on the chromatin fiber and internal interactions along the chromatin fiber. The four parameters we extract (α, Lc, Kc, and Dc) contain different information and are largely independent of each other (described in Figures S10A and S10B). By incorporating these experimentally extracted values into polymer models we have predicted that chromatin will decompact at a DSB and that this should lead to the extrusion of the damage from its local chromatin domain. We confirmed both these predictions in yeast by live imaging of an inducible site-specific DSB, either at *MAT* or in the rDNA array. Consistently, an earlier study modeled human Chr 11 using the expression-dependent Dynamic Loop Model (Zhang and Heermann, 2014), in which loops create

Figure 5. Predicted Monomer Extrusion to the Periphery of Its Local Domain upon Loss of Forces between Monomers, and Confirmation with an rDNA DSB

(A) Steady-state configuration of a β-polymer model (β = 1.5 and n = 33 with Lennard-Jones interactions) where the middle monomer (n = 17) is colored in red and its neighbors (n = 16, 18) in green.

(B and C) (B) Modeling predicts this outcome upon removing inter-monomer interactions in a β-polymer at n = 17 and (C) at n = 16, 17, 18.

(D) Two trajectories following a monomer unaffected by the extrusion (n = 10) and the middle monomer (n = 17) (forces removed as in C). At time t = 0 (S_p initial point, in red), the interactions for monomers n = 16, 17, 18 are instantaneously removed. Over 0.05 s, the color changes gradually to green until the end point E_p.

(E) Average distance of each monomer from the center of mass corresponding to (A) full line, (B) dashed line, and (C) dotted line.

(F) The average anomalous exponent α for all different monomers during the extrusion process for case (C).

(G) Strain schematic (GA-6587) showing an I-SceI cut site sequence that has been inserted into the rDNA along with an adjacent *tetO* array, which is visualized by TetR-mRFP binding (red arrows). Cells harbor two plasmids containing either a galactose inducible *I-SCEI* or *NOP1-CFP* (Supplemental Information). When the locus is cleaved by I-SceI and the DSB moves outside the nucleolus, Rad52-YFP can be recruited and forms a focus (red arrows). Rad52 is largely excluded from the nucleolus (Torres-Rosell et al., 2007).

(H) The Lc and α for the strain in (G), derived from trajectories taken at Δt = 80 ms ± 25 μM LatA before and after 2-hr I-SceI induction. LatA was added for the last 1 hr of HO induction. Corresponding k_c and D_c values, as well as values for all parameters in the absence of LatA can be found in Figure S9. ***p ≤ 0.001.

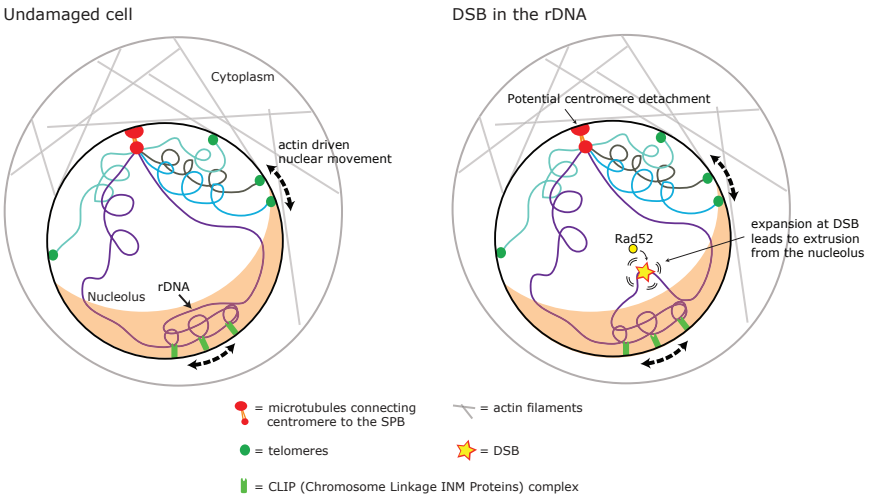

Figure 6. Expansion of Chromatin and Domain Extrusion Provoked by a DSB

Yeast chromosomes are anchored to the nuclear periphery in multiple ways: (1) their centromeres attach to the spindle pole body, (2) telomeres interact through multiple anchors including Sir proteins, SUN domain protein Mps3, Esc1, and Ku, and (3) the CLIP complex can tether the rDNA to the nuclear periphery. Cytoplasmic actin filaments can drive nuclear rotation/precession. After a DSB is induced, local interactions at the break are reduced allowing the chromatin surrounding the break to expand. The loss of interactions leads to the extrusion of the DSB outside of the nucleolus, allowing repair factors like Rad52 to bind.

compartments that are transcriptionally active (fewer loops) or inactive (more loops). By simulation they also found that a break in either an active or inactive domain will shift the site of damage away from the center of mass of the domain. While it was not confirmed experimentally, this is fully consistent with our modeling and experimental results.

Our study does not rule out that loss of an extrinsic tether, such as centromere detachment, could alter chromatin dynamics as reported by others (Strecker et al., 2016). However, our results make it unlikely that such changes are the only driving force behind enhanced break movement. Rather, we argue that the expansion of chromatin at the site of the break due to histone modifications and/or eviction (Smeenk and van Attikum, 2013) enhances α and drives increased movement. While these may be enhanced or altered by events like centromere detachment, in our hands, MT depolymerization and centromere detachment (Bystricky et al., 2004) prior to DSB induction, masks any other increase in mobility. We note that it is crucial for all experimental studies of chromatin dynamics to take into account the effects of nuclear precession, to triage image stacks by cell-cycle stage, and to monitor cleavage efficiency. Without these controls, results are likely to be misleading.

We also present here a quantitative 3D-SIM technique that monitors locus volume, and we show that expansion following a DSB requires the INO80 chromatin remodeling complex. Other remodelers, such as the BAF complex (Swi/Snf or Rsc in yeast) may serve a similar role (Seeber et al., 2014). Importantly, the targeting of INO80 to an uncut locus similarly increases locus dynamics (Neumann et al., 2012), without changing local transcription activity, supporting the notion that the shifting or removal of nucleosomes increases long-range locus dynamics. This has profound implications concerning the impact of local histone modifications on the compaction and spatial behavior of larger chromatin domains. The relevance of our observations is made clear by two recent studies in which a global decompaction of chromatin was observed in response to UV-induced DNA damage in mammalian cells (Adam et al., 2016) and in response to histone degradation in yeast (Hauer et al., 2017). Both studies reinforce and extend the models we simulated here.

As mentioned previously, β-polymer models can only be used when the anomalous exponent is in the range of 0–0.5. This limits their application to constrained, sub-diffusive movement and means that they cannot be used to study directed motion. Nonetheless, most DNA movement has been shown to be subdiffusive (Albert et al., 2013; Amitai et al., 2015; Dion and Gasser, 2013; Weber et al., 2010, 2012). The β-polymer models do not account for possible impact of local heterogeneous crowding on the polymer. On the other hand, by adding other interactions, such as polymer bending or Lennard-Jones forces, we have been able to account accurately for the chromatin dynamics monitored by fluorescent SPTs. We note that movement arising from nuclear rotation/precession leads to an increase in the anomalous exponent α, with or without a DSB. Finally, we show that the problem of additive motion can be circumvented by measuring the dynamics of the locus at different timescales.

New microscopes that allow for 3D imaging without the use of moving stages such as the aberration-corrected multi-focal microscope (Abrahamsson et al., 2013) or a double-helix point spread function microscope (Backlund et al., 2014) will expand the impact of high resolution chromatin locus tracking in the near future, providing even larger datasets that are appropriate for analysis by the β-polymer model presented here.

EXPERIMENTAL PROCEDURES

Yeast Growth Conditions

Yeast strains used in this study are in Table S1. Yeast cultures were grown 30°C, and imaging was performed at 25°C. Strains were either W303 background or JKM179, as described in Table S1. The Ruby2 fluorophore plasmid was acquired from Lee et al. (2013). For DSB live-tracking experiments, yeast were grown at 30°C on YPAD prior to dilution into synthetic media containing 3% glycerol and 2% lactate (SCLG) for several generations prior to the addition of 2% galactose to induce expression of HO. Unless otherwise indicated, 2-hr induction of HO was used, and the efficiency of endonuclease cleavage at *MAT* was determined by quantitative PCR with TaqMan probes as previously described, and qPCR values were normalized to the SMC2 locus (van Attikum et al., 2007). Cutting efficiencies are summarized in Table S2. See Supplemental Experimental Procedures for details.

Microscopy

Live microscopy used a Nikon Eclipse Ti microscope, two EM-CCD Cascade II (Photometrics) cameras, an ASI MS-2000 Z-piezo stage, and a PlanApo ×100,

numerical aperture (NA) 1.45 total internal reflection fluorescence microscope oil objective and Visiview software. Fluorophores were excited at 561 (Ruby2, mCherry), 515 (YFP), and 491 (GFP) nm. GFP and mCherry/Ruby2 fluorescence were acquired simultaneously on separate cameras. A Semrock FF01-617/73-25 filter was used to capture the mCherry/Ruby2 signal on camera 1, and a Semrock FF02-525/40-25 filter was used to capture the GFP signal on camera 2. Time-lapse series were conducted taking eight optical slices per stack either every 80 ms for 1 min or 300 ms for 2 min. Each optical slice received either a 10-ms exposure for the 80-ms intervals or 30 ms for the 300-ms intervals. Nuclear volumes are based on an average haploid nuclear radius of 0.9 μm. Time-lapse image stacks were analyzed as in Dion et al. (2012), using a custom-made ImageJ (FIJI) plug-in, to extract coordinates of locus position from the movies. For structured illumination microscopy, and other specifics of staining and foci selection, see Supplemental Experimental Procedures. Spot tracking was carried out with the Fiji plugin Spot Tracker 2D (Neumann et al., 2012).

Extraction of Parameters, Modeling, and Simulations with Rouse Polymer

The extraction of biophysical parameters from the image stacks and their mathematical derivation are described in Supplemental Experimental Procedures. A Rouse polymer is a collection of monomers moving with a random Brownian motion coupled to a spring force originating from the nearest neighbors. We use other polymer models by adding interactions such as bending elasticity, which accounts for the persistence length of the polymer and Lennard-Jones forces (LJ), describing self-avoidance of each monomer pairs. Finally, we used Euler's scheme to generate Brownian simulations. At impenetrable boundary, each rigid monomer is reflected in the normal direction of the tangent plane. See Supplemental Experimental Procedures for details.

Error Propagation and Statistical Significance

Significance between α, Kc, Lc, and Dc values was tested using the non-parametric Kolmogorov-Smirnov (KS) test. p values are either indicated above the figure panels or by asterisks, where *p $\leq$ 0.05, **p $\leq$ 0.01, ***p$\leq$ 0.001, respectively. Error bars on graphs represent the SE unless otherwise stated. LacI-GFP spot size was shown to be normally distributed and then tested for differences using a two-tailed Student's t test (Graph Pad). Significance cut off was $p < 0.05$.

The Polymer Model

To account for the chromatin dynamics, we use the generalized polymer model called the β-polymer model (Amitai and Holcman, 2013b), which accounts for anomalous diffusive behavior with α in the range of 0–0.5, as measured for a yeast in vivo chromatin locus (Hajjoul et al., 2013). We use β-polymer model where all monomers are connected through a quadratic potential defined by

$$U_\beta(\boldsymbol{R}_1,..\boldsymbol{R}_N,\beta)=\frac{1}{2}\sum_{l,m}A_{lm}\boldsymbol{R}_l\boldsymbol{R}_m,$$

with coefficients

$$A_{l,m}=\sum_{p=1}^{N-1}\tilde{\kappa}_p\alpha_p^l\alpha_p^m=4\kappa\frac{2}{N}\sum_{p=1}^{N-1}sin^\beta\frac{p\pi}{2N}\cos\left(\left(l-\frac{1}{2}\right)\frac{p\pi}{N}\right)\ \cos\left(\left(m-\frac{1}{2}\right)\frac{p\pi}{N}\right)$$

and

$$\tilde{\kappa}_p=4\kappa\overset{\beta}{\sin}\left(\frac{p\pi}{2N}\right)\ \text{for}\ p=0..N-1.$$

In such a model, the strength of interaction $A_{l,m}$ decays with the distance $|l-m|$ along the chain. By definition, $1<\beta<2$ (Amitai and Holcman, 2013b) and the Rouse polymer is recovered for $\beta=2$, for which only nearest neighbors are connected.

SUPPLEMENTAL INFORMATION

Supplemental Information includes Supplemental Experimental Procedures, ten figures, and four tables and can be found with this article online at http://dx.doi.org/10.1016/j.celrep.2017.01.018.

AUTHOR CONTRIBUTIONS

A.S. and S.M.G. planned experiments and analyzed data. A.S. performed most experiments, and A.A. and D.H. carried out all polymer modeling, theoretical development of the analysis pipeline, and extracted biophysical parameters from imaging data. All four authors wrote the paper.

ACKNOWLEDGMENTS

We thank Luca Giorgetti and Vincent Dion for critically reading this manuscript. We thank Jan Eglinger, Laurent Gelman, and Steve Bourke for imaging support; Michael Lisby for strains; and the Gasser laboratory for exciting discussions. S.M.G. thanks the Swiss National Science Foundation (310030B_156936), the Human Frontier Science Program (RGP-0016), and the Novartis Research Foundation for support.

Received: April 18, 2016
Revised: December 2, 2016
Accepted: January 10, 2017
Published: January 31, 2017

REFERENCES

Abrahamsson, S., Chen, J., Hajj, B., Stallinga, S., Katsov, A.Y., Wisniewski, J., Mizuguchi, G., Soule, P., Mueller, F., Dugast Darzacq, C., et al. (2013). Fast multicolor 3D imaging using aberration-corrected multifocus microscopy. Nat. Methods *10*, 60–63.

Adam, S., Dabin, J., Chevallier, O., Leroy, O., Baldeyron, C., Corpet, A., Lomonte, P., Renaud, O., Almouzni, G., and Polo, S.E. (2016). Real-time tracking of parental histones reveals their contribution to chromatin integrity following DNA damage. Mol. Cell *64*, 65–78.

Agmon, N., Liefshitz, B., Zimmer, C., Fabre, E., and Kupiec, M. (2013). Effect of nuclear architecture on the efficiency of double-strand break repair. Nat. Cell Biol. *15*, 694–699.

Albert, B., Mathon, J., Shukla, A., Saad, H., Normand, C., Léger-Silvestre, I., Villa, D., Kamgoue, A., Mozziconacci, J., Wong, H., et al. (2013). Systematic characterization of the conformation and dynamics of budding yeast chromosome XII. J. Cell Biol. *202*, 201–210.

Amitai, A., and Holcman, D. (2013a). Diffusing polymers in confined microdomains and estimation of chromosomal territory sizes from chromosome capture data. Phys. Rev. Lett. *110*, 248105.

Amitai, A., and Holcman, D. (2013b). Polymer model with long-range interactions: Analysis and applications to the chromatin structure. Phys. Rev. E Stat. Nonlin. Soft Matter Phys. *88*, 052604.

Amitai, A., Toulouze, M., Dubrana, K., and Holcman, D. (2015). Analysis of single locus trajectories for extracting in vivo chromatin tethering interactions. PLoS Comput. Biol. *11*, e1004433.

Aten, J.A., Stap, J., Krawczyk, P.M., van Oven, C.H., Hoebe, R.A., Essers, J., and Kanaar, R. (2004). Dynamics of DNA double-strand breaks revealed by clustering of damaged chromosome domains. Science *303*, 92–95.

Backlund, M.P., Joyner, R., Weis, K., and Moerner, W.E. (2014). Correlations of three-dimensional motion of chromosomal loci in yeast revealed by the double-helix point spread function microscope. Mol. Biol. Cell *25*, 3619–3629.

Bell, A.C., and Felsenfeld, G. (1999). Stopped at the border: Boundaries and insulators. Curr. Opin. Genet. Dev. *9*, 191–198.

Bystricky, K. (2015). Chromosome dynamics and folding in eukaryotes: Insights from live cell microscopy. FEBS Lett. *589* (*20 Pt A*), 3014–3022.

Bystricky, K., Heun, P., Gehlen, L., Langowski, J., and Gasser, S.M. (2004). Long-range compaction and flexibility of interphase chromatin in budding yeast analyzed by high-resolution imaging techniques. Proc. Natl. Acad. Sci. USA *101*, 16495–16500.

Chen, X., Cui, D., Papusha, A., Zhang, X., Chu, C.D., Tang, J., Chen, K., Pan, X., and Ira, G. (2012). The Fun30 nucleosome remodeller promotes resection of DNA double-strand break ends. Nature *489*, 576–580.

Chiolo, I., Minoda, A., Colmenares, S.U., Polyzos, A., Costes, S.V., and Karpen, G.H. (2011). Double-strand breaks in heterochromatin move outside of a dynamic HP1a domain to complete recombinational repair. Cell *144*, 732–744.

Cho, N.W., Dilley, R.L., Lampson, M.A., and Greenberg, R.A. (2014). Interchromosomal homology searches drive directional ALT telomere movement and synapsis. Cell *159*, 108–121.

Chubb, J.R., Boyle, S., Perry, P., and Bickmore, W.A. (2002). Chromatin motion is constrained by association with nuclear compartments in human cells. Curr. Biol. *12*, 439–445.

Chung, D.K., Chan, J.N., Strecker, J., Zhang, W., Ebrahimi-Ardebili, S., Lu, T., Abraham, K.J., Durocher, D., and Mekhail, K. (2015). Perinuclear tethers license telomeric DSBs for a broad kinesin-and NPC-dependent DNA repair process. Nat. Comm. *6*, 7742.

Dillon, N., Trimborn, T., Strouboulis, J., Fraser, P., and Grosveld, F. (1997). The effect of distance on long-range chromatin interactions. Mol. Cell *1*, 131–139.

Dimitrova, N., Chen, Y.C.M., Spector, D.L., and de Lange, T. (2008). 53BP1 promotes non-homologous end joining of telomeres by increasing chromatin mobility. Nature *456*, 524–528.

Dion, V., and Gasser, S.M. (2013). Chromatin movement in the maintenance of genome stability. Cell *152*, 1355–1364.

Dion, V., Kalck, V., Horigome, C., Towbin, B.D., and Gasser, S.M. (2012). Increased mobility of double-strand breaks requires Mec1, Rad9 and the homologous recombination machinery. Nat. Cell Biol. *14*, 502–509.

Dion, V., Kalck, V., Seeber, A., Schleker, T., and Gasser, S.M. (2013). Cohesin and the nucleolus constrain the mobility of spontaneous repair foci. EMBO Rep. *14*, 984–991.

Gartenberg, M.R., Neumann, F.R., Laroche, T., Blaszczyk, M., and Gasser, S.M. (2004). Sir-mediated repression can occur independently of chromosomal and subnuclear contexts. Cell *119*, 955–967.

Hajjoul, H., Mathon, J., Ranchon, H., Goiffon, I., Mozziconacci, J., Albert, B., Carrivain, P., Victor, J.-M., Gadal, O., Bystricky, K., and Bancaud, A. (2013). High-throughput chromatin motion tracking in living yeast reveals the flexibility of the fiber throughout the genome. Genome Res. *23*, 1829–1838.

Hauer, M.H., Seeber, A., Singh, V., Thierry, R., Amitai, A., Eglinger, J., Holcman, D., Owen-Hughes, T., and Gasser, S.M. (2017). Histone degradation in response to DNA damage triggers general chromatin decompaction. Nat. Struct. Mol. Biol. Published online January 9, 2017. http://dx.doi.org/10.1038/nsmb.3347.

Heun, P., Laroche, T., Shimada, K., Furrer, P., and Gasser, S.M. (2001). Chromosome dynamics in the yeast interphase nucleus. Science *294*, 2181–2186.

Horigome, C., Oma, Y., Konishi, T., Schmid, R., Marcomini, I., Hauer, M.H., Dion, V., Harata, M., and Gasser, S.M. (2014). SWR1 and INO80 chromatin remodelers contribute to DNA double-strand break perinuclear anchorage site choice. Mol. Cell *55*, 626–639.

Horigome, C., Bustard, D.E., Marcomini, I., Delgoshaie, N., Tsai-Pflugfelder, M., Cobb, J.A., and Gasser, S.M. (2016). PolySUMOylation by Siz2 and Mms21 triggers relocation of DNA breaks to nuclear pores through the Slx5/Slx8 STUbL. Genes Dev. *30*, 931–945.

Jakob, B., Splinter, J., Durante, M., and Taucher-Scholz, G. (2009). Live cell microscopy analysis of radiation-induced DNA double-strand break motion. Proc. Natl. Acad. Sci. USA *106*, 3172–3177.

Jakob, B., Splinter, J., Conrad, S., Voss, K.O., Zink, D., Durante, M., Löbrich, M., and Taucher-Scholz, G. (2011). DNA double-strand breaks in heterochromatin elicit fast repair protein recruitment, histone H2AX phosphorylation and relocation to euchromatin. Nucleic Acids Res. *39*, 6489–6499.

Kepten, E., Bronshtein, I., and Garini, Y. (2013). Improved estimation of anomalous diffusion exponents in single-particle tracking experiments. Phys. Rev. E Stat. Nonlin. Soft Matter Phys. *87*, 052713.

Krawczyk, P.M., Borovski, T., Stap, J., Cijsouw, T., ten Cate, R., Medema, J.P., Kanaar, R., Franken, N.A.P., and Aten, J.A. (2012). Chromatin mobility is increased at sites of DNA double-strand breaks. J. Cell Sci. *125*, 2127–2133.

Kruhlak, M.J., Celeste, A., Dellaire, G., Fernandez-Capetillo, O., Müller, W.G., McNally, J.G., Bazett-Jones, D.P., and Nussenzweig, A. (2006). Changes in chromatin structure and mobility in living cells at sites of DNA double-strand breaks. J. Cell Biol. *172*, 823–834.

Lee, S., Lim, W.A., and Thorn, K.S. (2013). Improved blue, green, and red fluorescent protein tagging vectors for S. cerevisiae. PLoS ONE *8*, e67902.

Levi, V., Ruan, Q., Plutz, M., Belmont, A.S., and Gratton, E. (2005). Chromatin dynamics in interphase cells revealed by tracking in a two-photon excitation microscope. Biophys. J. *89*, 4275–4285.

Lottersberger, F., Karssemeijer, R.A., Dimitrova, N., and de Lange, T. (2015). 53BP1 and the LINC Complex Promote Microtubule-Dependent DSB Mobility and DNA Repair. Cell *163*, 880–893.

Marshall, W.F. (2002). Order and disorder in the nucleus. Curr. Biol. *12*, R185–R192.

Marshall, W.F., Straight, A., Marko, J.F., Swedlow, J., Dernburg, A., Belmont, A., Murray, A.W., Agard, D.A., and Sedat, J.W. (1997). Interphase chromosomes undergo constrained diffusional motion in living cells. Curr. Biol. *7*, 930–939.

Mekhail, K., and Moazed, D. (2010). The nuclear envelope in genome organization, expression and stability. Nat. Rev. Mol. Cell Biol. *11*, 317–328.

Miné-Hattab, J., and Rothstein, R. (2012). Increased chromosome mobility facilitates homology search during recombination. Nat. Cell Biol. *14*, 510–517.

Nagai, S., Dubrana, K., Tsai-Pflugfelder, M., Davidson, M.B., Roberts, T.M., Brown, G.W., Varela, E., Hediger, F., Gasser, S.M., and Krogan, N.J. (2008). Functional targeting of DNA damage to a nuclear pore-associated SUMO-dependent ubiquitin ligase. Science *322*, 597–602.

Nakajima, M., Kumada, K., Hatakeyama, K., Noda, T., Peters, J.M., and Hirota, T. (2007). The complete removal of cohesin from chromosome arms depends on separase. J. Cell Sci. *120*, 4188–4196.

Nelms, B.E., Maser, R.S., MacKay, J.F., Lagally, M.G., and Petrini, J.H. (1998). In situ visualization of DNA double-strand break repair in human fibroblasts. Science *280*, 590–592.

Neumann, F.R., Dion, V., Gehlen, L.R., Tsai-Pflugfelder, M., Schmid, R., Taddei, A., and Gasser, S.M. (2012). Targeted INO80 enhances subnuclear chromatin movement and ectopic homologous recombination. Genes Dev. *26*, 369–383.

Ptashne, M. (1986). Gene regulation by proteins acting nearby and at a distance. Nature *322*, 697–701.

Roukos, V., Voss, T.C., Schmidt, C.K., Lee, S., Wangsa, D., and Misteli, T. (2013). Spatial dynamics of chromosome translocations in living cells. Science *341*, 660–664.

Ryu, T., Spatola, B., Delabaere, L., Bowlin, K., Hopp, H., Kunitake, R., Karpen, G.H., and Chiolo, I. (2015). Heterochromatic breaks move to the nuclear periphery to continue recombinational repair. Nat. Cell Biol. *17*, 1401–1411.

Seeber, A., Dion, V., and Gasser, S.M. (2013). Checkpoint kinases and the INO80 nucleosome remodeling complex enhance global chromatin mobility in response to DNA damage. Genes Dev. *27*, 1999–2008.

Seeber, A., Dion, V., and Gasser, S.M. (2014). Remodelers move chromatin in response to DNA damage. Cell Cycle *13*, 877–878.

Smeenk, G., and van Attikum, H. (2013). The chromatin response to DNA breaks: Leaving a mark on genome integrity. Annu. Rev. Biochem. *82*, 55–80.

Soutoglou, E., Dorn, J.F., Sengupta, K., Jasin, M., Nussenzweig, A., Ried, T., Danuser, G., and Misteli, T. (2007). Positional stability of single double-strand breaks in mammalian cells. Nat. Cell Biol. *9*, 675–682.

Spichal, M., Brion, A., Herbert, S., Cournac, A., Marbouty, M., Zimmer, C., Koszul, R., and Fabre, E. (2016). Evidence for a dual role of actin in regulating chromosome organization and dynamics in yeast. J. Cell Sci. *129*, 681–692.

Starr, D.A., and Fridolfsson, H.N. (2010). Interactions between nuclei and the cytoskeleton are mediated by SUN-KASH nuclear-envelope bridges. Ann. Rev. Cell Dev. Biol. *26*, 421–424.

Strecker, J., Gupta, G.D., Zhang, W., Bashkurov, M., Landry, M.-C., Pelletier, L., and Durocher, D. (2016). DNA damage signalling targets the kinetochore to promote chromatin mobility. Nat. Cell Biol. *18*, 281–290.

Taddei, A., and Gasser, S.M. (2012). Structure and function in the budding yeast nucleus. Genetics *192*, 107–129.

Tapley, E.C., and Starr, D.A. (2013). Connecting the nucleus to the cytoskeleton by SUN-KASH bridges across the nuclear envelope. Curr. Opin. Cell Biol. *25*, 57–62.

Torres-Rosell, J., Sunjevaric, I., De Piccoli, G., Sacher, M., Eckert-Boulet, N., Reid, R., Jentsch, S., Rothstein, R., Aragón, L., and Lisby, M. (2007). The Smc5-Smc6 complex and SUMO modification of Rad52 regulates recombinational repair at the ribosomal gene locus. Nat. Cell Biol. *9*, 923–931.

Tsouroula, K., Furst, A., Rogier, M., Heyer, V., Maglott-Roth, A., Ferrand, A., Reina-San-Martin, B., and Soutoglou, E. (2016). Temporal and spatial uncoupling of DNA double strand break repair pathways within mammalian heterochromatin. Mol. Cell *63*, 293–305.

van Attikum, H., Fritsch, O., and Gasser, S.M. (2007). Distinct roles for SWR1 and INO80 chromatin remodeling complexes at chromosomal double-strand breaks. EMBO J. *26*, 4113–4125.

Verdaasdonk, J.S., Vasquez, P.A., Barry, R.M., Barry, T., Goodwin, S., Forest, M.G., and Bloom, K. (2013). Centromere tethering confines chromosome domains. Mol. Cell *52*, 819–831.

Weber, S.C., Theriot, J.A., and Spakowitz, A.J. (2010). Subdiffusive motion of a polymer composed of subdiffusive monomers. Phys. Rev. E Stat. Nonlin. Soft Matter Phys. *82*, 011913.

Weber, S.C., Spakowitz, A.J., and Theriot, J.A. (2012). Nonthermal ATP-dependent fluctuations contribute to the in vivo motion of chromosomal loci. Proc. Natl. Acad. Sci. USA *109*, 7338–7343.

Zhang, Y., and Heermann, D.W. (2014). DNA double-strand breaks: Linking gene expression to chromosome morphology and mobility. Chromosoma *123*, 103–115.

Cell Reports, Volume *18*

Supplemental Information

Visualization of Chromatin Decompaction and Break Site Extrusion as Predicted by Statistical Polymer Modeling of Single-Locus Trajectories

Assaf Amitai, Andrew Seeber, Susan M. Gasser, and David Holcman

Supplementary Material

Visualization of chromatin decompaction and break site extrusion as predicted by statistical polymer modeling of single locus trajectories

Amitai, Seeber, Gasser and Holcman

Inventory

1 - Detailed Supplemental Experimental Procedures

Yeast growth conditions and cleavage induction method

Yeast strains used in this study are in Table S1. Yeast cultures were grown at 30°C, and imaged at 25°C. Strains were either W303 background or JKM179 as previously described (Dion et al., 2012; van Attikum et al., 2007). The Ruby2 fluorophore plasmid was acquired from Addgene (Lee et al., 2013). LatA and Nocodazole were dissolved in DMSO, and were added 1 h after galactose addition at a final concentration of 25μM and 50 μM respectively. Both treated and control cultures were adjusted to 1% DMSO. For live cell imaging, 5 ml of YPAD (2% Bactopeptone, 1% yeast extract, 0.01% adenine, 2% glucose) was inoculated and grown over night. In the morning the culture was diluted to $2x10^6$ cells per ml in synthetic complete media containing 3% glycerol and 2% lactate (SCLG). The cells were then grown for a minimum of 4 hours or until the culture doubled 1.5 times. The Gal1-10p driven *HO* gene was induced for 2 h by adding galactose to the culture to a final concentration of 2%. These growth conditions differ to those used previously for galactose induction (Horigome et al., 2015) where a diluted overnight YPAD culture is allowed to grow for ~10 hours in SCLGg (containing 0.05% glucose), before addition of galactose. Cell growth conditions for 3D-SIM imaging were similar to those used for live cell imaging except that YPLG (2% Bactopeptone, 1% yeast extract, 3% glycerol and 2% lactate) media was used instead of synthetic complete media. Before galactose addition the cells were synchronized in G1 phase by the addition of 1 μg/ml alpha factor for 1.5 h. For S-phase cells, cultures were released from α-factor into media + 2% galactose for 30 min.

DNA was extracted for quantitative PCR (QPCR) by spinning down 1 ml of cells and resuspending them in 100 μl of 200 mM LiAc (lithium acetate) containing 1% SDS (sodium dodecyl sulfate). The samples were incubated at 70 °C for 15 min after which 300 μl of 96% ethanol was added. The samples were then vortexed briefly and centrifuged at maximum speed for 3 minutes to collect DNA. The supernatant was removed and 100 μl of nuclease free water was added. Cell debris was pelleted by a 1 min high speed spin at maximum speed and 0.5-1 μl of the supernatant was used in a QPCR reaction. This method has been tested for QPCR (Looke et al., 2011). The efficiency of DSB induction was determined by QPCR with TaqMan probes as previously described (van Attikum et al., 2007) and the results are in Table S2. QPCR values were normalized to the *SMC2* locus (van Attikum et al., 2007) and primer and probe sequences are available on request.

We used the galactose inducible I-SceI-expressing strain (GA-6587 containing the I-SceI expressing plasmid pWJ1108) with a cleavage consensus in the rDNA (Torres-Rosell et al., 2007), because it was well characterized. In addition, the nucleolus was visualized in this strain by transformation of cells with a plasmid containing NOP1-CFP (SG-3453). In Torres-Rosell et al., the authors show that after 2h of cut induction (the conditions we use), 50% of I-SceI cut loci move outside of the nucleolus and 40% move to its periphery. A minority (10%) remain inside after I-SceI induction. Importantly, only ~10% I-SceI sites are found outside of the nucleolus in cells without I-Sce1 induction.

Live cell microscopy

Live microscopy was done at 25°C on a Nikon Eclipse Ti microscope, two EM-CCD Cascade II (Photometrics) cameras, an ASI MS-2000 Z-piezo stage and a PlanApo x100, NA 1.45 total internal reflection fluorescence microscope oil objective and Visiview software. Fluorophores were excited at 561 nm (Ruby2) and 491 nm (GFP), and emitted fluorescence was acquired simultaneously on separate cameras (Semrock FF01-617/73-25 filter for mCherry/Ruby2 and Semrock FF02-525/40-25 filter for GFP). Time-lapse series were streamed taking 8 optical slices per stack either every 80 ms for 60 s or 300 ms for 120 s, with 10 ms and 30 ms exposure times per slice respectively with laser powers set to ~7-12% for either laser line. Gain was set to 800. Nuclear volumes are based on an average haploid nuclear radius of 0.9 µm. Time-lapse image stacks were analyzed as in (Dion et al., 2012), using a custom made ImageJ (FIJI) plug-in (Sage et al., 2005), to correct for translational movement and to extract locus coordinates.

Structured illumination microscopy (SIM)

Structured illumination images were acquired at 23°C on a Zeiss Elyra S.1 microscope with a Andor iXon 885 EM-CCD camera using a HR diode 488 nm 100nW solid state laser, BP 525-580 + LP 750 filter and a PLAN-APOCHROMAT 63x N.A. 1.4 oil DIC objective lens. Cells were first fixed in freshly dissolved paraformaldehyde (PFA) 4% w/v for 5 min, washed 3 times in PBS and then attached glass slide using Concanavalin A. A thin SIM grade Zeiss 1.5 glass coverslip was used while imaging. Cells were fully sectioned by 50 slices with 0.1 nm intervals taken at 50 ms exposures per slice using 5 rotations of the illumination grid. Brightfield images of the cells were also acquired using an X-Cite PC 120 EXFO Metal Halide lamp. Zen Black was used to process the images using manual settings including Raw Scale. An automatic noise filter was used within the range of -4 to -6. The pixel size of the images after processing is 39 nm. 3D stacks were segmented using Ilastik and the subsequent probability masks projected onto the image using a custom Matlab script to determine the spot volumes. Volumes were

filtered to exclude spots smaller than 200 and greater than 3000 voxels.

Actin filament staining

10 µl of Rhodamine phalloidin (6.6 µm) was added to 100 µl of PFA fixed cells (4% paraformaldehyde for 5 min) and stained overnight. After washing in PBS the cells were imaged using SIM as above, with the 561 nm laser and appropriate emission filter. 60 z slices were acquired with a 100 nm step size using 5 rotations of the structured illumination grid.

The same aliquot of fixed cells was used for an actin Western blot. Sample buffer + 0.1 M DTT were added to the cells and they were heated to 95°C for 1 h to reverse crosslinking. Samples were run on a 4-12% SDS-PAGE gel and blotted using a Transblot turbo machine. The membrane was blocked in TENT (40 mM Tris-HCl (pH 7.5), 1mM EDTA (pH 8.0), 150 mM NaCl and 0.05% Tween-20) + 5% milk for 1 h. Actin was stained with a mouse anti-actin antibody (Millipore MAB1501, 1:10000) in TENT + 5% milk followed by a HRP conjugated mouse secondary antibody (1:10000). Ponceau S staining revealed total protein content.

Selection of foci and extraction of parameters

Due to the linearity of the equations, the dynamics of a Rouse polymer can be studied by projecting the equations on any axis. The parameters we calculated (Lc, α, kc, and Dc) can be estimated separately in the projected equations. Because other motion such as nucleus precession can influence the parameter estimation, we computed the anomalous α in both spatial axes separately (α_x and α_y), as any additional motion of the nucleus can influence α (Figure 2A). In Figure S3B, we show how the α estimate for a SPT of a Rouse polymer changes when a drift is added. We find that drift increases α to 0.66 (intermediate time interval, red line) from α= 0.5 (black line). Indeed, high values of α are the signature of an additive drift. In the presented results, we consider the α best representing the system to be the smaller value and thus consider that $\alpha = Min\{\alpha_x, \alpha_y\}$. In addition, we excluded nuclei containing aberrantly large steps which are defined as steps ≥ 500 nm for the imaging regimes of Δt = 80 ms or 300 ms, where a step is given by the difference $|\mathbf{R}_c((k+1)\Delta t) - \mathbf{R}_c(k\Delta t)|$. While α is estimated on a single axis, Lc, kc and Dc are estimated using both the x and y axis.

Effect of an external force on locus motion

We computed the anomalous exponent α (see below for derivation) from the projection of the dynamics on each axis of an orthogonal frame. The value of α computed for each direction for many cells, was often larger than 0.5 (Fig. 1). To interpret these values, we consider that an

additional force can be applied to the locus. We implemented this force using numerical simulations in two conditions: either the force was deterministic (directed) or it was random. We then computed the anomalous exponent α from the first six points of the time auto-correlation function, power-law ($C(t) = C \times t^{\alpha}$, where C is a constant).

An external deterministic force increases the anomalous exponent α

A deterministic force acting on a polymer affects any monomer motion. In practice such added motion can account for nuclear rotation, long time reorganization or simply measurement artifacts. Using a Rouse polymer embedded into a constant drift field with amplitude $|\mathbf{v}| = 0.2D/b$ (see Fig. S3A), monomers are described by

$$\frac{dR_{i,n}}{dt} = -D\nabla_{R_{i,n}}U(\boldsymbol{R}) + \sqrt{2D}\frac{dw_{i,n}}{dt}, \quad (1)$$

where

$$U(\boldsymbol{R}) = U_{\text{Rouse}}(\boldsymbol{R}_1, .. \boldsymbol{R}_N) + U_{\text{drift}}(\boldsymbol{R}_1, .. \boldsymbol{R}_N), \quad (2)$$

with

$$U_{\text{Rouse}}(\boldsymbol{R}_1, \ldots, \boldsymbol{R}_N) = \frac{1}{2}\kappa \sum_{i=1}^{N-1} (\boldsymbol{R}_{n+1} - \boldsymbol{R}_n)^2, \quad (3)$$

where $\kappa = \frac{3k_BT}{b^2}$, b is the standard deviation of the bond length and

$$U_{\text{drift}}(\boldsymbol{R}_1, \ldots, \boldsymbol{R}_N) = -\sum_n \frac{\boldsymbol{v} \cdot \boldsymbol{R}_n}{D}. \quad (4)$$

The anomalous exponent α is computed in intermediate time regime (Fig. S3A) and statistics of the simulations with such drift reveals that α=0.66 (Fig. S3B) (compared to α=0.5 for a Rouse polymer). Over longer periods of time, the motion of the center of mass becomes ballistic. In summary, adding a deterministic drift to the motion of a polymer increases α, providing an explanation for values scored > 0.5.

Oscillating forces on monomers increases the anomalous exponent

To further evaluate the effect of external forces on a monomer motion, we now consider those with oscillating properties (Fig. S3C), so that the total energy in eq. (1) is now

$$U(\boldsymbol{R}_1, .. \boldsymbol{R}_N) = U_{\text{Rouse}}(\boldsymbol{R}_1, .. \boldsymbol{R}_N) + U_{\text{osc}}(\boldsymbol{R}_1, .. \boldsymbol{R}_N), \quad (5)$$

with

$$U_{\text{osc}}(\boldsymbol{R}_1, \ldots, \boldsymbol{R}_N) = \sum_n (\boldsymbol{A} \cdot \boldsymbol{R}_n) \sin(\omega t + \theta_n), \quad (6)$$

where A, ω are constants and the phases θ_n can be chosen as follows. There are two extreme

cases: either all $\theta_n = 0$ for $n = 1..N$ or θ_n : $\mathrm{U}(0,2\pi)$ are random variables chosen uniformly distributed. We observe that increasing the amplitude A or the frequency ω increases the anomalous exponent value (Fig. S3D). For example, for $A = k_T/b = 1$ and $\omega = b^2/D$, where θ_n are randomly chosen, the anomalous exponent increases from $\alpha = 0.5$ (Rouse) to 0.64. We conclude that any deterministic motion added on the DNA locus will produce an increase of the anomalous exponent α.

Ghosh and Gov (Ghosh and Gov, 2014) use an alternative approach to model the effect of ATP-dependent active fluctuations, by considering exponentially correlated colored noise acting on the monomers of a semiflexible polymer. In this case the colored noise also resulted in anomalous motion with an exponent much higher than the one obtained with a Gaussian noise ($\alpha = 3/4$ for a semiflexible polymer). This result confirms that values of $\alpha > 0.5$ can be explained by an external force component acting on chromatin and not simply reflect changes in internal forces among monomers.

We note that the action of ATPase-driven motor proteins or of mechanical properties of the nucleus can be modeled by adding local oscillatory forces on some monomers (Fig. S3C). By increasing the magnitude of these oscillatory forces the α of monomers increases. For example, for oscillatory forces with random phases acting on each of the monomers (force amplitude of $A = k_T/b = 1$ and oscillation frequency $\omega = b^2/D$), the α computed from our numerical simulations increases from 0.5 to 0.64 (Fig. S3D). Given that the impact of an oscillatory force on chromatin depends on its intrinsic characteristic time ($\tau = 2\pi/\omega$), these effects could also explain the changes in α values measured at different time intervals.

Implementing excluded volume interactions

We used other polymer models than Rouse by adding interactions such as bending elasticity, which accounts for the persistence length of the polymer and Lennard-Jones forces (LJ), describing self-avoidance of each monomer pair. To account for the LJ forces, we use the potential energy defined by

$$U(\mathbf{R}_1,..\mathbf{R}_N) = U_{spring}(\mathbf{R}_1,..\mathbf{R}_N) + U_{LJ}(\mathbf{R}_1,..\mathbf{R}_N), \tag{7}$$

where the spring potential is

$$U_{spring}(\mathbf{R}_1,..\mathbf{R}_N) = \frac{1}{2}\kappa\sum_{i=1}^{N-1}(|\mathbf{r}_{i,i+1}| - l_0)^2, \tag{8}$$

where l_0 is the equilibrium length of a bond, $\kappa = \frac{3}{s_{l_0}^2}$ and s_{l_0} is the standard deviation of the bond length. We chose the empirical relation $s_{l_0} = 0.2 l_0$. The Lennard-Jones potential is

$$U_{LJ}(\mathbf{R}_1,..\mathbf{R}_N) = \sum_{i,j,i\neq j} U_{LJ}^{i,j}(\mathbf{r}_{i,j}), \tag{9}$$

with $\mathbf{r}_{i,j} = \mathbf{R}_i - \mathbf{R}_j$ and

$$U_{LJ}^{i,j}(\mathbf{r}_{i,j}) = \begin{cases} 4\left[\left(\frac{\sigma}{\mathbf{r}_{i,j}}\right)^{12} - 2\left(\frac{\sigma}{\mathbf{r}_{i,j}}\right)^{6} + \frac{1}{4}\right] & \text{for } |\mathbf{r}_{i,j}| \geq 2^{1/6}\sigma \\ 0 & \text{for } |\mathbf{r}_{i,j}| < 2^{1/6}\sigma, \end{cases} \tag{10}$$

where σ is the size of the monomer. With the choice $l_0 = 2\sigma$, the springs which materialize bonds, cannot cross each other in stochastic simulations using eq. 7, above. We do not account here for bending elasticity. Finally, we used Euler's scheme to generate Brownian simulations (Schuss, 2009). At an impenetrable boundary, each rigid monomer is reflected in the normal direction of the tangent plane.

Estimating the anomalous diffusion exponent α and the diffusion coefficient

We computed the auto-correlation (AC) function or the MSD using the classical estimator (Schuss, 2009)

$$C(t) = \frac{1}{N_p - q}\sum_{k=1}^{N_p - q} (\mathbf{R}_c(k\Delta t) - \mathbf{R}_c(k\Delta t + q\Delta t))^2 \qquad q = 1..N_p - 1, \tag{11}$$

where $t = q\Delta t$, is the time difference between the trajectory frames and N_p is the number of points in the trajectory. In many studies the AC function is referred to as the MSD function (Dion et al., 2012; Mine-Hattab and Rothstein, 2012). The MSD is defined as the squared displacement with respect to the initial trajectory position, averaged over time:

$$\text{MSD(t)} = \left\langle \left(R_c(t) - R_c(0)\right)^2 \right\rangle.$$

For short times, $C(t)$ or *MSD(t)* increases as a power law

$$C(t) \approx Ct^{\alpha}, \tag{12}$$

where $C > 0$. To extract the coefficient α, we computed $C(t)$ from empirical trajectories and

fitted the first six points of the curve to a power law. A chromatin or DNA locus is characterized experimentally by α<1 (Kepten et al., 2013; Weber et al., 2010), while for normal diffusion α=1. In the Rouse polymer model (Doi and Edwards, 1986), the anomalous exponent is α=0.5 computed for intermediate time regime.

To compute the diffusion coefficient of the tagged monomer, we use the following empirical estimator (Schuss, 2009)

$$D_c \approx \frac{1}{4\Delta t}\sum_{k=1}^{N_p-1}(\mathbf{R}_c(k\Delta t)-\mathbf{R}_c((k+1)\Delta t))^2, \tag{13}$$

For short time intervals $\Delta t = b^2/D$, the locus motion is Brownian and the diffusion coefficient is well approximated by eq.(13).

Estimating the effective spring coefficient (*k*c)

Because the chromatin interacts locally with its environment, we estimated this interaction using a polymer model (Amitai et al., 2015), by a harmonic well of strength k acting on a single monomer R_n. The potential energy of the interaction is

$$U(\mathbf{R}_n)=\frac{1}{2}k(\mathbf{R}_n-\boldsymbol{\mu})^2, \tag{14}$$

where $\boldsymbol{\mu}$ is the fixed position of the interaction. The velocity of an observed monomer c, averaged over many trajectories is driven by this interacting force, following the relation

$$\lim_{\Delta t\to 0}E\{\frac{\mathbf{R}_c(t+\Delta t)-\mathbf{R}_c(t)}{\Delta t}\,|\,\mathbf{R}_c(t)=\mathbf{x}\}=-Dk_{cn}(\mathbf{x}-\boldsymbol{\mu}), \tag{15}$$

where $\mathbf{R}_c(t)$ is the position of locus c at time t. D is the diffusion coefficient and $E\{.\,|\,\mathbf{R}_c(t)=\mathbf{x}\}$ means averaging over trajectory realizations such that the condition $\mathbf{R}_c(t)=\mathbf{x}$ is satisfied (Amitai et al., 2015). Relation (16) links the average velocity of the observed monomer c to the force applied at a distance $|c-n|$. For a Rouse polymer, with a potential well of type (14), the effective spring coefficient is given by

$$k_{cn}=\frac{k\kappa}{\kappa+|c-n|k}, \tag{16}$$

where κ is the monomer-monomer spring coefficient. We estimated k_c from the empirical

locus trajectories $\mathbf{R}_c(t)$ by $k_c \approx \frac{1}{2(N_p-1)} \sum_{i=1}^{2} \sum_{h=1}^{N_p-1} \frac{R_c^i((h+1)\Delta t) - R_c^i(h\Delta t)}{D_c \Delta t (R_c^i(h\Delta t) - \langle R_c^i \rangle)}$, (17)

where i varies over the spatial direction (in two dimensions, we sum over the x and y components) and N_p is the number of points in the trajectory. In practice, the quantity $\langle R_c^i \rangle$ is computed by averaging over the trajectory. The diffusion coefficient D_c can be computed by using eq. 13.

Properties of the the length of constraint (Lc)

The length of constraint Lc was defined as the standard deviation (SD) of the locus position with respect to its mean averaged over time and approximated for a trajectory containing N_p by empirical estimation

$$L_C = \sqrt{\mathrm{Var}(\mathbf{R}_c)} \approx \sqrt{\frac{1}{N_p} \sum_{k=1}^{N_p} (\mathbf{R}_c(k\Delta t) - \langle \mathbf{R}_c \rangle)^2},$$

Here are some basic properties when N_p is large enough:

1- For a ballistic trajectory, with a constant speed v, then $\mathbf{R}_c(k\Delta t) = vk\Delta t + \mathbf{R}_c(0)$ and $L_C \approx \frac{v\Delta t N_P}{3}$.

2- For a free Brownian trajectory, by the large number theory, the estimator converges to the mean and $L_C \approx \sqrt{D\Delta t N_P}$.

3- For a confined Brownian motion into a ball of radius R and long time asymptote, the empirical estimator for Lc converges to $\frac{R}{\sqrt{2}}$.

4- For an Ornstein-Ulenbeck process, which is the motion of a particle in a harmonic potential of strength *k*, for long time asymptote, the estimator for Lc converges to,

$$L_C \approx \frac{k_B T}{k}, \quad (18)$$

where $k_B T$ is the thermal energy.

Consequences of choosing a time interval for imaging chromatin dynamics

Here we briefly discuss why different time intervals can affect the values obtained for the four extracted parameters and in particular α. To do this we will use the Rouse polymer model (Doi

and Edwards, 1986), which describes a polymer consisting of a linear chain of N beads that are connected by a spring. The polymer's dynamics are characterized by an ensemble of relaxation times $\tau_p^{-1} = 4D\kappa \sin^2(p\pi/2N)$, $(p = 1..N-1)$, where κ is the spring coefficient between neighboring monomers, *D* is the diffusion coefficient of single monomer and *N* is the polymer length. When a time step Δt, is chosen for a measurement, this choice imposes that all time relaxation events of the polymer (Doi and Edwards, 1986) below $\Delta t \approx \tau_p$ do not influence the motion of the polymer. In other words, choosing a time step is equivalent to monitoring the dynamics of only a fraction of the polymer.

An analogy is the following: depending where you stand on a moving snake, you may see only the head moving. As you move towards the tail, the middle of the body becomes visible. Thus standing at a given location on the snake is equivalent of choosing the time step Δt. Another analogy is with the vibration of a string: The human ear can only process frequencies above 20 Hz and frequencies below this are not detected. The time step in this case is equivalent to the highest frequency we can hear. Therefore, when we observe a chromatin locus at a time interval $\Delta t = 300\,\text{ms}$, changes in chromatin happening on shorter time scales such as $\Delta t = 80\,\text{ms}$, are lost, as illustrated schematically in Figure 1D.

Error propagation and statistics

Significance between α, Kc, Lc and Dc values was tested using the non-parametric Kolmogorov-Smirnov (KS) test. P-values are either indicated above the figure panels or by asterisks, where, *, ** and *** correspond to P values of ≤ 0.05, ≤ 0.01,≤ 0.001, respectively. Error bars on graphs represent the standard error unless otherwise stated. LacI-GFP spot size was shown to be normally distributed and then tested for differences using a two-tailed Student's t-test (Graph Pad). Significance cut off was P < 0.05. All P values are in Table S4.

β-polymer models

To account for the chromatin dynamics, we use the generalized polymer model called the β-polymer model (Amitai and Holcman, 2013), which accounts for anomalous diffusive behavior with α in the range of [0-0.5], as measured for a yeast *in vivo* chromatin locus (Hajjoul et al., 2013). We use β-polymer model where all monomers are connected through a quadratic potential defined by

$$U_\beta(\boldsymbol{R}_1,..\boldsymbol{R}_N,\beta) = \frac{1}{2}\sum_{l,m} A_{lm}\,\boldsymbol{R}_l\boldsymbol{R}_m, \qquad (19)$$

with coefficients

$$A_{l,m} = \sum_{p=1}^{N-1} \tilde{\kappa}_p \alpha_p^l \alpha_p^m = 4\kappa \frac{2}{N} \sum_{p=1}^{N-1} \sin^{\beta} \frac{p\pi}{2N} \cos\left(\left(\mathrm{l} - \frac{1}{2}\right)\frac{p\pi}{N}\right) \cos\left(\left(\mathrm{m} - \frac{1}{2}\right)\frac{p\pi}{N}\right) \qquad (20)$$

and

$$\tilde{\kappa}_p = 4\kappa \overset{\beta}{\sin}\left(\frac{p\pi}{2N}\right) \text{ for } p = 0..N-1. \qquad (21)$$

In such a model, the strength of interaction $A_{l,m}$ decays with the distance $|l-m|$ along the chain. By definition, 1<β<2 (Amitai and Holcman, 2013) and the Rouse polymer is recovered for $\beta = 2$, for which only nearest neighbors are connected.

2 - Supplemental Tables

Table S1: Strains used in this study

All yeast strains are derived from GA-1081 which is in the JKM179 background. We prepared two isogenic strains for each mutant and for GA-8862, which is referred to as "wild-type" throughout. The two *MATα* clones were used interchangeably with identical results.

Strain number	**Genotype**	**Reference**
GA-1081 (JKM179)	*MAT$_\alpha$ ade1 leu2-3,112 lys5 trp1::hisG ura3-52 hml::ADE1 hmr::ADE1 ade3::PGAL-HO*	(Moore and Haber, 1996)
GA-8862	*JKM179; MATα, ΔHO hml::ADE1 hmr::ADE1 ade3::GALHO ade1-100 leu2-3, 112 lys5 trp1::hisG ura3-52 NUP49-Ruby2 - KanMx, GFP-LacI:Leu2, MAT::lacO repeats:TRP1*	This study
GA-8863	*JKM179; MATα, ΔHO hml::ADE1 hmr::ADE1 ade3::GALHO ade1-100 leu2-3, 112 lys5 trp1::hisG ura3-52 NUP49-Ruby2-KanMx, GFP-LacI:Leu2, MAT::lacO repeats:TRP1*	This study
GA-8921	*JKM179; MATα, ΔHO hml::ADE1 hmr::ADE1 ade3::GALHO ade1-100 leu2-3, 112 lys5 trp1::hisG ura3-52 NUP49-Ruby2-KanMx, GFP-LacI:Leu2, MAT::lacO repeats:TRP1, arp8::NAT*	This study
GA-8922	*JKM179; MATα, ΔHO hml::ADE1 hmr::ADE1 ade3::GALHO ade1-100 leu2-3, 112 lys5 trp1::hisG ura3-52 NUP49-Ruby2-KanMx, GFP-LacI:Leu2, MAT::lacO repeats:TRP1, arp8::NAT*	This study
GA-8067	*JKM179; MATa, ΔHO hml::ADE1 hmr::ADE1 ade3::GALHO ade1-100 leu2-3, 112 lys5 trp1::hisG ura3-52, GFP-LacI:Leu2, MAT::lacO repeats:TRP1*	This study
GA-9602	*JKM179; MATa, ΔHO hml::ADE1 hmr::ADE1 ade3::GALHO ade1-100 leu2-3, 112 lys5 trp1::hisG ura3-52, GFP-LacI:Leu2, MAT::lacO repeats:TRP1, arp8::NAT*	This study
GA-9045	*JKM179; MATα, ΔHO hml::ADE1 hmr::ADE1 ade3::GALHO ade1-100 leu2-3, 112 lys5 trp1::hisG ura3-52, GFP-LacI:Leu2, MAT::lacO repeats:TRP1, SPC29-Ruby2*	This study
ML118-1D (GA-6587)	*URA3::tetOx224::I-Sce1::rDNA TetR-mRFP(iYGL119W) RAD52-YFP*	(Torres-Rosell et al., 2007)

Table S2: HO endonuclease cutting efficiencies

Compiled cut efficiencies for the indicated time of induction (addition of 2% galactose) for the HO endonuclease. Strains are isogenic to JKM179 and are all *MAT*α other than GA-8067 and GA-9602, which are *MAT**a*** allowing for α-factor synchronization.

Strain	**Relevant genotype**	**Drug treatment (60 min)**	**Min after galactose addition (induced HO endonuclease)**	**% of intact *MAT***		**Imaging interval Δt (ms)**	**Number of foci analyzed**
GA-8862/3	wild-type	No drug	0	100		80	33
						300	30
GA-8862/3	wild-type	No drug	120	11.5 ± 2.83		80	19
						300	35
GA-8921/2	*arp8Δ*	No drug	0	100		80	20
GA-8921/2	*arp8Δ*	No drug	120	35 ± 2.79		80	16
GA-8862	wild-type	LatA (25 μM)	0	100		80	28
						300	28
GA-8862	wild-type	LatA (25 μM)	120	20 ± 2.4		80	47
						300	28
GA-8862	wild-type	Nocodazole (50 μM)	0	100		80	31
						300	28
GA-8862	wild-type	Nocodazole (50 μM)	120	17 ± 1.2		80	28
						300	22
GA-8067	wild-type	No drug	0	G1	100	-	924
GA-8067	wild-type	No drug	0	S	100	-	683
GA-8067	wild-type	No drug	30	G1	7 ± 1.03	-	630
GA-8067	wild-type	No drug	30	S	6 ± 1	-	1037
GA-9602	*arp8Δ*	No drug	0	G1	100	-	253
GA-9602	*arp8Δ*	No drug	0	S	100	-	247
GA-9602	*arp8Δ*	No drug	30	G1	12 ± 0.49	-	436
GA-9602	*arp8Δ*	No drug	30	S	13 ± 0.13	-	374

Table S3: Parameters for simulation of self-avoiding polymers

Description	Parameters	Value
Polymer persistence length	l_0	30nm
Diffusion constant	D	$8\times10^{-3}\,\mu\mathrm{m}^2/\mathrm{s}$
Encounter radius	ε	5nm
Spring constant	κ	$\frac{3}{(0.2*l_0)^2}\,\mathrm{Nm}^{-1}$
Monomer diameter	σ	30nm

Table S4: Volumes of LacI-GFP Foci

The volumes of the LacI-GFP foci were determined as described in Supplemental Materials for strains GA-8067 (WT) and GA-9602 (*arp8Δ*). P-values that indicate the significance of the differences between measured volumes was determined by a 2 tailed t-test. Only G1 cut and uncut in either strain were not significant. Values are as follows: WT G1 uncut vs G1 cut: 0.9698; WT G1 uncut vs S uncut: 5.3E-27; WT S uncut vs S cut: 1.34E-09; WT G1 cut vs S cut: 1.2E-40; *arp8*Δ G1 uncut vs G1 cut: 0.1337; *arp8*Δ G1 uncut vs S uncut: 9.29E-44; *arp8*Δ S uncut vs S cut: 1.34E-09; *arp8*Δ G1 cut vs S cut: 6.99E-32.

Genotype	Phase and condition	Mean spot volume (μm^3)	SD	Foci counted
WT	G1 uncut	0.069	0.030	924
WT	G1 cut	0.069	0.031	683
WT	S uncut	0.090	0.041	630
WT	S cut	0.109	0.086	1037
*arp8*Δ	G1 uncut	0.076	0.035	253
*arp8*Δ	G1 cut	0.071	0.033	247
*arp8*Δ	S uncut	0.154	0.098	436
*arp8*Δ	S cut	0.133	0.085	374

3 - Supplemental Figures

Figure S1: Imaging regimes do not activate the DNA damage response, related to Figure 1.

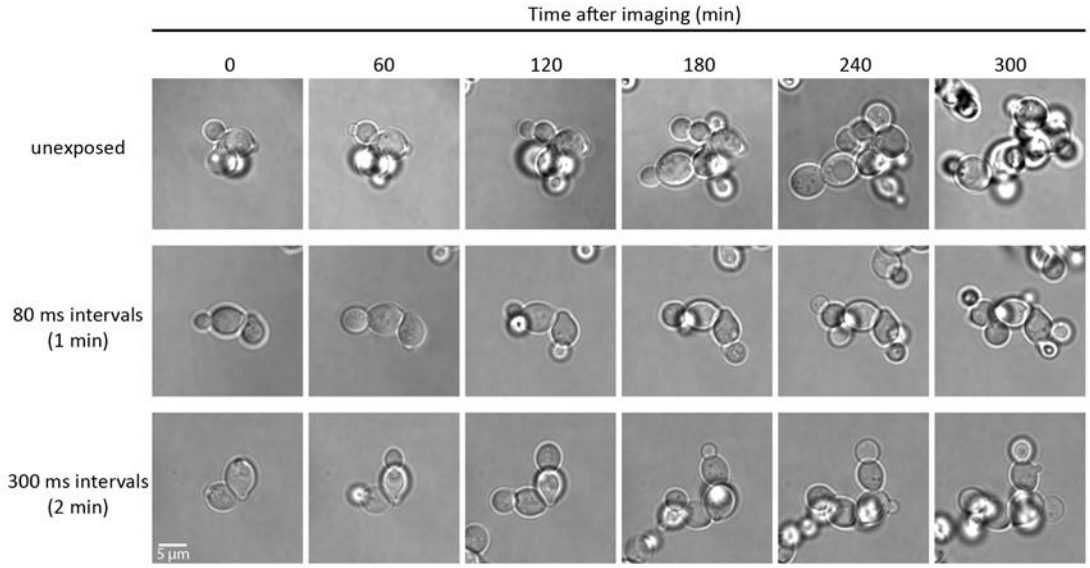

Figure S1: Yeast cells (GA-8862) were exposed to either the 80 ms or 300 ms interval imaging regimes described in the main text, or were left unexposed. Brightfield images were captured every 60 min for 5 h after fluorescence imaging. In no case did the cells manifest a checkpoint arrest or delayed cell cycle progression for at least two rounds of mitosis. Related to Figure 1.

Figure S2: Extracting values for the effective diffusion coefficient (Dc), related to Figure 1

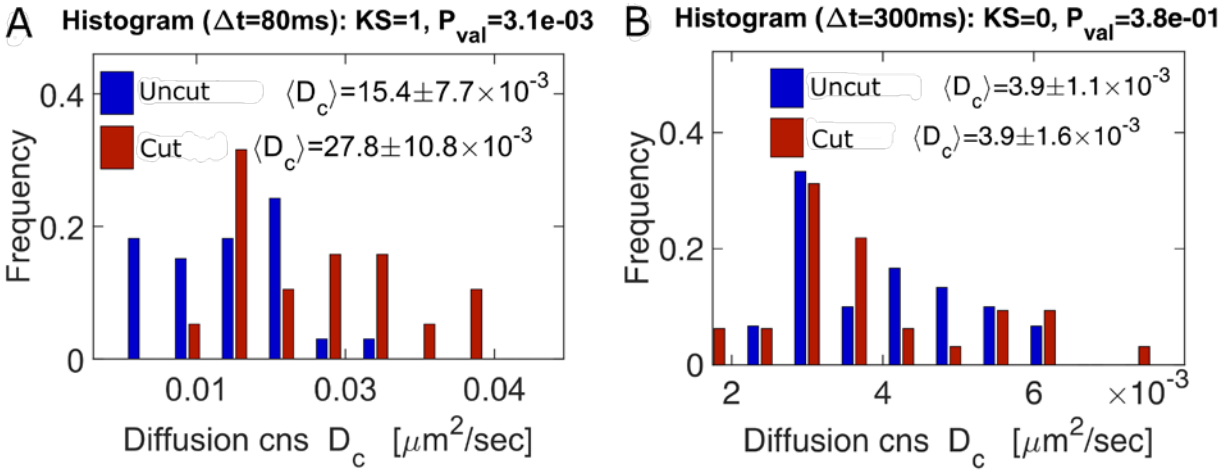

Figure S2: We extracted Dc for the locus trajectories under cut and uncut conditions using eq. 13, described in Experimental procedures (below). Changes in the diffusion coefficient before and after induction of a DSB are quantified at the *MAT* locus after cleavage (HO induction during 2h, red) or non-cleaved (no HO endonuclease, blue) for (**A**) 60 s trajectories (Δt = 80 ms) or **(B)** 120 s trajectories (Δt = 300 ms). Related to Figure 1; strains are as in Figure 1.

Figure S3: Effect of an external force on locus motion, related to Figure 2

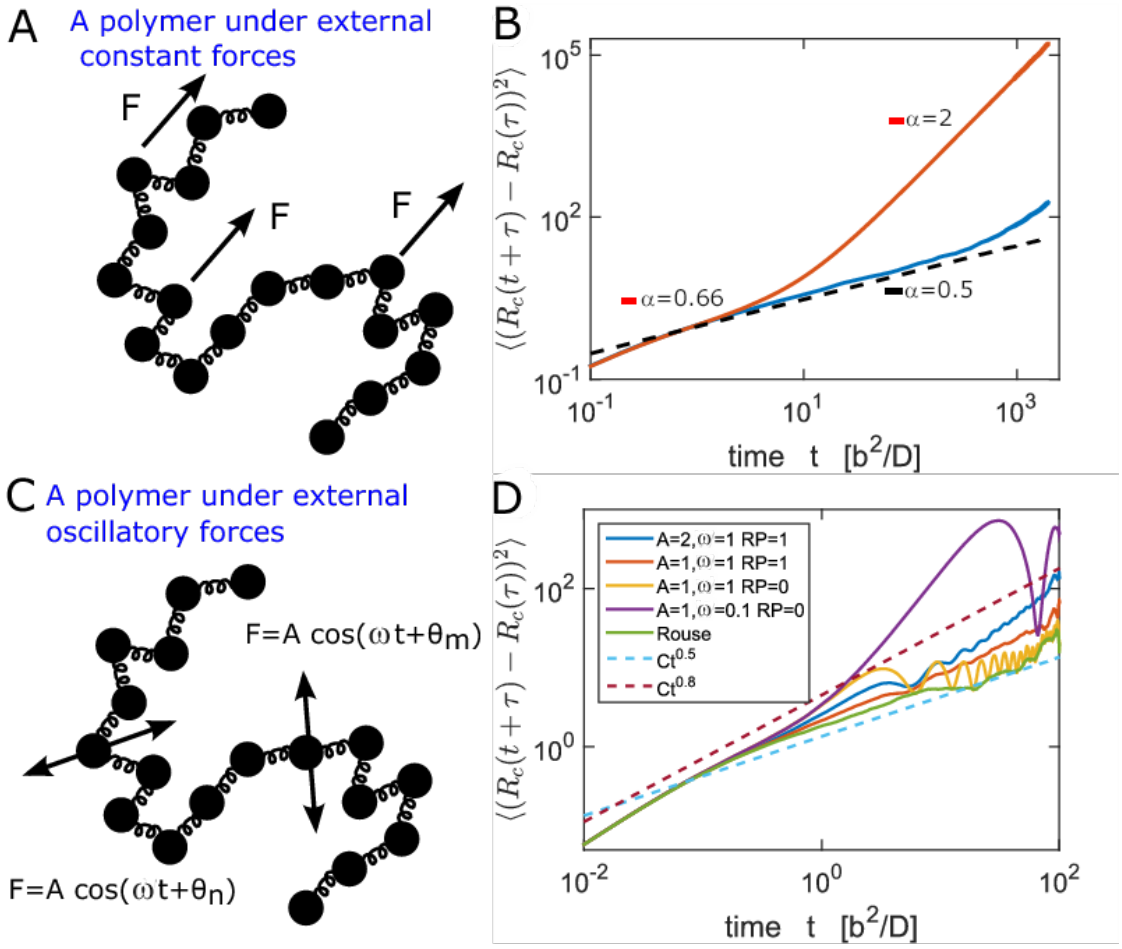

Figure S3: (A) A polymer drifting under the influence of an external force acting on all monomers. **(B)** Time correlation function estimated from Brownian simulations of a Rouse polymer ($\beta=2$, blue line), where the first monomer is followed. At intermediate time scales, the particle performs anomalous diffusion with $\alpha=0.5$ (black dashed line). The time correlation function is computed for the first monomer (Rouse polymer) under drift (red line). When a directed force is applied on all monomers the anomalous exponent increases to $\alpha=0.66$ at intermediate time regime and converges to ($\alpha=2$) for the ballistic regime at longer times. **(C)** Schematic of a polymer where independent oscillatory forces are acting on all monomers. **(D)** Time correlation function of the middle monomer of a Rouse polymer ($N=33$), where an oscillating force is acting on all monomers (Eq. (6)). The phase of force can be the same for all monomers (RP=0) or random (RP=1). We show the correlation function for several values of the amplitude A and the frequencies ω, compared to the Rouse polymer, with no oscillating force, for which the anomalous exponent is 0.5 (green). Hatched trend lines (Ct^{α}, where $\alpha=0.5$, blue and $\alpha=0.8$, red) are shown.

Figure S4: Depolymerization of actin cables by LatA at the concentration used in Figure 2

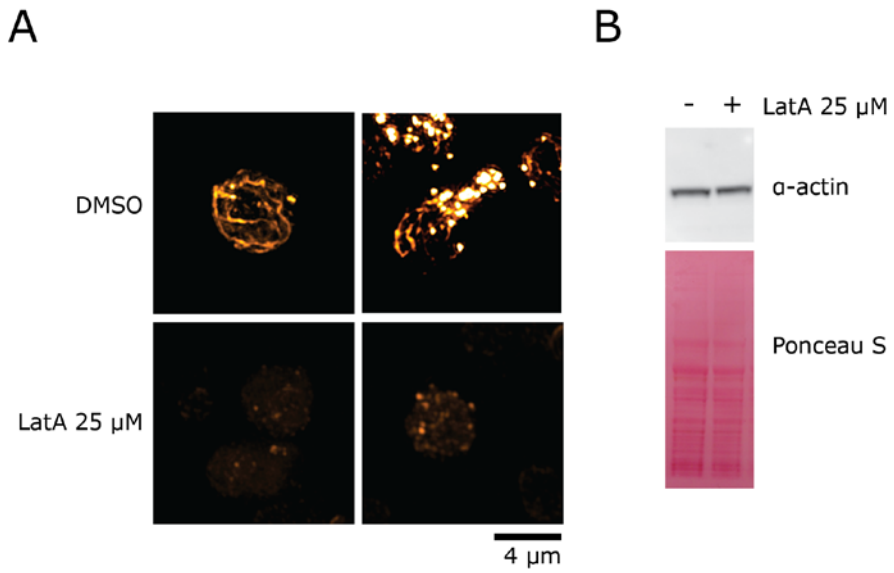

Figure S4: (A) Logarithmically growing yeast cells (GA-8862) in synthetic complete media with 2% glucose were stained with Rhodamine phalloidin to visualize actin cables after 1 h exposure to 25 µm Latrunculin A (LatA) in DMSO or DMSO alone. Identical staining and imaging conditions are used ± LatA. **(B)** Western blot shows no actin degradation under these conditions. Related to Figure 2.

Figure S5: Effect of LatA on spindle pole body and chromatin movement, related to Figure 2

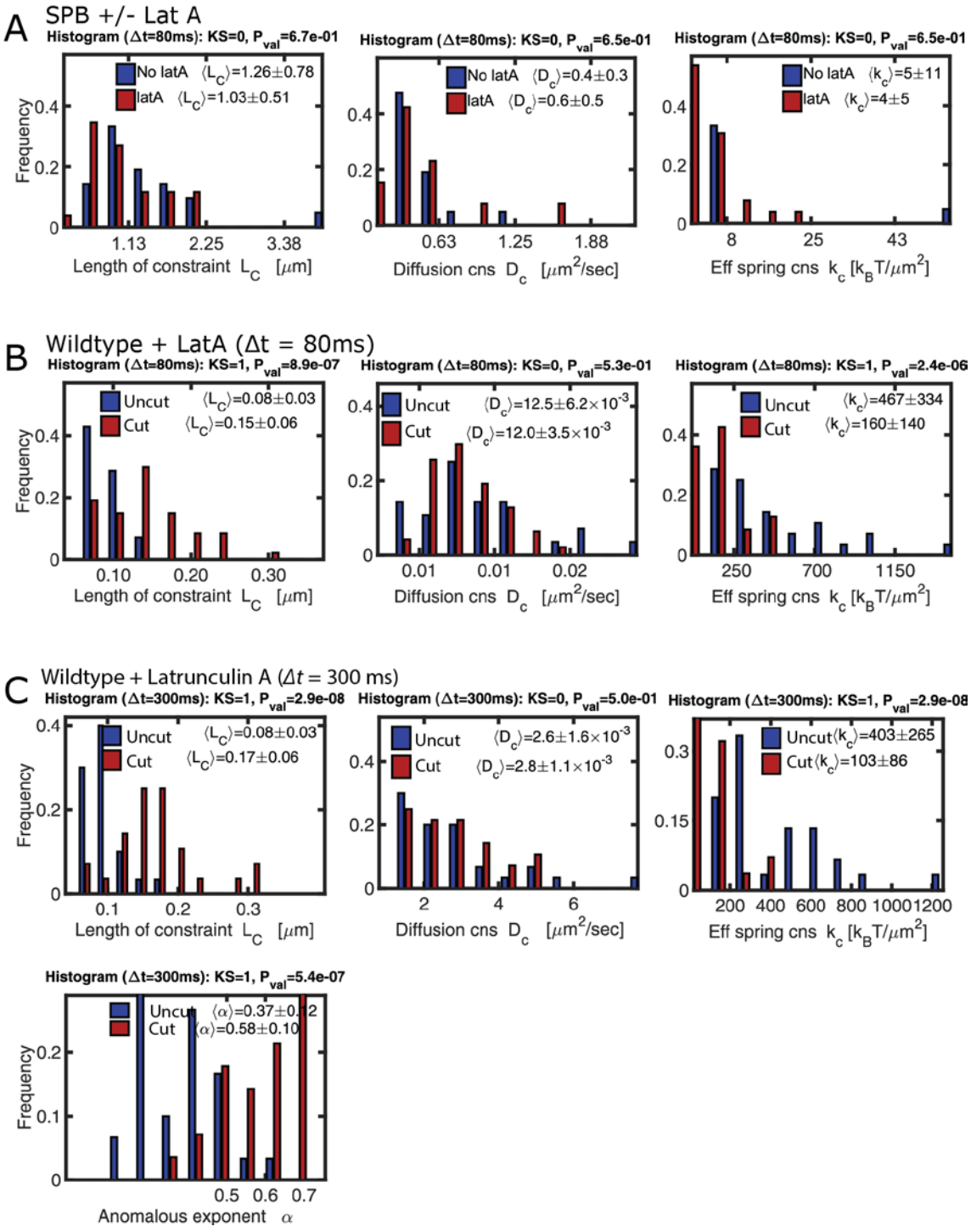

Figure S5: (A) Lc, Dc and kc of the Spindle pole body (SPB tagged by Spb29-Ruby2) + LatA (1h) (strain, GA-9045) **(B)** Lc, kc and Dc of the *MAT* locus before and after 2 h cut induction + LatA in the Δt=80 ms regime (strains, GA-8862/8863). **(C)** or 300 ms regime. LatA was added for the last hour of cut induction. Related to Figure 2. (strains as B).

Figure S6: Trajectory parameters extracted from *ARP8+* and *arp8Δ* cells, related to Figure 4

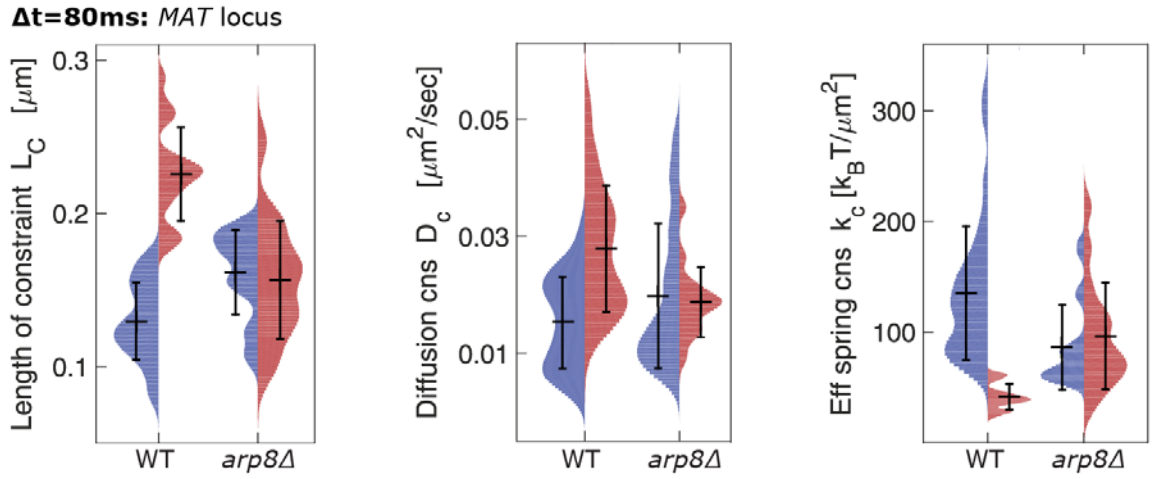

Figure S6: Lc, kc and Dc of the *MAT* locus in ARP8+ (WT) and *arp8Δ* cells after 2 h cut induction using the Δt=80 ms regime. Blue indicates no HO endonuclease induction, red is after 2 h HO induction. Strains used are (GA-8921/GA-8922). All trajectories come from S phase cells selected from an asynchronous culture. Related to Figure 4**.**

Figure S7: Steady state configuration of a β-polymer with Lennard-Jones forces, related to Figure 4

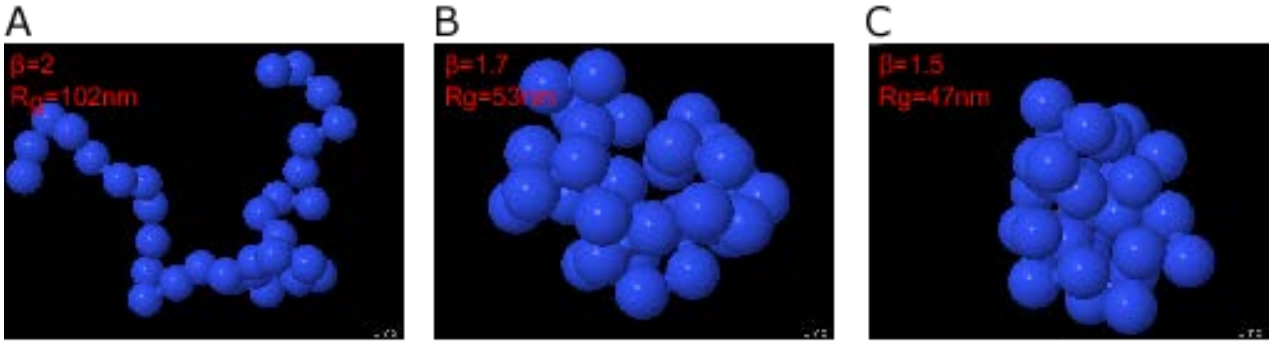

Figure S7: The steady-state configuration of a β-polymer with both inter-monomer interactions and additional self-avoiding interactions (Lennard-Jones forces) for **(A)** *β=2*, **(B)** *β=1.7* and **(C)** *β=1.5*. The radius of gyration (Rg) measures the degree of compaction associated with *β* and is shown here to depend on the value of *β*. The blue balls represent monomers are of radius 30 nm. Related to Figure 4.

Figure S8: Dynamic decondensation of a β-polymer, related to Figure 5

Following a local release of the polymer forces, there is a dynamic rearrangement of the chromatin simulated in Figure S8. This decondensation process is simulated for two polymer chains and for different interacting monomers characterized by β=1.5 and β=1.3. The numerical procedure is the following: at an initial time $t = 0$, we instantaneously relax the long-range forces at three consecutive monomers *n=16,17,18*. The simulations shows that the relaxed monomers are drifting outside the center of mass and are expelled or extruded toward the surface of the polymer.

Although the extrusion period was very short, it could be much longer *in vivo*, since it can occur gradually and the chromatin fiber will be much longer. Additional constraints can also be taken into account, such as anchoring or interactions with other chromatin or the nuclear membrane that will influence the relaxation time.

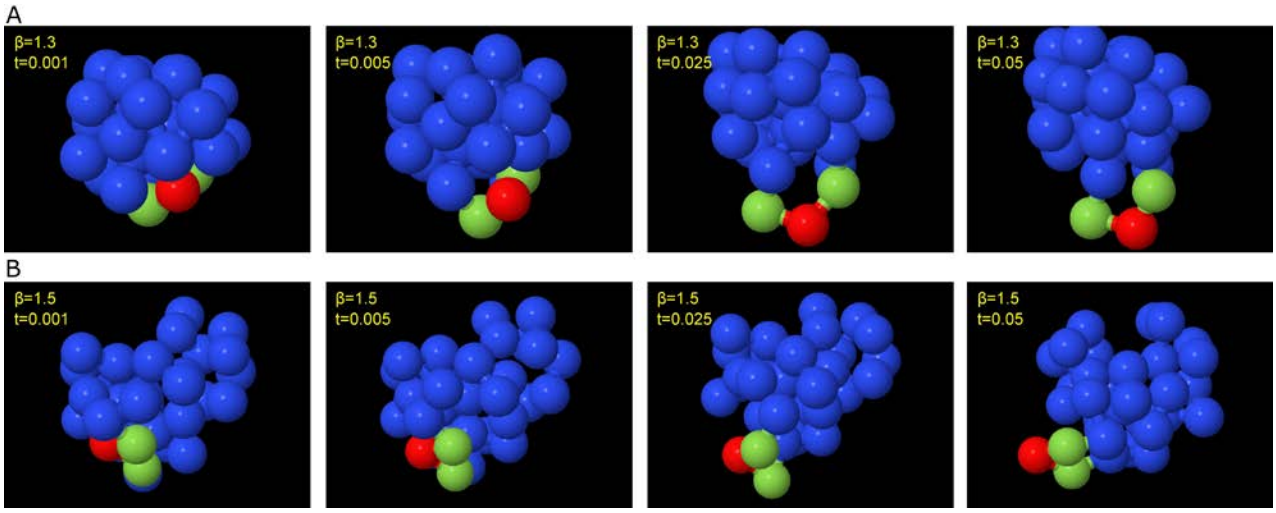

Figure S8: The intra-polymer forces on for monomers *n=16,17,18* (in chain of length *N=33*) are removed at time *t=0*. Snapshot of the relaxation dynamics **(A)** for *β=1.3* and **(B)** for *β=1.5*. The middle monomer *n=17* (red) is surrounded by *n=17,18* (green). For simulation the monomer diffusion coefficient is $D = 8 \times 10^{-3} \mu m^2 / s$. Related to Figure 5.

Figure S9: Dynamics of rDNA locus before and after cut induction related to Figure 5

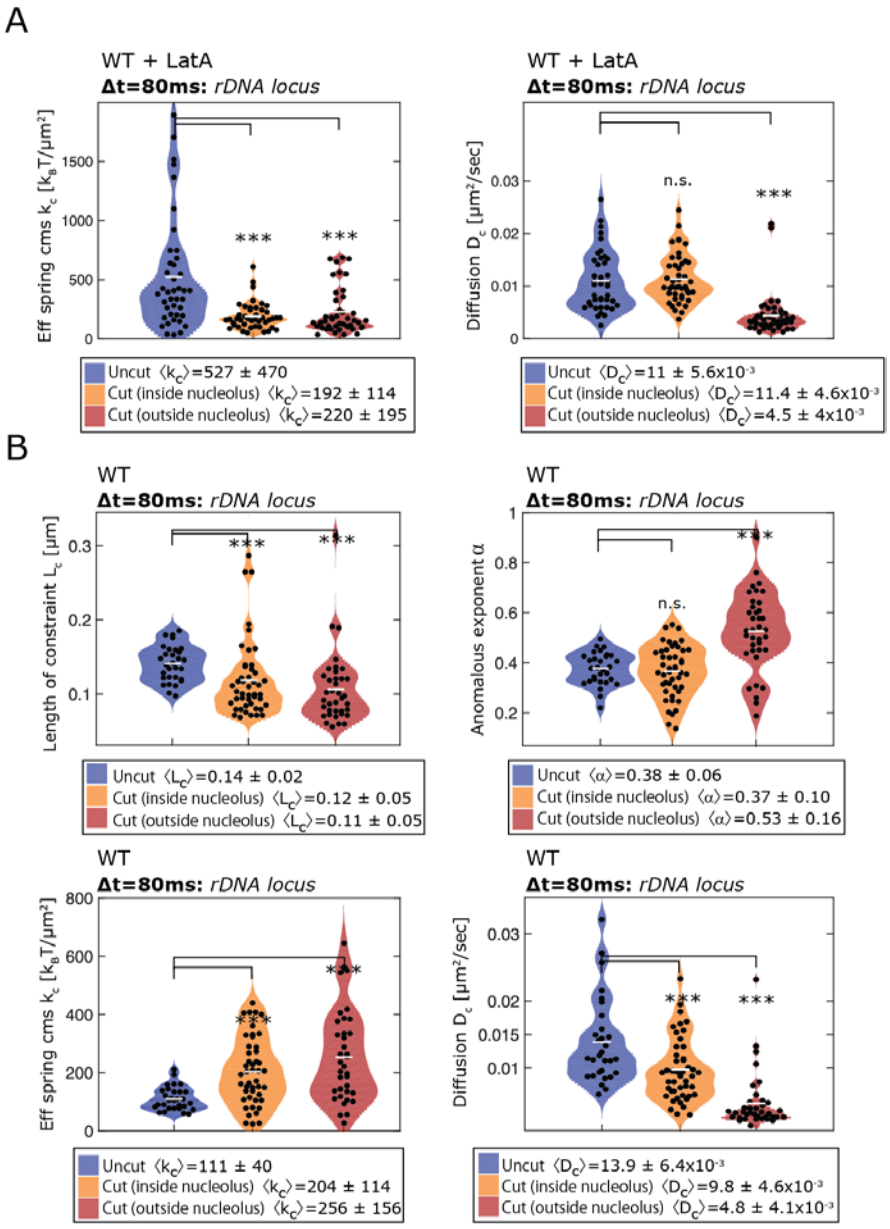

Figure S9: (A) Dc and kc of a TetR-mRFP at the rDNA locus after 2 h I-SceI induction using the Δt=80 ms regime with or without 25 µm LatA for the last hour of cut induction (related to Figure 5GH). All movies acquired for "Cut (outside nucleolus)" contain a Rad52 focus that colocalises with the TetR-mRFP spot. **(B)** Lc, α, kc and Dc of TetR-mRFP at the rDNA locus after 2 h I-SceI using the Δt=80 ms regime without LatA. ***, **,***** indicate P ≤ 0.05, ≤ 0.01, ≤ 0.001 respectively. Strains used are GA-6587 with plasmids SG-3453 and pWJ1108. We observe increased α for the cut and shifted rDNA locus but decreased movement (Dc). The drop in Dc is unclear but may reflect binding of Rad51.

Figure S10: Correlation between the statistical parameters, related to the Discussion

In this section we clarify the relationship between the 4 estimated parameters (Lc, Kc, Dc, and α). Kc is computed from the first statistical moment of the displacement eq. (15 SI). It is independent of α and Dc which are rather computed from the second moment of the displacement, supplemental eqs. 11, 12 and 13. These estimators (first moment *vs*. second moment) are expected to be independent. We confirm this by comparing the parameters computed for an uncut *MAT* locus at Δt =80ms and Δt =300ms (see Figure S10AB). When Δt=300ms the correlation coefficient between Lc and Dc is larger. While for Δt=80ms the value of the correlation coefficients of Lc with α and Dc is small.

When the confinement of a chromatin locus is driven by a tethering force, the length of confinement Lc is inversely proportionally to the constant Kc as shown in equation 18 and Figures S10AB, and Amitai et al., 2015. For other types of motion, this relationship is not necessarily the same, as explained in the supplemental section, "Properties of the the length of constraint (Lc)". The algebraic relationship we have observed indicates that confinement of this locus arises from a tethering force and not necessarily crowding. Moreover, the information contained in α is different from the one in Dc. α has no dimension and it is obtained by fitting the correlation function by a power law $C(t) \approx Ct^{\alpha}$, as described above in the main text. The effective diffusion coefficient has the physical units of $\mu m^2/s$ and is computed from supplemental eq. 15. We confirm that α and Dc are uncorrelated (Figure S10AB). In the context of the β-polymer model, α reflects the level of chromatin condensation.

In summary, the four parameters are computed from the first and second statistical moments of the displacement. There are in general not redundant and provide independent information about the dynamics of the underlying physical process that has generated the single particle trajectories. The numerical code to compute the four parameters is accessible at http://bionewmetrics.org/ in the "Nuclear Organization section" or https://amitaiassaf.github.io/.

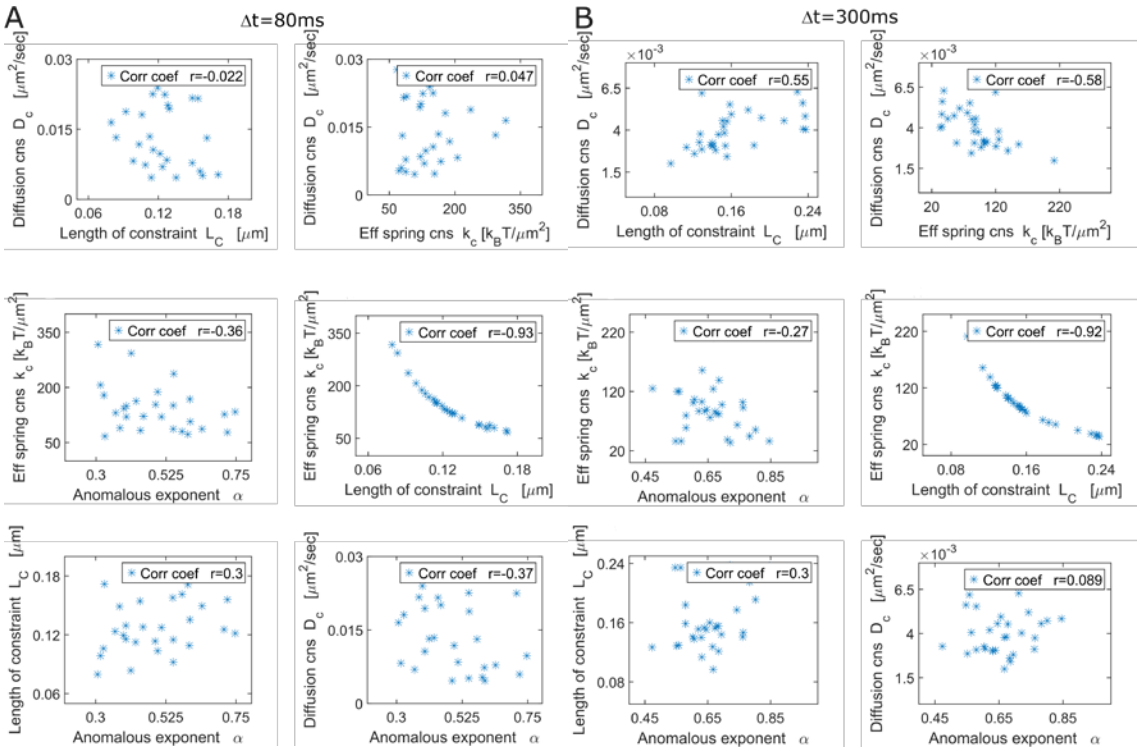

Figure S10: Correlation between the extracted parameters (A) Scatter plots and correlation coefficients between the four parameters (Lc, Kc, Dc, and α) estimated from trajectories of a uncut *MAT* locus using image capture time intervals of 80 ms. (B) As A but using image capture time intervals of 300 ms.

4 - References

Amitai, A., and Holcman, D. (2013). Polymer model with long-range interactions: analysis and applications to the chromatin structure. Phys Rev E Stat Nonlin Soft Matter Phys *88*, 052604.

Amitai, A., Toulouze, M., Dubrana, K., and Holcman, D. (2015). Analysis of Single Locus Trajec-tories for Extracting In Vivo Chromatin Tethering Interactions. PLoS Comp Biol *11*, e1004433.

Dion, V., Kalck, V., Horigome, C., Towbin, B.D., and Gasser, S.M. (2012). Increased mobility of double-strand breaks requires Mec1, Rad9 and the homologous recombination machinery. Nature Cell Biology *14*, 502-U221.

Doi, M., and Edwards, S.F. (1986). The Theory of Polymer Dynamics. Oxford: Clarendon Press.

Ghosh, A., and Gov, N.S. (2014). Dynamics of active semiflexible polymers. Biophys J *107*, 1065-1073.

Hajjoul, H., Mathon, J., Ranchon, H., Goiffon, I., Mozziconacci, J., Albert, B., Carrivain, P., Victor, J.-M., Gadal, O., and Bystricky, K. (2013). High-throughput chromatin motion tracking in living yeast reveals the flexibility of the fiber throughout the genome. Genome research *23*, 1829-1838.

Horigome, C., Dion, V., Seeber, A., Gehlen, L.R., and Gasser, S.M. (2015). Visualizing the spatiotemporal dynamics of DNA damage in budding yeast. Methods in molecular biology (Clifton, NJ) *1292*, 77-96.

Kepten, E., Bronshtein, I., and Garini, Y. (2013). Improved estimation of anomalous diffusion exponents in single-particle tracking experiments. Phys Rev E Stat Nonlin Soft Matter Phys *87*, 052713.

Lee, S., Lim, W.A., and Thorn, K.S. (2013). Improved blue, green, and red fluorescent protein tagging vectors for *S. cerevisiae*. PLoS One *8*, e67902.

Looke, M., Kristjuhan, K., and Kristjuhan, A. (2011). Extraction of genomic DNA from yeasts for PCR-based applications. Biotechniques *50*, 325-328.

Mine-Hattab, J., and Rothstein, R. (2012). Increased chromosome mobility facilitates homology search during recombination. Nat Cell Biol *14*, 510-517.

Moore, J.K., and Haber, J.E. (1996). Cell cycle and genetic requirements of two pathways of nonhomologous end-joining repair of double-strand breaks in *Saccharomyces cerevisiae*. Mol Cell Biol *16*, 2164-2173.

Sage, D., Neumann, F.R., Hediger, F., Gasser, S.M., and Unser, M. (2005). Automatic tracking of individual fluorescence particles: application to the study of chromosome dynamics. IEEE Trans Image Process *14*, 1372-1383.

Schuss, Z. (2009). Diffusion and Stochastic Processes. An Analytical Approach. Springer-Verlag, New York, NY.

Torres-Rosell, J., Sunjevaric, I., De Piccoli, G., Sacher, M., Eckert-Boulet, N., Reid, R., Jentsch, S., Rothstein, R., Aragon, L., and Lisby, M. (2007). The Smc5-Smc6 complex and SUMO modification of Rad52 regulates recombinational repair at the ribosomal gene locus. Nat Cell Biol *9*, 923-931.

van Attikum, H., Fritsch, O., and Gasser, S.M. (2007). Distinct roles for SWR1 and INO80 chromatin remodeling complexes at chromosomal double-strand breaks. Embo J *26*, 4113-4125.

Weber, S.C., Theriot, J.A., and Spakowitz, A.J. (2010). Subdiffusive motion of a polymer composed of subdiffusive monomers. Phys Rev E Stat Nonlin Soft Matter Phys *82*, 011913.

CHAPTER 6: RPA MEDIATES RECRUITMENT OF MRX TO FORKS AND DOUBLE-STRAND BREAKS TO HOLD SISTER CHROMATIDS TOGETHER

Andrew Seeber[1,2], Anna Maria Hegnauer[1], Nicole Hustedt[1,3], Ishan Deshpande[1,2], Jérôme Poli[1], Jan Eglinger[1], Philippe Pasero[4], Heinz Gut[1], Miki Shinohara[5], Karl-Peter Hopfner[6], Kenji Shimada[1], and Susan M. Gasser [1,2]

1) Friedrich Miescher Institute for Biomedical Research, Maulbeerstrasse 66, CH-4058 Basel, Switzerland.

2) University of Basel, Faculty of Natural Sciences, Klingelbergstrasse 50, CH-4056 Basel, Switzerland

3) current address: The Lunenfeld-Tanenbaum Research Institute, Mount Sinai Hospital, 600 University, Avenue, Toronto, Canada

4) Institute of Human Genetics, CNRS UPR 1142 Montpellier, France

5) Institute for Protein Research, Osaka University, Suita, Osaka 565-0871, Japan

6) Gene Center LMU Munich, Feodor-Lynen Str. 25, 81377 Munich, Germany

Molecular Cell 2016, Volume 64, pp 951-966

Summary

The Mre11-Rad50-Xrs2 (MRX) complex is related to SMC complexes that form rings capable of holding two distinct DNA strands together. MRX functions at stalled replication forks and double-strand breaks (DSBs). A mutation in the N-terminal OB fold of the 70 kDa subunit of yeast replication protein A, *rfa1-t11*, abrogates MRX recruitment to both types of DNA damage. The *rfa1* mutation is functionally epistatic with loss of any of the MRX subunits for survival of replication fork stress or DSB recovery, although it does not compromise end-resection. High-resolution imaging shows that either the *rfa1-t11* or the *rad50Δ* mutation lets stalled replication forks collapse and allows the separation not only of opposing ends but of sister chromatids at breaks. Given that cohesin loss does not provoke visible sister separation as long as the RPA-MRX contacts are intact, we conclude that MRX also serves as a structural linchpin holding sister chromatids together at breaks.

In this article we show MRX that is epistatic with *rfa1-t11* in response to replication stress. We show that Rfa1 and MRX can interact through the N-terminal OB fold of Rfa1. This interaction facilitates the recruitment of MRX to stalled replication forks and DSBs. We prove the theory that MRX may hold sister chromatids together DSBs by advanced imaging assays. Importantly, we show that MRX appears to hold sister chromatids together at breaks in the absence of cohesin.

Author contributions: I note that this was a community project that spanned multiple generations. A.S., K.S., A.M.H. and S.M.G planned most experiments, analyzed data and A.S., K.S., and S.M.G wrote the manuscript. A.S. specifically performed experiments in Figures 1C and E; 2F, 3A-F, 4A-D, 5A-C, 6 and 7. N.H. carried out the EMAP and all analysis, J.P. did Rad50 ChIP-chip, I.D. did MST, purified Rfa1 and determined rfa1-t11 structure guided by H.G., M.S. did the NHEJ assay, J.E. wrote scripts for image analysis, K.S. created strains and confirmed EMAP synergies, and K-P.H. modeled the Rad50-Mre11 structure and peptide position. P.P. supervised DNA combing and ChIP-chip data.

Article

Molecular Cell

RPA Mediates Recruitment of MRX to Forks and Double-Strand Breaks to Hold Sister Chromatids Together

Graphical Abstract

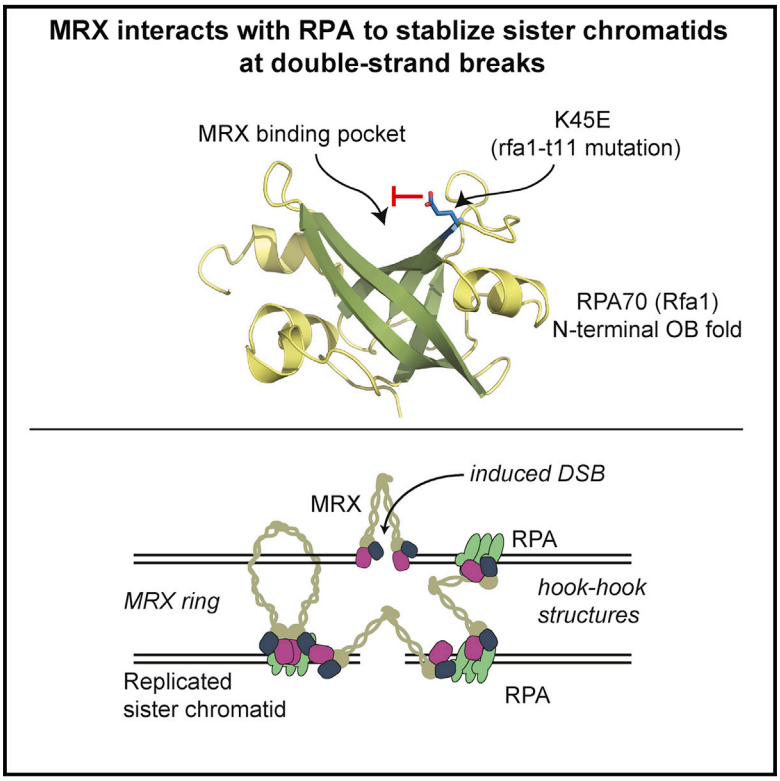

Authors

Andrew Seeber, Anna Maria Hegnauer, Nicole Hustedt, ..., Karl-Peter Hopfner, Kenji Shimada, Susan M. Gasser

Correspondence

susan.gasser@fmi.ch

In Brief

Seeber et al. show that the MRX (MRN) complex is recruited to stalled replication fork and double-strand breaks through the N-terminal OB fold of Rfa1. They show that this interaction is crucial for holding both sister chromatids and ends together at breaks independently of cohesin.

Highlights

- MRX is epistatic with *rfa1-t11* in response to replication stress
- Rfa1 and MRX interact through the N-terminal OB fold of Rfa1
- Rfa1 recruits MRX to stalled forks and double-strand breaks
- RPA-MRX interaction holds sisters together at breaks independently of cohesin

Accession Numbers

5M1X
GSE88816

Seeber et al., 2016, Molecular Cell *64*, 951–966
December 1, 2016
http://dx.doi.org/10.1016/j.molcel.2016.10.032

CellPress

Molecular Cell
Article

RPA Mediates Recruitment of MRX to Forks and Double-Strand Breaks to Hold Sister Chromatids Together

Andrew Seeber,[1,2] Anna Maria Hegnauer,[1] Nicole Hustedt,[1,6] Ishan Deshpande,[1,2] Jérôme Poli,[1] Jan Eglinger,[1] Philippe Pasero,[3] Heinz Gut,[1] Miki Shinohara,[4] Karl-Peter Hopfner,[5] Kenji Shimada,[1] and Susan M. Gasser[1,2,7,*]
[1]Friedrich Miescher Institute for Biomedical Research, Maulbeerstrasse 66, 4058 Basel, Switzerland
[2]University of Basel, Faculty of Natural Sciences, Klingelbergstrasse 50, 4056 Basel, Switzerland
[3]Institute of Human Genetics, CNRS UPR 1142, 34090 Montpellier, France
[4]Institute for Protein Research, Osaka University, Suita, Osaka 565-0871, Japan
[5]Gene Center LMU Munich, Feodor-Lynen Strasse 25, 81377 Munich, Germany
[6]Present address: The Lunenfeld-Tanenbaum Research Institute, Mount Sinai Hospital, 600 University Avenue, Toronto, ON M5G 1X5, Canada
[7]Lead Contact
*Correspondence: susan.gasser@fmi.ch
http://dx.doi.org/10.1016/j.molcel.2016.10.032

SUMMARY

The Mre11-Rad50-Xrs2 (MRX) complex is related to SMC complexes that form rings capable of holding two distinct DNA strands together. MRX functions at stalled replication forks and double-strand breaks (DSBs). A mutation in the N-terminal OB fold of the 70 kDa subunit of yeast replication protein A, *rfa1-t11*, abrogates MRX recruitment to both types of DNA damage. The *rfa1* mutation is functionally epistatic with loss of any of the MRX subunits for survival of replication fork stress or DSB recovery, although it does not compromise end-resection. High-resolution imaging shows that either the *rfa1-t11* or the *rad50Δ* mutation lets stalled replication forks collapse and allows the separation not only of opposing ends but of sister chromatids at breaks. Given that cohesin loss does not provoke visible sister separation as long as the RPA-MRX contacts are intact, we conclude that MRX also serves as a structural linchpin holding sister chromatids together at breaks.

INTRODUCTION

The DNA damage and intra-S phase checkpoints are important response mechanisms that allow cells to deal with damage from exogenous or endogenous sources both by arresting the cell cycle when necessary and by activating the appropriate repair machinery (Ciccia and Elledge, 2010; Harrison and Haber, 2006; Hustedt et al., 2013). Central to the checkpoint response are the conserved checkpoint kinases Mec1-Ddc2 (ATR-ATRIP) and Tel1 (ATM). Importantly, the trimeric complex that binds single-strand DNA (ssDNA), replication protein A (RPA), acts as a recruitment platform for checkpoint and repair proteins, including but not limited to Mec1-Ddc2 and 9-1-1, the DNA damage clamp, both at stalled forks and at DNA double-strand breaks (DSBs) (Paciotti et al., 2000; Rouse and Jackson, 2002; Xu et al., 2008; Zou and Elledge, 2003; Kanoh et al., 2006; Majka et al., 2006). The failure of RPA to coat ssDNA results in replication catastrophe and also compromises homologous recombination (HR), underscoring the crucial role of this complex (Hustedt et al., 2013; Toledo et al., 2013). Although checkpoint activation coordinates cell cycle events, the maintenance of the physical structure of a stalled fork or a DSB is also crucial for repair, especially repair that is based on recombination with a sister chromatid (Bjergbaek et al., 2005; Petermann and Helleday, 2010; San Filippo et al., 2008; Wang et al., 2004).

Structural maintenance of chromosomes (SMC) complexes are central to long-range chromatin organization and are required for the proper meiotic segregation of replicated DNA, chromosome condensation, and homology-based DNA repair (Uhlmann, 2016). SMC proteins are characterized by a distinct coiled-coil domain that contains a hinge, allowing the coil to fold back on itself, bringing the N- and C-terminal globular domains together (Hirano, 2006). The best characterized SMC protein complex is cohesin, which comprises two SMC proteins, Smc1/3, and two non-SMC proteins, Scc1 (Mcd1) and Scc3. The latter serve as a clasp to bridge the head domains of Smc1/3. This complex keeps sister chromatids paired, particularly in G2 and prometaphase (Uhlmann et al., 1999). Cohesin is also recruited to DSBs and stalled replication forks, where it contributes to repair (Heidinger-Pauli et al., 2008; Ström et al., 2007; Ström and Sjögren, 2007; Unal et al., 2004, 2007) and replication fork recovery (Tittel-Elmer et al., 2012).

The Mre11/Rad50/Xrs2 (MRX) complex is structurally similar to cohesin and is often characterized as the first responder to a DSB (Lisby et al., 2004). MRX promotes the initiation of end-resection with the co-factor Sae2 (CtIP) (Garcia et al., 2011; Lengsfeld et al., 2007; Mimitou and Symington, 2008; Williams et al., 2009). Although abundant data implicate MRX in

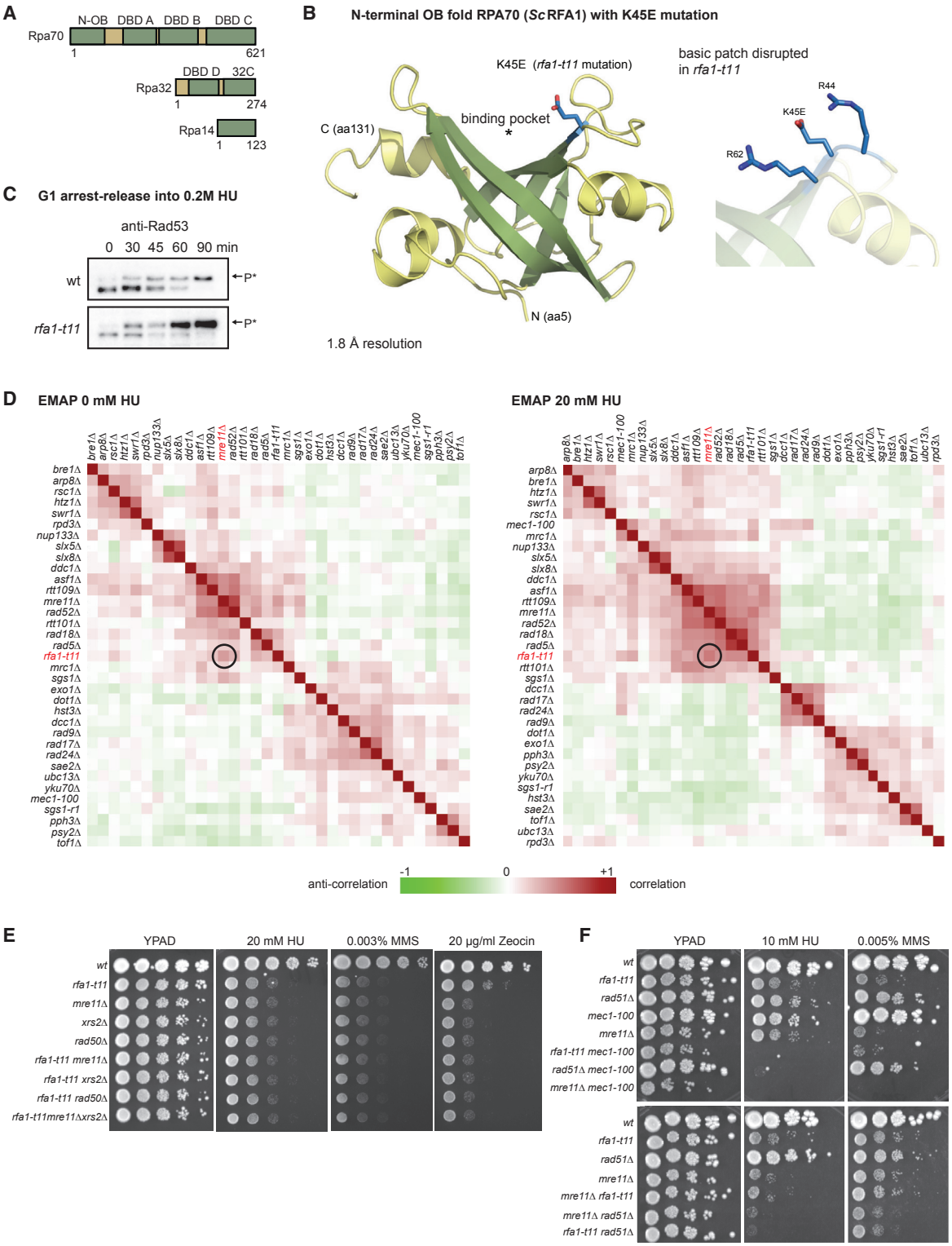

Figure 1. *rfa1-t11* Is Checkpoint Proficient and Is Epistatic with Loss of MRX on HU

(A) Diagram of the three subunits of RPA. Rfa1 (*Sc*RPA70) contains four OB domains. Unlike the others, the N-OB binds DNA poorly but binds proteins.

(B) Crystal structure of budding yeast Rfa1-t11$_{1–132}$ in cartoon with the five-stranded β-barrel forming the OB fold colored in dark green. Residues 1–4 are not shown. The E45 side chain is indicated in blue atom colors, while helices and coiled elements are in pale yellow. *Putative MRX-binding site. Right: E45 in the Rfa1-t11$_{1–132}$ structure with residues R44, K45E, and R62 displayed as sticks and blue atom colors. K45E disrupts this basic patch.

(legend continued on next page)

checkpoint activation, telomere elongation, and initiation of resection (reviewed in Stracker and Petrini, 2011; Lafrance-Vanasse et al., 2015), only a few studies have asked whether it plays a structural role at damage. Supporting this, it was shown that the two sides of a DSB separate from each other in ~12%–15% of cells lacking MRX (Kaye et al., 2004; Lobachev et al., 2004). MRX is thought to form a dimer complex with two Rad50 subunits, which, like Smc1 and Smc3 in cohesin, have long coiled-coil arms that can stretch up to ~600 Å (de Jager et al., 2001a; Hopfner et al., 2002; Moreno-Herrero et al., 2005). These coiled-coil arms can dimerize at their tips through a zinc hook domain, allowing the formation of ring-like structures or higher order oligomers that could hold two DNA molecules together (de Jager et al., 2001b; Hopfner et al., 2002). Functional studies showing that the hook domain is essential for MRX function in DNA repair, telomere maintenance, and meiotic DSB formation (Hohl et al., 2011; Wiltzius et al., 2005) are consistent with this hypothesis but do not prove it. Genetic data also implicate MRX in the repair of DSBs by sister chromatid exchange (González-Barrera et al., 2003; Hartsuiker et al., 2001).

Our study starts from the discovery of an epistatic relationship between a point mutation in the large subunit of RPA, *rfa1-t11*, and null alleles of *MRE11*, *RAD50*, or *XRS2*, under conditions of replication stress in *S. cerevisiae*. The *rfa1-t11* allele bears a single point mutation (K45E) in the N-oligonucleotide binding (OB) fold of Rfa1, which renders the strain deficient for both mitotic and meiotic recombination, although end-resection occurs normally (Dubrana et al., 2007; Umezu et al., 1998). We show here that *rfa1-t11* fails to stabilize stalled replication forks, leading to fork collapse. Rather than impairing activation of the S phase checkpoint, *rfa1-t11* reduces the recruitment of MRX to both stalled replication forks and DSBs in vivo, resulting in an inability to restart stalled forks and end separation at DSBs. We show that Rfa1 and MRX interact in an *rfa1-t11*-sensitive manner in vitro. Finally, we find that MRX holds sisters and break ends together in an RPA-dependent manner at DSBs in vivo, even when cohesin is inactivated. This provides direct evidence that MRX plays a structural role at stalled replication forks and breaks.

RESULTS

The *rfa1-t11 K45E* Mutation Disrupts a Basic Patch in Rfa1's N-OB Binding Pocket

The ssDNA-binding protein RPA is composed of three subunits, all of which are essential for cell viability in budding yeast (Figure 1A). The largest subunit (ScRpa70 or Rfa1) contains 4 OB fold domains, three of which are implicated in ssDNA binding, while the N-terminal OB-fold serves as a recruitment platform for other proteins involved in replication stress and DSB repair, including Ddc2/ATRIP and Sgs1 in budding yeast, and Rad9 and p53 in mammalian cells (Ball et al., 2007; Bochkareva et al., 2005; Dutta et al., 1993; Flynn and Zou, 2010; Hegnauer et al., 2012; Xu et al., 2008).

In earlier studies, RPA was mutagenized for non-lethal mutations, in order to identify crucial binding partners and domain-specific functions (Binz and Wold, 2008; Umezu et al., 1998; Zou et al., 2006). A previously characterized mutation, *rfa1-t11* (K45E), was reported to be specifically defective in HR, while supporting normal DNA replication (Kanoh et al., 2006; Wang and Haber, 2004). The lysine-to-glutamate charge reversal maps to the binding pocket of the N-terminal OB fold. Intriguingly, it confers recessive sensitivity to hydroxyurea (HU), which induces replication stress by inhibiting dNTP synthesis (Figure S1A), although without HU there was no delay in S phase entry: replication forks fire and progress without pausing or forming aberrant recombination intermediates (Figures S1B and S1C).

To understand the structural changes provoked by the K45E substitution, we expressed, purified, and crystallized the mutant N-terminal OB fold of yeast Rfa1 (aa 1–132) and solved its structure at 1.8 Å (Figure 1B; Table 1) using the single-wavelength anomalous diffraction method (Supplemental Experimental Procedures). Indeed, the *rfa1-t11* mutation disrupts a basic patch in the binding pocket of the N-terminal OB fold, as the mutant residue protrudes into the binding cleft. Given that the ligands of this domain are acidic, we predicted that this K45E mutation might interfere with protein-protein interactions that are important at stalled forks.

The N-terminal OB domain is responsible for the recruitment of ATRIP/Ddc2 to ssDNA and activation of the ATR kinase (Rouse and Jackson, 2002; Zou and Elledge, 2003). Mec1-Ddc2 is responsible for the vast majority of Rad53 phosphorylation induced by replication stress (Hustedt et al., 2013). Therefore, we tested for defects in checkpoint activation on a synchronized population of *rfa1-t11* cells, after releasing from G1 arrest into 0.2 M HU for 90 min. Rad53, however, was efficiently activated in the *rfa1-t11* mutant and showed a pronounced shift in electrophoretic migration (Figure 1C). A similar assay in a strain bearing *rfa1-t11* combined with *tel1Δ* showed the same shift, arguing that Rad53 activation on HU is primarily mediated by Mec1 (Figure S1D). Importantly, impaired Mec1 kinase activation is not responsible for the *rfa1-t11* mutant's sensitivity to HU.

MRX and rfa1-t11 Show Similar Epistatic Miniarray Profile Patterns in Response to Replication Stress

To identify *rfa1-t11*'s pathway of action, we performed an epistatic miniarray profile (EMAP) to compare the growth of *rfa1-t11* and 34 other query strains crossed to 1,311 deletion strains or decreased abundance by mRNA perturbation (DAmP) alleles, grown in 0, 20, or 100 mM HU (Hustedt et al., 2015). This resulted in a gene network of 45,885 interactions that had either synergistic or suppressive effects or failed to grow altogether on HU (Figures 1A, S2A, and S2B). One can correlate the patterns of sensitivity to identify genetic pathways affected similarly by specific mutants, because mutants that share phenotypic correlations often share functionality (Morrison

(C) Western blot showing Rad53 phosphorylation upshift (*) after release from α-factor into 0.2 M HU in WT and *rfa1-t11* strains.
(D) Heatmaps of Pearson correlation coefficients showing patterns of synergism between 1,311 nuclear proteins in 0 and 20 mM HU. Red indicates a correlation, while green indicates an anti-correlation. Black ring highlights the strong correlation between *rfa1-t11* and *mre11Δ*.
(E) A 10-fold dilution series showing epistasis of MRX components with *rfa1-t11* on genotoxic drugs.
(F) Additivity with *mec1-100* and *rad51Δ*. All strains are W303 *RAD5+* isogenic strains (Table S1).

Table 1. Crystallographic Data Collection and Refinement Statistics

	Rfa1-t11$_{1-132}$ Se-Met Peak[a]
Data Collection	
Space group	P 2_1
Unit cell dimensions	
a, *b*, *c* (Å)	29.62, 115.35, 69.03
α, β, γ (°)	90.0, 90.7, 90.0
Resolution range (Å)[b]	50.0–1.8 (1.85–1.80)
Wavelength (Å)	0.97941
Completeness (%)[b]	95.4 (86.2)
Redundancy[b]	2.4 (2.3)
R_{sym}[b]	0.079 (0.527)
$I/\sigma(I)$[b]	8.0 (1.7)
CC (1/2) (%)[b]	99.5 (67.9)
Unique reflections	80,762
Refinement	
R_{work}	0.164
R_{free}	0.214
Resolution range (Å)	44.3–1.8
Reflections (all)	41,721
Reflections (test set)	2,086 (5%)
Number of atoms	4,246
Figure of merit	0.415
B Factors (Å^2)	
Overall	31.7
Protein	31.0
Solvent	39.4
RMSD	
Bond lengths (Å)	0.01
Bond angles (°)	1.05
Ramachandran Plot	
Allowed (%)	100.0
Outliers (%)	0.0

RMS, root mean square.
[a]Data collection statistics are reported for unmerged Friedel pairs.
[b]Values in parentheses refer to the highest-resolution shell.

et al., 2007). For example, the histone variant *HTZ1* pattern correlates best with the nucleosome remodeler *SWR1*, which incorporates Htz1 into nucleosomes (Figures 1D and S2B).

To our surprise we found that *rfa1-t11* correlated most strongly with *mre11Δ* in both the absence and presence of 20 mM HU (Figure 1D). On 100 mM HU (Figure S2B), the EMAP pattern of *rfa1-t11* correlated additionally with *mec1-100*, an S phase defective allele of Mec1 kinase that is particularly sensitive to HU (Paciotti et al., 2001). Consistently, at 100 mM HU the *rfa1-t11* and *mre11Δ* EMAPs were similar to the template switch pathway, whereas at 20 mM the patterns of sensitivity scored for *mre11Δ* and *rfa1-t11* resemble a null allele of replication fork component *mrc1*Δ. This led to a deeper examination of the genetic relationship of *rfa1-t11*, *mec1-100*, and the MRX complex.

We created double mutants of *rfa1-t11* with deletions of *MRE11*, *RAD50*, or *XRS2* and tested them for epistasis on a range of DNA-damaging agents. Confirming the EMAP, we found that the sensitivity of *rfa1-t11* for growth on HU is completely epistatic with *mre11Δ*, *rad50Δ*, or *xrs2Δ*. That is, single and double mutants had nearly identical survival rates on HU (Figure 1E). The same is true for the triple mutant, *rfa1-t11 mre11Δ xrs2Δ*, on either HU or methyl methanesulfonate (MMS), an alkylating agent that also delays replication fork progression. On Zeocin, which induces single- and double-strand breaks, the two complexes again appeared to act on a common survival pathway, as the double mutants lacked additivity, although MRX loss of function alleles were significantly more sensitive than *rfa1-t11*. Nonetheless, these data confirmed that *rfa1-t11* likely acts through MRX and not on a parallel repair pathway at stalled forks and DSBs.

We next tested whether the *rfa1-t11* allele is epistatic or additive with mutations in Mec1, the checkpoint kinase, or the recombination protein Rad51. If *rfa1-t11*'s main defect were an inability to load or modulate Rad51 on HU (Kantake et al., 2003), one would expect these two mutants to be epistatic. However, neither *rad51Δ* nor *mec1-100* was epistatic with the *rfa1-t11* allele (Figure 1F), each showing a synthetic lethality with *rfa1-t11* on HU. Similarly, *ddc1Δ*, which compromises the 9-1-1 complex, showed synthetic lethality in combination with *rfa1-t11* on HU (data not shown). Our data suggest that RPA works with MRX to maintain replication fork integrity on HU, defining a pathway that acts in parallel to checkpoint activation and to Rad51 (Figure 1F). Consistently, *rad51Δ* was synergistically sensitive with *mre11Δ* and *mec1-100* on HU or MMS (Figure 1F).

The Replication Fork Is Unable to Resume after HU-Induced Arrest in the rfa1-t11 Mutant

To examine how *rfa1-t11* affects replication fork integrity, we scored the resumption of replication after release from an acute fork arrest in 0.2 M HU. After 6 hr on HU, the recovery rate for *mec1-100* cells is <10% of wild-type (wt) levels, while both the *mre11Δ* and *rfa1-t11* strains reduce recovery to about 20% of WT levels. Strikingly, the *rfa1-t11* mutant is again completely epistatic with the loss of Mre11 and is synergistically lethal with *mec1-100* (Figure 2A). This places the *rfa1-t11* defect on the pathway through which MRX ensures fork restart on HU (Figures 1D, 1E, and S2).

To see if this reflects the loss of DNA polymerase α (polα) at forks arrested by 0.2 M HU, we scored the presence of polα at forks that were arrested synchronously near early firing origins, using chromatin immunoprecipitation (ChIP) (Cobb et al., 2003). In contrast to results in an isogenic WT background, we scored a striking loss of DNA polα at *ARS607* in the *rfa1-t11* mutant (Figure 2B). This does not reflect an impaired checkpoint response, as there is no polα at the late firing origin *ARS501* (Figure 2B). In contrast, in *mec1-100* cells, impaired Rad53 activation allows late origin firing (Cobb et al., 2005).

To see if the resumption of DNA synthesis after HU arrest is compromised by *rfa1-t11*, we performed a DNA combing assay that measures fork progression by incorporation of BrdU, a thymidine analog, after a transient exposure to 0.2 M HU and release into HU-free media. Whereas WT forks resume

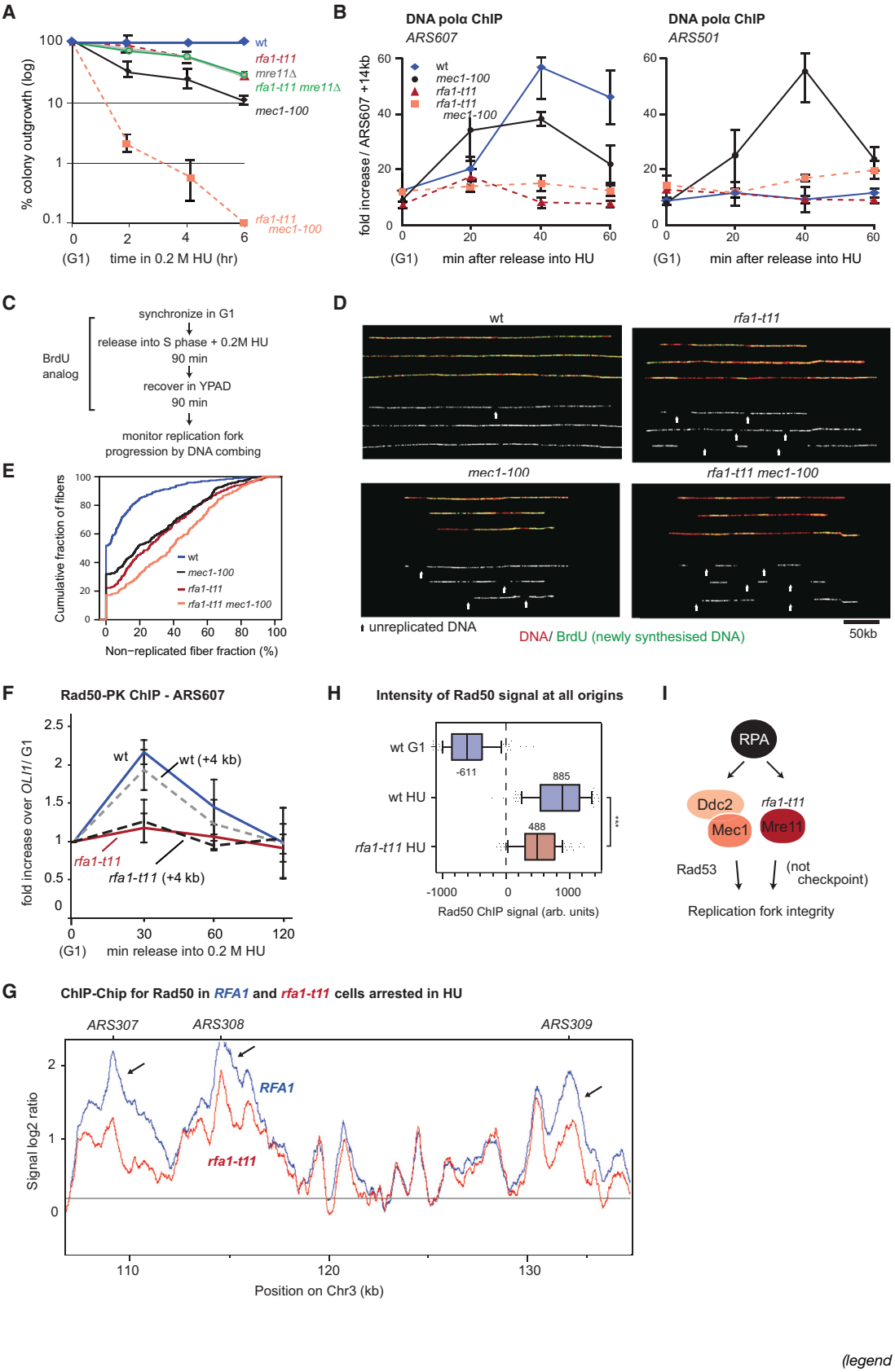

(legend on next page)

elongation, the *rfa1-t11* mutant is strongly impaired in the resumption of DNA synthesis (Figures 2D and 2E, white arrows). Again, we note that the *rfa1-t11* defect is additive with *mec1-100*. Similar phenotypes have been observed in MRX deletion alleles, although not for nuclease-deficient Mre11 mutants (Tittel-Elmer et al., 2009).

rfa1-t11 Interferes with Recruitment of MRX to Stalled Replication Forks

Given the epistasis of *mre11Δ* with *rfa1-t11*, we examined whether the K45E mutation in RPA compromises the recruitment of MRX to stalled replication forks. We performed PK-tagged Rad50 ChIP after treatment with 0.2 M HU in WT and mutant strains. Indeed, by quantitative ChIP for Rad50-PK, we found that Rad50 recruitment to stalled forks at *ARS607* was compromised by the *rfa1-t11* mutation (Figure 2F). To make sure that this was a general phenomenon and not unique to one site, we performed genome-wide ChIP of HA-tagged Rad50 on cells synchronously released from α-factor into 0.2 M HU. Figure 2G shows the pattern of Rad50 binding across a typical domain on Chr3, which includes several origins and non-origin binding sites. Whereas Rad50 binding at non-origin sites was not impaired in the *rfa1-t11* strain, its signal was strongly reduced at origins. We integrated this over all origins of the yeast genome (Figure 2H) and found ≥50% reduction in MRX (Rad50) at origins on HU. Combining our data with observations of Tittel-Elmer et al. (2012), we propose that Rfa1 recruits MRX to stalled replication forks, the failure of which allows replication fork collapse on HU soon after origin firing. This pathway of fork maintenance is independent of Rad53 activation (Figure 2I).

MRX Interacts with RPA through the N-OB Fold of Rfa1

The epistasis and recruitment data on HU suggested that RPA might directly bind MRX. To detect this interaction and monitor its response to the *rfa1-t11* mutation, we co-immunoprecipitated Rad50-PK from extracts of WT and *rfa1-t11* strains, probing for Rfa1 with an antibody that reacts equally with mutant and WT Rfa1 (Figure 3A). We find that Rad50 can indeed co-precipitate Rfa1, while it binds rfa1-t11 less efficiently (Figure 3B). The converse precipitation (i.e., by anti-Rfa1) confirmed that the MRX interaction was sensitive to the *rfa1-t11* mutation. The binding did not depend on DNA or RNA, since recovery was unchanged after treatment with Benzonase, which degrades nucleic acids (Figures 3B and S3A). Pull-downs from cell extracts using antibody specific for Xrs2 recovered Rad50 and Rfa1 but failed to recover rfa1-t11 (Figure 3B).

To determine the component of MRX that binds Rfa1, we repeated the Rad50-PK pull-down from extracts of *mre11Δ* or *xrs2Δ* strains. Rad50-PK precipitates a lower amount of Rfa1 in the absence of either Mre11 or Xrs2, suggesting either the existence of multiple contacts between Rfa1 and MRX or a need for MRX complex integrity for the interaction (Figure 3C). A double point mutation in Xrs2 (*xrs2-AA*) that disrupts Mre11 binding and/or the truncation (*xrs2-664*) of the Xrs2 C terminus (Shima et al., 2005) compromised Rfa1 recovery to the same extent as *rfa1-t11* in *XRS2*$^{+}$ cells (Figure S3B), suggesting a role for MRX conformation or complex integrity in Rfa1 interaction.

Finally, we examined the specificity of binding by comparing yeast two-hybrid (Y2H) interactions of Rfa1 with rfa1-t11. Intriguingly, both Mre11 and Xrs2 bound Rfa1 by Y2H, but only Xrs2 binding was *rfa1-t11* sensitive (Figures S3C and S3D). Y2H with Rad50 was not possible because the cloned fusions were lethal. Unfortunately, Y2H does not exclude that the endogenous MRX subunits form tertiary complexes with the bait during the assay, and thus from the Y2H and pull-down results we concluded only that multiple contact sites exist between MRX and RPA, with a subset being sensitive to the *rfa1-t11* mutation.

To map the interactions more precisely, we used a scanning peptide microarray that consisted of 206 18-aa-long peptides (overlapping by 9 aa), covering all of MRX, except the coiled-coiled arms of Rad50. The peptides were spotted onto glass slides in triplicate and were incubated with purified recombinant Rfa1 or *rfa1-t11* N-OB domains (Figure 3D). Bound proteins were visualized through anti-Rfa1 staining and a secondary Alexa647-tagged antibody, whose fluorescence was quantified on a protein array analyzer (ImageJ plugin; see Supplemental Experimental Procedures). The efficiency of binding of either Rfa1 or rfa1-t11 is plotted in Figure 3E, and the full list of peptides and their associated intensities are listed in Table S2.

We scored several clusters of Rfa1-binding peptides that were sensitive to the *rfa1-t11* mutation: namely, in the nuclease domain of Mre11, in the ATPase domain of Rad50, and two defined regions in Xrs2, one each in the N-terminal FHA domain and the C-terminal Mre11-binding domain (Figure 3E). When mapped onto the 3D structure of Mre11-Rad50 (Seifert et al., 2015), the peptides cluster in two surface areas: the double-stranded DNA (dsDNA) binding cleft of the Rad50 dimer, and a surface patch on the lateral side of the Mre11 phosphodiesterase domain (Figure 3F). Although peptides from Xrs2 also showed differential interaction, two of these map to binding sites for other proteins, and they do not cluster as do those in Mre11 or

Figure 2. Resumption of Replication after HU-Induced Stalling Fails in the *rfa1-t11* Mutant

(A) Recovery assay after G1 arrest with α-factor and release into 0.2 M HU of indicated mutants (*rfa1-t11*, *mre11Δ*, and *mec1-100*; n = 3).

(B) ChIP of DNA polα at either the early-firing ARS607 or late-firing ARS501 (Cobb et al., 2003) after release from G1 arrest into in 0.2 M HU (n = 3).

(C) Experimental scheme of DNA combing: synchronized cells are released into 0.2 M HU with a BrdU analogue for 90 min, after which the HU is washed out and the cells are allowed to recover again with analogue. DNA was combed and new synthesis was visualized by antibodies against BrdU and DNA.

(D) Example images of DNA combing with gaps (white arrows) and shorter lengths of newly synthesized DNA in mutant backgrounds.

(E) Cumulative frequency graph showing the non-replicated fiber fraction in WT and mutant strains.

(F) Rad50-PK ChIP to ARS607 after release from α-factor into 0.2 M HU (n = 3).

(G) Example plots of genome-wide Rad50-HA ChIP-chip showing loss of Rad50 at origins 307–309 in *rfa1-t11*.

(H) Boxplots of Rad50 ChIP-chip signals at all origins after release in to 0.2 M HU for 60 min at 25°C, in indicated strains. Error bars represent the SEM.

(I) Model placing *rfa1-t11* on a pathway with MRX, parallel to Mec1 activation, to confer replication fork integrity.

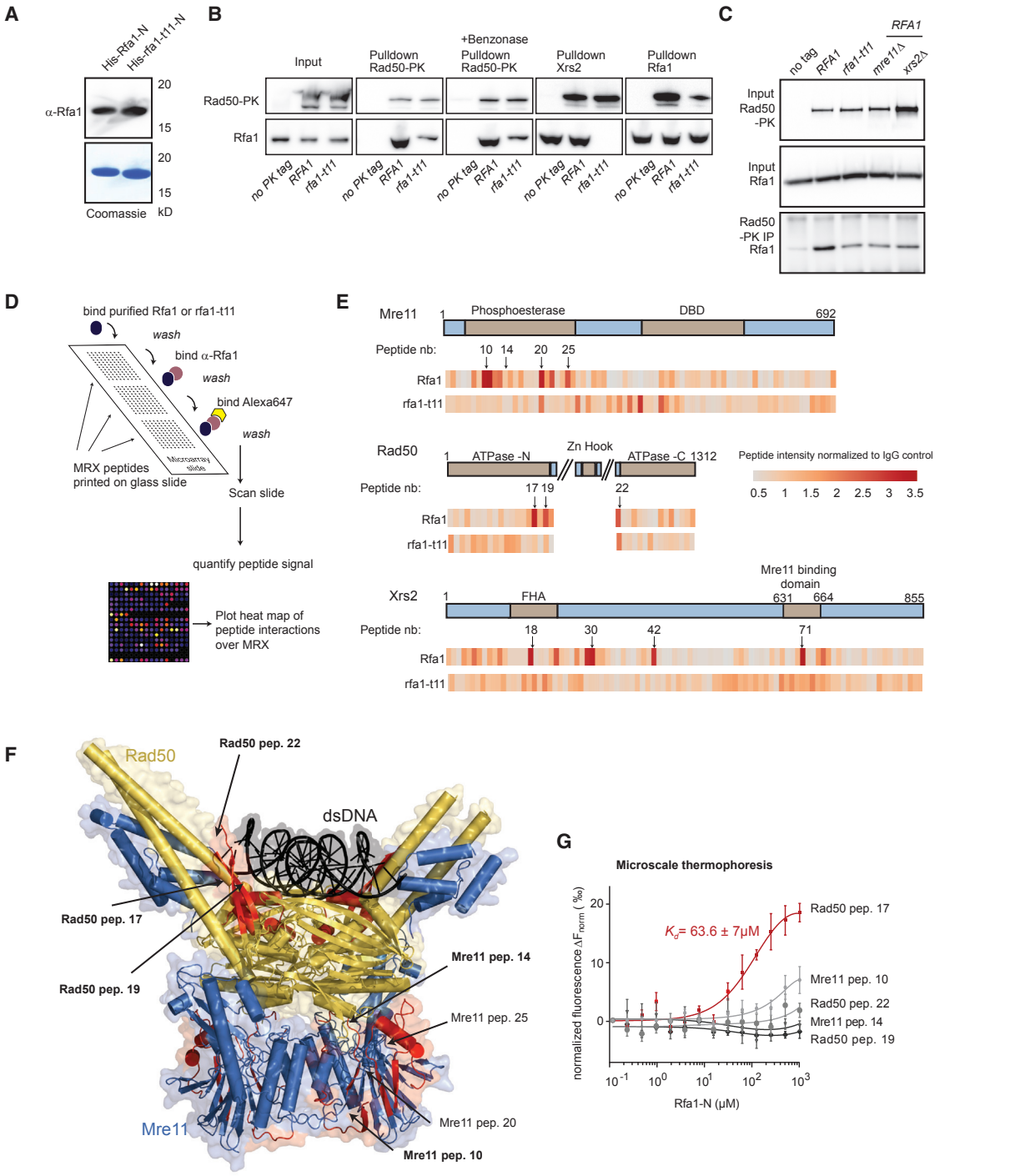

Figure 3. The Interaction between MRX and Rfa1 Is Disrupted in *rfa1-t11*

(A) Western blot showing that the Rfa1 antibody recognizes the N-OB of both Rfa1 and rfa1-t11 equally.

(B) Co-immunoprecipitation from yeast extracts in WT RFA1 and *rfa1-t11* using either antibodies against the PK tag, Xrs2, or Rfa1. Samples were Benzonase treated (Figure S3A).

(C) Rad50-PK co-immunoprecipitation as in (A) using the indicated mutants.

(D) Scheme of MRX scanning peptide microarray probed with N-OB of either Rfa1 or rfa1-t11. Two hundred six peptides (18 aa each) were spotted onto a glass slide for binding to Rfa1 or rfa1-t11 N-OB from (A). Supplemental Experimental Procedures describe signal detection and quantitation.

(E) Interaction heatmaps for either Rfa1 or rfa1-t11 across MRX. Arrows indicate regions of strong (red) binding sensitive to the *rfa1-t11* mutation (n = 3).

(legend continued on next page)

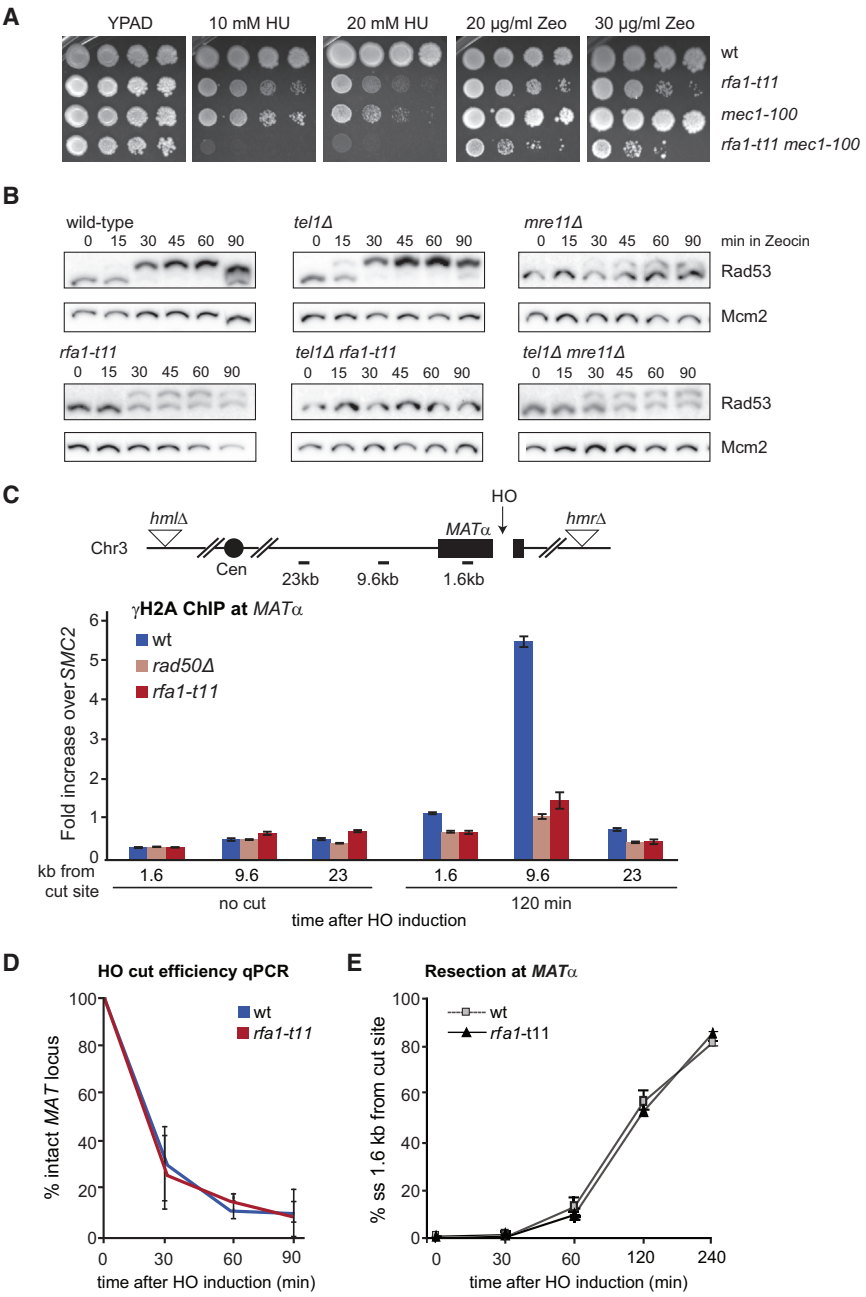

Figure 4. *rfa1-t11* Has a Diminished Checkpoint Response to DSBs, but Resection Is Intact

(A) A 10× dilution series on YPAD ± HU and Zeocin of isogenic strains with the indicated genotypes.

(B) Western blot showing Rad53 phosphorylation upshift after release from α-factor into 250 μg/ml Zeocin. No Rad53 phosphorylation was detectable in *tel1Δ rfa1-t11*. Mcm2 is the loading control.

(C) γH2A ChIP to a HO-induced DSB at *MATα* (van Attikum et al., 2007) at 120 min after cut induction (n = 4).

(D) Cut efficiency time course from Figure 5A showing that WT and *rfa1-t11* have similar cut efficiencies. After replication, both sisters are likely to be cut at once.

(E) QAOS assay showing equal accumulation of ssDNA at 1.6kb from the DSB at *MATα* in WT and *rfa1-t11*, reproduced from Dubrana et al. (2007). Error bars represent SEM.

rfa1-t11 Impairs Mec1-Dependent Checkpoint Activation at DSBs

Because *rfa1-t11* had previously been shown to be important to recruit Ddc2 (ATRIP) and Mec1 (ATR) to a DSB (Dubrana et al., 2007; Zou and Elledge, 2003), we next interrogated its genetic relationship with *mec1-100* on Zeocin, which induces both single- and double-strand breaks. Although *rfa1-t11* is sensitive to Zeocin, *mec1-100* has a mild slow-growth phenotype (Figure 4A). In contrast to growth on HU, where the combination of *rfa1-t11* and *mec1-100* was synthetically lethal, the combination of *rfa1-t11* and *mec1-100* was only slightly additive on Zeocin. MRX both helps recruit the DNA damage checkpoint kinase Tel1 (ATM) to DSBs (Nakada et al., 2003a, 2003b) and promotes resection to allow Ddc2-Mec1 activation, explaining their epistasis.

To check the epistatic relationship of Rfa1 and Mre11 on Zeocin, we scored the effects of *rfa1-t11*, *mre11Δ*, *tel1Δ*, and their pairwise combinations on Rad53 phosphorylation. We found that *rfa1-t11* and *mre11Δ* mutations compromised checkpoint activation by Zeocin to a similar degree (Figure 4B), yet in the case of *rfa1-t11*, the impaired checkpoint response was strongly additive with *tel1Δ*; that is, the *tel1Δ rfa1-t11* completely failed to activate the DNA damage checkpoint

Rad50. Microscale thermophoresis (MST) showed that the Rad50 peptide 17 had the highest affinity for Rfa1-N (Figure 3G). The other peptides tested showed weaker binding. This does not rule out that they contribute to a binding site but suggests that the ATPase-domain of Rad50 contains a key interaction site, which is indeed sensitive to the K45E mutation.

(F) Crystal structure of *Chaetomium thermophilum* Mre11-Rad50 dimer with dsDNA (Seifert et al., 2015). Peptides scored in the microarray as strongly interacting with RFA1 OB fold domain are highlighted in red.

(G) Purified Rfa1-N (dilution series from 0.12 to 1,000 μM) was incubated with 25 μM Cy5-labeled Rad50 and Mre11 peptides for 15 min at rt. Dissociation constant K_d of 63.6 ± 7 μM is for Rad50 peptide 17 and Rfa1-N (n = 3), error bars represent SEM, and ΔF_{norm} (‰) represents change in fluorescence during thermophoresis normalized to initial fluorescence. A detailed list of peptides is provided in Table S2.

(Figure 4B). This suggests that the *rfa1-t11* defect in checkpoint at DSBs arises from the loss of Mec1 (ATR) activity. Indeed, by ChIP *rfa1-t11* and *rad50Δ* were shown to reduce the accumulation of phosphorylated H2A (γH2A, a Mec1 target), at an HO-induced DSB (Figure 4C). We conclude that *rfa1-t11* compromises the Mec1 checkpoint response at DNA breaks (i.e., on Zeocin) but does not impair Mec1 activation at stalled forks. This difference likely stems from the redundancy of co-activators and mediators at stalled forks, namely, 9-1-1, Dbp11, Dna2, Mrc1, Sgs1, and RPA (Hustedt et al., 2013). We note that although DSB activation of checkpoint kinases was compromised by *rfa1-t11*, both the efficiency of HO endonuclease cleavage and resection rates were at WT levels (Figure 4DE).

rfa1-t11 Reduces Recruitment of MRX to DSBs and Reduces Repair Efficiency

To see whether RPA is implicated in the recruitment or stabilization of MRX at DSBs, possibly by binding either a short overhang or an internal ssDNA stretch, we measured the recruitment Rad50-PK to a HO endonuclease-induced DSB at *MAT* by ChIP. Consistent with previously published results, MRX binding is strongest at early time points and close to the cut site (compare 0.6 versus 1.6 kb probes). This interaction is reduced (although not entirely eliminated) in the *rfa1-t11* mutant (Figure 5A). Consistently, Mre11-YFP focus formation was reduced by roughly 50% in response to Zeocin in the *rfa1-t11* mutant (Figure 5B). One further function attributed to MRX at DSBs is the recruitment of cohesin (Unal et al., 2004, 2007). We therefore tested whether *rfa1-t11*, like *rad50*Δ, fails to recruit cohesin to an HO-induced DSB. ChIP for cohesin subunit Scc1-HA (Mcd1) at a DSB confirmed that both mutants reduce cohesin recruitment similarly after HO induction (Figure 5C).

In contrast to the observation that *rfa1-t11* decreases MRX levels at DSBs, it was recently reported that the loss of Sae2 leads to more MRX at DSBs (Chen et al., 2015; Gobbini et al., 2015). We therefore tested whether *sae2*Δ would compensate for the reduced RPA-MRX binding in the *rfa1-t11* mutant. Indeed, growth defects of *rfa1-t11* on Zeocin, HU, MMS and the topoisomerase I inhibitor camptothecin, were partially rescued by the elimination of Sae2 (Figure S3E). Again, this supports the model that *rfa1-t11* confers sensitivity to DNA damage because of impaired MRX recruitment.

To see if *rfa1-t11* affects DSB repair by a pathway other than HR, we tested the impact of the mutation on repair by end-joining of two incompatible DSBs that flank a *URA3* reporter gene (Ma et al., 2003; Matsuzaki et al., 2012). After cleavage and repair, the survivors are either URA^- (indicating repair by microhomology-mediated repair of non-complementary DSB ends following resection) or URA^+ (precise end-ligation). Like mutations in the MRX complex, *rfa1-t11* reduced the recovery of both URA^- and URA^+ colonies (Figure 5D). Importantly, the *xrs2Δ* mutation is epistatic with *rfa1-t11* in this assay (Iwasaki et al., 2016), consistent with drop assays on Zeocin that place MRX and Rfa1 on the same repair pathway. Given that *rfa1-t11* does not block resection, we suggest that RPA acts by recruiting or stabilizing MRX at breaks, allowing it to hold the two break ends together for either precise or imprecise end-joining.

RFA1 OB Fold Integrity Is Necessary to Allow MRX to Hold the Ends of a DSB Together

We next tested whether *rfa1-t11* directly interferes with the end-tethering activity of MRX by scoring the separation of ends by tagged with different fluorescent protein fusions on either side of an inducible DSB (Kaye et al., 2004; Lobachev et al., 2004). As expected, following cleavage by a galactose-inducible I-SceI endonuclease, the loss of MRX integrity provoked a significant increase in DSB end separation in cells arrested at G2/M by the DNA damage checkpoint (Figure 6A; see also Kaye et al., 2004; Lobachev et al., 2004). Importantly, the level of end separation scored for *mre11Δ* and *rad50Δ* mutants was the same for *rfa1-t11* (Figure 6A).

The fact that *rfa1-t11* compromised cohesin loading (Figure 5C) led us to test whether this mutation interferes with the tight association of sister chromatids, which we could score in a strain bearing a *lacO* array adjacent to the HO-induced break at *MATα* (Figure 6B). Sister cohesion at DSBs is commonly ascribed to cohesin, but on the basis of its architecture and dimensions, MRX should also be able to hold sister chromatids together (Hopfner et al., 2002). To test a potential role for MRX in sister-sister pairing at breaks, we used multiple DSB imaging approaches. First, super-resolution structured illumination microscopy (SIM) was used to analyze small changes in the area occupied by the paired *lacO* arrays adjacent to a break, in late S/G2 phase cells. Second, we performed high-speed time-lapse imaging of the arrays to measure the kinetics of separation following break induction, in unarrested S phase cells. Finally, we examined the maintenance of sister-sister juxtaposition after efficient DSB induction in cells that are arrested by microtubule depolymerization and fixed, comparing *rfa1-t11* with mutants in cohesin and MRX.

We first confirmed that we can resolve two sister chromatids with 3D SIM imaging of the cleaved *MATα* locus (Figure 6BC). Following projection of the 3D image stack to a 2D plane for a large number of late S phase cells, we found that the volume and shape of the fluorescent *lacO* signal are significantly larger in the *rfa1*-t11 mutant, even though the sisters only fully separated in <1% of cells (Figure 6CD). We next confirmed the validity of this spot-size assay by using a strain in which the essential cohesin subunit Scc1 (Mcd1) was cleaved by a galactose-induced TEV protease (Figure 6D). The efficiency of Scc1 cleavage was documented by western blot (Figures S4A and S4B). In S phase cells, we scored a robust increase in the area occupied by the cut-proximal *lacO* focus after Scc1 cleavage, presumably reflecting compromised pairing of sister chromatids (Figures 6D, red arrow and S4C). We applied the same analysis to the strain bearing a HO-mediated DSB at the *MATα* locus adjacent to a *lacO* array (Figure 6B). In WT cells there is a slight increase in array area as cells progress from G1 to S phase; at 120 min after HO induction, there is again a slight increase in locus size (Figure 6D). In the *rfa1-t11* or *rad50Δ* strains, however, the size of the *lacO* signal stemming from the two sisters, increased more significantly than was detected upon Scc1 cleavage (Figure 6D; 0.9 versus 0.6 μm^2).

Given that chromatin loci show continual movement in living cells, and that fixation can introduce artifacts, we examined the behavior of the *lacO* arrays on the two tagged sisters using

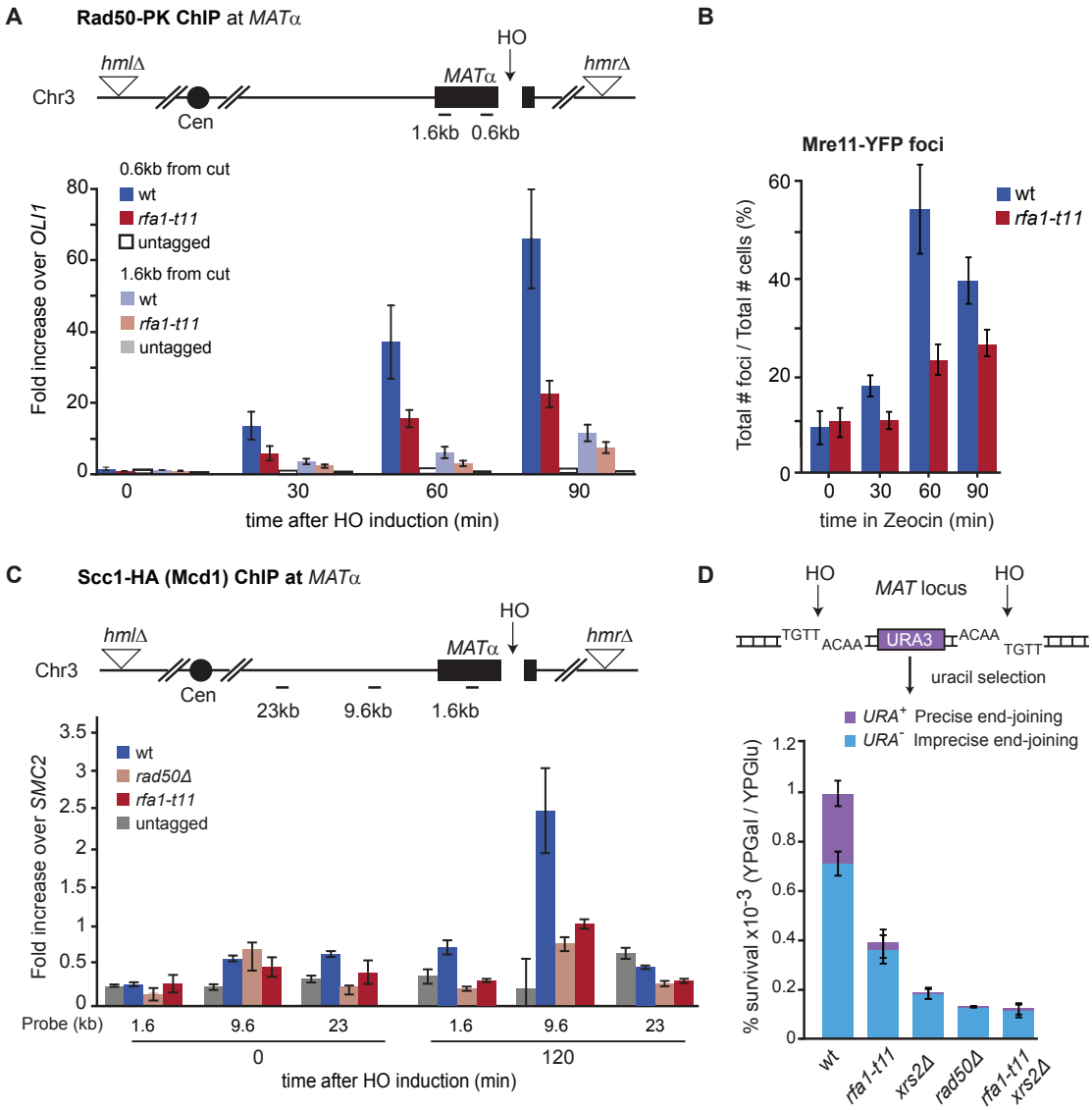

Figure 5. *rfa1-t11* Reduces the Recruitment of MRX to DSBs

(A) Rad50-PK ChIP at an HO-induced DSB at *MATα* on Chr3 in asynchronous cells (n = 5) (for probes, see van Attikum et al., 2007). HO cut efficiencies for each experiment are in Table S3. We assume that both sisters are cut, given the high rate of cleavage scored for individual loci.

(B) Mre11-YFP foci accumulation after 250 μg/ml Zeocin (n ≥ 65). Details are provided in Table S4.

(C) Scc1-HA ChIP to an HO-induced DSB at 120 min after induction (n = 4) as in (A).

(D) Scheme of the NHEJ repair pathways that yield either *URA*− (imprecise end-joining) or *URA*+ (precise end-joining) phenotypes (Matsuzaki et al., 2012). Graph shows the percentage *URA*− and *URA*+ survivors in various genotypes (n = 3).

Error bars represent SEM except for (B), in which they represent the SD.

a high-speed, high-resolution imaging assay with and without cut induction (Figure 7). In the strains used in Figure 6B, we acquired z stacks on a spinning-disk confocal microscope (8× 0.2 nm z stacks, 10 ms exposure) continuously over 1 min, yielding 750 stacks per movie at a 3D spatial resolution of ~256 nm. The movies were projected stack by stack on to a 2D plane for analysis by the ImageJ (Fiji) plugin Trackmate (Supplemental Experimental Procedures), and we quantified the percentage of frames in which two spots can be resolved. Again we used the TEV-cleavable Scc1 strain to confirm that we can monitor a loss of sister chromatid cohesion at a tagged *ARS607* (Figures S4D and S4E). Spot separation was very low in a normal WT S phase (~2% of frames separated), while after 1 hr TEV induction, separation increased to ~11% (Figure S4E).

Next we induced HO-mediated cleavage at *MATα* (Figure 7A) and monitored sister chromatid dynamics in WT, *rad50Δ*, or *rfa1-t11* cells. After 2 hr of HO induction in WT S phase cells, 8% of the frames showed resolution of the two sisters into two

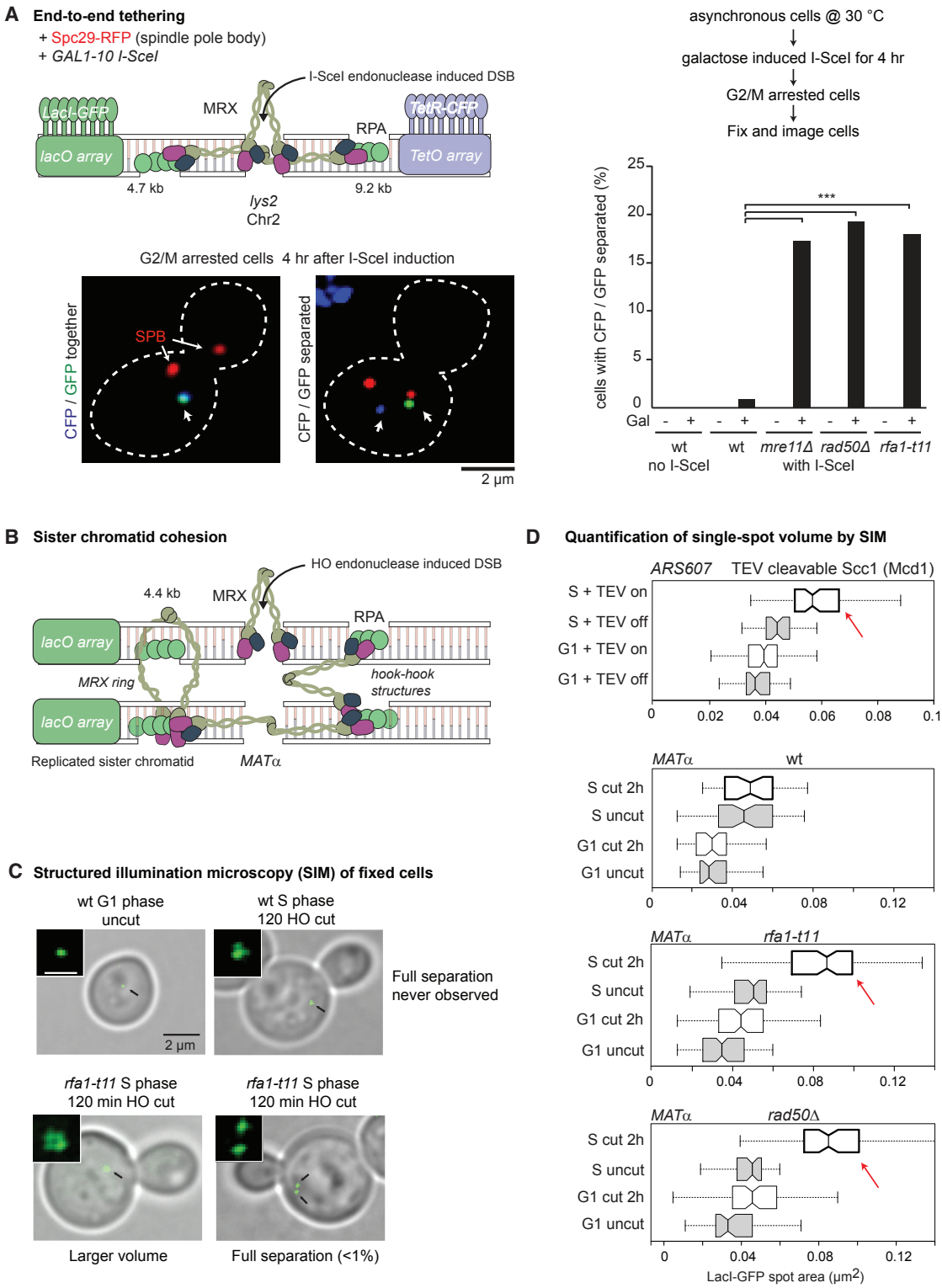

Figure 6. RFA1-Mediated Recruitment of MRX to DSBs Is Necessary for Tethering Ends and Sister Chromatids

(A) Scheme of strain used for tracking both sides of a galactose inducible I-SceI DSB on Chr2. LacO/LacI-GFP tags one side and TetO/TetR-CFP the other (Lobachev et al., 2004). MRX can tether ends through Rad50's hook domain by directly binding to the DSB end or by interaction with RPA. Examples of separation of GFP/CFP signals after I-SceI cut induction. Graph shows the percentage separated GFP/CFP in large budded cells ($n \geq 107$). For details and statistics, see Table S4. Cells scored were late G2/M (large bud and SPBs <0.6 µm apart). For uncleaved controls, mid-S and G2/M cells were scored.

(legend continued on next page)

spots, while in either *rad50Δ* or *rfa1-t11* strains, 16% to 19% of the frames had separated sisters (Figure 7B). We ruled out that this is an artifact of galactose addition by expressing HO in a strain that is resistant to cleavage, *mata*^{inc}. In conclusion, sister chromatid juxtaposition at a DSB is compromised by loss of MRX or its recruitment through RPA.

To see if this reflects compromised bridging through MRX itself or a failure to recruit and load cohesin at the DSB (Figure 5C; Unal et al., 2007), we tested the effects of destabilizing Scc1 (Mcd1) at the base of the cohesin ring (Figure 7A). Specifically, we scored sister *lacO* foci pairing at the induced cut at *MATα* in a temperature sensitive allele of Scc1 called *mcd1-1* (Heidinger-Pauli et al., 2008). Previous studies showed that a 1 hr incubation at the non-permissive temperature (37°C) was sufficient to inactivate cohesin. Our time-lapse imaging showed that without DSB induction, S phase *mcd1-1* cells have separated *lacO* foci in ~25% of frames at 37°C (Figure 7C). Remarkably, after DSB induction following cohesin inactivation (1 hr at 37°C), spot separation was actually reduced to 5%, suggesting that the induction of the break stabilizes sister-sister pairing. Importantly, this effect was lost by combining the *mcd1-1* mutant with *rfa1-t11* (Figure 7C). The simplest interpretation of this is that MRX holds sister chromatids together at a DSB, even in the absence of functional cohesin. We note that this result is in contrast to a previous report in which a DSB was not sufficient to keep sisters together (Unal et al., 2007), although in that case, the experimental setup involved a 2 hr induction of two adjacent DSBs after 4 hr of Nocodazole arrest. Under that condition, cohesin seemed to contribute to sister cohesion.

To rule out kinetic limitations of our time-lapse assay, which scores unfixed cells immediately after cleavage, we tested an experimental setup much like that used by Unal et al. (2007). The cells were grown to log phase, and nocodazole was added at the same time as either glucose (no HO cut) or galactose (induction of HO). After 1 hr, cells were shifted to 37°C to inactivate cohesin, and cells were fixed and imaged. G2/M cells were scored for LacI-GFP spot separation (Figure 7D). Remarkably we found that whereas loss of the cohesin ring (*mcd1-1* at 37°C) allowed sisters to separate at an uncut locus, sister pairing was restored in a manner dependent on Rad50 (MRX) and a functional Rfa1 N-terminal OB fold after cut induction (Figures 7D–7F). This argues that upon DSB induction, the recruitment of MRX by Rfa1 is necessary and sufficient to hold both DSB ends and two broken sister chromatids together, as this can be achieved in the absence of intact cohesin (Figure 7F).

DISCUSSION

Since their discovery and description, a role of SMC-family protein complexes in the tethering of broken DNA ends or in the maintenance of sister chromatid pairing has been debated (Huang and Kolodner, 2005; Nasmyth and Haering, 2005; Uhlmann, 2016). MRX is closely related to cohesin, condensin, and the SMC5/6 complex, and we document here an "SMC-like" function for the MRX complex at DSBs, where it appears to both hold ends together and contribute to the pairing of broken sisters. In this function, MRX recruitment is compromised by a mutation in the N-terminal domain of Rfa1. This helps answer the long-standing question of how MRX is targeted to sites of damage.

rfa1-t11 and MRX Mutations Work Epistatically to Compromise Fork Integrity under Stress

By EMAP analysis against a panel of 1,311 knockout alleles, we found that the sensitivity of *rfa1-t11* to HU parallels that of *mre11Δ* (Figure 1). Although the MRX interaction with RPA is not entirely compromised by the *rfa1-t11* mutation, in all fork-stalling and recovery assays performed *rfa1-t11* acted epistatically with MRX mutations. Consistently, MRX recruitment to HU-stalled forks is compromised by the *rfa1-t11* mutation, yet *rfa1-t11* does not impair activation of the replication checkpoint on HU. Rad53 is efficiently phosphorylated in both the *mre11Δ* and *rfa1-t11* strains on HU (Kanoh et al., 2006). As expected, *rfa1-t11* defects are additive with *mec1-100*, an S phase-specific allele of the ATR kinase, Mec1, which fails to activate Rad53 in response to replication stress (Cobb et al., 2005; Hustedt et al., 2015). At stalled forks, MRX is thought both to process fold-back structures, preventing ligation or over-resection, and to tether replicated sisters together, prior to the loading of cohesin (Tittel-Elmer et al., 2012).

The MRX Complex Has a Structural Role at DSBs

We also document a clear but unanticipated role for Rfa1 in the recruitment and stability of MRX at DSBs (Figures 5, 6, and 7). MRX tethering by RPA at breaks in late S phase contributes both to end-to-end tethering and the juxtaposition of broken sisters (late S/G2). On Zeocin, the *rfa1-t11* mutation compromises Mec1-dependent Rad53 activation (Figure 4), which likely reflects a role for the Rfa1 N-terminal OB fold in the recruitment of Mec1-Ddc2 at DSB (Zou and Elledge, 2003; Dubrana et al., 2007). Again, we have tested the effects of *rfa1-t11* in a range of yeast backgrounds, generating the mutant allele by de novo mutagenesis. In all cases, *rfa1-t11* was epistatic to *mre11Δ*.

A previous study documented a role for MRX in the recruitment of cohesin at breaks (Unal et al., 2007). We confirmed this, but we found that it is MRX, not cohesin, that holds sisters together at breaks at early time points. Our experiments differ from theirs in two significant ways: first, they induced two sets of DSBs near each other, while we induced only one. Second, Unal

(B) Construct used to measure sister chromatid pairing at an HO-induced DSB. Cut efficiencies are scored for each experiment (Table S3). MRX can hold sister chromatids together at DSBs through Rad50 hook-hook interactions or its ring structure.
(C) Examples of bright-field/GFP merged SIM images of WT and *rfa1-t11* fixed cells bearing the construct at time indicated after cleavage induction (B). Insets show enlarged LacI-GFP foci (scale bar represents 0.5 μm). The focus area is quantified by Fiji (Table S4). Fully separated foci were never observed in WT S phase cells and rarely in *rfa1-t11* cells. Foci were nonuniform in *rfa1-t11* and *rad50Δ*.
(D) Boxplots of LacI-GFP spot areas before and after 1 hr TEV induction (upper plot) or 2 hr after HO cut (lower three plots) ($n \geq 35$). Full statistics are provided in Table S4.

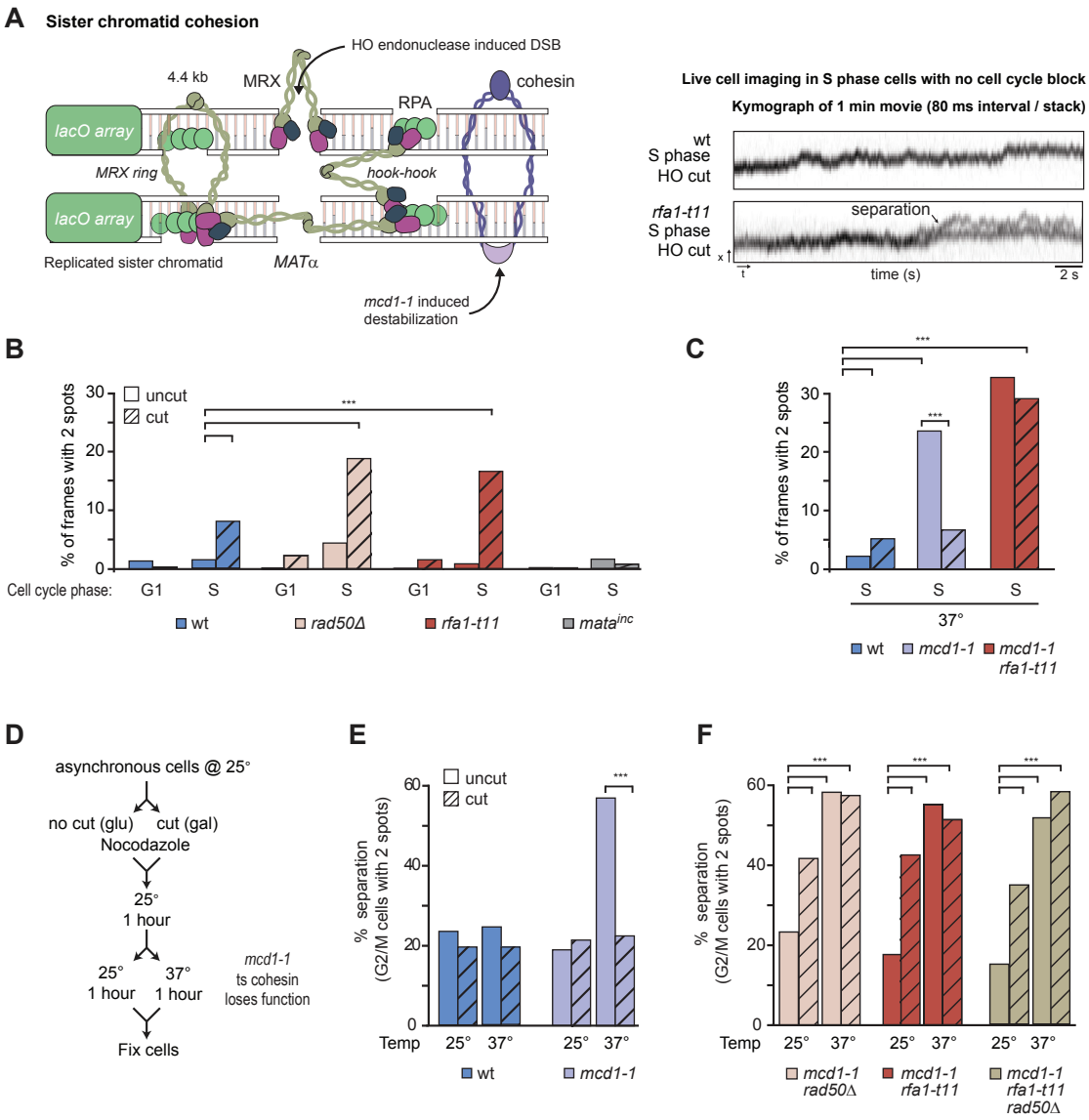

Figure 7. MRX Is Sufficient and Necessary to Hold Sister Chromatids Together at DSBs

(A) Construct used to measure changes in sister chromatid pairing at a HO induced DSB at *MATα*. Cohesin binding is later and more distant from the cut site. Right: an example kymograph of live cell imaging of a LacI-GFP spot projected through the x axis over time in WT versus *rfa1-t11* after 120 min galactose induction of HO. Black arrows indicate separation events. Uncut conditions are on glucose.

(B and C) Quantitation of the number of frames containing two LacI-GFP spots at either 25°C (B) or 37°C (C) ($n \geq 5$). All details and statistics are provided in Table S4, and example movies are available in the Supplemental Information.

(D) Experimental layout for the sister chromatid cohesion assay using the construct in (A). Asynchronous cultures of indicated mutants were grown at 25°C until log phase, 15 μg/ml nocodazole and either glucose (no cut) or galactose (cut) were added. Growth for 1 hr preceded a shift to 37°C and fixation.

(E) Quantitation of the number of G2/M cells with separated sister chromatids (two spots) in the indicated isogenic strains carrying the construct in (A).

(F) Quantitation as in (E) for the indicated mutants ($n \geq 201$) (see Table S4 for statistics). *$p < 0.005$. HO cut efficiencies are provided in Table S3.

et al. (2007) first treated cells with the microtubule-depolymerizing drug nocodazole for 4 hr before inducing the DSB for a further 2 hr. This extended arrest in G2/M may alter the behavior of the break.

It is unclear how MRX contributes to cohesin loading, as the two proteins do not interact (Tittel-Elmer et al., 2012). It may simply be that MRX holds sisters together to allow cohesin loading. In any case, it appears that through its interaction with Rfa1, MRX serves an additional role at DSBs by stabilizing both end-to-end and sister-sister contacts.

A recent study examined the role of the Rad50 zinc hook in DSB repair by monitoring sister chromatid exchange in mitosis. Those investigators found that strains with mutations in the zinc hook domain that partially impair hook dimerization without

blocking complex assembly have milder effects on sister chromatin exchange than full *RAD50* deletions (Hohl et al., 2015). We propose that these hook mutations reduce, but do not ablate, Rad50 dimerization. At a DSB multiple MRX molecules bind and even with a weakened Rad50 hook, their combined effect may be sufficient to hold both ends and sisters together (Figures 6 and 7). Cohesin may provide further structural support later in repair.

Rfa1 Interaction Sites on MRX Are Relevant to Biological Function and Human Disease

The validated interaction sites between Rfa1 and MRX cluster in two major sites. One is located in the DNA-binding cleft of the Rad50 dimer. In the presence of ATP, Rad50 primarily binds dsDNA and duplexes with extended 3′ overhangs (Seifert et al., 2015). Thus, the location of the interacting peptides would be consistent with a side-by-side binding of Rad50 and RPA at ssDNA/dsDNA junctions. The second cluster of interacting peptides maps to a surface on the N-terminal phosphodiesterase domain of Mre11 (peptides 9–12; Table S3), which was recently shown to be mutated in Mre11 hypomorphic alleles that suppress the damage sensitivity of *sae2Δ* (Seifert et al., 2015). This mutation allows easier MRX removal from ssDNA during the later stages of HR (Chen et al., 2015).

In addition, the Mre11 peptide 25 (aa 217–234), which binds Rfa1 in an *rfa1-t11*-sensitive manner in vitro, contains a site that is mutated in patients suffering from ataxia-telangiectasia-like disease (ATLD; Mre11 mutations W210C and W243R) (Fernet et al., 2005; Regal et al., 2013; Schiller et al., 2012). Very close to this interaction site is the *mre11-58* mutation (H213Y), which confers a rad50-S-like phenotype (Usui et al., 1998), affecting Mre11's nuclease activity and/or its interaction to Nbs1/Xrs2 (Schiller et al., 2012). The fact that this domain interacts with Rfa1 in an *rfa1-t11*-sensitive manner suggests that a loss of Rfa1 binding may also contribute to the ATLD phenotypes. We note that some interactions sites may require switching between open and closed conformational states of MRX (Lim et al., 2011; Möckel et al., 2012) and that some of Rfa1-MRX interactions are insensitive to the *rfa1-t11* mutation. In the case of Mre11 peptides 37–39, interaction was enhanced with the mutant Rfa1 domain. Intriguingly, this conserved Mre11 region is deleted in some ATLD patients (Δ340–366) who are predisposed to pulmonary adenocarcinoma (Regal et al., 2013).

High-Speed and Super-Resolution Imaging Allows New Insights into Chromatin Biology

We have been able to analyze sister chromatid pairing with super-resolution microscopy of short fluorescent tags either on the two sisters or both sides of a DSB. Although the resolution achieved here (250 nm and 80 ms 3D stack imaging) is sufficient to document sister separation, the imaging method can be improved to provide even more information about the forces that hold sisters together. Extending these experiments to include other SMC proteins such as condensin or the SMC5/6 complex will surely provide a fuller understanding of long-range chromatin interactions in living cells.

EXPERIMENTAL PROCEDURES

Yeast Growth Conditions, Plasmids, Repair Assays and ChIP

All strains used were derived from W303-1A or JKM179 (see Table S1). EMAP, drop assays, and DNA-combing methods are described in Supplemental Experimental Procedures. Cohesin experiments used nocodazole at 15 μg/ml with the yeast culture adjusted to 1% DMSO before nocodazole addition. Imprecise and precise NHEJ assays were as in Matsuzaki et al. (2012). ChIP experiments were performed as described in Cobb et al. (2003). For ChIP-chip and associated bioinformatics analysis, see Tittel-Elmer et al. (2012).

Protein Purification, Structure Studies, Peptide Arrays, and Microscale Thermophoresis

Details are presented in Supplemental Experimental Procedures. The scanning peptide array covered all of MRX except the coiled-coil domains of Rad50, with 18-aa-long peptides with 9 aa overlap spotted onto a glass slide by JPT Peptide Technologies.

Microscopy and Error Calculation

Details for live and fixed fluorescent imaging and quantitative analysis including spot volume and spot separation in time lapse movies are described in Supplemental Experimental Procedures. Structured illumination imaging used a Zeiss Elyra S.1 microscope with an Andor iXon 885 EMCCD camera.

Error bars on graphs represent the SEM unless otherwise stated. Categorical data such as the one- versus two-spot cohesin assay was tested for significance using a two-tailed Fisher's exact test (GraphPad), computing exact p values using the method of summing small p values. The large spot separation movie data set was tested for significance using a chi-square with Yates correction test (GraphPad) against the relevant strain genotype uncut. Continuous data such as LacI-GFP spot size was shown to be normally distributed and then tested for differences using a two-tailed Student's t test (GraphPad). Significance cutoff was $p < 0.05$. All p values are listed in Table S4.

ACCESSION NUMBERS

The accession numbers for the rfa1-t11 N-OB crystal structure and the Rad50 ChIP-chip data reported in this paper are PDB: 5M1X and GEO: GSE88816, respectively.

SUPPLEMENTAL INFORMATION

Supplemental Information includes Supplemental Experimental Procedures, four figures, four tables, and one movie and can be found with this article online at http://dx.doi.org/10.1016/j.molcel.2016.10.032.

AUTHOR CONTRIBUTIONS

A.S., K.S., and S.M.G. planned experiments, analyzed data, and wrote the manuscript. A.S. and A.M.H. performed most experiments. N.H. carried out the EMAP. J.P. performed Rad50 ChIP-chip. I.D. performed MST, purified Rfa1, and determined rfa1-t11 structure, guided by H.G. M.S. performed the NHEJ assay. J.E. wrote scripts for image analysis. A.S., A.M.H., N.H., and K.S. created strains. K.-P.H. modeled the Rad50-Mre11 structure and peptide position. P.P. and J.P. supervised DNA combing.

ACKNOWLEDGMENTS

We thank J. Bianco and the Pasero lab for assistance, M. Stadler for statistical analysis, L. Gelman and S. Bourke for imaging help, C. Soustelle and A. Nicolas for the *rfa1-t11* plasmid, M. Kawai for technical assistance, J. Cobb for advice, K. Lobachev, K. Bloom, D. Koshland, and M. Resnick for strains, and J. Petrini for the Mre11 antibody. We thank V. Dion, U. Rass, and S.M.G. lab members for proofreading. The S.M.G. laboratory thanks the Swiss National Science Foundation (310030B_156936), Human Frontier Science Program (RGP0016), European Molecular Biology Organization, and Novartis

Research Foundation for support. K.-P.H acknowledges funding by the ERC (advanced grant ATMMACHINE 322869).

Received: August 3, 2016
Revised: September 29, 2016
Accepted: October 21, 2016
Published: November 23, 2016

REFERENCES

Ball, H.L., Ehrhardt, M.R., Mordes, D.A., Glick, G.G., Chazin, W.J., and Cortez, D. (2007). Function of a conserved checkpoint recruitment domain in ATRIP proteins. Mol. Cell. Biol. *27*, 3367–3377.

Binz, S.K., and Wold, M.S. (2008). Regulatory functions of the N-terminal domain of the 70-kDa subunit of replication protein A (RPA). J. Biol. Chem. *283*, 21559–21570.

Bjergbaek, L., Cobb, J.A., Tsai-Pflugfelder, M., and Gasser, S.M. (2005). Mechanistically distinct roles for Sgs1p in checkpoint activation and replication fork maintenance. EMBO J. *24*, 405–417.

Bochkareva, E., Kaustov, L., Ayed, A., Yi, G.S., Lu, Y., Pineda-Lucena, A., Liao, J.C., Okorokov, A.L., Milner, J., Arrowsmith, C.H., and Bochkarev, A. (2005). Single-stranded DNA mimicry in the p53 transactivation domain interaction with replication protein A. Proc. Natl. Acad. Sci. U S A *102*, 15412–15417.

Chen, H., Donnianni, R.A., Handa, N., Deng, S.K., Oh, J., Timashev, L.A., Kowalczykowski, S.C., and Symington, L.S. (2015). Sae2 promotes DNA damage resistance by removing the Mre11-Rad50-Xrs2 complex from DNA and attenuating Rad53 signaling. Proc. Natl. Acad. Sci. U S A *112*, E1880–E1887.

Ciccia, A., and Elledge, S.J. (2010). The DNA damage response: making it safe to play with knives. Mol. Cell *40*, 179–204.

Cobb, J.A., Bjergbaek, L., Shimada, K., Frei, C., and Gasser, S.M. (2003). DNA polymerase stabilization at stalled replication forks requires Mec1 and the RecQ helicase Sgs1. EMBO J. *22*, 4325–4336.

Cobb, J.A., Schleker, T., Rojas, V., Bjergbaek, L., Tercero, J.A., and Gasser, S.M. (2005). Replisome instability, fork collapse, and gross chromosomal rearrangements arise synergistically from Mec1 kinase and RecQ helicase mutations. Genes Dev. *19*, 3055–3069.

de Jager, M., Dronkert, M.L., Modesti, M., Beerens, C.E., Kanaar, R., and van Gent, D.C. (2001a). DNA-binding and strand-annealing activities of human Mre11: implications for its roles in DNA double-strand break repair pathways. Nucleic Acids Res. *29*, 1317–1325.

de Jager, M., van Noort, J., van Gent, D.C., Dekker, C., Kanaar, R., and Wyman, C. (2001b). Human Rad50/Mre11 is a flexible complex that can tether DNA ends. Mol. Cell *8*, 1129–1135.

Dubrana, K., van Attikum, H., Hediger, F., and Gasser, S.M. (2007). The processing of double-strand breaks and binding of single-strand-binding proteins RPA and Rad51 modulate the formation of ATR-kinase foci in yeast. J. Cell Sci. *120*, 4209–4220.

Dutta, A., Ruppert, J.M., Aster, J.C., and Winchester, E. (1993). Inhibition of DNA replication factor RPA by p53. Nature *365*, 79–82.

Fernet, M., Gribaa, M., Salih, M.A., Seidahmed, M.Z., Hall, J., and Koenig, M. (2005). Identification and functional consequences of a novel MRE11 mutation affecting 10 Saudi Arabian patients with the ataxia telangiectasia-like disorder. Hum. Mol. Genet. *14*, 307–318.

Flynn, R.L., and Zou, L. (2010). Oligonucleotide/oligosaccharide-binding fold proteins: a growing family of genome guardians. Crit. Rev. Biochem. Mol. Biol. *45*, 266–275.

Garcia, V., Phelps, S.E., Gray, S., and Neale, M.J. (2011). Bidirectional resection of DNA double-strand breaks by Mre11 and Exo1. Nature *479*, 241–244.

Gobbini, E., Villa, M., Gnugnoli, M., Menin, L., Clerici, M., and Longhese, M.P. (2015). Sae2 function at DNA double-strand breaks is bypassed by dampening Tel1 or Rad53 activity. PLoS Genet. *11*, e1005685.

González-Barrera, S., Cortés-Ledesma, F., Wellinger, R.E., and Aguilera, A. (2003). Equal sister chromatid exchange is a major mechanism of double-strand break repair in yeast. Mol. Cell *11*, 1661–1671.

Harrison, J.C., and Haber, J.E. (2006). Surviving the breakup: the DNA damage checkpoint. Annu. Rev. Genet. *40*, 209–235.

Hartsuiker, E., Vaessen, E., Carr, A.M., and Kohli, J. (2001). Fission yeast Rad50 stimulates sister chromatid recombination and links cohesion with repair. EMBO J. *20*, 6660–6671.

Hegnauer, A.M., Hustedt, N., Shimada, K., Pike, B.L., Vogel, M., Amsler, P., Rubin, S.M., van Leeuwen, F., Guénolé, A., van Attikum, H., et al. (2012). An N-terminal acidic region of Sgs1 interacts with Rpa70 and recruits Rad53 kinase to stalled forks. EMBO J. *31*, 3768–3783.

Heidinger-Pauli, J.M., Unal, E., Guacci, V., and Koshland, D. (2008). The kleisin subunit of cohesin dictates damage-induced cohesion. Mol. Cell *31*, 47–56.

Hirano, T. (2006). At the heart of the chromosome: SMC proteins in action. Nat. Rev. Mol. Cell Biol. *7*, 311–322.

Hohl, M., Kwon, Y., Galván, S.M., Xue, X., Tous, C., Aguilera, A., Sung, P., and Petrini, J.H. (2011). The Rad50 coiled-coil domain is indispensable for Mre11 complex functions. Nat. Struct. Mol. Biol. *18*, 1124–1131.

Hohl, M., Kochańczyk, T., Tous, C., Aguilera, A., Krężel, A., and Petrini, J.H. (2015). Interdependence of the rad50 hook and globular domain functions. Mol. Cell *57*, 479–491.

Hopfner, K.P., Craig, L., Moncalian, G., Zinkel, R.A., Usui, T., Owen, B.A., Karcher, A., Henderson, B., Bodmer, J.L., McMurray, C.T., et al. (2002). The Rad50 zinc-hook is a structure joining Mre11 complexes in DNA recombination and repair. Nature *418*, 562–566.

Huang, M.E., and Kolodner, R.D. (2005). A biological network in Saccharomyces cerevisiae prevents the deleterious effects of endogenous oxidative DNA damage. Mol. Cell *17*, 709–720.

Hustedt, N., Gasser, S.M., and Shimada, K. (2013). Replication checkpoint: tuning and coordination of replication forks in S phase. Genes (Basel) *4*, 388–434.

Hustedt, N., Seeber, A., Sack, R., Tsai-Pflugfelder, M., Bhullar, B., Vlaming, H., van Leeuwen, F., Guénolé, A., van Attikum, H., Srivas, R., et al. (2015). Yeast PP4 interacts with ATR homolog Ddc2-Mec1 and regulates checkpoint signaling. Mol. Cell *57*, 273–289.

Iwasaki, D., Hayashihara, K., Shima, H., Higashide, M., Terasawa, M., Gasser, S.M., and Shinohara, M. (2016). The MRX complex ensures NHEJ fidelity through multiple pathways including Xrs2-FHA-dependent Tel1 activation. PLoS Genet. *12*, e1005942.

Kanoh, Y., Tamai, K., and Shirahige, K. (2006). Different requirements for the association of ATR-ATRIP and 9-1-1 to the stalled replication forks. Gene *377*, 88–95.

Kantake, N., Sugiyama, T., Kolodner, R.D., and Kowalczykowski, S.C. (2003). The recombination-deficient mutant RPA (rfa1-t11) is displaced slowly from single-stranded DNA by Rad51 protein. J. Biol. Chem. *278*, 23410–23417.

Kaye, J.A., Melo, J.A., Cheung, S.K., Vaze, M.B., Haber, J.E., and Toczyski, D.P. (2004). DNA breaks promote genomic instability by impeding proper chromosome segregation. Curr. Biol. *14*, 2096–2106.

Lafrance-Vanasse, J., Williams, G.J., and Tainer, J.A. (2015). Envisioning the dynamics and flexibility of Mre11-Rad50-Nbs1 complex to decipher its roles in DNA replication and repair. Prog. Biophys. Mol. Biol. *117*, 182–193.

Lengsfeld, B.M., Rattray, A.J., Bhaskara, V., Ghirlando, R., and Paull, T.T. (2007). Sae2 is an endonuclease that processes hairpin DNA cooperatively with the Mre11/Rad50/Xrs2 complex. Mol. Cell *28*, 638–651.

Lim, H.S., Kim, J.S., Park, Y.B., Gwon, G.H., and Cho, Y. (2011). Crystal structure of the Mre11-Rad50-ATPγS complex: understanding the interplay between Mre11 and Rad50. Genes Dev. *25*, 1091–1104.

Lisby, M., Barlow, J.H., Burgess, R.C., and Rothstein, R. (2004). Choreography of the DNA damage response: spatiotemporal relationships among checkpoint and repair proteins. Cell *118*, 699–713.

Lobachev, K., Vitriol, E., Stemple, J., Resnick, M.A., and Bloom, K. (2004). Chromosome fragmentation after induction of a double-strand break is an active process prevented by the RMX repair complex. Curr. Biol. *14*, 2107–2112.

Ma, J.L., Kim, E.M., Haber, J.E., and Lee, S.E. (2003). Yeast Mre11 and Rad1 proteins define a Ku-independent mechanism to repair double-strand breaks lacking overlapping end sequences. Mol. Cell. Biol. *23*, 8820–8828.

Majka, J., Binz, S.K., Wold, M.S., and Burgers, P.M. (2006). Replication protein A directs loading of the DNA damage checkpoint clamp to 5′-DNA junctions. J. Biol. Chem. *281*, 27855–27861.

Matsuzaki, K., Terasawa, M., Iwasaki, D., Higashide, M., and Shinohara, M. (2012). Cyclin-dependent kinase-dependent phosphorylation of Lif1 and Sae2 controls imprecise nonhomologous end joining accompanied by double-strand break resection. Genes Cells *17*, 473–493.

Mimitou, E.P., and Symington, L.S. (2008). Sae2, Exo1 and Sgs1 collaborate in DNA double-strand break processing. Nature *455*, 770–774.

Möckel, C., Lammens, K., Schele, A., and Hopfner, K.P. (2012). ATP driven structural changes of the bacterial Mre11:Rad50 catalytic head complex. Nucleic Acids Res. *40*, 914–927.

Moreno-Herrero, F., de Jager, M., Dekker, N.H., Kanaar, R., Wyman, C., and Dekker, C. (2005). Mesoscale conformational changes in the DNA-repair complex Rad50/Mre11/Nbs1 upon binding DNA. Nature *437*, 440–443.

Morrison, A.J., Kim, J.A., Person, M.D., Highland, J., Xiao, J., Wehr, T.S., Hensley, S., Bao, Y., Shen, J., Collins, S.R., et al. (2007). Mec1/Tel1 phosphorylation of the INO80 chromatin remodeling complex influences DNA damage checkpoint responses. Cell *130*, 499–511.

Nakada, D., Matsumoto, K., and Sugimoto, K. (2003a). ATM-related Tel1 associates with double-strand breaks through an Xrs2-dependent mechanism. Genes Dev. *17*, 1957–1962.

Nakada, D., Shimomura, T., Matsumoto, K., and Sugimoto, K. (2003b). The ATM-related Tel1 protein of Saccharomyces cerevisiae controls a checkpoint response following phleomycin treatment. Nucleic Acids Res. *31*, 1715–1724.

Nasmyth, K., and Haering, C.H. (2005). The structure and function of SMC and kleisin complexes. Annu. Rev. Biochem. *74*, 595–648.

Paciotti, V., Clerici, M., Lucchini, G., and Longhese, M.P. (2000). The checkpoint protein Ddc2, functionally related to S. pombe Rad26, interacts with Mec1 and is regulated by Mec1-dependent phosphorylation in budding yeast. Genes Dev. *14*, 2046–2059.

Paciotti, V., Clerici, M., Scotti, M., Lucchini, G., and Longhese, M.P. (2001). Characterization of mec1 kinase-deficient mutants and of new hypomorphic mec1 alleles impairing subsets of the DNA damage response pathway. Mol. Cell. Biol. *21*, 3913–3925.

Petermann, E., and Helleday, T. (2010). Pathways of mammalian replication fork restart. Nat. Rev. Mol. Cell Biol. *11*, 683–687.

Regal, J.A., Festerling, T.A., Buis, J.M., and Ferguson, D.O. (2013). Disease-associated MRE11 mutants impact ATM/ATR DNA damage signaling by distinct mechanisms. Hum. Mol. Genet. *22*, 5146–5159.

Rouse, J., and Jackson, S.P. (2002). Lcd1p recruits Mec1p to DNA lesions in vitro and in vivo. Mol. Cell *9*, 857–869.

San Filippo, J., Sung, P., and Klein, H. (2008). Mechanism of eukaryotic homologous recombination. Annu. Rev. Biochem. *77*, 229–257.

Schiller, C.B., Lammens, K., Guerini, I., Coordes, B., Feldmann, H., Schlauderer, F., Möckel, C., Schele, A., Strässer, K., Jackson, S.P., and Hopfner, K.P. (2012). Structure of Mre11-Nbs1 complex yields insights into ataxia-telangiectasia-like disease mutations and DNA damage signaling. Nat. Struct. Mol. Biol. *19*, 693–700.

Seifert, F.U., Lammens, K., and Hopfner, K.P. (2015). Structure of the catalytic domain of Mre11 from *Chaetomium thermophilum*. Acta Crystallogr. F Struct. Biol. Commun. *71*, 752–757.

Shima, H., Suzuki, M., and Shinohara, M. (2005). Isolation and characterization of novel xrs2 mutations in Saccharomyces cerevisiae. Genetics *170*, 71–85.

Stracker, T.H., and Petrini, J.H. (2011). The MRE11 complex: starting from the ends. Nat. Rev. Mol. Cell Biol. *12*, 90–103.

Ström, L., and Sjögren, C. (2007). Chromosome segregation and double-strand break repair - a complex connection. Curr. Opin. Cell Biol. *19*, 344–349.

Ström, L., Karlsson, C., Lindroos, H.B., Wedahl, S., Katou, Y., Shirahige, K., and Sjögren, C. (2007). Postreplicative formation of cohesion is required for repair and induced by a single DNA break. Science *317*, 242–245.

Tittel-Elmer, M., Alabert, C., Pasero, P., and Cobb, J.A. (2009). The MRX complex stabilizes the replisome independently of the S phase checkpoint during replication stress. EMBO J. *28*, 1142–1156.

Tittel-Elmer, M., Lengronne, A., Davidson, M.B., Bacal, J., François, P., Hohl, M., Petrini, J.H., Pasero, P., and Cobb, J.A. (2012). Cohesin association to replication sites depends on rad50 and promotes fork restart. Mol. Cell *48*, 98–108.

Toledo, L.I., Altmeyer, M., Rask, M.B., Lukas, C., Larsen, D.H., Povlsen, L.K., Bekker-Jensen, S., Mailand, N., Bartek, J., and Lukas, J. (2013). ATR prohibits replication catastrophe by preventing global exhaustion of RPA. Cell *155*, 1088–1103.

Uhlmann, F. (2016). SMC complexes: from DNA to chromosomes. Nat. Rev. Mol. Cell Biol. *17*, 399–412.

Uhlmann, F., Lottspeich, F., and Nasmyth, K. (1999). Sister-chromatid separation at anaphase onset is promoted by cleavage of the cohesin subunit Scc1. Nature *400*, 37–42.

Umezu, K., Sugawara, N., Chen, C., Haber, J.E., and Kolodner, R.D. (1998). Genetic analysis of yeast RPA1 reveals its multiple functions in DNA metabolism. Genetics *148*, 989–1005.

Unal, E., Arbel-Eden, A., Sattler, U., Shroff, R., Lichten, M., Haber, J.E., and Koshland, D. (2004). DNA damage response pathway uses histone modification to assemble a double-strand break-specific cohesin domain. Mol. Cell *16*, 991–1002.

Unal, E., Heidinger-Pauli, J.M., and Koshland, D. (2007). DNA double-strand breaks trigger genome-wide sister-chromatid cohesion through Eco1 (Ctf7). Science *317*, 245–248.

Usui, T., Ohta, T., Oshiumi, H., Tomizawa, J., Ogawa, H., and Ogawa, T. (1998). Complex formation and functional versatility of Mre11 of budding yeast in recombination. Cell *95*, 705–716.

van Attikum, H., Fritsch, O., and Gasser, S.M. (2007). Distinct roles for SWR1 and INO80 chromatin remodeling complexes at chromosomal double-strand breaks. EMBO J. *26*, 4113–4125.

Wang, X., and Haber, J.E. (2004). Role of *Saccharomyces* single-stranded DNA-binding protein RPA in the strand invasion step of double-strand break repair. PLoS Biol. *2*, E21.

Wang, X., Ira, G., Tercero, J.A., Holmes, A.M., Diffley, J.F., and Haber, J.E. (2004). Role of DNA replication proteins in DSB-induced recombination in *S. cerevisiae*. Mol. Cell. Biol. *24*, 6891–6899.

Williams, R.S., Dodson, G.E., Limbo, O., Yamada, Y., Williams, J.S., Guenther, G., Classen, S., Glover, J.N., Iwasaki, H., Russell, P., and Tainer, J.A. (2009). Nbs1 flexibly tethers Ctp1 and Mre11-Rad50 to coordinate DNA double-strand break processing and repair. Cell *139*, 87–99.

Wiltzius, J.J., Hohl, M., Fleming, J.C., and Petrini, J.H. (2005). The Rad50 hook domain is a critical determinant of Mre11 complex functions. Nat. Struct. Mol. Biol. *12*, 403–407.

Xu, X., Vaithiyalingam, S., Glick, G.G., Mordes, D.A., Chazin, W.J., and Cortez, D. (2008). The basic cleft of RPA70N binds multiple checkpoint proteins, including RAD9, to regulate ATR signaling. Mol. Cell. Biol. *28*, 7345–7353.

Zou, L., and Elledge, S.J. (2003). Sensing DNA damage through ATRIP recognition of RPA-ssDNA complexes. Science *300*, 1542–1548.

Zou, Y., Liu, Y., Wu, X., and Shell, S.M. (2006). Functions of human replication protein A (RPA): from DNA replication to DNA damage and stress responses. J. Cell. Physiol. *208*, 267–273.

Molecular Cell, Volume *64*

Supplemental Information

RPA Mediates Recruitment of MRX to Forks and Double-Strand Breaks to Hold Sister Chromatids Together

Andrew Seeber, Anna Maria Hegnauer, Nicole Hustedt, Ishan Deshpande, Jérôme Poli, Jan Eglinger, Philippe Pasero, Heinz Gut, Miki Shinohara, Karl-Peter Hopfner, Kenji Shimada, and Susan M. Gasser

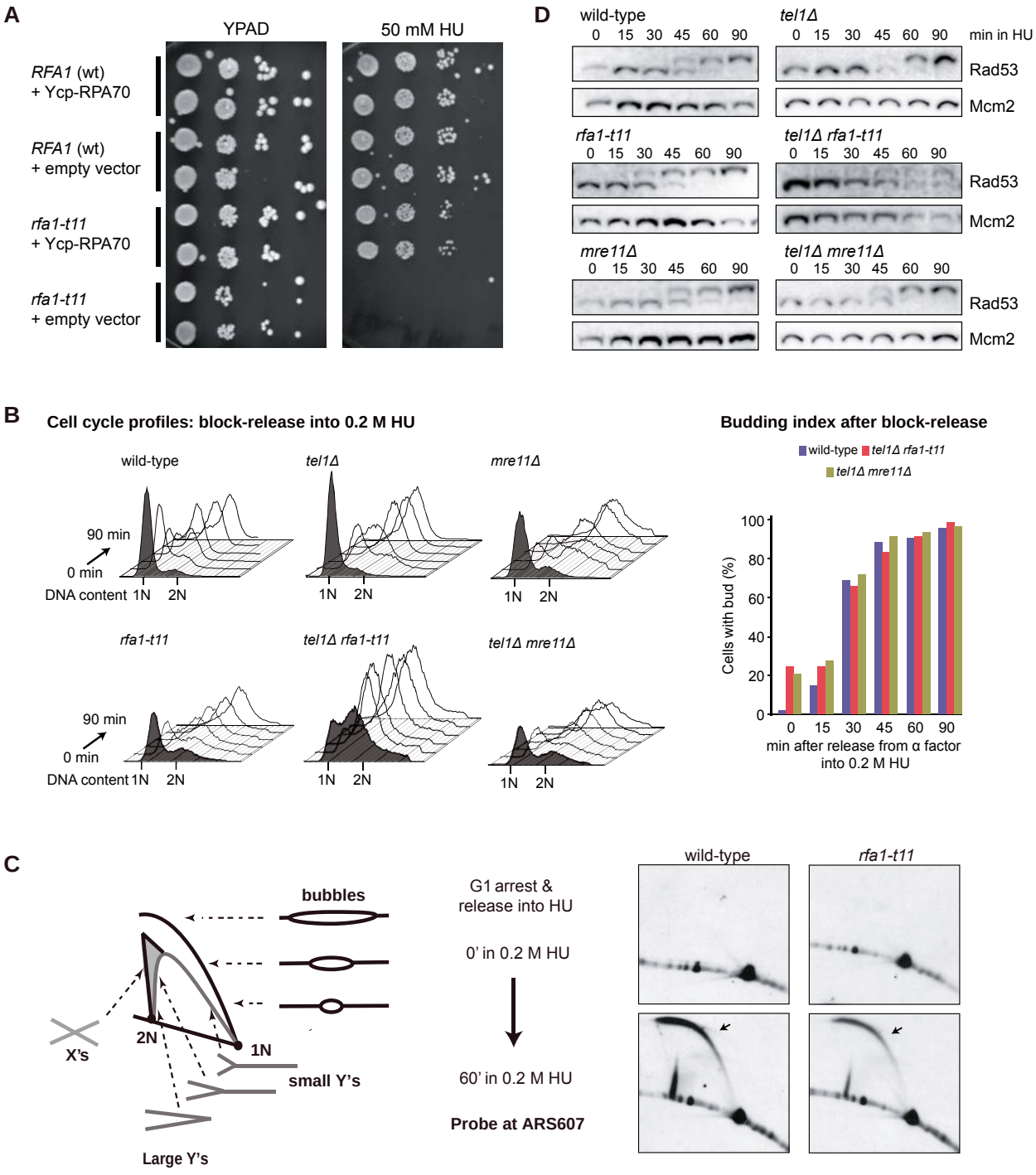
A
YPAD
50 mM HU
RFA1 (wt) + Ycp-RPA70
RFA1 (wt) + empty vector
rfa1-t11 + Ycp-RPA70
rfa1-t11 + empty vector
D
wild-type
tel1Δ
0 15 30 45 60 90
min in HU
Rad53
Mcm2
rfa1-t11
tel1Δ rfa1-t11
mre11Δ
tel1Δ mre11Δ
B
Cell cycle profiles: block-release into 0.2 M HU
wild-type
tel1Δ
mre11Δ
90 min
0 min
DNA content 1N 2N
rfa1-t11
tel1Δ rfa1-t11
tel1Δ mre11Δ
Budding index after block-release
wild-type tel1Δ rfa1-t11
tel1Δ mre11Δ
Cells with bud (%)
0 20 40 60 80 100
0 15 30 45 60 90
min after release from α factor into 0.2 M HU
C
bubbles
X's
2N
1N
small Y's
Large Y's
G1 arrest & release into HU
0' in 0.2 M HU
60' in 0.2 M HU
Probe at ARS607
wild-type
rfa1-t11

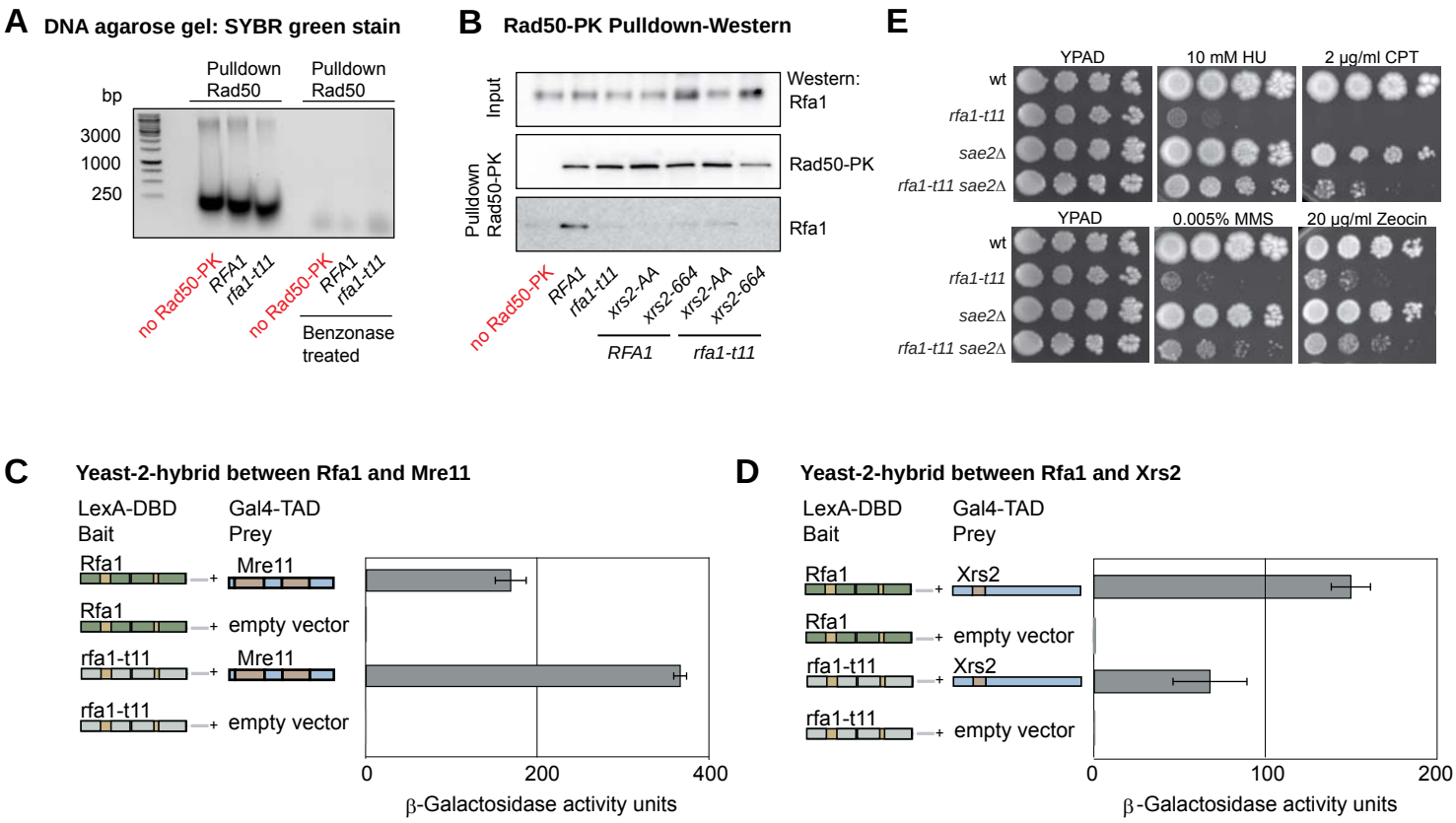
A
DNA agarose gel: SYBR green stain
bp
3000
1000
250
Pulldown Rad50
Pulldown Rad50
no Rad50-PK
RFA1
rfa1-t11
no Rad50-PK
RFA1
rfa1-t11
Benzonase treated
B
Rad50-PK Pulldown-Western
Input
Pulldown Rad50-PK
Western: Rfa1
Rad50-PK
Rfa1
no Rad50-PK
RFA1
rfa1-t11
xrs2-AA
xrs2-664
xrs2-AA
xrs2-664
RFA1
rfa1-t11
E
YPAD
10 mM HU
2 µg/ml CPT
wt
rfa1-t11
sae2Δ
rfa1-t11 sae2Δ
YPAD
0.005% MMS
20 µg/ml Zeocin
wt
rfa1-t11
sae2Δ
rfa1-t11 sae2Δ
C
Yeast-2-hybrid between Rfa1 and Mre11
LexA-DBD Bait
Gal4-TAD Prey
Rfa1
Mre11
Rfa1
empty vector
rfa1-t11
Mre11
rfa1-t11
empty vector
0
200
400
β-Galactosidase activity units
D
Yeast-2-hybrid between Rfa1 and Xrs2
LexA-DBD Bait
Gal4-TAD Prey
Rfa1
Xrs2
Rfa1
empty vector
rfa1-t11
Xrs2
rfa1-t11
empty vector
0
100
200
β-Galactosidase activity units

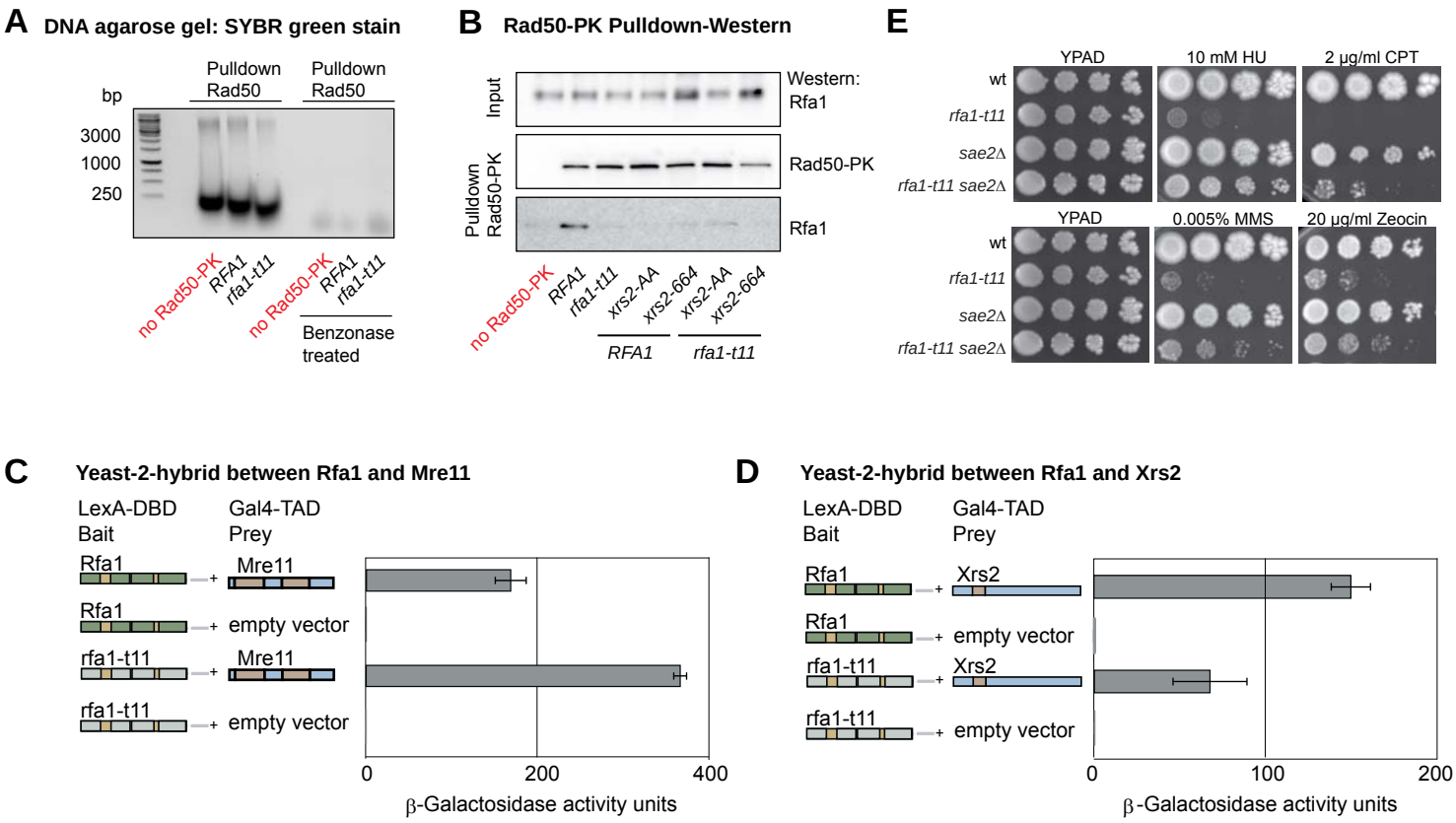
A
DNA agarose gel: SYBR green stain
bp
3000
1000
250
Pulldown Rad50
Pulldown Rad50
no Rad50-PK
RFA1
rfa1-t11
no Rad50-PK
RFA1
rfa1-t11
Benzonase treated
B
Rad50-PK Pulldown-Western
Input
Pulldown Rad50-PK
Western: Rfa1
Rad50-PK
Rfa1
no Rad50-PK
RFA1
rfa1-t11
xrs2-AA
xrs2-664
xrs2-AA
xrs2-664
RFA1
rfa1-t11
E
YPAD
10 mM HU
2 µg/ml CPT
wt
rfa1-t11
sae2Δ
rfa1-t11 sae2Δ
YPAD
0.005% MMS
20 µg/ml Zeocin
wt
rfa1-t11
sae2Δ
rfa1-t11 sae2Δ
C
Yeast-2-hybrid between Rfa1 and Mre11
LexA-DBD Bait
Gal4-TAD Prey
Rfa1
Mre11
Rfa1
empty vector
rfa1-t11
Mre11
rfa1-t11
empty vector
0
200
400
β-Galactosidase activity units
D
Yeast-2-hybrid between Rfa1 and Xrs2
LexA-DBD Bait
Gal4-TAD Prey
Rfa1
Xrs2
Rfa1
empty vector
rfa1-t11
Xrs2
rfa1-t11
empty vector
0
100
200
β-Galactosidase activity units

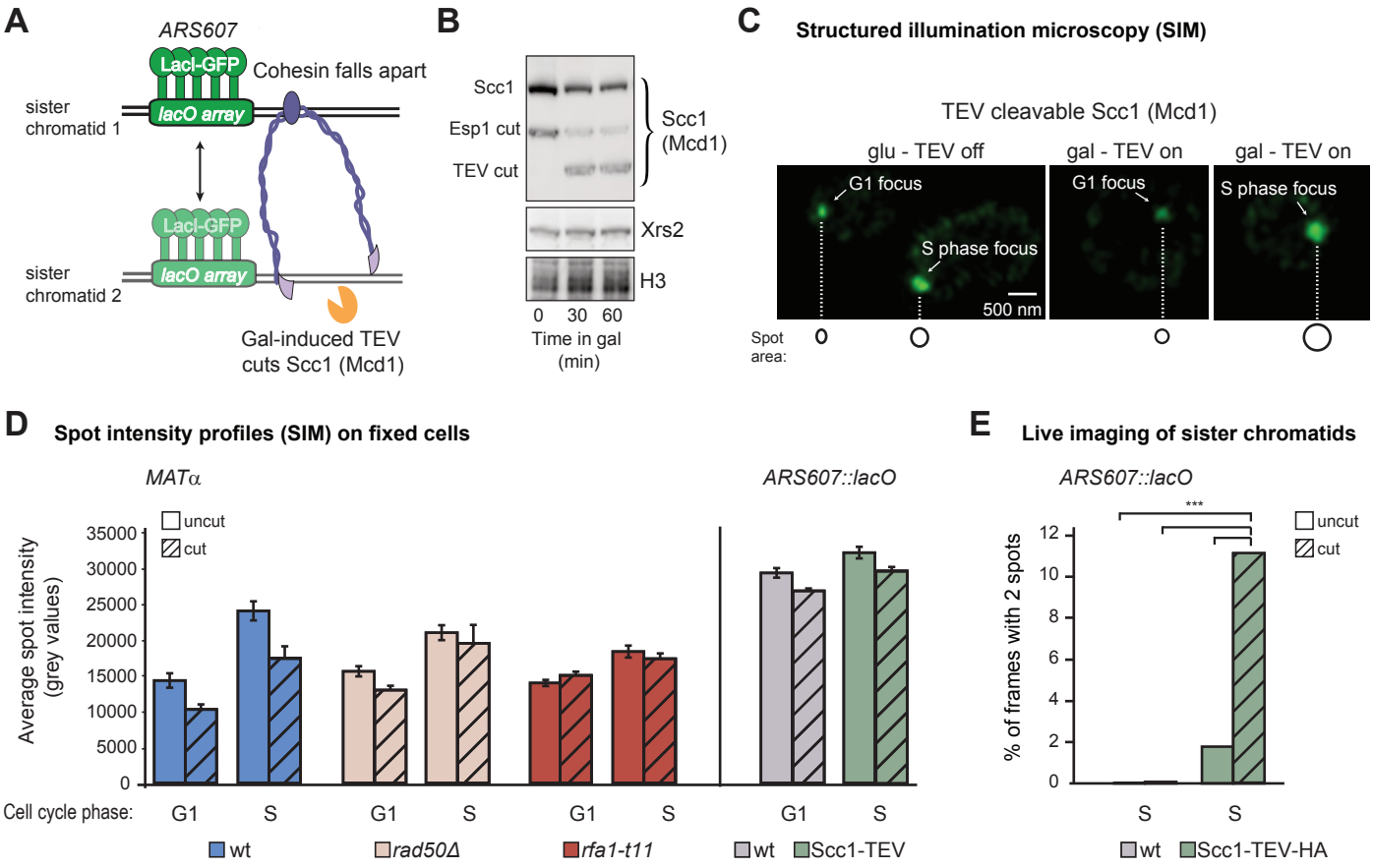
A
ARS607
LacI-GFP
Cohesin falls apart
sister chromatid 1
lacO array
LacI-GFP
sister chromatid 2
lacO array
Gal-induced TEV cuts Scc1 (Mcd1)
B
Scc1
Esp1 cut
TEV cut
Scc1 (Mcd1)
Xrs2
H3
0 30 60
Time in gal (min)
C
Structured illumination microscopy (SIM)
TEV cleavable Scc1 (Mcd1)
glu - TEV off
gal - TEV on
gal - TEV on
G1 focus
S phase focus
G1 focus
S phase focus
500 nm
Spot area:
D
Spot intensity profiles (SIM) on fixed cells
MATα
ARS607::lacO
Average spot intensity (grey values)
uncut
cut
35000
30000
25000
20000
15000
10000
5000
0
Cell cycle phase:
G1 S G1 S G1 S G1 S
wt
rad50Δ
rfa1-t11
wt
Scc1-TEV
E
Live imaging of sister chromatids
ARS607::lacO
% of frames with 2 spots
***
uncut
cut
12
10
8
6
4
2
0
S S
wt
Scc1-TEV-HA

Seeber et al., Supplemental Material

Supplemental Figures S1-S4

Supplemental Figure legends S1-S4

Supplemental Movie legend S1

Supplemental Tables and legends S1-S4, Tables S1, S2 and S4 are uploaded as separate files

Supplemental Experimental procedures

Supplemental References

Supplemental figure legends

Figure S1. The recessive mutation *rfa1-t11* progresses normally through unperturbed S phase, and supports both origin firing and checkpoint activation on HU, related to figure 1

(A) 10x dilution series on YPAD ± 50 mM HU for wild-type (wt) and *rfa1-t11* strains containing a plasmid expressing either a wild-type *RFA1*, *rfa1-t11* or empty vector, showing that *rfa1-t11* is a recessive mutation. (B) Cell cycle profiles of propidium iodide (PI) stained nuclei after release from α-factor into 0.2 M HU. Right panel is budding index of wild-type, *tel1Δ rfa1-t11* and *tel1Δ mre11Δ* cells showing similar release profiles, to confirm proper progression into S phase. (C) Illustration highlighting key features of a 2D gel. 2D gel images showing replication fork firing at ARS607 (see Supplemental experimental procedures) in wt and *rfa1-t11* in the presence of 0.2 M HU. Black arrows highlight replication bubble arcs. (D) Western blot showing Rad53 activation (phosphorylation upshift detected by antibody) after release from α-factor into 0.2 M HU in the indicated isogenic strains. Mcm2 is used as a loading control.

Figure S2. Quantitative genetic interaction mapping of 1311 query strains reveals an epistatic relationship between *rfa1-t11* and MRX mutants, related to figure 1

(A) EMAP results showing the growth of double mutants on 0, 20, 100 mM HU. Yellow indicates an epistatic/suppressive interaction. Blue indicates a synergistic/additive interaction. Grey squares represent no growth due to cell death. (B) Heat maps of Pearson correlation coefficients showing patterns of synergism between 1311 nuclear proteins in untreated and 100 mM HU conditions. Red indicates a correlation while green indicates an anti-correlation. Black ring highlights the strong

correlation between *rfa1-t11* and *mre11Δ.* The 0 mM HU heat map is a duplication from Figure 1D to allow comparison with the 100 mM HU heat map.

Figure S3. MRX complex physical interactions with *rfa1-t11* and genetic interaction with *sae2Δ,* related to figure 3

(A) DNA agarose gel stained with SYBR green showing the effect of treatment of yeast extracts with 1250 units of Benzonase. These samples were used for immunoprecipitations in Fig. 3A. All subsequent yeast extracts treated with Benzonase prior to IP for 30 min on ice. (B) Rad50-PK pulldown in wt, *rfa1-t11* and the indicated *xrs2* mutants: xrs2-AA consists of two point mutations that disrupt Mre11 binding and xrs2-664 is a truncation of its entire C-terminus but maintains partial Mre11 binding. (C,D) Yeast-2-hybrid between Rfa1 or rfa1-t11 and Mre11 or Xrs2. Error bars represent the SEM, *n=3.* (E) 10x dilution series on YPAD ± indicated amounts of HU, CPT, MMS and Zeocin in combinations of wild-type, *sae2Δ* and *rfa1-t11* strains.

Figure S4. TEV cleavage of Scc1 (Mcd1) results in expansion of a genetically tagged locus and uncoordinated sister chromatid dynamics, related to figure 4

(A) Construct illustrating galactose-inducible TEV protease which cuts Scc1, allowing sister chromatids to separate. (B) Time course Western blot after galactose induction of a strain bearing TEV protease, showing full length (FL) Scc1, the resulting fragment after cleavage by Esp1 (Separase) or the form cut by TEV protease. Histone H3 is used as a loading control. Xrs2 levels do not change upon TEV induction. (C) Example images of foci at *ARS607* before and after galactose-induced cleavage. Black circles highlight spot area in S phase cells and upon galactose-induction for 60 mins (TEV on). (D) Spot intensity profiles of SIM foci from experiments in Figure 6, $n \geq 35$. Full details and statistics are available in Table S4. (E) Quantitation of the percentage of frames containing 2 spots in movies ± TEV induction and a control strain that does not contain the galactose inducible TEV, $n \geq 10$. Full details and statistics are available in Table S4. Asterisks indicate a p value < 0.005.

Supplemental movie legend

Movie S1. Example movies of sister chromatid separation at induced DSBs, related to figure 7

Example movies of LacI-GFP spots located at the LacO array adjacent to the *MAT* locus. Movies are acquired and processed as described in Fig 7. Top row, left to right: wt S phase 37 °C uncut, wt S phase 37 °C cut 2h, *mcd1-1* S phase 37 °C uncut, *mcd1-1* S phase 37 °C cut 2h. Middle row: *rfa1-t11* S phase 37

°C uncut, *rfa1-t11* S phase 37 °C cut 2h, *rfa1-t11 mcd1-1* S phase 37 °C uncut, *rfa1-t11 mcd1-1* S phase 37 °C cut 2h. Bottom row: *rad50Δ* S phase 25 °C uncut, *rad50Δ* S phase 25 °C cut 2h. Scale bar = 2 μm.

Supplemental tables and table legends

Table S1 – Yeast strains and plasmids, related to figures 1-7 (included as an additional excel file)

Table S2 - Summary of peptide binding data (included as an additional excel file), related to figure 3

Table S3 - Cut efficiencies of strains used in experiments, related to figures 4,5,6,7

Table S4 – Summary of statistics of microscopy experiments (included as an additional excel file), related to figures 5, 6, 7

Table S3 - Cut efficiencies of strains used in experiments, related to figures 4,5,6,7

Strain	Relevant genotype	Temperature °C	Min after addition of galactose (HO induction)	% of intact MAT
GA6405	wild-type	30	0	100
			30	35 ± 14.36
			60	18 ± 3.08
			90	17 ± 3.9
GA6406	*rfa1-t11*	30	0	100
			30	32 ± 14.28
			60	22 ± 1.45
			90	16 ± 9.13
GA8858	wild-type	25	0	100
			120	23 ± 2.56
GA8256	*rad50Δ*	25	0	100
			120	21 ± 9.45
GA8569	*rfa1-t11*	25	0	100
			120	2 ± 1.44
GA8067	wild-type (untagged)	30	0	100
			120	21 ± 0.74
GA9194	*Scc1-3HA*	30	0	100
			120	18 ± 1.65
GA9241	*Scc1-3HA rad50Δ*	30	0	100
			120	10 ± 1.68
GA9246	*Scc1-3HA rfa1-t11*	30	0	100
			120	9 ± 0.62
GA8067	wild-type	25	0	100
			120	24 ± 2.1
GA9229	*mcd1-1*	25	0	100
			120	16 ± 0.89
GA9288	*mcd1-1 rfa1-t11*	25	0	100
			120	19 ± 1.25
GA9291	*mcd1-1 rad50Δ*	25	0	100
			120	1 ± 0.02
GA9247	*mcd1-1 rfa1-t11 rad50Δ*	25	0	100
			120	22 ± 2.3
GA8067	wild-type	37	0	100
			120	23 ± 1.3
GA9229	*mcd1-1*	37	0	100
			120	10 ± 0.56
GA9288	*mcd1-1 rfa1-t11*	37	0	100
			120	9 ± 1.82
GA9291	*mcd1-1 rad50Δ*	37	0	100
			120	24 ± 2.35
GA9247	*mcd1-1 rfa1-t11 rad50Δ*	37	0	100
			120	27 ± 2

Supplemental experimental procedures

Yeast strains and EMAP assay

The *rfa1-t11* allele was generated by transforming *NheI*-linearized plasmid *pKU2-rfa1-t11* into W303-1A (Soustelle et al., 2002). Cells were selected for the plasmid-borne *URA3* marker and plated on 5-fluoroorotic acid (5-FOA). The mutant was confirmed by sequencing and sensitivity to MMS and HU. Yeast strains were at grown at 30°C in YPAD media, unless stated differently. For experiments involving galactose driven induction of genes, yeast was grown in sterile filtered YPLGg media consisting of 1% yeast extract, 2% bactopeptone, 2% lactic acid, 3% glycerol and 0.05% glucose. Samples were always harvested in log phase cultures. EMAP was performed as in Hustedt *et al.,* 2015.

Drop tests and recovery assays

For drop assays, overnight cultures were diluted to a starting density of OD600 = 0.5 and serial 1:10 dilutions were plated on YPAD or the appropriate selective medium containing the indicated concentrations of MMS, HU or Zeocin. For liquid recovery or survival assays, overnight cultures were diluted to OD600 = 0.15 and grown for 3 h. Cultures were synchronized with α factor and were released into YPAD containing 0.2 M HU. After the indicated time points, relevant dilutions were plated onto YPAD and colonies were counted after 3 to 4 days. Recovery in (%) is the fraction of colonies at the indicated doses compared to the untreated control (0h) normalized to the survival of WT cells for each time point. Cut efficiency of the HO endonuclease at *MAT* was determined as in Horigome *et al.,* 2014, and reflects cleavage of both sisters, which have identical sequence. Primer sequences are available.

2D gels

Neutral/neutral 2D agarose gels were performed as described (Huberman et al., 1987; Wu and Gilbert, 1995). Genomic DNA was isolated from cells at a density of $5x10^6$–$1x10^7$ from GA-4973 and GA-5048using a G-20 column (QIAGEN) followed by digestion with *Pst*I. Genomic DNA was separated on a 0.4% agarose gel in TBE for 40 h at 0.6 V/cm in the first dimension and on a 1.2% agarose gel in TBE at 3 V/cm for 18 h. Replication intermediates at ARS607 were detected after Southern blotting and hybridization with a DIG-labeled probe. The relative ratio of fork firing is expressed as signal of bubble arc to the amount of 1N linear fragments, normalized to wild-type.

DNA combing

Dynamic molecular combing was performed as described previously (Michalet et al., 1997; Tourriere et al., 2005). Wild-type (GA-5382), *rfa1-t11* (GA-5383), *mec1-100* (GA-5385), and *rfa1-t11 mec1-100* (GA-5386) were arrested in G1. 20 min before release into S phase 0.4 mg/ml IdU was added. Cells were incubated for 90 min in YPAD containing 0.2 M HU and 0.4 mg/ml IdU, then washed and released into fresh YPAD in presence of 0.4mg/ml CldU for additional 90 min. IdU and CldU were detected with anti-BrdU antibodies (BD44-Becton Dickinson and BU1/75-AbCys, respectively). Due to cross-reaction of the IdU- and CldU-specific antibodies, both channels are shown together as "replicated fiber fraction" (green/white channels Fig. 2D). DNA molecules were counter-stained with an anti-DNA antibody (MAB3034, Chemicon) and an anti-mouse IgG coupled to Alexa 647 (Molecular Probes). A Leica DM6000B microscope was used to record the images, which were processed as described (Pasero et al., 2002). DNA fibers from 4 independent experiments were analyzed using MetaMorph. R was used for statistical analysis. Each experiment was checked for batch effects, before all DNA fibers per strain were pooled and analyzed by a paired Wilcox test. DNA fibers analyzed from *rfa1-t11*, *mec1-100* and *rfa1-t11 mec1-100* cells were significantly different from wild-type cells ($P<0.05$).

Co-immunoprecipitation (Pulldown) and Chromatin immunoprecipitation (ChIP)

ChIP was performed as described in Cobb et al., 2003. G1-synchronized cells were released into 0.2 M HU-containing media at 30 °C for approximately 1 h and fixed with 1% formaldehyde at the indicated time points. Monoclonal anti-HA was used to precipitate HA-tagged DNA pol α (Cdc17-3HA). Cell extracts were incubated with BSA-saturated Dynabeads coupled to anti-HA antibody for 2 h at 4 °C. As a background control we used BSA-coupled Dynabeads without antibody. Real-time PCR was used for amplification of the precipitated DNA regions. Sequences for the primers/probes that amplify regions in the *S. cerevisiae* genome correspond to ARS607, a site 14 kb away from ARS607 and ARS501 as described in (Cobb et al., 2003). For quantification, Applied Biosystems 7500 Fast Real-time PCR System and software was used. The data for each strain are the average of 3 independent experiments with real-time PCR performed in duplicate (standard error of the mean is indicated by the error bars). Absolute fold enrichment at ARS607 or ARS501 was calculated for each time point as follows: the signal from the anti-HA-coupled Dynabeads was divided by the signal from the BSA-coated Dynabeads, after both signals were first normalized to the signal from input DNA. Relative enrichment at ARS607 or ARS501 was obtained by normalizing the absolute enrichment at ARS607 or ARS501 to the absolute

enrichment at a locus 14 kb away from ARS607. Rad50-HA ChIP-chip was performed and analyzed as in Tittel-Elmer et al., 2012.

Co-immunoprecipitations were done as in (Hustedt et al., 2015) with the following modifications: Roche complete protease inhibitor tablets (Sigma 04693116001) were used at double the recommended concentration to prevent Rad50 degradation and phosphatase inhibitors were not added. 1250 units of Benzonase (Sigma E1014) was added for 30 min on ice after bead beating to digest both RNA and DNA. Since Rfa1 bound non-specifically to beads a stringent wash was used consisting of: 10 mM Tris PH 8.0, 500 mM LiAC, 0.2% NP-40, 0.5% Na-deoxycholate, 1 mM EDTA. Washes were done 3 x 5mins at 4 °C using a circular shaker set to 750 rpm.

Western blotting and antibodies

Western blotting of TCA precipitated proteins separated on a SDS-PAGE gel (Invitrogen) was performed as in (Seeber et al., 2013). Transfer was done using Biorad Turbo blot system onto PVDF membranes. Anti-actin was from Millipore (#MAB1501) and anti-Mcm2 was purchased from Santa Cruz (#6680). Rad53 protein was detected using a custom-made mouse monoclonal antibody (GenScript) against the FHA2 domain of Rad53. Anti-γH2A is a custom-made polyclonal antibody that is specific for phospho-S129 in yeast H2A. Anti-Rfa1 is a polyclonal antibody raised against purified yeast RPA consisting of all three subunits and was purchased from Agrisera (#AS07214). Anti-PK was purchased from Acris antibodies (#SM1691). Anti-Mre11 is a rabbit polyclonal antibody (kind gift of John Petrini; Sloan Kettering Memorial Hospital, #59567). Monoclonal anti-HA 12CA5 was from Santa Cruz (#sc-57592).

Yeast two hybrid analyses

Two-hybrid analyses were performed using galactose inducible bait and prey as described (Bjergbaek et al., 2005). The lacZ reporter pSH18-34, the bait and the prey were transformed into EGY191 cells (GA-1211). After glucose depletion, 2% galactose was added to the exponentially growing culture to induce the fusion proteins. The β-galactosidase assay for permeabilized cells was used to detect and quantify protein-protein interactions. Four independent transformants were analyzed in two or more independent experiments. Western blot analysis was used to check the expression of the fusion proteins (data not shown). B-galactosidase units are defined as OD420/(OD600*dilution*time(min)).

FACS analysis

For FACS, cultures were grown as for Western blotting. A 1 ml sample was taken for each time-point and was spun down and fixed in 70% ethanol and stored at 4 °C. When ready for analysis samples were

sedimented and resuspended in 50 mM Tris-HCL pH 7.5 + 200 µg/ml RNase A and digested for 2 h at 37 °C. Samples were then sedimented and resuspended in 50 mM Na-Citrate pH 7.0 + 10 µg/ml PI. Samples were stained overnight at 4 °C. The following morning the samples were briefly sonicated and diluted in more Na-Citrate + PI. Samples were measured on a Becton Dickinson FACS Calibur and at least 10 000 cells were measured.

Protein expression and purification

Budding yeast Rfa1-t11$_{1-132}$ was cloned into pOPINF vector using the In-Fusion system (Clontech) (Berrow et al., 2007) and expressed in *E. coli* B834s cells (Novagen) grown in seleno-methionine-supplemented medium (Molecular Dimensions). Recombinant protein was affinity purified via an N-terminal $(His)_6$ tag using Ni^{2+}-NTA Superflow (Qiagen) according to manufacturer's instructions. The $(His)_6$ tag was removed by HRV 3C protease digestion and the protein was further purified by anion exchange using 1 ml HiTrap Capto Q column (GE Healthcare) followed by gel filtration on a HiLoad 16/60 Superdex 75 column (GE Healthcare) in 20 mM Tris pH 8.0, 150 mM NaCl, 0.02% NaN_3 and 1 mM TCEP. The purified protein was concentrated to 20 mg/ml, flash-frozen in liquid N_2 and stored at -80°C.

Peptides and peptide microarray

Scanning peptide array was designed to cover all of MRX excluding the coiled-coil domains of Rad50, using 18 amino acids long peptides with 9 amino acid overlap. Peptides were synthesized and spotted onto a glass slide by JPT Peptide Technologies GmbH according to the PepStar microarray protocol. Rfa1$_{1-132}$ and rfa1-t11$_{1-132}$ purified peptides were incubated on the peptide glass slide at a concentration of 0.3 mg/ml in a humid chamber at 4 °C for 1 h. The peptide slide was then washed 5x5 times in TBS-Buffer + 0.1% Tween20 (TBS-T) with gentle agitation. Next, the primary Rfa1 antibody was incubated at a 1:10000 dilution in TBS-T with the slide for 1 h at 4 °C. The slide was washed as above. The fluorescent Alexa antibodies (Alexa647 anti-rabbit against the Rfa1 antibody and Alexa555 anti-mouse for the IgG control) were used at a 1:10000 dilution and incubated as above. Slide was then washed again as in the previous step followed by 5x5 min washes in deionized water. All solutions were filtered with a 0.2 µm filter. The slide was dried with a stream of air and immediately scanned with a Zeiss Axioimager Z1 microscope. Images were stitched using Zen Blue software and analysis was done using the protein array analyzer plugin for Fiji (ImageJ) (Carpentier and Henault, 2010).

N-terminal Cy5-labeled peptides of *S. cerevisiae* Rad50 (^{145}-VPKAILEYVIFCHQEDSL-^{162}; ^{163}-WPLSEPSNLKKKFDEIFQ-^{180}; ^{1171}-IRSDEVSSTVKGKSYNYR-^{1188}) and *S. cerevisiae* Mre11 (^{82}-DKPCELELLSDPSQVFHY-^{99}; ^{118}-VFGISGNHDDASGDSLLC-^{135}; ^{136}-PMDILHATGLINHFGKVI-^{153}) were purchased

from JPT Peptide Technologies (Berlin, Germany). Peptides were dissolved in 0.1 M Tris pH 8.0 and stored as 4 mM stock solutions at -80^{0}C until use.

Microscale thermophoresis (MST)

Experiments were carried out in 20 mM Tris buffer pH 8.0 containing 150 mM NaCl, 0.05 % Tween-20 and 0.5 mg/ml BSA. Purified *S. cerevisiae* Rfa1-N (residues 1-132) and Cy5-labeled Rad50 and Mre11 peptides were centrifuged at 13200 *g* for 5 min at room temperature prior to the assays. A dilution series of Rfa1-N yielding 14 different protein concentrations starting from 0.12 µM to 1000 µM was mixed separately with labeled Rad50 and Mre11 peptides at a fixed concentration of 25 µM. After 15 min incubation at room temperature, followed by centrifugation at 5000 *g* for 5 min, approximately 4 µL of each solution was filled into Monolith NT Premium Coated Capillaries (NanoTemper Technologies GmbH). Thermophoresis was measured using a Monolith NT.115 instrument (NanoTemper Technologies GmbH) at 23°C with 5 s / 30 s / 5 s laser off/on/off times, respectively. Instrument parameters were adjusted to 1-20 % LED power and 20 % MST power. Data of three independently pipetted measurements were analyzed (NT Analysis software version 1.5.41, NanoTemper Technologies GmbH) using the signal from thermophoresis and plotted using GraphPad Prism version 6.01 (La Jolla, CA, USA).

Name	Sequence	Protein	K_d ± SEM (µM)
VPK	VPKAILEYVIFCHQEDSL	Rad50	63.6 ± 7
DKP	DKPCELELLSDPSQVFHY	Mre11	n.d.
IRS	IRSDEVSSTVKGKSYNYR	Rad50	n.d.
VFG	VFGISGNHDDASGDSLLC	Mre11	n.d.
WPL	WPLSEPSNLKKKFDEIFQ	Rad50	n.d.
PMD	PMDILHATGLINHFGKVI	Mre11	n.d.

Crystallization

Crystals of Rfa1-t11$_{1-132}$ were grown at 20 °C using the sitting-drop vapor diffusion method after mixing 0.1 µl of Rfa1-t11$_{1-132}$ (20 mg/ml in 20 mM Tris pH 8.0, 150 mM NaCl, 0.02% NaN_3 and 1 mM TCEP) with 0.1 µl of reservoir containing 200 mM ammonium fluoride and 20% (w/v) PEG 3350. Crystals were transferred into a cryo-solution (20 mM Tris pH 8.0, 150 mM NaCl, 200 mM ammonium fluoride, 20%

(w/v) PEG 3350, 24 % (v/v) ethylene glycol) and flash frozen in liquid N_2 for data collection. Diffraction data were collected at the Swiss Light Source, Paul Scherrer Institut, Villigen, Switzerland.

Atomic coordinates and structure factors for Rfa1-t11$_{1-132}$ have been deposited in the Protein Data Bank under accession code 5M1X.

Structure determination and model building

Reflection data were indexed, integrated, and scaled using XDS (Kabsch, 2010). The structure of Rfa1-t11$_{1-132}$ was solved using the AutoSol pipeline implemented in the PHENIX package via SAD, using four seleno-methionine sites per molecule (Adams et al., 2010). The initial AutoSol structural model was manually completed and refined by the crystallographic simulated annealing routine followed by individual B-factor refinement in PHENIX. The final model was obtained after several cycles of manual rebuilding in COOT (Emsley et al., 2010) followed by refinement rounds in PHENIX and BUSTER (Bricogne et al, 2010). The Rfa1-t11$_{1-132}$ structure was validated using Molprobity (Chen et al., 2010) and COOT. Structural images for Figure 1B were prepared with PyMOL (DeLano Scientific; http://pymol.sourceforge.net/). Data collection and refinement statistics are found in Table 1.

DSB end separation assay

The DSB end separation assay was performed as in (Lobachev et al., 2004).

Microscopy

Live microscopy used an Olympus IX81 microscope equipped with a Yokogawa CSU-X1 scan head, an EM-CCD Cascade II (Photometrics), a ASI MS-2000 Z-piezo stage and a PlanApo x100, NA 1.45 total internal reflection fluorescence microscope oil objective. Fluorophores were excited at 567 nm (mCherry, ~30 µW), 515 nm (YFP, ~65 µW) and 491 (GFP, ~75 µW). Time-lapse series (1 min) of 8 optical slices per stack were streamed for 750 timepoints. Live cell cultures were imaged for a maximum of 60 minutes. Fixation of cells was done using 4% PFA for 1 min followed by washing 3x and then resuspending the cells in PBS. Mre11-YFP and cohesin spot separation experiments of fixed cells were acquired using 50 ms exposures of 50 slices with 0.2 µm intervals. For experiments where the DSB was marked on either side of the break 100 ms exposures were used with 50 slices at 0.2 µm intervals. Images were deconvolved and where necessary, channel aligned, using Huygens Pro.

Microarray slides were scanned with a Zeiss Axioimager Z1 microscope with a Plan-APOCHROMAT 10x/0.45 M27 objective lens and either Alexa555 or Alexa647 filter. The light source used was an X-Cite 120 EXFO Metal Halide lamp and images were detected on an Axiocam 506 camera. 50 ms exposures

were used for the Alexa555 signal and 100 ms exposures for the Alexa647 signal. 120 tiles were taken, covering the whole peptide array and then stitched together using Zen Blue software.

Structured illumination images were acquired on a Zeiss Elyra S.1 microscope with a Andor iXon 885 EMCCD camera using a HR diode 488 100nW solid state laser, BP 525-580 + LP 750 filter and a PLAN-APOCHROMAT 63x N.A. 1.4 oil DIC objective lens. Cells were fixed to a glass slide using Concanavalin A and a thin SIM grade Zeiss 1.5 glass coverslip was used while imaging. Cells were fully sectioned by 50 slices with 0.1 nm intervals taken at 50 ms exposures per slice using 5 rotations of the illumination grid. Brightfield images of the cells were also acquired using an X-Cite PC 120 EXFO Metal Halide lamp. Zen Black was used to process the images using automatic settings but retaining the raw scale.

Spot volume analysis

Spot volumes were determined by first creating a maximum intensity projection of the acquired 3D SIM stack. Fiji (ImageJ) was then used to segment the images to allow for easy particle detection and determination of both area and mean intensity of each particle. Particle detection and segmentation was done using the same setting for all images. The detected particles where then overlaid on the corresponding bright field images to allow for cell cycle phase determination.

Spot separation movie analysis

Time lapse movies were maximum intensity projected and spot separation was measured in the X and Y dimensions using the Fiji spot tracking plugin Trackmate (Jaqaman et al., 2008) with the following settings: Differences of Gaussian (DoG) detector with estimated blob diameter 0.3 µm, sub-pixel localization enabled, LAP tracker with frame to frame linking, segment gap closing (maximum frame gap of 20 frames), track segment splitting and track segment merging set to maximum distances of 0.5 µm. Length of splitting evens were analyzed using a custom Fiji script available on request.

Supplemental references

Adams, P.D., Afonine, P.V., Bunkoczi, G., Chen, V.B., Davis, I.W., Echols, N., Headd, J.J., Hung, L.W., Kapral, G.J., Grosse-Kunstleve, R.W.*, et al.* (2010). PHENIX: a comprehensive Python-based system for macromolecular structure solution. Acta crystallographica Section D, Biological crystallography *66*, 213-221.

Berrow, N.S., Alderton, D., Sainsbury, S., Nettleship, J., Assenberg, R., Rahman, N., Stuart, D.I., and Owens, R.J. (2007). A versatile ligation-independent cloning method suitable for high-throughput expression screening applications. Nucleic Acids Res *35*, e45.

Bjergbaek, L., Cobb, J.A., Tsai-Pflugfelder, M., and Gasser, S.M. (2005). Mechanistically distinct roles for Sgs1p in checkpoint activation and replication fork maintenance. Embo J *24*, 405-417.

Carpentier, G., and Henault, E. (2010). Protein Array Analyzer for ImageJ. Proceedings of the ImageJ User and Developer Conference, pp. 238-240.

Chen, V.B., Arendall, W.B., 3rd, Headd, J.J., Keedy, D.A., Immormino, R.M., Kapral, G.J., Murray, L.W., Richardson, J.S., and Richardson, D.C. (2010). MolProbity: all-atom structure validation for macromolecular crystallography. Acta crystallographica Section D, Biological crystallography *66*, 12-21.

Cobb, J.A., Bjergbaek, L., Shimada, K., Frei, C., and Gasser, S.M. (2003). DNA polymerase stabilization at stalled replication forks requires Mec1 and the RecQ helicase Sgs1. Embo j *22*, 4325-4336.

Cobb, J.A., Schleker, T., Rojas, V., Bjergbaek, L., Tercero, J.A., and Gasser, S.M. (2005). Replisome instability, fork collapse, and gross chromosomal rearrangements arise synergistically from Mec1 kinase and RecQ helicase mutations. Genes Dev *19*, 3055-3069.

Dion, V., Kalck, V., Seeber, A., Schleker, T., and Gasser, S.M. (2013). Cohesin and the nucleolus constrain the mobility of spontaneous repair foci. EMBO Rep *14*, 984-991.

Dubrana, K., van Attikum, H., Hediger, F., and Gasser, S.M. (2007). The processing of double-strand breaks and binding of single-strand-binding proteins RPA and Rad51 modulate the formation of ATR-kinase foci in yeast. J Cell Sci *120*, 4209-4220.

Emsley, P., Lohkamp, B., Scott, W.G., and Cowtan, K. (2010). Features and development of Coot. Acta crystallographica Section D, Biological crystallography *66*, 486-501.

Golemis, E.A., Serebriiskii, I., Finley, R.L., Jr., Kolonin, M.G., Gyuris, J., and Brent, R. (2011). Interaction trap/two-hybrid system to identify interacting proteins. Current protocols in neuroscience / editorial board, Jacqueline N Crawley [et al] *Chapter 4*, Unit 4.4.

Hegnauer, A.M., Hustedt, N., Shimada, K., Pike, B.L., Vogel, M., Amsler, P., Rubin, S.M., van Leeuwen, F., Guenole, A., van Attikum, H.*, et al.* (2012). An N-terminal acidic region of Sgs1 interacts with Rpa70 and recruits Rad53 kinase to stalled forks. Embo j *31*, 3768-3783.

Heun, P., Laroche, T., Shimada, K., Furrer, P., and Gasser, S.M. (2001). Chromosome dynamics in the yeast interphase nucleus. Science *294*, 2181-2186.

Huberman, J.A., Spotila, L.D., Nawotka, K.A., el-Assouli, S.M., and Davis, L.R. (1987). The in vivo replication origin of the yeast 2 microns plasmid. Cell *51*, 473-481.

Hustedt, N., Seeber, A., Sack, R., Tsai-Pflugfelder, M., Bhullar, B., Vlaming, H., van Leeuwen, F., Guenole, A., van Attikum, H., Srivas, R.*, et al.* (2015). Yeast PP4 interacts with ATR homolog Ddc2-Mec1 and regulates checkpoint signaling. Mol Cell *57*, 273-289.

Jaqaman, K., Loerke, D., Mettlen, M., Kuwata, H., Grinstein, S., Schmid, S.L., and Danuser, G. (2008). Robust single-particle tracking in live-cell time-lapse sequences. Nature methods *5*, 695-702.

Lee, S.E., Moore, J.K., Holmes, A., Umezu, K., Kolodner, R.D., and Haber, J.E. (1998). Saccharomyces Ku70, mre11/rad50 and RPA proteins regulate adaptation to G2/M arrest after DNA damage. Cell *94*, 399-409.

Lobachev, K., Vitriol, E., Stemple, J., Resnick, M.A., and Bloom, K. (2004). Chromosome fragmentation after induction of a double-strand break is an active process prevented by the RMX repair complex. Curr Biol *14*, 2107-2112.

Ma, J.L., Kim, E.M., Haber, J.E., and Lee, S.E. (2003). Yeast Mre11 and Rad1 proteins define a Ku-independent mechanism to repair double-strand breaks lacking overlapping end sequences. Mol Cell Biol *23*, 8820-8828.

Michalet, X., Ekong, R., Fougerousse, F., Rousseaux, S., Schurra, C., Hornigold, N., van Slegtenhorst, M., Wolfe, J., Povey, S., Beckmann, J.S.*, et al.* (1997). Dynamic molecular combing: stretching the whole human genome for high-resolution studies. Science *277*, 1518-1523.

Pasero, P., Bensimon, A., and Schwob, E. (2002). Single-molecule analysis reveals clustering and epigenetic regulation of replication origins at the yeast rDNA locus. Genes Dev *16*, 2479-2484.

Seeber, A., Dion, V., and Gasser, S.M. (2013). Checkpoint kinases and the INO80 nucleosome remodeling complex enhance global chromatin mobility in response to DNA damage. Genes Dev *27*, 1999-2008.

Soustelle, C., Vedel, M., Kolodner, R., and Nicolas, A. (2002). Replication protein A is required for meiotic recombination in Saccharomyces cerevisiae. Genetics *161*, 535-547.

Tittel-Elmer, M., Lengronne, A., Davidson, M.B., Bacal, J., Francois, P., Hohl, M., Petrini, J.H., Pasero, P., Cobb, J.A. (2012). Cohesin association to replication sites depends on rad50 and promotes fork restart. Mol Cell *48,* 98-108.

Tourriere, H., Versini, G., Cordon-Preciado, V., Alabert, C., and Pasero, P. (2005). Mrc1 and Tof1 promote replication fork progression and recovery independently of Rad53. Mol Cell *19*, 699-706.

Wu, J.R., and Gilbert, D.M. (1995). Rapid DNA preparation for 2D gel analysis of replication intermediates. Nucleic Acids Res *23*, 3997-3998.

CHAPTER 7: CONCLUDING REMARKS AND FUTURE PROSPECTS

In this thesis I have explored three separate projects connected by the underlying theme of DNA damage. All three projects used *S. cerevisiae* as a model organism and relied heavily on microscopy-based techniques to test their core hypotheses. The first two projects focused on how DNA damage changes the dynamics of chromatin. The third project was a more mechanistic study of the role of the MRX complex at DSBs and stalled replication forks. This section is divided into three summaries of the main conclusions of Chapters 4, 5, and 6, followed by a discussion of the direction future work related to these projects should take.

i) The mechanism of DNA-damage-induced chromatin mobility

In Chapter 4 I investigated the mechanisms that drive damage-induced chromatin motion both at the site of a DSB (in *cis*) or at other undamaged loci (in *trans*). We found that movement of undamaged chromosomal loci stimulated in *trans* by DNA damage, shows increased movement in a dose-dependent manner (Figure 1). This was ATP-dependent, and required activation of the DNA damage checkpoint. Importantly, we could show that activation of the DNA damage checkpoint in the absence of damage by artificial tethering of checkpoint proteins to a chromosomal locus was sufficient to increase movement both in *cis* as well as in *trans*. Continuing previous work (Neumann et al., 2012) we could show that the INO80 chromatin-remodeling complex is required for both in *cis* and in *trans* movement (Figure 1). Interestingly, other chromatin remodeling enzymes, such as Chd1 or Swr1, do not seem to be required for damage-induced chromatin movement.

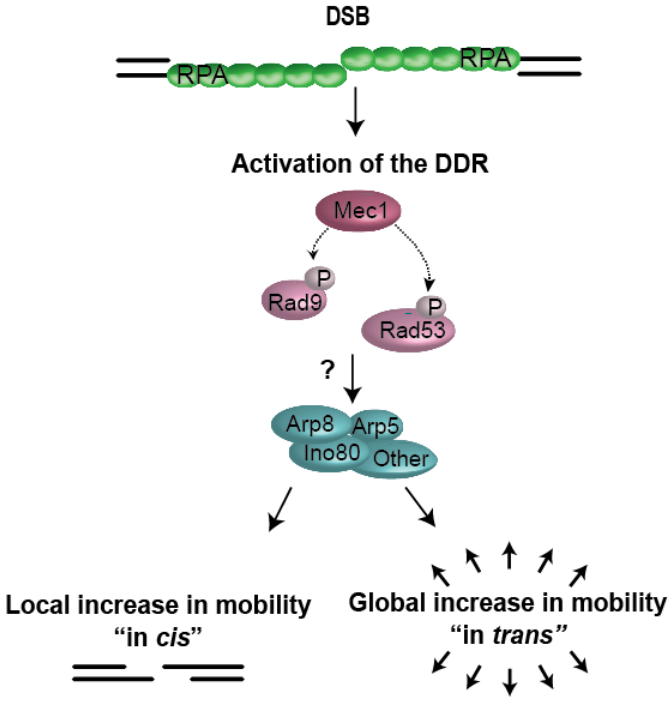

Figure 1: Graphical summary of the key findings in Chapter 4. Resection at a DSB leads to accumulation of ssDNA and binding of RPA. This signals the recruitment of repair proteins and activates the DDR. Global chromatin movement (in *trans)* is enhanced by checkpoint kinase activation and requires Mec1, Rad9 and Rad53. Increased movement of a DSB only requires Mec1 and Rad9 (Dion et al., 2012). Downstream from checkpoint activation, the INO80 subunits Arp5 and Arp8 are required for both in *cis* and in *trans* movement. It is still unknown which subunits of INO80 need to be phosphorylated to regulate damage-induced increased chromatin motion.

ii) Polymer modeling of chromatin loci allows local chromatin structure to be predicted

In Chapter 5 we investigated what new insights could be made into changes in chromatin structure at the site of an inducible DSB by statistical analysis of single-particle trajectories. First, we updated our imaging regime in order to use robust statistics to extract a number of parameters from single-particle trajectories, such as the diffusion coefficient, the character of the movement (anomalous diffusion), the forces acting on the chromatin, and the confinement of the locus. We were able to determine that nuclear "rocking" is a major contributor to chromatin motion, and that this effect can be reduced by depolymerization of the actin cytoskeleton using Latrunculin A. Removal of this "rocking" let us study pure chromatin motion.

We extracted parameters from trajectories of the locus in both cut and uncut conditions. Using the parameters extracted from these conditions we modeled chromatin using a β-polymer model (Amitai and Holcman, 2013). Our simulations predicted that chromatin would expand at the site of a DSB: this was confirmed by super-resolution imaging where we measured the volume of GFP-LacI foci bound to a *lacO* array. As observed by others (Neumann et al., 2012; Strecker et al., 2016) we found that the INO80 complex is required to increase the movement of a DSB, and that DSBs do not expand in an INO80 mutant. Our simulations also predicted that a break would move to the periphery of its local domain, driven simply by modification of the chromatin surrounding the break – no active force is needed.

In summary, this research describes a workflow that takes single-particle trajectories of DSBs and extracts a series of parameters. These parameters give useful information about the motion of the locus. In addition, they can be used in polymer simulations to make predictions about local chromatin structure at the observed sites: these can then be tested (see Figure 2).

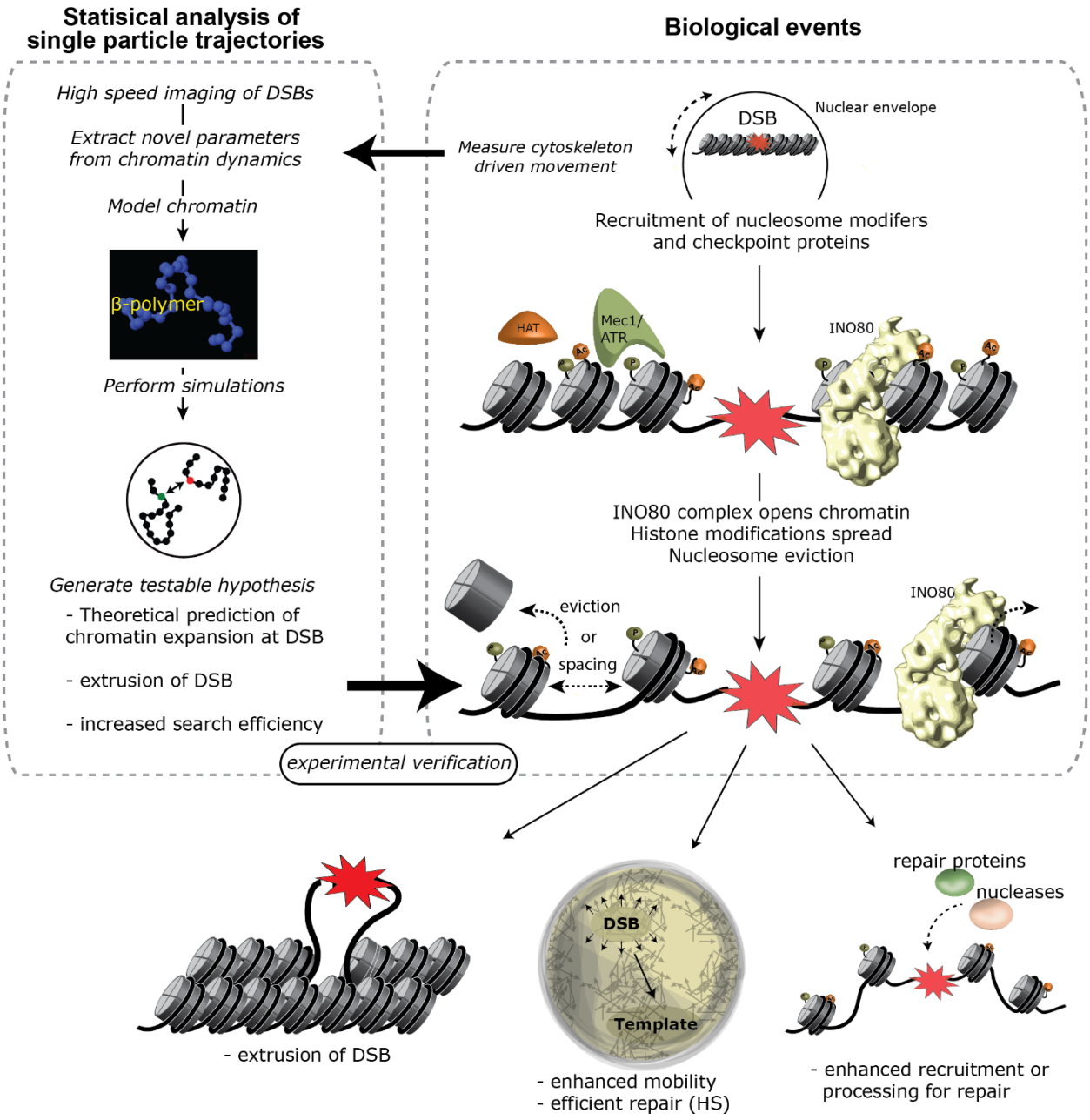

.

Figure 2: Using statistical analysis of single-particle trajectories to model chromatin and make predictions about its structure and mechanics. See section ii) for details.

iii) The role and mechanism of recruitment of the MRX complex to stalled replication forks and DSBs

Chapter 6 reports a long investigation into understanding the functional epistasis behind the recombination-defective *rfa1-t11* mutant allele and mutants of the MRX complex. We describe a mechanism whereby RPA recruits the MRX complex through the N-terminal OB fold of Rfa1 to both stalled replication forks and DSBs. MRX binds to the N-OB fold of Rfa1 through multiple configurations, including through the ATPase domain or Rad50. At stalled replication forks, the interaction between Rfa1 and MRX is crucial to prevent fork collapse. Interestingly, checkpoint activation is unaffected in the *rfa1-t11* mutant after hydroxyurea treatment. At DSBs the interaction allows the MRX complex to hold sister chromatids and the end of DSBs together to ensure faithful DNA repair (see Figure 3). Importantly, MRX holds sisters together at DSBs independently of cohesin.

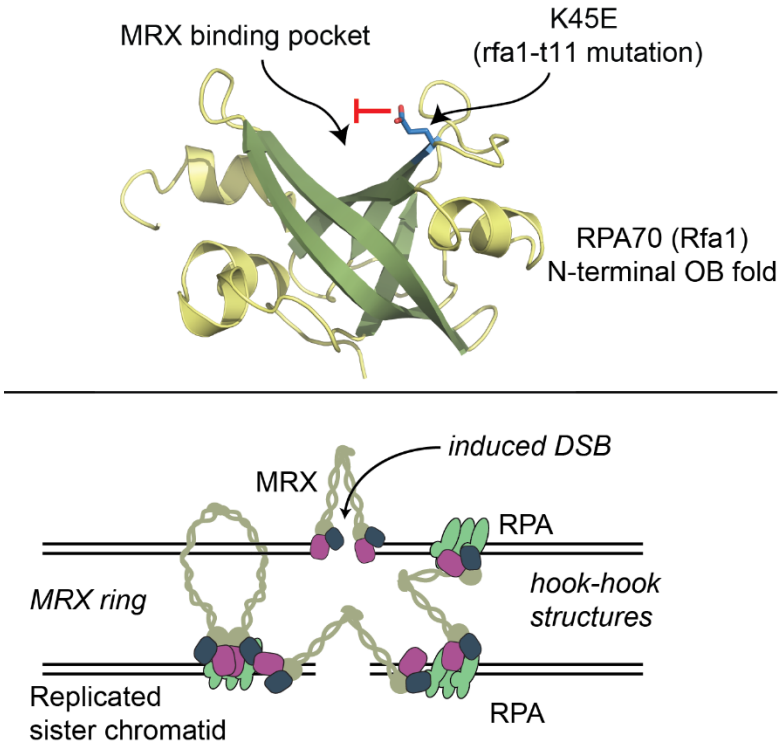

Figure 3: Upper panel – Crystal structure of the N-terminal OB fold of Rfa1 showing the rfa1-t11 mutation. This single amino acid substitution of lysine 45 to a glutamate disrupts the basic batch surrounding K45. Lower panel – The MRX complex is recruited to a DSB where it can hold sister chromatids as well as the ends of a DSB together.

Future directions

An important question that is not answered in this thesis concerns how the DNA damage checkpoint signals to the INO80 complex to bring about damage-induced chromatin motion (in *cis* or in *trans*). One possibility could be due to the fact that subunits of the INO80 complex are directly phosphorylated by Mec1 and Rad53 (Hustedt et al., 2015; Morrison et al., 2007). One known target is Ies4, a subunit of INO80 that does not significantly alter DNA repair, and is phosphorylated by Mec1/Tel1 (Hustedt et al., 2015; Morrison et al., 2007). Another possibility is that the checkpoint may indirectly signal to INO80, facilitating its recruitment through, for instance, phosphorylation of H2A (Morrison et al., 2004; van Attikum et al., 2004). However, this is unlikely to be the mechanism that drives damage-induced chromatin motion since deletion of *RAD9*, which abrogates increased movement does not affect H2A phosphorylation (Seeber et al., 2013). Chromatin motion analysis of Ies4 phosphorylation mutants would be an easy way to start to approach this question. Following this, a more in-depth analysis of the phosphorylation of INO80 by DNA damage checkpoint kinases would be required.

In the introduction I raised multiple concerns about issues arising from Strecker et al., 2016. The reason for this is that at the moment there are two major hypotheses that claim to explain damage-induced chromatin movement. Strecker et al. claim that *cis* and *trans* damage-induced movement both arise from centromere (and telomere) detachment. This is also supported by the observation that artificial centromere detachment can increase chromatin movement (Strecker et al., 2016; Verdaasdonk et al., 2013). Our lab claims that movement arises from changes in chromatin structure brought about by the INO80 nucleosome remodeling complex (Dion et al., 2012; Hauer et al., 2017; Neumann et al., 2012; Seeber et al., 2013). Both sides of this debate implicate the DNA damage checkpoint as important, and both sides show the need for INO80. It remains a possibility that these two hypotheses are not mutually exclusive and that both are affecting movement through the same pathway or through the same enzyme complex that has more than one function. Experiments to test this are ongoing.

In Hauer et al. (2017) we show that DNA damage induced by the radiomimetic drug Zeocin or IR causes degradation of histones on DNA in a manner dependent on INO80 and the DNA damage checkpoint. Other DSB repair proteins, such as Rad51, or other chromatin remodeling complexes, such as Swr1, are not required. This loss of histones is associated with an expansion of chromatin and a subsequent increase in chromatin movement. We conclude that this loss of histones is what drives the increase in mobility. Two important controls support this conclusion. The first evidence comes from the stufy of a mutant bearing a double deletion of the *S. cerevisiae* high mobility group box 1 (HMGB1) homologues (*NHP6A* and *NHP6B*), which has been shown to have approximately 20% less nucleosome density on DNA (Celona et al., 2011). This results in increased chromatin movement compared to a wild-type strain, even in the absence of DNA damage. The second control is a *S. cerevisiae* strain where single copies of both histone H3 and H4 are expressed under an inducible promoter. Shutting off this promoter reduces total histone levels on DNA by approximately 20-30%. Chromatin movement of undamaged loci in this histone-depleted state results in increased chromatin movement, much like in the *nhp6* double mutant. One caveat might be that the depletion of histone H4 causes declustering of kinetochores (Bouck and Bloom, 2007). This effect likely stems from disruption of the nucleosome at the centromere that contains Cse4 (centromere-specific histone H3-like protein, also called CenH3; Henikoff and Henikoff, 2012). Consistent with this hypothesis the depletion of normal H3 does not have the same effect as it is not present at centromeres. Thus, while nucleosome loss certainly drives increased chromatin movement, it is not clear whether this effect stems from disruption of centromere attachment to the spindle pole body or from a change in

structure of the chromatin fiber in general. To resolve this important issue, the kinetochores in the double *nhp6* mutant could be examined to see if they are partially declustered. If they are not declustered, then chromatin movement driven by nucleosome loss can be separated from that of movement based on centromere detachment.

It should also be noted here that mutants that disrupt the INO80 complex have been shown to disrupt centromere structure in *S. cerevisiae* (Chambers et al., 2012). This leads to chromosome segregation errors and can generate aneuploidy. However, chromatin motion in undamaged INO80 mutants is no different to wild-type even though they have a disrupted centromere structure (Neumann et al., 2012; Seeber et al., 2013; Strecker et al., 2016). INO80 does affect chromatin structure at loci where increased movement is observed (Hauer et al., 2017; Neumann et al., 2012; Seeber et al., 2013) and, specifically, is necessary for DSB expansion (see Chapter 5). In addition, artificially targeting the INO80 complex to a chromosomal locus is sufficient to increase its mobility (Neumann et al., 2012). While one could argue that a single DSB could cause centromere detachment, it is not obvious how targeting INO80 to a specific locus in the middle of a chromosome arm would also affect the centromere of the same chromosome. The regulation of INO80 in response to damage, how it causes histone degradation, and resolving the issue of whether or not centromere detachment drives damage-induced chromatin motion remain open and interesting lines of future research.

Expanding chromatin movement assays to mammalian cells would also be interesting, in order to see if the same mechanisms are conserved in higher eukaryotes. For instance, does loss of HMGB1 in mammalian cells also cause a general increase in mobility? Damage-induced mobility does appear to be conserved in mammalian cells (summarized in the Introduction), but the understanding of how exactly it is regulated is still at an early stage. The fact that centromeres in mammalian cells only become attached to the centriole after nuclear envelope breakdown argues that other factors must serve to increase interphase DSB movement besides centromere release. Are these the same factors as in *S. cerevisiae*, such as chromatin remodeling enzymes? It would also be of interest to investigate if damage-induced histone loss is conserved in mammalian cells. Related to this is the question of whether chromatin expands in mammalian cells due to DNA damage. While the effect of microtubules has been somewhat elucidated (Lottersberger et al., 2015), the contribution of the actin cytoskeleton to mammalian chromatin movement is not completely clear. The increased mobility of uncapped telomeres does not seem to be affected by Latrunculin A treatment (Dimitrova et al., 2008), and bulk movement of chromatin measured by diffusion of photoactivated PA-GFP tagged histone H4 also appears unaffected (Wiesmeijer et al., 2008). However, uncapped telomeres already show increased dynamics which may mask any effect of Latrunculin A. The measurement of chromatin diffusion as done by Wiesmeijer et al., was not quantitative, and in the words of the authors, "Cells treated with Latrunculin revealed a change in cellular and nuclear morphology, which made it more difficult to interpret the movement of photoactivated chromatin regions in time-lapse experiments". It would still be worthwhile for the result of the effect of Latrunculin A treatment on the movement of a normal mammalian chromatin locus to be published to settle this issue.

In the Introduction, I explained that one proposed function of damage-induced chromatin movement might be to enhance the efficiency of homology search during homologous recombination: I also highlighted the evidence for and against the hypothesis. This hypothesis has yet to be directly tested and is certainly worth investigating.

The MRX(N) complex is highly studied, with an average of 50 articles published on the topic per year since the early 2000s. The majority of these articles investigate the role of MRX in some aspect of DNA repair, with a minority focusing on the role of MRX in replication fork stability or telomere

length maintenance. MRX is thus a competitive field with the majority of "low-hanging fruit" experiments already done. This does not mean that there is nothing left to do.

There are still many aspects of aspects of MRX function at DSBs or stalled replication forks to understand. In particular, how exactly MRX binds to the N-OB fold of Rfa1 is a difficult question to answer. Both MRX and RPA are difficult to work with, and MRX appears to contain multiple binding sites for Rfa1. Since we have the crystallization protocol for Rfa1 N-OB, and because this peptide crystalizes readily, it would be interesting to try and co-crystallize the confirmed Rad50 interacting peptide that binds Rfa1 in a *rfa1-t11* sensitive manner (see Chapter 6).

Our study has shown that it is possible for MRX to hold sister chromatids together at sites of DNA damage. This function could be studied more in-depth since we do not know how MRX physically does this (i.e. using rings or hook-hook structures; Figure 3). It would also be interesting to know what the minimal required length of the long coiled-coil arms of Rad50 is, to be able to encircle or tether sister chromatids. Finally, it would be important to test if the sister chromatid stability function of MRX that we observe in yeast is conserved in mammalian cells.

Many proteins such as the transcription factor, TFIIH (Compe et al., 2012) or the repair protein, BRCA1 (Hatchi et al., 2015), have been shown to function in multiple biological processes, playing roles that were unanticipated at the time of their discovery. TFIIH, for instance, was first characterized as a general transcription factor and was later shown to be necessary to open DNA, allowing the incision and excision of damaged nucleotides (Compe et al., 2012). In contrast, BRCA1 was first described as an important tumor suppressor gene due to its DNA repair activity and role in the DNA damage response (Roy et al., 2012). This function has now broadened with the publication of data that links BRCA1's repair activity to transcription (Hatchi et al., 2015). Hatchi et al., show that BRCA1 one is necessary to prevent transcriptional DNA damage arising at nearby R-loops (RNA:DNA hybrids). The mechanism of this damage suppression is not clear but involves the interaction of BRCA1 with senataxin, an RNA/DNA helicase (Santos-Pereira et al., 2015), and subsequent recruitment of BRCA1/senataxin complexes to R-loop associated transcription termination regions (Hatchi et al., 2015).

Like, BRCA1, the MRX complex may also be involved in transcription. While there is scant published evidence of a role for MRX in transcription, there are hints. For example, all three subunits of the mammalian MRN complex interact with the transcriptional coactivator, p300 (Jung et al., 2005). In addition, recruitment of the MRN complex (in conjunction with topoisomerase I) modulates enhancer activation (Puc et al., 2015). Here, topoisomerase I is thought to relieve torsional stress arising from the synthesis of RNA at enhancers. While the authors propose that MRN may be recruited to remove "stalled" topoisomerase I from DNA (Puc et al., 2015), it is not clear that this is actually occurring. Finally, unpublished results from Peter Stirling's laboratory indicate that in the absence of MRX, more R-loops are generated with a concomitant increase in γH2A foci. Both of these affects can be rescued by the overexpression of RNase HI, showing that MRX appears, much like BRCA1, to suppress transcriptional DNA damage arising from RNA-DNA hybrids.

In collaboration with the Pasero laboratory, we are now investigating the role of MRX in transcription. Exciting new data suggest that MRX may be able to regulate transcription through genome organization (Jérôme Poli, unpublished data). These unpublished results, which I have participated in collecting and analyzing, use the well-studied galactose inducible promoter *GAL1-10* locus (Brickner et al., 2016; Cabal et al., 2006; Kalverda et al., 2008; Texari et al., 2013). Upon activation in galactose, this locus relocates to the nuclear pores. Our results show that, in cells lacking functional MRX, the *GAL1-10* does not relocate to the nuclear periphery. We show that MRX is normally recruited to this

locus and that in its absence, fine tuning of transcription at *GAL1-10* is defective. Interestingly, mutants in MRX also exhibit altered histone marks, including H3K4ac, and have reduced nucleosome density at the *GAL1-10* promoter (Poli et al., *in preparation)*. Further studies will focus on determining if and how the MRX complex could link chromatin position in the nucleus to its conformation/organization at the gene level. These results are the first to show a role for the MRX complex in transcriptional regulation, and will be an exciting new aspect of the MRX complex to research.

In conclusion, this thesis has validated the existence of DNA damage-induced chromatin movement., through mechanisms that act both in *cis* and in *trans*. It has shown that both the DNA damage checkpoint and INO80 are key regulators of movement. This thesis shows that combining polymer models with single particle trajectory analysis of chromosomal loci can lead to novel predictions about local chromatin structure. Finally, this thesis has proved that the MRX complex is required to hold sister chromatids together at breaks independently of cohesin. Understanding the role of chromatin movement in DNA repair as well as the mechanism of damage-induced movement remains a challenge, for which *S. cerevisiae* has proven to be a capable and relevant model organism.

References

Amitai, A., and Holcman, D. (2013). Polymer model with long-range interactions: analysis and applications to the chromatin structure. Phys Rev E Stat Nonlin Soft Matter Phys *88*, 052604.

Bouck, D.C., and Bloom, K. (2007). Pericentric chromatin is an elastic component of the mitotic spindle. Current biol. *17*, 741-748.

Brickner, D.G., Sood, V., Tutucci, E., Coukos, R., Viets, K., Singer, R.H., and Brickner, J.H. (2016). Subnuclear positioning and interchromosomal clustering of the *GAL1-10* locus are controlled by separable, interdependent mechanisms. Mol Biol Cell *27*, 2980-2993.

Cabal, G.G., Genovesio, A., Rodriguez-Navarro, S., Zimmer, C., Gadal, O., Lesne, A., Buc, H., Feuerbach-Fournier, F., Olivo-Marin, J.-C., and Hurt, E.C. (2006). SAGA interacting factors confine sub-diffusion of transcribed genes to the nuclear envelope. Nature *441*, 770-773.

Celona, B., Weiner, A., Di Felice, F., Mancuso, F.M., Cesarini, E., Rossi, R.L., Gregory, L., Baban, D., Rossetti, G., and Grianti, P. (2011). Substantial histone reduction modulates genomewide nucleosomal occupancy and global transcriptional output. PLoS Biol *9*, e1001086.

Chambers, A.L., Ormerod, G., Durley, S.C., Sing, T.L., Brown, G.W., Kent, N.A., and Downs, J.A. (2012). The INO80 chromatin remodeling complex prevents polyploidy and maintains normal chromatin structure at centromeres. Genes Dev, *26*, 2590-2603.

Compe, E., and Egly, J.-M. (2012). TFIIH: when transcription met DNA repair. Nature Reviews Molecular Cell Biology *13*, 343-354.

Dimitrova, N., Chen, Y.C., Spector, D.L., and de Lange, T. (2008). 53BP1 promotes non-homologous end joining of telomeres by increasing chromatin mobility. Nature *456*, 524-528.

Dion, V., Kalck, V., Horigome, C., Towbin, B.D., and Gasser, S.M. (2012). Increased mobility of double-strand breaks requires Mec1, Rad9 and the homologous recombination machinery. Nat Cell Biol *14*, 502-509.

Hatchi, E., Skourti-Stathaki, K., Ventz, S., Pinello, L., Yen, A., Kamieniarz-Gdula, K., Dimitrov, S., Pathania, S., McKinney, K.M., and Eaton, M.L. (2015). BRCA1 recruitment to transcriptional pause sites is required for R-loop-driven DNA damage repair. Molecular Cell *57*, 636-647.

Hauer, M., Seeber, A., Singh, V., Thierry, R., Amitai, A., Eglinger, J., Holcman, D., Owen-Hughes, T., and Gasser, S. (2017). Histone degradation in response to DNA damage triggers general chromatin decompaction. NSMB *24*, 99-107.

Henikoff, S., and Henikoff, J.G. (2012). "Point" centromeres of *Saccharomyces* harbor single centromere-specific nucleosomes. Genetics *190*, 1575-1577.

Hustedt, N., Seeber, A., Sack, R., Tsai-Pflugfelder, M., Bhullar, B., Vlaming, H., van Leeuwen, F., Guénolé, A., van Attikum, H., and Srivas, R. (2015). Yeast PP4 interacts with ATR homolog Ddc2-Mec1 and regulates checkpoint signaling. Molecular Cell *57*, 273-289.

Jung, S.Y., Malovannaya, A., Wei, J., O'Malley, B.W., and Qin, J. (2005). Proteomic analysis of steady state nuclear hormone receptor coactivator complexes. Mol. Endocrin. *19*, 2451-2465.

Kalverda, B., Röling, M.D., and Fornerod, M. (2008). Chromatin organization in relation to the nuclear periphery. FEBS letters *582*, 2017-2022.

Lottersberger, F., Karssemeijer, R.A., Dimitrova, N., and de Lange, T. (2015). 53BP1 and the LINC Complex Promote Microtubule-Dependent DSB Mobility and DNA Repair. Cell *163*, 880-893.

Morrison, A.J., Highland, J., Krogan, N.J., Arbel-Eden, A., Greenblatt, J.F., Haber, J.E., and Shen, X. (2004). INO80 and gamma-H2AX interaction links ATP-dependent chromatin remodeling to DNA damage repair. Cell *119*, 767-775.

Morrison, A.J., Kim, J.A., Person, M.D., Highland, J., Xiao, J., Wehr, T.S., Hensley, S., Bao, Y., Shen, J., Collins, S.R*., et al.* (2007). Mec1/Tel1 phosphorylation of the INO80 chromatin remodeling complex influences DNA damage checkpoint responses. Cell *130*, 499-511.

Neumann, F.R., Dion, V., Gehlen, L.R., Tsai-Pflugfelder, M., Schmid, R., Taddei, A., and Gasser, S.M. (2012). Targeted INO80 enhances subnuclear chromatin movement and ectopic homologous recombination. Genes Dev *26*, 369-383.

Puc, J., Kozbial, P., Li, W., Tan, Y., Liu, Z., Suter, T., Ohgi, K.A., Zhang, J., Aggarwal, A.K., Rosenfeld, M.G. (2015). Ligand-dependent enhancer activation regulated by topoisomerase-I activity. Cell *160,* 367-380.

Roy, R., Chun, J., and Powell, S.N. (2012). BRCA1 and BRCA2: different roles in a common pathway of genome protection. Nature Reviews Cancer *12*, 68-78.

Santos-Pereira, J.M., and Aguilera, A. (2015). R loops: new modulators of genome dynamics and function. Nat Rev Genet *16*, 583–597.

Seeber, A., Dion, V., and Gasser, S.M. (2013). Checkpoint kinases and the INO80 nucleosome remodeling complex enhance global chromatin mobility in response to DNA damage. Genes Dev *27*, 1999-2008.

Strecker, J., Gupta, G.D., Zhang, W., Bashkurov, M., Landry, M.-C., Pelletier, L., and Durocher, D. (2016). DNA damage signalling targets the kinetochore to promote chromatin mobility. Nature cell biology *18*, 281-290.

Texari, L., Dieppois, G., Vinciguerra, P., Contreras, M.P., Groner, A., Letourneau, A., and Stutz, F. (2013). The nuclear pore regulates GAL1 gene transcription by controlling the localization of the SUMO protease Ulp1. Molecular Cell *51*, 807-818.

van Attikum, H., Fritsch, O., Hohn, B., and Gasser, S.M. (2004). Recruitment of the INO80 complex by H2A phosphorylation links ATP-dependent chromatin remodeling with DNA double-strand break repair. Cell *119*, 777-788.

Verdaasdonk, J.S., Vasquez, P.A., Barry, R.M., Barry, T., Goodwin, S., Forest, M.G., and Bloom, K. (2013). Centromere tethering confines chromosome domains. Mol Cell *52*, 819-831.

Wiesmeijer, K., Krouwels, I.M., Tanke, H.J., and Dirks, R.W. (2008). Chromatin movement visualized with photoactivable GFP-labeled histone H4. Differentiation *76*, 83-90.

APPENDICES

List of abbreviations

53BP1: p53 binding protein 1, a critical DSB repair protein that antagonizes DNA end resection to promote repair by non-homologous end joining and plays a critical role in the DNA damage checkpoint

alt-NHEJ: alternative non-homologous end joining, a mutagenic pathway in which previously resected DNA ends are ligated together, also called microhomology-mediated NHEJ (MM-NHEJ)

ATR: ataxia telangiectasia and Rad3-related protein, a critical protein kinase in the DNA damage response pathway. Mec1 in *S. cerevisiae*.

D-loop: displacement loop, the DNA structure caused by strand invasion that displaces one strand of the duplex DNA that serves as the template for HR

DSB: DNA double-strand break, a DNA lesion in which both strands of DNA are broken

HC: heterochromatin, highly condensed, and predominantly repetitive and transcriptionally repressed chromatin region that reside at the nuclear periphery and/or in intranuclear depots.

HP1: heterochromatin protein 1, a chromodomain-containing protein that associates with heterochromatin

HR: homologous recombination, a major pathway of DSB repair that requires a homologous template

IR: ionizing radiation consisting of particles, X-rays, or gamma rays with sufficient energy to cause ionization in the medium through which it passes.

KASH: Klarsicht/Anc-1/Syne1 homology, a family of orthologous tail-anchored outer nuclear membrane proteins that make up the cytoplasmic aspect of the LINC complex

LINC complex: linker of nucleoskeleton and cytoskeleton, a complex of inner nuclear membrane SUN proteins and outer nuclear membrane KASH proteins that spans the nuclear envelope

LOH: loss of heterozygosity

MRX(N): Mre11-Rad50-Xrs2 (Nbs1 in mammals) complex, important for DSB repair and stabilization of stalled replication forks

MSD: mean squared displacement

NHEJ: non-homologous end joining, a major pathway of DSB repair that involves direct ligation of the DSB

NPC: nuclear pore complex, the massive protein complex that stabilizes nuclear pores and controls the bidirectional traffic of macromolecules in and out of the nucleus

NORs: nucleolar organization regions, the regions of the genome that give rise to nucleoli, later established as being the rDNA

OB fold: oligonucleotide binding fold.

rDNA: ribosomal DNA, the repetitive region of the genome that is composed of repeats of the genes encoding the ribosomal rRNA subunits. It resides in the nucleolus

R-loops: an R-loop is a three-stranded nucleic acid structure, composed of a DNA:RNA hybrid and the associated non-template single-stranded DNA (ssDNA).

rRNA: the RNAs produced from the rDNA that make up the bulk of the ribosomes

RPA: replication protein A, a trimeric (Rfa1,2,3) complex that binds ssDNA, coating it during replication and DNA repair and acting as a major protein recruitment scaffold

SDSA: synthesis-dependent strand annealing, a template-dependent repair mechanism that proceeds without Holliday junction intermediates and leads to non-crossover products

SMC5/6: a cohesin-related protein complex important for genome integrity, linked to SUMOylation activity

SSA: single-strand annealing, a template-independent (but homology-dependent) repair mechanism in which the copy number of tandem repeats can be reduced after DSB resection

ssDNA: single strand DNA

STUbL: SUMO-targeted ubiquitin ligase, a family of proteins that induce ubiquitination of target proteins and require prior SUMOylation

SUMO: small ubiquitin-like modifier, a small protein that can be conjugated to lysine residues on target proteins

SUN: Sad1/Unc84, a family of orthologous integral inner nuclear membrane proteins that make up the nuclear aspect of the LINC complex

TRF2: telomere repeat (binding) factor, a component of the Shelterin complex that protects chromosome ends

Non-thesis related contributions

This is a summary of contributions that I made during my PhD to other bodies of work not directly related to my thesis. Where necessary I state my contribution.

Peer-reviewed Publications

Poli, J., Gerhold, C.-B., Tosi, A., Hustedt, N., **Seeber, A.**, Sack, R., Herzog, F., Pasero, P., Shimada, K., and Hopfner, K.-P. (2016). Mec1, INO80, and the PAF1 complex cooperate to limit transcription replication conflicts through RNAPII removal during replication stress. Genes & Development 30, 337-354.

Here I developed a microfluidic live-cell assay and analysis suite based on the image processing program ICY to monitor the levels of fluorescently tagged proteins in cells. In this case I measured the levels of Rpb1 and Paf1 after treatment with HU.

Hauer, M., **Seeber, A.**, Singh, V., Thierry, R., Amitai, A., Kryzhanovska, M., Eglinger, J., Holcman, D., Owen-Hughes, T. (2016) Histone degradation in response to DNA damage enhances chromatin dynamics and recombination rates. Nature Structural and Molecular Biology, 24, 99-107.

In 2013 during publication of my Genes & Development paper I obtained the first result showing that histones are lost and that chromatin expands in response to Zeocin treatment. I contributed these initial results which Michael then expanded and built his work on. I also contributed directly to this article by providing tracking data of loci in damage conditions as well as establishing the automated live cell assay to monitor protein levels in the nucleus after DNA damage that was used in Poli et al. Finally, I performed the integration efficiency assay in Figure 8a and some of the imaging in Figure 8b.

Hustedt, N., **Seeber, A.**, Sack, R., Tsai-Pflugfelder, M., Bhullar, B., Vlaming, H., van Leeuwen, F., Guénolé, A., van Attikum, H., and Srivas, R. (2015). Yeast PP4 interacts with ATR homolog Ddc2-Mec1 and regulates checkpoint signaling. Molecular Cell 57, 273-289.

In this work I did the microscopy consisting of counting Ddc2, Psy2 and Rfa1 foci after treatment with HU or Zeocin. In addition, I developed an assay to measure FRET between these proteins confirming Nicole's biochemical work.

Shimada, K., Filipuzzi, I., Stahl, M., Helliwell, S.B., Studer, C., Hoepfner, D., **Seeber, A.**, Loewith, R., Movva, N.R., and Gasser, S.M. (2013). TORC2 signaling pathway guarantees genome stability in the face of DNA strand breaks. Molecular Cell 51, 829-839.

At the beginning of my PhD in Susan's lab I was learning how to do CHEF gels and doing chromatin mobility assays. At the time Rodney Rothstein was using caffeine as a way to prevent damage induced chromatin movement through inhibition of Mec1/Tel1. I attempted to repeat his results but rather found that caffeine combined with Zeocin strongly increased the damage induced movement response. I showed by CHEF gel that caffeine and Zeocin together caused the same yeast chromosome shattering that Kenji was observing, certainly due to the fact that caffeine does not specifically inhibit Mec1/Tel1 and will inhibit many other kinases including those in the TOR pathway. While we didn't use my result in the paper we did use it as a reply to a specific reviewer comment.

Chen, J., Young, S.M., Allen, C., **Seeber, A.**, Péli-Gulli, M.-P., Panchaud, N., Waller, A., Ursu, O., Yao, T., and Golden, J.E. (2012). Identification of a small molecule yeast TORC1 inhibitor with a multiplex screen based on flow cytometry. ACS Chemical Biology 7, 715-722.

While I was in Robbie Loewith's lab in Geneva I was working with many small molecule inhibitors of TORC1 and in this case contributed by characterizing one of these inhibitors. I did this by monitoring the phosphorylation state of targets of TORC1 by western blot.

Review articles and book chapters

Horigome, C., Dion, V., **Seeber, A.**, Gehlen, L.R., and Gasser, S.M. (2015). Visualizing the spatiotemporal dynamics of DNA damage in budding yeast. Methods in Molecular Biology (Clifton, NJ) 1292, 77-96.

Here I contributed to writing the methods section on chromatin mobility assays.

Chen, J., Young, S.M., Allen, C., Waller, A., Ursu, O., Strouse, J.J., Yao, T., Golden, J.E., Peterson, B.R., Foutz, T.D., **Seeber, A.,** et al. (2010). Profiling a Selective Probe for RTG Branch of Yeast TORC1 Signaling Pathway. Probe Reports from the NIH Molecular Libraries Program

Here the data from Chen et al., was published as a report from the NIH Molecular Libraries Program.

Patent

"Methods for increasing the frequency of gene targeting by chromatin modification"

Inventors: Hauer, M., **Seeber, A**. and Gasser, S.M.,

Curriculum Vitae

Andrew Seeber

andy.seeber@gmail.com

33 Riehentorstrasse · 4058 Basel · +44 (0) 78 625 2126

Date of Birth: 28 October 1987 | Citizenship: South Africa/Ireland

Civil Status: Married to Michelle DiPietro | Residency: Switzerland, C Permit

PRESENT POSITION

Friedrich Miescher Institute for Biomedical Research — Basel, CH

PhD Student — 11.2011 - Present

EDUCATION

Friedrich Miescher Institute for Biomedical Research — Basel, CH

University of Basel — 11.2011 - Present

PhD, Genetics

Dissertation: "*Chromatin dynamics in DNA double-strand break repair*"

University of Geneva — Geneva/Basel, CH

NCCR Frontiers in Genetics PhD rotation program — 10.2010 – 11.2011

Hong Kong University of Science and Technology — Kowloon, HK

NUIG Funded Exchange Fellowship — 1.2009 – 7.2009

National University of Ireland, Galway — Galway, IE

Bachelor of Biomedical Science, 1st Class Hons — 9.2006 – 6.2010

RESEARCH EXPERIENCE

Friedrich Miescher Institute for Biomedical Research — Basel, CH

PhD student; Advisor: Susan M. Gasser — 11.2011 - Present

Chromatin dynamics in DNA double-strand break repair

- Developed an imaging regime to study chromatin dynamics in living cells
- Identified the biological mechanism that drives chromatin movement
- Characterized how sister chromatids are held together at double-strand breaks

Advanced Imaging Center, Janelia Research Campus Ashburn,USA

Janelia Research Campus visitor program 8.2015 – 9.2015

PhD student; Advisor: Teng-Leong Chew

Applying aberration-corrected multifocus microscopy to chromatin dynamics

Cold Spring Harbor Laboratory NY, USA

Yeast Genetics and Genomics course 7.2011 – 8.2011

Advisors: Prof. Jeffery Strathern and Prof. Jeffery S. Smith

Intensive training course in the use of S. cerevisiae as a model organism

Friedrich Miescher Institute for Biomedical Research Basel, CH

3rd Rotation, NCCR Frontiers in Genetics 5.2011 – 11.2011

Advisor: Prof. Susan M. Gasser

Interaction of the MRX complex with RPA at DSBs and stalled replication forks

University of Geneva Geneva, CH

2nd Rotation, NCCR Frontiers in Genetics 2.2011 – 5.2011

Advisor: Prof. David Shore

Sir protein interaction at an irreparable DSB

University of Geneva Geneva, CH

1st Rotation, NCCR Frontiers in Genetics 10.2010 – 2.2011

Advisor: Prof. Robbie Loewith

Investigation of downstream targets of yeast protein kinase

National University of Ireland, Galway Galway, IE

Science Foundation Ireland Student Fellowship 5.2010 – 9.2010

Advisor: Prof. Noel F. Lowndes

Investigation of the target residues of the tudor domains of 53Bp1 and Crb2

Diaceutics, International Management and Consulting Firm Galway, IE

Advisor: Patrick Considine, PhD 6.2010 – 9.2010

Creation of a database of patents, products and services of diagnostic companies

National University of Ireland, Galway Galway, IE

Final Year Laboratory Project 9.2009 – 1.2010

Advisor: Prof. Andrew Flaus

Recombinant expression and purification of histone H1.2 and its effect on a DNA-bound nucleosome

National University of Ireland, Galway Galway, IE

Biochemical Society Summer Studentship 6.2009 – 9.2009

Advisor: Prof. Heinz-Peter Hasheuer

Creation and recombinant expression of a trimeric mutant of replication protein A, in a single vector with a triple alanine mutation on the p32 subunit

SKILLS AND TECHNIQUES

- Genetic manipulations in budding yeast
- Chromatin immunoprecipitation and quantitative PCR
- Protein microarrays
- Co-immunoprecipitation of protein complexes
- Fluorescence live-cell microscopy
  - Confocal and spinning disk
  - Structured illumination (SIM), PALM
  - FRET and FRAP
- Image processing and analysis of large image datasets

LEADERSHIP EXPERIENCE

Friedrich Miescher Institute for Biomedical Research Basel, CH

Graduate student advisor and microscopy expert 2014-2016

Trained multiple graduate students in a range of techniques including live-cell and super-resolution microscopy and the use of S. cerevisiae as a model organism

The University of Hong Kong Pok Fu Lam, HK

Anatomy demonstrator and prepared prosections 1.2009 – 5.2009

Assisted in gross anatomical and histological laboratory practical sessions

National University of Ireland, Galway Galway, IE

Vice Auditor of the Galway Film Society 2008 – 2009

National University of Ireland, Galway Galway, IE

Student Support Worker 7.2007 – 5.2010

Tutoring students with learning (dyslexia) disabilities in biochemistry

GRANTS AND AWARDS

Carl Singer Foundation award	8.2014
Biochemical Society travel grant	9.2011
Swiss Society for Biochemistry special grant for junior scientists	8.2011
NCCR – Frontiers in Genetics, travel grant	8.2011
Science Foundation Ireland student fellowship	5.2010 – 9.2010
Biochemical Society Summer studentship	6.2009 – 9.2009
NUIG fellowship to Hong Kong University of Science and Technology	1.2009 – 7.2009

PROFESSIONAL ASSOCIATIONS

Member of the Biochemical Society (UK) 2009 - present

INVITED CONFERENCE TALKS

Research Center for the Mathematics on Chromatin Live Dynamics 11.2016

"Using single-particle trajectory statistics and polymer simulations to analyze and predict changes in chromatin structure"

39th Annual Meeting of the Molecular Biology Society of Japan 11.2016

"*Change in local chromatin structure during homology search"*

At the Intersection of DNA Replication and Genome Maintenance, ICGEB Trieste 6.2016

"RPA recruits MRX to forks and breaks to hold replicated sister chromatids together"

International Centre for Theoretical Physics Chromatin Workshop, Trieste 9.2014

"Chromatin (modifiers) and the dynamic chromatin response to DNA damage"

FASEB, Yeast Chromosome Structure, Replication and Segregation 7.2014

"Stable interaction between MRX and RPA is required for stalled fork recovery and maintenance of DSB structure for repair"

TriRhena transcription and chromatin club 2.2013

"Checkpoint kinases regulate global chromatin mobility after DSB induction"

Nucleosome 4D Barcelona Retreat 10.2012

"How checkpoint kinases influence global chromatin dynamics"

Image DDR meeting, Sussex

"How checkpoint kinases influence global chromatin dynamics" 9.2012

NCCR – Frontiers in Genetics Annual Meeting 6.2012

"How checkpoint kinases influence global chromatin dynamics"

PATENTS

Inventors: Hauer, M., **Seeber, A**. and Gasser, S.M., 11.2016

"Methods for increasing the frequency of gene targeting by chromatin modification"

PEER-REVIEWED PUBLICATIONS

Chen, J., Young, S.M., Allen, C., **Seeber, A.**, Péli-Gulli, M.-P., Panchaud, N., Waller, A., Ursu, O., Yao, T., and Golden, J.E. (2012). Identification of a small molecule yeast TORC1 inhibitor with a multiplex screen based on flow cytometry. ACS Chemical Biology 7, 715-722.

Shimada, K., Filipuzzi, I., Stahl, M., Helliwell, S.B., Studer, C., Hoepfner, D., **Seeber, A.**, Loewith, R., Movva, N.R., and Gasser, S.M. (2013). TORC2 signaling pathway guarantees genome stability in the face of DNA strand breaks. Molecular Cell 51, 829-839.

Dion, V., Kalck, V., **Seeber, A.**, Schleker, T., and Gasser, S.M. (2013). Cohesin and the nucleolus constrain the mobility of spontaneous repair foci. EMBO Reports 14, 984-991.

Seeber, A., Dion, V., and Gasser, S.M. (2013). Checkpoint kinases and the INO80 nucleosome remodeling complex enhance global chromatin mobility in response to DNA damage. Genes & Development 27, 1999-2008.

Hustedt, N., **Seeber, A.**, Sack, R., Tsai-Pflugfelder, M., Bhullar, B., Vlaming, H., van Leeuwen, F., Guénolé, A., van Attikum, H., and Srivas, R. (2015). Yeast PP4 interacts with ATR homolog Ddc2-Mec1 and regulates checkpoint signaling. Molecular Cell 57, 273-289.

Poli, J., Gerhold, C.-B., Tosi, A., Hustedt, N., **Seeber, A.**, Sack, R., Herzog, F., Pasero, P., Shimada, K., and Hopfner, K.-P. (2016). Mec1, INO80, and the PAF1 complex cooperate to limit transcription replication conflicts through RNAPII removal during replication stress. Genes & Development 30, 337-354.

Seeber, A., Hegnauer, A.M., Hustedt, N., Deshpande, I., Poli, J., Eglinger, J., Pasero, P., Gut, H., Shinohara, M., Hopfner, K.P., Shimada, K., Gasser, S.M. (2016) RPA Mediates Recruitment of MRX to Forks and Double-Strand Breaks to Hold Sister Chromatids Together. Molecular Cell, 64, 951-966.

Hauer, M., **Seeber, A.**, Singh, V., Thierry, R., Amitai, A., Kryzhanovska, M., Eglinger, J., Holcman, D., Owen-Hughes, T. (2017) Histone degradation in response to DNA damage enhances chromatin dynamics and recombination rates. Nature Structural and Molecular Biology, 24, 99-107.

Amitai, A.*, **Seeber, A.***, Gasser, S.M., Holcman, D., Visualization of Chromatin Decompaction and Break Site Extrusion as Predicted by Statistical Polymer Modeling of Single-Locus Trajectories. Cell Reports, 18, 1200-1214.

*equal contribution

REVIEW ARTICLES AND BOOK CHAPTERS

Chen, J., Young, S.M., Allen, C., Waller, A., Ursu, O., Strouse, J.J., Yao, T., Golden, J.E., Peterson, B.R., Foutz, T.D., **Seeber, A.,** et al. (2010). Profiling a Selective Probe for RTG Branch of Yeast TORC1 Signaling Pathway. Probe Reports from the NIH Molecular Libraries Program

Seeber, A., Hauer, M., and Gasser, S.M. (2013). Nucleosome remodelers in double-strand break repair. Current Opinion in Genetics & Development 23, 174-184.

Seeber, A., Dion, V., and Gasser, S.M. (2014). Remodelers move chromatin in response to DNA damage. Cell Cycle 13, 877-878.

Horigome, C., Dion, V., **Seeber, A.**, Gehlen, L.R., and Gasser, S.M. (2015). Visualizing the spatiotemporal dynamics of DNA damage in budding yeast. Methods in Molecular Biology (Clifton, NJ) 1292, 77-96.

Seeber, A., and Gasser, S.M. (2017). Chromatin organization and dynamics in double-strand break repair. Current Opinion in Genetics & Development 43, 9-16.

REFERENCES

Susan M. Gasser, PhD
Director of FMI
Professor of Molecular Biology
Quantitative Biology
FMI
Maulbeerstrasse 66
4058 Basel
Switzerland
+41 61 697 66 51
susan.gasser@fmi.ch

Noel F. Lowndes, PhD
Professor of Biochemistry
Biochemistry
NUI, Galway
Galway
Ireland
+353 86 023 6600
noel.lowndes@nuigalway.ie

Vincent Dion, PhD
SNF Professor
CIG
University of Lausanne
Lausanne
Switzerland
+41 76 737 9888
vincent.dion@unil.ch

Acknowledgements

This thesis would not have been possible without the support, guidance and teaching of Susan M. Gasser. I thank the NCCR - Frontiers in Genetics PhD program. The first year of rotations allowed me to start my PhD research on an excellent foundation. I am grateful to David Shore and Robbie Loewith, both of whom hosted me in their laboratories and supported me during a family crisis. In particular, Cyril Ribeyere in David Shore's group taught me a number of essential yeast experimental techniques.

When I joined Susan's lab I worked with two exquisitely talented, albeit very different scientists. Kenji Shimada's talents extend to everything, making him the lab guru: he is also a patient advisor and was essential in finishing the MRX project. Vincent Dion, "my post-doc", taught me a number of important techniques but, more importantly, he taught me, along with Susan, how to focus my efforts into concentrated productivity.

My special thanks go out to my other thesis committee members, Noel F. Lowndes and Ulrich Rass. I have known Noel since I did a summer research project in his lab. I hold Noel in the highest esteem not only because he is a talented scientist but because when he has given me advice, he always thinks of my best interests. Uli started his lab at the same time as I started my PhD. I admire his scientific rigor and persistence. Uli is filled with great ideas and it is easy to spend hours discussing concepts and experiments with him.

An important thank you goes to Monika Tsai, without whom the lab would run a lot more like an Italian train than a Swiss one. I wish her the best for when she retires next year and many happy years sailing. Another thank you is needed for Veronique Kalck and Razel Arpagaus who maintain the lab in a clean and well-organized way. Thank you to Sara Oakeley for proofreading this thesis.

The FMI microscopy facility, FAIM, has been essential to my PhD research. Without the expertise and experience of Laurent Gelman and Steve Bourke, and the excellent image analysis skills of Raphael Thierry and Jan Eglinger, my PhD would simply not have been the same.

I also thank all the former and current members of the Gasser lab. Joining the lab is like joining a family with a history of multiple generations. The environment is demanding but I feel that this is merely part of the tempering process in the training of a competent, critical scientist. Collaborating with Michael Hauer, Jerome Poli, Christian Gerhold, Nicole Hustedt, Vincent Dion, Daphne Cabianca, Ishan Deshpande, and Kenji Shimada has been deeply fulfilling. I also thank Anna Maria Hegnauer for establishing the base upon which I built a large portion of my PhD. I thank my external collaborators, David Holcman and Assaf Amitai, who forced me to push my limits and introduced me to the world of polymer physics.

Finally, special recognition goes to my patient wife, Michelle DiPietro, and my parents Patrick and Deirdre Seeber who have always supported me.